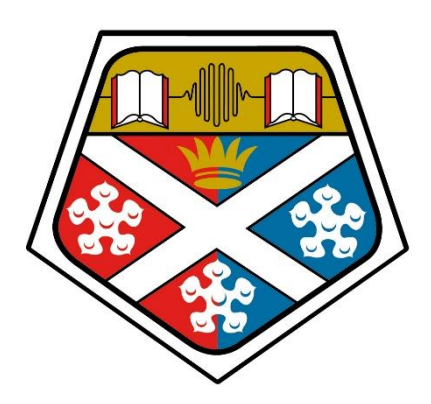
# Biofilm Development and Regulation in *Bacillus* subtilis Under Static and Flow Conditions and Effects of *Ginkgo biloba* Leaf Extract

Sara Drais MSc, BSc (Hons)

# Civil and Environmental Engineering Department University of Strathclyde



A thesis submitted in the fulfilment of the requirements for the degree

of

**Doctor of Philosophy** 

2025

This thesis is the result of the author's original research. It has been composed by the author and has not been previously submitted for examination which has led to the award of a degree. The copyright of this thesis belongs to the author under the terms of the United Kingdom Copyright Acts as qualified by University of Strathclyde Regulation 3.50. Due acknowledgement must always be made of the use of any material contained in, or derived from, this thesis.

Signed: Social

Date: 21st August 2025

# Thesis Abstract

Biofilms are structured communities of microorganisms embedded in an extracellular matrix, capable of adhering to surfaces and withstanding chemical, mechanical, and environmental stresses. They play essential roles in natural ecosystems but also cause major challenges in clinical, industrial, and environmental contexts due to their persistence and resistance to treatment. While Bacillus subtilis (B. subtilis) serves as a well-established model for studying biofilm development, the combined influence of hydrodynamic forces and natural antibiofilm compounds on its structure and regulation remains poorly understood. Existing studies have largely focused on static systems, microfluidic-scale observations, and clinical pathogens, offering limited insight into the macroscale architecture and transcriptional responses of B. subtilis biofilms under flow conditions. Furthermore, although Ginkgo biloba leaf extract (GBLE) has been shown to exhibit antimicrobial or antibiofilm activity against several clinically relevant bacteria, it has not previously been tested against B. subtilis or applied to flow-grown biofilms. Studying these responses under macroscale flow conditions is essential, as such environments are common in natural, clinical and industrial systems, while the use of GBLE reflects the urgent need for environmentally sustainable antibiofilm strategies. This thesis addresses these gaps by investigating the structural and molecular adaptations of B. subtilis biofilms to fluid flow regimes (unidirectional and bidirectional flow) and their responses to GBLE. A combination of confocal laser scanning microscopy, quantitative image analysis, RT-qPCR, and RNA Sequencing was used to examine biofilm morphology, matrix organisation, cellular differentiation, and transcriptional regulation under static and flow conditions, with and without GBLE supplementation.

This work shows that GBLE acts primarily as an antibiofilm agent against B. subtilis, with concentration-dependent inhibition of biofilm formation. GBLE greatly influenced agar colony biofilms, promoting motility (except at 400 and 500  $\mu$ g/mL) and inducing cellular differentiation. Microscopy revealed pronounced morphological changes, including the development of disorganised Van Gogh bundles (single cell chains), intracellular alterations, and increased amyloid production, suggesting differentiation into amyloid-producing cell types as a mechanism to reinforce extracellular matrix and persist under stress.

Under unidirectional flow, biofilms were entirely composed of aligned Van Gogh bundles and developed novel higher-order architectures, including spore aggregates, extracellular matrixrich foundation layers and rope-like twisted bundles of filaments ("Van Gogh ropes"), which

are believed to enhance mechanical stability and tensile strength against shear stress. GBLE disrupted these biofilms, reducing biomass and interfering with bundle organisation, thereby compromising the stability of flow-grown biofilms.

Exposure to bidirectional flow produced even greater structural heterogeneity, with biofilms exhibiting higher biomass and porosity compared to biofilms under unidirectional flow, and unique raised folds containing nutrient channels. These folds likely facilitate mass transport, spatial differentiation, and resilience under fluctuating hydrodynamic stress. GBLE treatment significantly reduced biomass and disrupted these complex architectures, further underscoring its potential as a natural biofilm-control strategy under dynamic flow conditions.

At the molecular level, gene expression analyses in planktonic cultures revealed that GBLE repressed key regulators of matrix production, development, motility, sporulation, and stress tolerance, while selectively inducing pathways linked to oxidative stress resistance and ribosome stabilisation, indicative of a shift toward survival rather than active biofilm development. Comparative transcriptomics across static, unidirectional, and bidirectional flow confirmed that flow regimes strongly activate transcription, with bidirectional flow inducing the broadest response, consistent with the structural complexity observed microscopically.

Together, these findings demonstrate that *B. subtilis* biofilms display remarkable plasticity under flow, adapting through novel structural and genetic strategies to withstand mechanical forces, while GBLE represents a promising environmentally sustainable antibiofilm agent that reduces biomass and disrupts biofilm organisation without strong bactericidal pressure.

Together, these findings extend current biofilm development models to incorporate macroscale flow environments and demonstrate the value of integrating microscopic analysis with transcriptomics, applied to industrially relevant environments. The work provides new insight into the physical and regulatory plasticity of *B. subtilis* biofilms and offers a foundation for developing context-specific, environmentally responsible biofilm control approaches.

# Acknowledgements

In the name of Allah, the Most Gracious, the Most Merciful. I bear witness that there is no God but Allah, and I bear witness that Muhammad, peace be upon him, is His servant and Messenger. My deepest thanks are to Allah for granting me the strength to persevere, the patience to overcome challenges, and the guidance to complete this work. All achievements are by His grace, and to Him I am forever grateful.

I stand in unwavering solidarity with the people of Palestine, Sudan, Congo, and all oppressed nations whose lives, land, labour, and resources continue to be exploited by colonial powers for material gain. May their resistance and struggles for freedom and justice prevail against genocidal systems built on oppression, occupation and ethnic cleansing.

I would like to thank my primary supervisor, Prof Vernon Phoenix, for his invaluable advice, unwavering guidance, and mentorship. My gratitude extends to my secondary supervisor, Prof Gail McConnell, for her technical input that helped shape my lab experiments.

I would like to thank my parents, Hafida and Abdelali, and my brothers, Ismail and Ahmed, for their immense support, encouragement, and endless love. I am deeply grateful to my husband, Tnany, for his unwavering belief in me, for patiently listening to my endless explanations, and for offering constant encouragement even during the most challenging stages of this journey. His love, understanding, and steadfast support have been a foundation I could always rely on. I also wish to thank my dear nephew, Ilyas, whose love, laughter, and innocence have brought immeasurable joy to my life and inspired me to keep moving forward with hope and positivity.

My appreciation also goes to my cherished friends, Maggie, Cynthia, Aleks, Matt and Natascia, for their support, laughter and distractions, needed throughout my academic journey.

I would also like to extend my affection and gratitude to my cats, Hmirbi and Bella, whose companionship, warmth, and occasional comic relief have brought me comfort and joy throughout this journey.

# Symbols

a.u. arbitrary units

degrees degrees

 $\sigma \hspace{1cm} \text{sigma}$ 

M molar

 $\mu g \hspace{1cm} micrograms$ 

 $\mu m \qquad \qquad micrometres$ 

 $\mu L$  microliters

mL millilitres

mM millimolar

n number

# **Abbreviations**

A. baumannii Acinetobacter baumannii

agr accessory gene regulator

AHLs acyl-homoserine lactones

AMR antimicrobial resistance

B. subtilis Bacillus subtilis

C. acnes Cutibacterium acnes

CESRs cell envelope stress responses

cDNA coding DNA

CIP clean-in-place

CLABSIs central line-associated bloodstream infections

CLSM Confocal Laser Scanning Microscope

CO<sub>2</sub> carbon dioxide

Ct cycle threshold

DBP disinfection by-product

DNA deoxyribonucleic acid

E. coli Escherichia coli

E. faecalis Enterococcus faecalis

ECF extracytoplasmic function

ECM extracellular matrix

eDNA extracellular DNA

EDTA ethylenediaminetetraacetic acid

EHEC Enterohemorrhagic E. coli O157:H7

EPS extracellular polymeric substances

FDBs food-borne diseases

Fe–S iron–sulfur

GbE Ginkgo biloba extracts

GBEE Ginkgo biloba exocarp extracts

GBLE Ginkgo biloba leaf extract

GFP green fluorescent protein

Gfp green fluorescent protein (gene)

H. pylori Helicobacter pylori

LB Luria-Bertani

L. monocytogenes Listeria monocytogenes

M. luteus Micrococcus luteus

MBC minimum bactericidal concentration

MIC microbiologically induced corrosion

MIC minimum inhibitory concentration

MRSA methicillin-resistant *Staphylococcus aureus* 

NaCl sodium chloride

NAPs nucleoid-associated proteins

N. A. numerical aperture

OCT optical coherence tomography

OD optical density

P. aeruginosa Pseudomonas aeruginosa

P. fluorescens Pseudomonas fluorescens

padj adjusted p-value

PCR polymerase chain reaction

PNAG poly-N-acetylglucosamine

PSMs phenol-soluble modulins

qPCR quantitative polymerase chain reaction

QS quorum sensing

RNA ribonucleic acid

RT-qPCR Reverse Transcription quantitative Polymerase Chain Reaction

S. aureus Staphylococcus aureus

S. epidermidis Staphylococcus epidermidis

S. gordonii Streptococcus gordonii

S. haemolyticus Staphylococcus haemolyticus

S. maltophilia Stenotrophomonas maltophilia

S. saprophyticus Saprophytic staphylococcus

S. pyogenes Streptococcus pyogenes

S. putrefaciens Shewanella putrefaciens

SIPBS Strathclyde Institute of Pharmacy and Biomedical Sciences

spp. species

STEC Shiga toxin—producing Escherichia coli

T. maritima Thermotoga maritima

TCM Traditional Chinese Medicine

TE buffer Tris-EDTA buffer

tRNAs Transfer RNAs

UV ultraviolet

V. cholera Vibrio cholera

VST variance-stabilising transformation

ΔΔCt Delta Delta Cycle threshold

ΔCt Delta Cycle threshold

# Table of Contents

1. n		uction: Biofilm Development Across Scales - Foundations, Dynamics Under Flo <sup>o</sup> Irdens, Control Strategies, and the Potential of <i>Ginkgo biloba</i> -Derived Antibiof	,
Δę	gents		1
	1.1. A	bstract	1
	1.2. Ir	ntroduction and Scope	1
	1.2.1.	Objectives of this chapter:	2
	1.2.2.	Terminology	3
	1.2.3.	Why Bacillus subtilis?	3
	1.3. H	istorical Evolution of Biofilm Theory	3
	1.3.1.	Early Microscopy and the Recognition of Sessile Communities	3
	1.3.2.	The Costerton Paradigm and the Primacy of the Sessile Lifestyle	4
	1.3.3.	The Five-Step Developmental Model	5
	1.3.4.	Limitations of the Classic Five Step Model	6
	1.3.5.	Expanded Conceptual Models: Aggregation, Growth, Disaggregation	7
	1.3.6.	From Ecology to Evolution-Development and Systems Perspectives	9
	1.4. C	ore Conceptual Elements Across Biofilm Models	.10
	1.4.1.	Matrix Centrality	11
	1.4.2.	Physiological Heterogeneity and Microenvironments	12
	1.4.3.	Cell–Cell Signalling, Social Interactions, and Public Goods	13
	1.4.4.	Mechanics, Hydrodynamics, and Biofilm Architecture	14
	1.4.5.	Dispersal, Detachment, and Lifecycle Transitions	15
	1.5. B	acillus subtilis as a Model for Biofilm Development and an Engineering Model	.16
	1.5.1.	Strain Diversity, Domestication, and Environmental Relevance	16
	1.5.2.	Matrix Architecture in B. subtilis	17
	1.5.3.	Genetic Regulatory Network Overview	19
	1.5.4.	Phenotypic Differentiation and Developmental Progression	21
	1.5.5.	Environmental and Engineering Cues Affecting B. subtilis Biofilms	23
	1.6. B	iofilm Development in Dynamic Systems and Under Fluid Flow	.24
	1.6.1.	Shear Regimes: Laminar, Transitional, Turbulent	24
	1.6.2.	Secondary Flows, Fluid Friction, and Streamer Formation	27
	1.6.3.	Mass Transfer, Nutrient Limitation, and Chemical Conditioning Films	28

	1.7.	Burden of Biofilms Across Sectors	.29
	1.8.	Biofilm Control Strategies in Industry: Conventional and Emerging Approaches.	.30
	1.8.1.	Chemical Biocides and Disinfectants	31
	1.8.2.	Physical and Mechanical Interventions and Surface Modification and Coatings	31
	1.8.3.	Biological and Ecological Controls	32
	1.8.4.	Matrix-Targeting Enzymes and Disassembly Signals	32
	1.8.5.	Monitoring, Sensing, and Control Loops	33
	1.9.	Ginkgo biloba: a Potential Natural Antibiofilm Agent	.33
	1.9.1.	Compound Classes from Ginkgo biloba	33
	1.9.2.	Spectrum of Activity Against Priority and Foodborne Organisms	34
	1.9.3.	Mechanistic Insights	35
	1.9.4.	Limitations of Static Models in Evaluating Ginkgo biloba Antibiofilm Efficacy	35
	1.10.	Knowledge Gaps and Research Opportunities	.36
	1.10.1	Genotype and Environment Interactions	36
	1.10.2	Linking Gene Regulation to Biofilm Mechanics and Detachment	36
	1.10.3	8. Natural Product Translation Under Realistic Conditions: Ginkgo biloba	37
	1.11.	Thesis Overview	.38
	1.11.1.	Chapter 2: Investigating the Antibiofilm and Antimicrobial Activity of Ginkgo bilo.	ba
	Leaf Exti	ract Against <i>Bacillus subtilis</i> Static Biofilms	.39
	1.11.2.	Chapter 3: Fluid Flow-Induced Morphological Adaptations in Bacillus subtilis	
	Biofilms	and Their Inhibition by <i>Ginkgo biloba</i> Leaf Extract	.39
	1.11.3.	Chapter 4: Structural Adaptation of <i>Bacillus subtilis</i> Biofilms to Bidirectional Flow	,
		. Disruptive Effect of <i>Ginkgo biloba</i> Leaf Extract	
	1 11 4	Chapter 5: Gene Expression Rewiring and Biofilm Morphogenesis in <i>Bacillus subt</i>	ilic
		to Ginkgo biloba Leaf Extract and Fluid Flow	
	•	References	
	1.12.	References	.42
2. A		tigating the Antibiofilm and Antimicrobial Activity of <i>Ginkgo biloba</i> Leaf Extract cillus subtilis Static Biofilms	.55
	2.1.	Abstract	.55
	2.2.	Introduction	.55
	2.3.	Materials and Methods	.60

	2.3.1	Bacterial Strain, Culture Conditions and Growth Curves Measurements	60
	2.3.2	Impact of GBLE on Bacterial Planktonic Growth	60
	2.3.3	Impact of GBLE on Static Biofilm Formation and Adhesion	61
	2.3.4	Impact of GLBE Concentration on Bacterial Colony Morphology and Motility	61
	2.3.5	Confocal Laser Scanning Microscopy	62
	2.4.	Results	62
	2.4.1	. Impact of GBLE on Bacterial Planktonic Growth	62
	2.4.2	Microtiter Dish Biofilm Assay	69
	2.4.3	, , ,	
	2.5.	Discussion	97
	2.5.1	. Impact of GBLE on Planktonic Growth	97
	2.5.2	. Impact of GBLE on Agar Colony Biofilms	99
	2.5.3	. Impact of GBLE on static Biofilms	.101
	2.5.4	. Impact of GBLE on TasA Amyloid Fibres	.104
	2.6.	Conclusion	.107
	2.7.	References	.108
	2.8.	Appendix	.113
	3.	Fluid Flow-Induced Morphological Adaptations in <i>Bacillus subtilis</i> Biofilms and	
	Their In	hibition by <i>Ginkgo biloba</i> Leaf Extract	.114
	3.1.	Abstract	.114
3.2	2. Intro	duction	.114
	3.3.	Materials and Methods	.120
	3.3.1	Bacterial strain and Culture Conditions	.120
	3.3.2	Fluid Flow System Design and Imaging	.120
	3.4.	Results	.123
	3.4.1	Effect of flow on biofilm morphology	.123
	3.4.2	. Effect of 75 μg/mL GBLE on Flow Cell Biofilms	.139
	3.4.3	Effect of 400 μg/mL GBLE on Flow Cell Biofilms	.142
	3.5.	Discussion	.144
	3.5.1		
		tures	
	3.5.2	. Effect of Ginako biloba Leaf Extract on Flow Cell Biofilms	.154

3	3.6.	Conclusion	157
3	3.7.	References	158
4.	Struc	ctural Adaptation of <i>Bacillus subtilis</i> Biofilms to Bidirectional Flow and the	
• •		Effect of <i>Ginkgo biloba</i> Leaf Extract	165
2	1.1.	Abstract	165
2	1.2.	Introduction	165
2	1.3.	Material and Methods	170
	4.3.1	Bacterial Strain and Culture Conditions	170
	4.3.2	Bidirectional Fluid Flow System Design	171
	4.3.3	. Image Analysis	173
2	1.4.	Results	173
	4.4.1	. Effect of Unidirectional and Bidirectional Fluid Flow on Biofilms	173
	4.4.2	. Biofilm Architecture under Bidirectional Conditions	177
	4.4.3	Bidirectional Flow Induced the Formation of Folds	180
	4.4.4	. GBLE Disrupts Biofilm Architecture under Bidirectional Flow	187
2	1.5.	Discussion	190
	4.5.1	. Effect of Unidirectional and Bidirectional Fluid Flow on Biofilms	190
	4.5.2	. Biofilm Architecture under Bidirectional Conditions	194
	4.5.3	Bidirectional Flow Induces the Formation of Folds	195
	4.5.4	. GBLE Disrupts Biofilm Architecture under Bidirectional Flow	198
2	1.6.	Conclusion	199
4	1.7.	References	201
<u>.</u>		e Expression Rewiring and Biofilm Morphogenesis in <i>Bacillus subtilis</i> Exposed t	
Gir	kgo bild	oba Leaf Extract and Fluid Flow	
C	5.1.	Abstract	206
٦	Γogethe	er, these findings highlight the impact of phytochemical and mechanical cues	on
E	3. subti	lis biofilm formation. Flow regime shapes transcriptional breadth and structu	ıral
(	comple	xity, while GBLE independently suppresses core developmental pathways	
r	egardle	ess of culture condition.	207
r	<del>.</del> ၁	Introduction	207

	5.3.	Material and Methods	209
	5.3.1	. Growth conditions	209
	5.3.2	. Total RNA Isolation	210
	5.3.3 Reac	. cDNA Synthesis and Reverse Transcription Quantitative Polymerase Chain tion (RT-qPCR)	211
	5.3.4	. RNA-Seq, Data Processing and Differential Expression Analysis	211
	5.4.	Results	213
	5.4.1	. RT-qPCR: planktonic cultures supplemented with GBLE	213
	5.4.2	. RNA-Sequencing Results	225
	5.5.	Discussion	235
	5.5.1	. Impact of GBLE on planktonic cultures	235
	5.5.2	. Impact of GBLE on Cultures under Unidirectional Fluid Flow	241
	5.5.3	. Impact of a Continuous Unidirectional Flow on <i>B. subtilis</i>	244
	5.5.4	. Impact of a Continuous Bidirectional Flow on <i>B. subtilis</i>	246
	5.6.	Conclusion	248
	5.7.	References	250
	5.8.	Appendix	257
6	. Cond	clusion Chapter	258
	6.1.	Introduction	258
	6.2.	Integration of Structural Findings	258
	6.3.	Integration of Molecular Findings	260
	6.4.	Broader Scientific Implications	262
	6.5.	Applied Relevance	263
	6.6.	Future Directions	265
	6.7	Closing Remarks	266

# Tables

Table 4.1. Characteristic architectural features of Bacillus subtilis biofilms developed under	er
bidirectional flow, as visualised by confocal laser scanning microscopy (CLSM)1	79
Table 5.1. Functional roles and mutant phenotypes of key regulatory and structural genes	
involved in <i>Bacillus subtilis</i> biofilm development2	220
Table S5.1. Primers used in the RT-αPCR investigation in this chapter2	240

# Table of Figures

Figure 1.1. The classical five-step model of biofilm development5
Figure 1.2. The biofilm life cycle model proposed by Sauer et al. (2022)
Figure 1.3. Interplay between biological, molecular, and physical processes in biofilm
formation11
Figure 1.4. Schematic representation of the spatial organisation and functional
specialisation within a Bacillus subtilis biofilm18
Figure 1.5. Simplified model of the Bacillus subtilis biofilm regulatory network showing
transitions between planktonic and biofilm states
Figure 1.6. Fluorescent micrograph of a gfp-expressing <i>Pseudomonas aeruginosa</i> biofilm
streamer formed within a curved channel of a microfluidic device27
Figure 1.7. Estimated global economic impact of biofilms across major industrial sectors29
Figure 2.1. Growth (teal) and decline (salmon) start times from smoothed OD curves of
cultures grown with increasing GBLE63
Figure 2.2. Bacillus subtilis planktonic growth curves at 0 and 50 μg/mL Ginkgo Biloba Leaf
Ginkgo
Figure 2.3. Bacillus subtilis planktonic growth curves at 75 and 100 μg/mL Ginkgo Biloba
Leaf Extract, c and d respectively65
Figure 2.4. Bacillus subtilis planktonic growth curves at 150 and 175 μg/mL Ginkgo Biloba
Leaf Extract, e and f respectively66
Figure 2.5. Bacillus subtilis planktonic growth curves at 200 and 300 μg/mL Ginkgo Biloba
Leaf Extract, g and h respectively67
Figure 2.6. Bacillus subtilis planktonic growth curves at 400 and 500 μg/mL Ginkgo Biloba
Leaf Extract, i and j respectively68
Figure 2.7. Bacillus subtilis planktonic growth curves at 600 μg/mL Ginkgo Biloba Leaf
Extract, (k)69
Figure 2.8. Histogram showing the mean value of optical density (590 mm), in relation to
increasing concentrations of Ginkgo biloba leaf extract
Figure 2.9. Pictures of 0.3% LB agar petri dishes containing increasing concentrations of
GBLE and inoculated with <i>B. subtilis</i> culture to test swimming motility72
Figure 2.10. Pictures of 0.3% LB agar petri dishes containing increasing concentrations of
GBLE and inoculated with <i>B. subtilis</i> culture to test swimming motility73

<b>Figure 2.11.</b> Pictures of 0.3% LB agar petri dishes containing increasing concentrations of
GBLE and inoculated with <i>B. subtilis</i> culture to test swimming motility74
Figure 2.12. Pictures of 0.3% LB agar petri dishes containing increasing concentrations of
GBLE and inoculated with <i>B. subtilis</i> culture to test swimming motility75
Figure 2.13. Pictures of 0.3% LB agar petri dishes containing increasing concentrations of
GBLE and inoculated with <i>B. subtilis</i> culture to test swimming motility76
Figure 2.14. Pictures of 0.3% LB agar petri dishes containing increasing concentrations of
GBLE and inoculated with <i>B. subtilis</i> culture to test swimming motility77
Figure 2.15. Pictures of 0.6% agar petri dishes containing increasing concentrations of GBLE
and inoculated with <i>B. subtilis</i> culture79
Figure 2.16. Pictures of 0.6% agar petri dishes containing increasing concentrations of GBLE
and inoculated with <i>B. subtilis</i> culture80
Figure 2.17. Pictures of 0.6% agar petri dishes containing increasing concentrations of GBLE
and inoculated with <i>B. subtilis</i> culture81
Figure 2.18. Pictures of 0.6% agar petri dishes containing increasing concentrations of GBLE
and inoculated with <i>B. subtilis</i> culture82
Figure 2.19. Pictures of 0.6% agar petri dishes containing increasing concentrations of GBLE
and inoculated with <i>B. subtilis</i> culture83
Figure 2.20. Picture of 0.6% agar petri dishes containing 600 $\mu g/mL$ GBLE and inoculated
with <i>B. subtilis</i> culture84
Figure 2.21. Fluorescent images of gfp-expressing B. subtilis biofilms, grown without
GBLE86
Figure 2.22. Fluorescent images of gfp-expressing $\emph{B. subtilis}$ biofilms, grown with 50 $\mu g/mL$
GBLE87
Figure 2.23. Fluorescent images of $gfp$ -expressing $B$ . $subtilis$ biofilms, grown with 75 $\mu$ g/mL
GBLE
Figure 2.24. Microscopy images of <i>gfp</i> -expressing <i>Bacillus subtilis</i> biofilms treated with 100
μg/mL GBLE89
<b>Figure 2.25.</b> Microscopy images of <i>gfp</i> -expressing <i>Bacillus subtilis</i> biofilms treated with 200
μg/mL GBLE90
<b>Figure 2.26.</b> Microscopy images of <i>gfp</i> -expressing <i>Bacillus subtilis</i> biofilms treated with 300
ug/mL GRLF

<b>Figure 2.27.</b> Microscopy images of <i>gfp</i> -expressing <i>Bacillus subtilis</i> biofilms treated with 400
μg/mL GBLE92
<b>Figure 2.28.</b> Microscopy images of <i>gfp</i> -expressing <i>Bacillus subtilis</i> biofilms treated with 500
µg/mL GBLE93
Figure 2.29. Confocal laser scanning microscopy images of untreated gfp-expressing
Bacillus subtilis biofilms stained with EbbaBiolight 680
Figure 2.30. Confocal laser scanning microscopy images of gfp-expressing Bacillus subtilis
biofilms treated with 100 $\mu\text{g/mL}$ GBLE and stained with EbbaBiolight 68096
Figure 2.31. A) Van Gogh bundles characterised by van Gestel, Vlamakis and Kolter (2015)
on agar plates at the edge of Bacillus subtilis colonies. B) Van Gogh bundles seen in this
present study, in \textit{B. subtilis} JWV042 pellicle biofilms in response to 100 $\mu g/mL$ GBLE102
Figure S.2.32. Standard descriptive terms for bacterial colony morphology113
Figure 3.1. Schematic of the fluid flow set up used to grow biofilms under a fluid flow121
Figure 3.2. Fluorescent images of gfp-expressing B. subtilis biofilms grown under a fluid
flow, showing cloud- and wave-like morphology (a-b)
Figure 3.3. Fluorescent images of gfp-expressing B. subtilis biofilms grown under a fluid
flow, showing multiple Van Gogh bundles aligned
Figure 3.4. Fluorescent images (left) and light transmission images (right) of aggregates
seen within gfp-expressing B. subtilis biofilms grown under a pumped fluid flow129
Figure 3.5. Barplot showing the surface area (μm²) of individual <i>Bacillus subtilis</i> biofilm
aggregates formed under continuous unidirectional flow
Figure 3.6. Barplot showing the length ( $\mu m$ ) of individual $\textit{Bacillus subtilis}$ biofilm aggregates
developed under continuous unidirectional flow
Figure 3.7. Fluorescent image of rope-like structure seen within gfp-expressing B. subtilis
biofilm grown under a pumped flow of fluid
Figure 3.8. Fluorescent image of rope-like structures seen within gfp-expressing B. subtilis
biofilm grown under a pumped flow of fluid
Figure 3.9. Rope dimensions and correlation between rope length and average width134
Figure 3.10. Twist angle distribution of selected <i>B. subtilis</i> biofilm ropes under
unidirectional flow
Figure 3.11. Fluorescent images of gfp-expressing B. subtilis biofilms grown under a fluid
flow (a, b) and B. subtilis pellicle biofilms (c, d)

<b>Figure 3.12.</b> Fluorescent images of a <i>gfp</i> -expressing <i>B. subtilis</i> biofilm grown under a fluid
flow, attached to the wall of the flow cell
Figure 3.13. Fluorescent images of a <i>gfp</i> -expressing <i>B. subtilis</i> biofilm grown under a fluid
flow, supplemented with 75 $\mu$ g/mL GBLE
<b>Figure 3.14.</b> "The spoon". Fluorescent image of structure seen within the <i>B. subtilis</i> biofilm
grown under a continuous fluid flow of LB media supplemented with 75 $\mu\text{g/mL}$ GBLE141
Figure 3.15. Fluorescent images of a <i>gfp</i> -expressing <i>B. subtilis</i> biofilm grown under a fluid
flow, supplemented with 400 $\mu g/mL$ GBLE
Figure 4.1. Schematic of the bidirectional fluid flow set up used to grow biofilms under a
fluid flow
<b>Figure 4.2.</b> Fluorescent images of <i>gfp</i> -expressing <i>B. subtilis</i> biofilms grown under different
flow condition
Figure 4.3. Boxplots represent the distribution of mean gray values (a.u.), which are directly
proportional to biofilm density and biomass based on fluorescence intensity. $ \\  \dots \\                              $
Figure 4.4. Porosity of biofilms grown under bidirectional and unidirectional flow
conditions
Figure 4.5. Fluorescent images of gfp-expressing B. subtilis biofilms grown under a
bidirectional fluid flow
Figure 4.6. Fluorescent image of a region of a <i>gfp</i> -expressing <i>B. subtilis</i> biofilm containing
$two\ folds,\ developed\ under\ a\ bidirectional\ fluid\ flow,\ presented\ at\ different\ depths.\181$
<b>Figure 4.7</b> . Fluorescent image of a region of a <i>gfp</i> -expressing <i>B. subtilis</i> biofilm containing
four folds, developed under a bidirectional fluid flow, presented at different depths. $\ldots$ 182
Figure 4.8. (A) Boxplot showing the measured heights of different biofilm folds. (B) Fold
width profiles measured at five equidistant points across each fold. (C) Scatter plot showing
the relationship between overall fold width and fold height, grouped by fold ID184 $$
Figure 4.9. (A) Boxplots showing minimum (red), mean (blue), and maximum (green)
channel widths beneath individual folds. (B) Fold height-to-channel width ratio per fold. (C)
Scatter plot showing the relationship between fold height and channel width
Figure 4.10. Boxplots represent the distribution of thickness measurements ( $\mu m$ ) for each
group
Figure 4.11. Images (a–d) show representative fields of view at various magnifications188
Figure 4.12. Boxplots represent total biofilm volume ( $\mu m^3$ ) from biofilms grown under bi-
directional flow, grown either with GBLE (treated) or without GBLE (untreated)

Figure 4.13. Boxplots represent mean gray value (a.u.), which is directly proportional to
biofilm density and biomass
Figure 5.1. Relative expression of bslA in Bacillus subtilis planktonic cultures under
increasing concentrations of GBLE, in $\mu g/mL$ .
<b>Figure 5.2.</b> Relative expression of <i>TasA</i> in <i>Bacillus subtilis</i> planktonic cultures supplemented
with increasing concentrations of GBLE, in $\mu g/mL$
Figure 5.3. Relative expression of sIrR in Bacillus subtilis planktonic cultures under
increasing concentrations of GBLE, in $\mu g/mL$ .
Figure 5.4. Fold change in remB expression in Bacillus subtilis planktonic cultures in
response to increasing concentrations of GBLE, in $\mu\text{g/mL}217$
Figure 5.5. RT-qPCR analysis of SpoOA expression in Bacillus subtilis planktonic cultures
following addition of increasing concentrations of GBLE, in $\mu g/mL$
Figure 5.6. Fold change in comK expression in Bacillus subtilis planktonic cultures in
response to increasing concentrations of GBLE in $\mu g/mL$
Figure 5.7. RT-qPCR analysis of <i>Dps</i> expression in <i>Bacillus subtilis</i> planktonic cultures under
increasing concentrations of GBLE in $\mu g/mL$
Figure 5.8. Expression of sigM in Bacillus subtilis planktonic cultures in response to
increasing concentrations of GBLE, in $\mu g/mL$
Figure 5.9. Expression of YerD in Bacillus subtilis planktonic cultures in response to
increasing concentrations of GBLE in $\mu g/mL$
Figure 5.10. Fold change in abrB expression in Bacillus subtilis planktonic cultures treated
with increasing concentrations of GBLE in $\mu g/mL$
<b>Figure 5.11.</b> Expression profile of <i>sigD</i> in <i>Bacillus subtilis</i> planktonic cultures in response to
increasing concentrations of GBLE in $\mu g/mL$
Figure 5.12. Expression levels of LytA in Bacillus subtilis planktonic cultures across
increasing concentrations of GBLE, in $\mu g/mL$
Figure 5.13. The heatmap displays hierarchical clustering of genes with significant
differential expression (p < 0.05) across untreated control, 400 $\mu$ g/mL, and 600 $\mu$ g/mL
GBLE-treated samples (labelled treated_400 and treated_600 respectively)228
Figure 5.14. This heatmap shows differentially expressed genes between untreated and
GBLE-treated (400 $\mu g/mL$ ) <i>B. subtilis</i> cells grown under unidirectional flow230
<b>Figure 5.15.</b> The heatmap displays genes with significant differential expression (p $< 0.05$ )
between <i>Bacillus subtilis</i> cells in static and unidirectional flow environments232

<b>Figure 5.16.</b> Heatmap showing differentially expressed genes (adjusted p < 0.05) in <i>Bacillus</i>
subtilis cultures grown under static versus bidirectional flow conditions234
Figure 5.17. Representative macrocolonies of <i>B. subtilis</i> JWV042 grown on LB agar
supplemented with increasing concentrations of Ginkgo biloba leaf extract (GBLE)237
Figure 5.18. Confocal microscopy of <i>Bacillus subtilis</i> JWV042 pellicle biofilms treated with
100 μg/mL GBLE238
Figure 5.19. Confocal laser scanning microscopy of Bacillus subtilis JWV042 flow-cell
biofilms with and without GBLE treatment242
Figure 5.20. Confocal laser scanning microscopy comparison of <i>Bacillus subtilis</i> JWV042
$biofilms\ formed\ under\ static\ versus\ unidirectional\ continuous\ flow\ conditions,\ both\ without$
GBLE
Figure 5.21. Confocal laser scanning microscopy image of a Bacillus subtilis JWV042 biofilm
grown under bidirectional flow conditions

# 1. Introduction: Biofilm Development Across Scales - Foundations, Dynamics Under Flow, Industrial Burdens, Control Strategies, and the Potential of *Ginkgo biloba*-Derived Antibiofilm Agents

#### 1.1. Abstract

Biofilms are surface- or aggregate-associated microbial communities encased in self-produced extracellular polymeric substances (EPS). They are central to environmental processes, industrial systems, public health, and engineered water infrastructure. Foundational work during the "Costerton era" redefined sessile microbial lifestyles as the norm, driving decades of research into attachment, matrix biology, and antimicrobial resistance. The classic five-stage *Pseudomonas aeruginosa* (*P. aeruginosa*) biofilm model has since expanded to include non-attached aggregates, pellicles, and biofilms in complex ecological and industrial contexts.

This chapter reviews the evolution of biofilm theory, compares core concepts across models (matrix structure, heterogeneity, signalling, mechanics, and dispersal), and examines biofilm development under fluid flow, with attention to shear, secondary currents, and gravity.

Bacillus subtilis (B. subtilis) is discussed as a model organism linking developmental biology to environmental engineering, with a focus on its regulatory network and matrix composition. Comparative sections highlight features of *P. aeruginosa*, staphylococci, and mixed industrial biofilms. Industrial impacts are mapped across healthcare, water systems, food processing, and corrosion.

Conventional mitigation strategies are contrasted with emerging biological and natural product approaches. A focused review of *Ginkgo biloba*-derived compounds highlights broad-spectrum antibiofilm activity against key pathogens, acting through motility inhibition, matrix gene suppression, and quorum pathway interference.

# 1.2. Introduction and Scope

Biofilms are now recognised as the dominant growth mode for bacteria in natural, engineered, and host-associated environments (Costerton et al., 1995) (Hall-Stoodley, Costerton and Stoodley, 2004). Their presence underpins both beneficial processes, such as nitrification biofilters, granular sludge formation, and biocontrol on plant roots, as well as

problematic outcomes, including chronic device-associated infections, membrane biofouling, microbiologically influenced corrosion, and foodborne pathogen persistence on processing lines (Flemming et al., 2016) (Rodríguez-López et al., 2019) (Schultz et al., 2011). For civil and environmental engineers, biofilms represent both a valuable unit process to be harnessed and a contamination risk to be mitigated.

Despite decades of research, translating biofilm science into robust predictive and control frameworks remains challenging. Laboratory models often underrepresent the spatial, chemical, and hydrodynamic complexity found in full-scale systems (Sauer et al., 2022), in part due to strain domestication that alters biofilm phenotypes (Kovács and Kuipers, 2011) (Arnaouteli et al., 2021). Regulatory test methods, though essential for product validation and registration, frequently fail to replicate field-relevant conditions such as nutrient limitation, variable shear forces, and multispecies interactions (EPA, 2024) (ASTM International, 2021). These gaps highlight the need for an integrated approach that links molecular-level regulation to the emergent structure and behaviour of biofilm communities at larger scales, and ultimately to how these communities impact the performance and sustainability of real-world engineered systems.

## 1.2.1. Objectives of this chapter:

- 1. Trace the historical evolution of biofilm theory and the major conceptual models in the literature, highlighting how each contributed to current multi-scale thinking.
- 2. Provide an in-depth, engineering-oriented review of *Bacillus subtilis* (*B. subtilis*) biofilm genetics, regulation, and matrix biology, and compare with *Pseudomonas aeruginosa* (*P. aeruginosa*) and staphylococcal paradigms.
- 3. Examine biofilm development under dynamic hydrodynamic regimes relevant to pipes, reactors, distribution systems, and industrial equipment.
- 4. Map the industrial and economic burden of biofilms across sectors.
- Evaluate conventional and emerging industrial biofilm treatment strategies, with a focused assessment of evidence for natural antibiofilm agents derived from *Ginkgo biloba*.

### 1.2.2. Terminology

The term *biofilm* is used here in an inclusive sense to encompass surface-attached microbial communities, floating pellicles, and suspended aggregates that exhibit key biofilm-associated phenotypes, such as matrix encasement, altered gene expression, and enhanced tolerance to environmental stressors (Sauer et al., 2022) (Kragh et al., 2023). The term *matrix*, following Flemming and Wingender (2010), refers to the self-produced extracellular polymeric substances (EPS) comprising polysaccharides, proteins (including functional amyloids), extracellular DNA (eDNA), lipids, and associated biopolymers that provide structural and protective functions. *Burden* denotes quantifiable or estimated impacts of biofilms, such as economic losses, reductions in system efficiency, regulatory non-compliance, negative health outcomes, or infrastructure degradation (Flemming et al., 2016) (Cámara et al., 2022).

## 1.2.3. Why *Bacillus subtilis*?

Although non-pathogenic, *B. subtilis* has become a model organism for dissecting the genetic and regulatory logic of biofilm development, offering intriguing parallels to multicellular development and differentiation processes (Vlamakis et al., 2013) (Arnaouteli et al., 2021). Its ability to form a robust extracellular matrix and undergo phenotypic differentiation into functionally distinct subpopulations makes *B. subtilis* particularly attractive for biofilm studies. However, under certain conditions, *Bacillus* biofilms can also contribute to fouling and clogging in industrial water systems, such as filtration membranes or cooling circuits (Hoek, 2022). Due to its well-characterised regulatory network, *B. subtilis* serves as a powerful framework for linking molecular regulation to the emergent structure, mechanics, and function of biofilm communities.

# 1.3. Historical Evolution of Biofilm Theory

## 1.3.1. Early Microscopy and the Recognition of Sessile Communities

The recognition of biofilms as structured microbial communities can be traced back to early microscopic observations in the 19th century. In 1871, J. Burdon-Sanderson described "viscous intermediary substances" connecting rod-shaped bacteria on surfaces, while Ferdinand Cohn (1877) noted similar formations, both offering early glimpses into what we now understand as biofilm matrices. These surface-associated layers were not yet conceptualised as distinct biological systems but were often regarded as curious byproducts

of microbial growth. Around the same time, Louis Pasteur's investigations into fermentation and spoilage processes hinted at the industrial consequences of microbial aggregates, linking their presence to blockages and failures in fermentation vessels (Kragh et al., 2016). While these observations were largely descriptive and lacked a unifying theoretical framework, they presaged a critical realisation: that microbes do not merely exist as isolated cells but often form complex, matrix-bound collectives whose structure and behaviour are distinct from planktonic populations. The notion that microbial adhesion and surface persistence could drive persistent contamination would not be formalised until much later, but the groundwork had been quietly laid through these early accounts.

# 1.3.2. The Costerton Paradigm and the Primacy of the Sessile Lifestyle

A major conceptual leap in biofilm science emerged in the late 1970s through the work of J. William Costerton and colleagues, who redefined how microbial life was understood across natural and engineered environments. Rather than viewing bacteria primarily as free-floating (planktonic) entities, Costerton advanced a transformational idea: bacteria predominantly exist as surface-attached communities, embedded in a self-produced matrix of extracellular polymeric substances, a mode of life now recognised as the biofilm (Costerton, Geesey and Cheng, 1978) (Costerton et al., 1995). This "sessile lifestyle" was not merely a transient phase but foundational biological The Costerton paradigm introduced several key tenets that still shape modern biofilm theory. First, it emphasised irreversible adhesion to surfaces, mediated by adhesive glycocalyx polymers that anchor cells in place. Second, it described nutrient microzones within the biofilm matrix, defined as localized regions of metabolic activity shaped by diffusion gradients and substrate limitation. Third, and perhaps most disruptively, it revealed that biofilmembedded cells exhibit significantly higher tolerance to antibiotics and disinfectants than their planktonic counterparts, not due to genetic resistance alone but because of the protective properties of the matrix and altered metabolic states (Costerton, Geesey and Cheng, 1978) (Costerton et al., 1995). This paradigm prompted a re-evaluation of microbial persistence in diverse settings, from chronic infections (Hall-Stoodley, Costerton and Stoodley, 2004) to fouled membranes (Flemming, 2002) and industrial pipelines (Beech and Sunner, 2004). It also led to the development of new investigative tools, including advanced microscopy techniques for visualising biofilms on catheters (Donlan and Costerton, 2002),

teeth (Kolenbrander et al., 2010), and filtration systems (Herzberg and Elimelech, 2007). Importantly, it reframed control strategies: rather than targeting cells in suspension, effective interventions would now need to focus on disrupting the matrix, penetrating the biofilm structure, and preventing initial attachment (Høiby et al., 2010) (Bridier et al., 2011). The Costerton era marked a foundational shift, placing the biofilm, not the planktonic cell, at the centre of microbial ecology, pathogenesis, and systems design (Stoodley et al., 2002) (Costerton, Stewart and Greenberg, 1999).

## 1.3.3. The Five-Step Developmental Model

Building on continuous imaging studies of *P. aeruginosa*, Stoodley and co-workers introduced one of the most widely cited developmental models of biofilm formation (Fig. 1.1), summarised in five distinct stages: (1) reversible attachment, where individual planktonic cells transiently adhere to a surface; (2) irreversible attachment, involving stronger surface anchoring and production of extracellular polymeric substances (EPS); (3) maturation I, marked by early microcolony formation; (4) maturation II, characterised by complex three-dimensional structures such as mushroom-like towers with fluid channels; and finally (5) dispersal, where subsets of cells detach to colonise new niches (Stoodley et al., 2002) (Hall-Stoodley, Costerton and Stoodley, 2004).

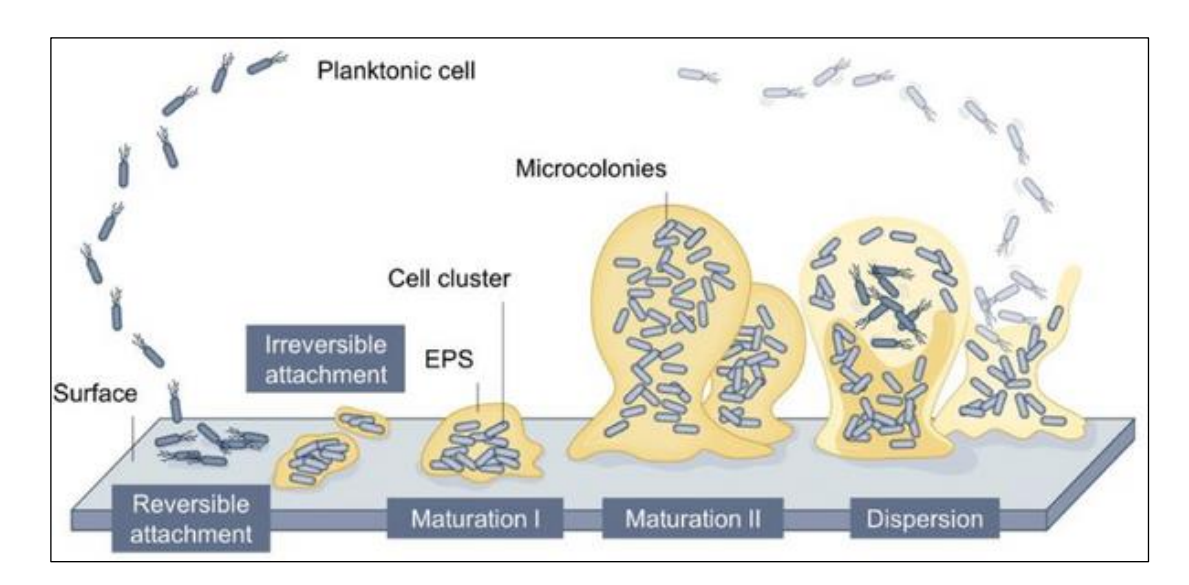


Figure 1.1. The classical five-step model of biofilm development. Planktonic bacterial cells first engage in reversible attachment to a surface, followed by irreversible attachment mediated by extracellular polymeric substances (EPS). Cells then form microcolonies and undergo maturation phases I and II, characterised by increased biomass, structural complexity, and matrix production. The final stage, dispersion, releases cells back into the planktonic state, enabling colonisation of new surfaces. From Zhang et al. (2025)

This model was made possible by real-time confocal microscopy and quantitative analyses of P. aeruginosa biofilms, which revealed the spatial and temporal dynamics of biofilm development in unprecedented detail. The architecture of the mature biofilm was found to support metabolic stratification, nutrient gradients, and cell differentiation, features that closely mirror developmental systems in multicellular organisms (Lawrence et al., 1991) (Walters, Roe and Stewart, 2003). Importantly, the Stoodley model was strengthened by transcriptional profiling studies, which linked each developmental stage to characteristic gene expression programs. For instance, early stages featured genes related to flagellar motility and chemotaxis, while the maturation stages upregulated genes involved in EPS synthesis, quorum sensing, and anaerobic metabolism (Whiteley et al., 2001) (Sauer and Camper, 2001). The clarity and intuitive structure of this model made it widely accessible across disciplines. It has since been featured in microbiology textbooks, regulatory guidance documents, and conceptual frameworks in clinical and industrial microbiology. Despite its original basis in *P. aeruginosa*, it has been applied to other species, such as *Staphylococcus* aureus (S. aureus), Escherichia coli (E. coli), and B. subtilis, though with recognised limitations due to species-specific biofilm dynamics (Karatan and Watnick, 2009) (Bridier et al., 2011).

## 1.3.4. Limitations of the Classic Five Step Model

While the Stoodley model of biofilm development was transformative, its generalisability beyond laboratory systems, particularly those based on *P. aeruginosa*, has been increasingly challenged. In many real-world environments, biofilm formation does not begin with surface attachment by individual cells, but instead arises through aggregation of suspended cells in hydrogels, mucus layers, or aqueous microenvironments. Examples include flocculated microbial clusters in activated sludge, pelagic marine snow in ocean systems, floating pellicles in static cultures, and mucosal aggregates in host tissues, all of which deviate significantly from the classical sequence of surface colonisation (Bjarnsholt et al., 2022) (Kragh et al., 2016). Biofilm architectures are also highly diverse, ranging from flat surface films and ridged colonies, to wrinkled pellicles, filamentous streamers, and even immobilised flocs (Flemming and Wingender, 2010) (Neu and Lawrence, 2015). These morphologies respond dynamically to local environmental conditions such as fluid shear, oxygen gradients, desiccation, or nutrient pulses. Such parameters can not only modulate the pace of development, but can reorder, skip, or reverse biofilm developmental stages altogether (Bridier et al., 2011). Additionally, multispecies and interkingdom biofilms, common in soils, industrial systems,

and host environments, exhibit structural and regulatory complexities absent from simplified monoculture models. These include fungal-bacterial scaffolds, metabolic cross-feeding, and cooperative matrix production, which defy the linear assumptions of canonical models (Nadell, Drescher and Foster, 2016). Collectively, these limitations highlight the need for a more flexible, context-dependent view of biofilm formation, one that accommodates diverse initiation mechanisms, architectural plasticity, and ecological interactions across space and time.

# 1.3.5. Expanded Conceptual Models: Aggregation, Growth, Disaggregation

The classical models of biofilm development, rooted in surface-attached paradigms, have come under increasing scrutiny for their limited applicability to diverse real-world systems. In response, Sauer et al. (2022) proposed a streamlined and inclusive three-event life cycle model for biofilm dynamics (Fig. 1.2), comprising aggregation or attachment, growth or accumulation, and disaggregation. This model is deliberately sceptical to surface requirement, allowing for parallel pathways such as combination of suspended aggregates, pellicle formation, or attachment from pre-existing flocs in dynamic systems. It shifts emphasis away from rigid, sequential stages and instead accommodates the fluidity and reversibility often observed in biofilm systems subjected to fluctuating conditions.

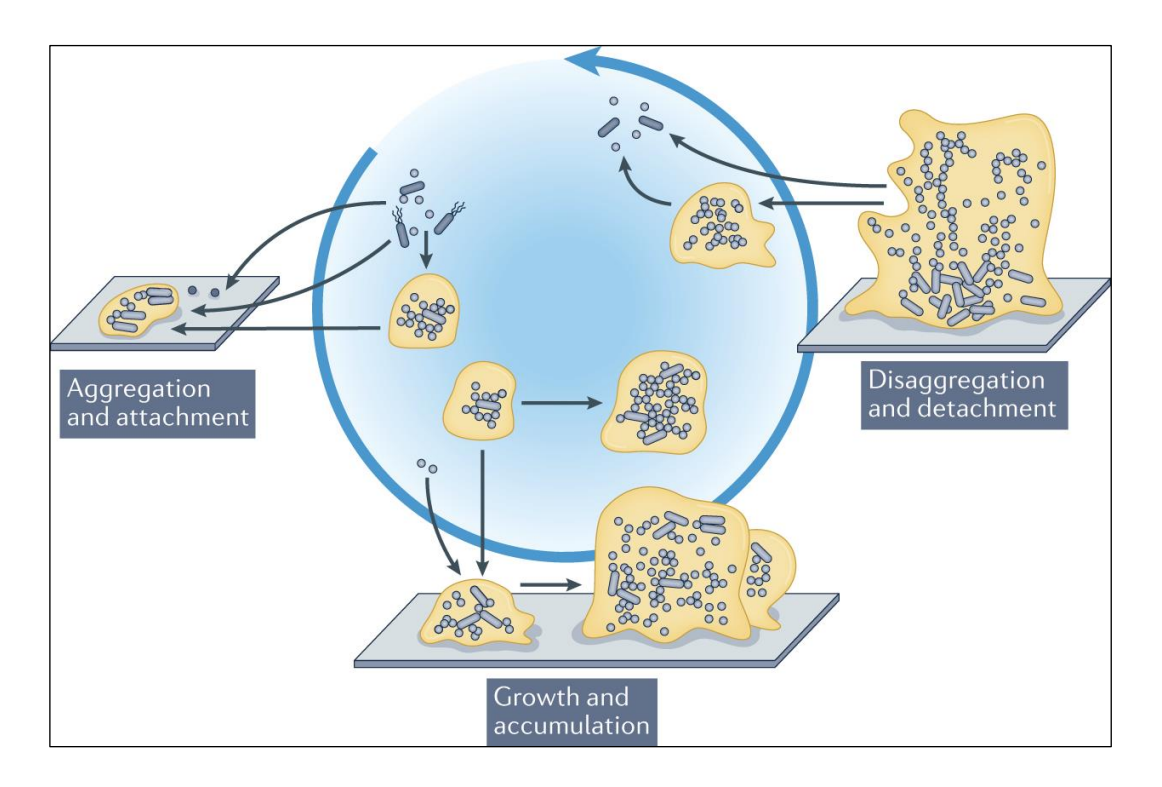


Figure 1.2. The biofilm life cycle model proposed by Sauer et al. (2022), expanding on the classical five-step framework. This model emphasises the dynamic and cyclical nature of biofilm development, encompassing initial aggregation and attachment of cells to a surface, growth and accumulation into structured communities, and eventual disaggregation and detachment of cells or aggregates. Detached cells may then reattach locally or colonise new surfaces, sustaining biofilm persistence across spatial and temporal scales. From Sauer et al. (2022)

Kragh et al. (2023) further expanded the scope of conceptual models by arguing that nonsurface-attached aggregates, which have been long observed in chronic infections, bioreactors, and wastewater systems, should also be considered biofilms. These structures exhibit hallmark biofilm characteristics such as extracellular matrix production, spatial organisation, quorum sensing, and enhanced tolerance to antibiotics and shear stress, despite lacking fixed substratum adhesion. This redefinition aligns with earlier calls by Percival et al. (2015) and Sloan et al. (2006) to recognise the functional phenotype over physical configuration as the defining feature of a biofilm.

These revised frameworks have significant implications for both clinical and industrial microbiology. For instance, suspended aggregates found in chronic wounds, cystic fibrosis lung mucus, or synovial fluid infections may be overlooked by surface-biased diagnostics and regulatory assays (Høiby et al., 2015) (Alhede et al., 2014). Similarly, in engineered environments, biofilm flocs in anaerobic digesters, granules in sequencing batch reactors, and turbulent streamers in membrane systems represent operationally important, yet non-canonical forms of biofilm life (Rittmann and McCarty, 2001) (Wanner et al., 2006).

Recognising these forms improves the ability of modelling frameworks to simulate detachment, transport, and downstream colonisation, which are critical to both bioprocess efficiency and infection spread.

By embracing a more phenotype-driven and systems-aware model, current thinking in biofilm science is shifting toward ecological and functional definitions of biofilms. Rather than requiring fixed surface attachment, the emphasis is increasingly placed on matrix production, collective behaviour, antimicrobial tolerance, and emergent properties, regardless of spatial configuration or attachment mode (Stoodley et al., 2002) (Flemming and Wuertz, 2019) (Kragh et al., 2023). This reflects an emerging consensus that structure, while still important, should not constrain our conceptual or practical understanding of biofilm behaviour across diverse and complex habitats, including host tissues, industrial pipelines, and aquatic systems (Nadell, Drescher and Foster, 2016) (Rumbaugh and Sauer, 2020). As such, biofilm is increasingly understood as a mode of bacterial life, rather than a rigid morphological state.

# 1.3.6. From Ecology to Evolution-Development and Systems Perspectives

Biofilms are now widely recognised as multicellular, evolutionarily structured communities, rather than mere accumulations of individual cells. This ecological framing highlights cooperation, resource sharing, and spatial assortment as key drivers of biofilm organisation and resilience. For example, public goods, such as extracellular matrix (ECM) components, can benefit the collective, but are susceptible to exploitation by non-producing cells, referred to as "cheaters", prompting evolutionary dynamics that shape architecture and function over time (Nadell, Xavier and Foster, 2009) (Oliveira et al., 2015).

Such evolutionary perspectives are deeply intertwined with developmental models, especially in species like *B. subtilis*, where subpopulations differentiate into matrix producers, motile cells, spores, or surfactin-producing scouts, governed by tightly regulated genetic circuits and bistable switches (Lopez et al., 2009) (Arnaouteli et al., 2021). These subpopulations contribute to architectural complexity and functional specialisation, mimicking division of labour seen in multicellular organisms.

Systems biology has further advanced biofilm understanding by linking chemical gradients, mechanical forces, and genetic regulation to emergent behaviours. Streamers are filamentous structures that develop under flow and cause rapid clogging in filtration systems

(Rusconi et al., 2010). For instance, their formation emerges from the coupling of shear forces, matrix viscoelasticity, and growth-driven instability (Rusconi et al., 2010).

These studies highlight that biofilm morphology is not static but dynamically regulated by feedback between the physical environment and gene expression.

Recent advances extend this systems view to engineering contexts, where biofilm behaviour under variable hydrodynamics, nutrient flux, and geometric constraints is modelled using cross-scale frameworks (Klapper et al., 2010). These integrate mesoscale structure, molecular regulation, and process-level consequences, offering predictive tools essential for civil and environmental engineering, such as modelling membrane biofouling, granular sludge stability, or reactor biofilm detachment thresholds (Picioreanu, van Loosdrecht and Heijnen, 2001) (de Kreuk, Pronk and van Loosdrecht, 2005) (Horn, Reiff and Morgenroth, 2003).

This combination of evolutionary, developmental, and systems-level perspectives reinforces the notion of biofilms as adaptive, dynamic collectives. It invites cross-disciplinary modelling that links genes to functions to outcomes, a crucial aspect for designing robust biofilm-informed interventions in both clinical and engineered ecosystems.

# 1.4. Core Conceptual Elements Across Biofilm Models

Although biofilm models differ in complexity and scale, from genetic circuits to fluid-structure interactions, several developmental processes are central (Fig. 1.3): matrix production, phenotypic differentiation, spatial structure, and environmental feedbacks (Flemming and Wingender, 2010) (Stoodley el al., 2002) (Arnaouteli et al., 2021). These elements interact nonlinearly, meaning changes at one level, such as shear stress, oxygen availability, or nutrient availability, can trigger shifts in biofilm architecture, metabolic activity, or detachment dynamics (Rusconi et al., 2010) (Nadell, Drescher and Foster, 2016). Grasping these interdependencies is essential for accurately predicting biofilm formation, resilience, and control in different environments, from water treatment systems to medical devices (Bjarnsholt et al., 2022).

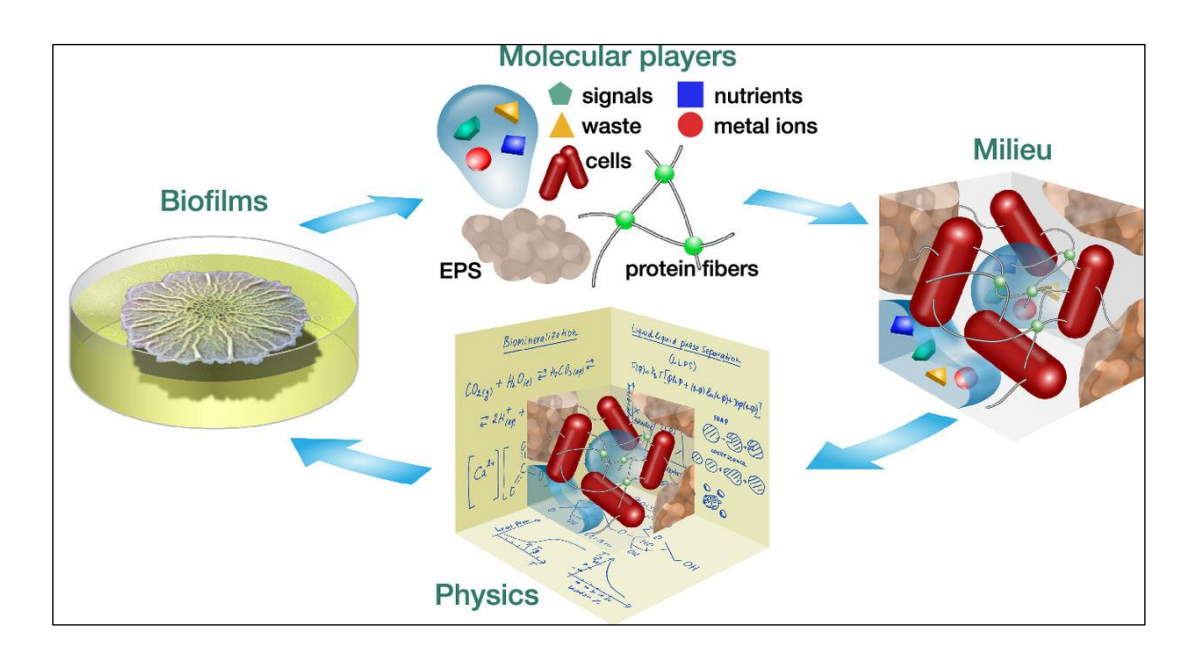


Figure 1.3. Interplay between biological, molecular, and physical processes in biofilm formation. Biofilms (left) are structured microbial communities embedded in an extracellular polymeric substance (EPS) matrix composed of protein fibres and other molecular components. Molecular players (top) include cells, nutrients, signals, waste products, and metal ions, which influence biofilm development and organisation. Within the biofilm milieu (right), these components interact with and are shaped by physical processes (bottom), such as biomineralisation and liquid—liquid phase separation, which contribute to structural stability, nutrient distribution, and mechanical resilience. From Chai, Zaburdaev and Kolter (2024)

#### 1.4.1. Matrix Centrality

The extracellular polymeric substance (EPS) matrix is widely regarded as the central structural and functional element of biofilms, distinguishing them from planktonic populations. This matrix provides the physical scaffold that holds cells together, anchors the community to surfaces, and creates a unique microenvironment that enables cooperative behaviours and emergent resilience (Flemming and Wingender, 2010) (Flemming, Neu and Wozniak, 2007). The matrix confers multiple critical properties: cohesion, surface adhesion, hydration, mechanical stability, retention of enzymes, and sorption of antimicrobials and heavy metals, all of which contribute to biofilm persistence in both clinical and industrial settings (Haque et al., 2021) (Jennings et al., 2021).

The composition of the matrix is highly variable and context-dependent, shaped by species-specific biosynthetic pathways, environmental conditions, and regulatory circuits. In *P. aeruginosa*, three primary polysaccharides (alginate, Psl, and Pel) play distinct roles in structure, cohesion, and immune evasion (Colvin et al., 2011). *S. aureus* and *S. epidermidis* produce poly-N-acetylglucosamine (PNAG), a positively charged polysaccharide important for biofilm accumulation on medical devices (Cue et al., 2012). In *B. subtilis*, the EPS matrix

contains exopolysaccharides, the amyloid protein TasA, and the hydrophobin-like protein BsIA, which together form a robust and hydrophobic architecture (Vlamakis et al., 2013) (Arnaouteli et al., 2021).

Beyond polysaccharides and proteins, biofilm matrices often include extracellular DNA (eDNA), released via autolysis or active secretion, and a variety of extracellular enzymes, lipids, and even outer membrane vesicles. These components play crucial roles in biofilm maturation, horizontal gene transfer, and intercellular communication, while also influencing matrix viscoelasticity (Petrova and Sauer, 2012).

Matrix heterogeneity contributes to the development of diffusion gradients for oxygen, nutrients, and waste products, which in turn create metabolically distinct subpopulations within the biofilm (Stewart and Franklin, 2008). It also governs the retention and deactivation of antibiotics or disinfectants and supports viscoelastic responses to flow and shear stress, contributing to streamer formation and clogging in fluidic systems (Rusconi et al., 2010).

Understanding the molecular composition, structure, and mechanical properties of the matrix is thus foundational for developing strategies to disrupt, penetrate, or prevent biofilm formation, whether in wound beds, catheter surfaces, or industrial membranes.

## 1.4.2. Physiological Heterogeneity and Microenvironments

Within biofilms, steep physicochemical gradients of oxygen, nutrients, pH, and metabolic by-products arise over remarkably short distances, due to limited diffusion and high local consumption (Stewart and Franklin, 2008). These gradients generate stratified physiological zones, with outer layers consisting of actively growing, metabolically responsive cells, while deeper layers may contain slow-growing, dormant, or persister-like cells, or even sporulating subpopulations, as seen in species like *B. subtilis* (Arnaouteli et al., 2021). In multispecies or industrially relevant consortia, these layers may also exhibit differential gene expression mosaics, where spatial cues drive localized expression of stress response, matrix production, or dispersal genes (Bjarnsholt et al., 2022).

This physiological heterogeneity is a key driver of biofilm resilience. For example, cells in nutrient-poor or anaerobic zones often enter metabolically inert states, rendering them less susceptible to antibiotics that target growth-related functions (Stewart and Franklin, 2008). Additionally, redox gradients and matrix chemistry modulate the penetration and efficacy of oxidising agents and disinfectants. Localised pH shifts or the presence of biofilm-bound ions

can impair the activity of chemical treatments before they reach the core of the biofilm, by creating microenvironments that reduce antimicrobial efficacy (Horswill et al., 2007). More broadly, biofilms exhibit resistance mechanisms such as reduced penetration, altered gene expression, and metabolic heterogeneity, which collectively hinder treatment success (Davies, 2003). Furthermore, the extracellular matrix itself acts as a diffusion barrier, retaining enzymes, binding antimicrobials, and creating microenvironments that shield interior cells from environmental stressors (Flemming and Wingender, 2010).

In both clinical and industrial settings, understanding and modelling this spatial complexity is critical for designing effective biofilm interventions, whether targeting chronic wound infections, biofouling on membranes, or biofilm corrosion in pipelines.

#### 1.4.3. Cell–Cell Signalling, Social Interactions, and Public Goods

Biofilm formation is inherently social, shaped by cell—cell signalling networks that coordinate gene expression in response to population density, environmental cues, and spatial structure. Quorum sensing (QS), defined as a system of chemical communication, allows bacteria to regulate communal behaviours such as EPS production, motility suppression, and virulence factor secretion in a density-dependent manner (Parsek and Greenberg, 2005). In *P. aeruginosa*, QS circuits based on acyl-homoserine lactones (AHLs) tightly control matrix synthesis, biofilm maturation, and dispersal, with additional roles in pathogenesis and interspecies competition (Ng and Bassler, 2009).

From an evolutionary perspective, biofilm behaviour aligns with social evolution theory, which frames microbial traits like matrix secretion as public goods, meaning resources that benefit nearby cells (Nadell, Drescher and Foster, 2016). In spatially structured environments, where clonemates are close together, cooperation, such as matrix production or nutrient sharing, is favoured. However, in less structured systems or under flow-induced detachment, non-producing cheaters can arise and exploit the benefits of cooperative neighbours without contributing themselves (Oliveira, Niehus and Foster, 2014).

In *B. subtilis*, cell-cell communication is orchestrated by peptide-based signalling networks, notably the ComX/ComP-ComA system and the surfactin-Spo0A feedback loop. These systems regulate transitions between motility, matrix production, and sporulation, allowing the population to synchronise development across environmental gradients (Vlamakis et al., 2008) (Arnaouteli et al., 2021). Specifically, ComX, a secreted pheromone, activates the

ComP-ComA two-component system, which in turn primes the cells for matrix gene expression; while surfactin, a biosurfactant, triggers Spo0A phosphorylation, initiating differentiation into biofilm-forming or sporulating states depending on environmental context and signal intensity (Lopez et al., 2009).

In Gram-positive pathogens such as *S. aureus*, the accessory gene regulator (agr) QS system mediates the transition between adherence and dispersal phenotypes. At low cell density, surface adhesins are expressed to promote colonisation. At higher densities, agr induces phenol-soluble modulins (PSMs) and secreted enzymes that promote biofilm dispersal, aiding spread to new sites and immune evasion (Peschel and Otto, 2013) (Schwartz et al., 2012). Disruption of these systems alters the balance between stable colonisation and transmission, with major implications for chronic infection and device-associated biofilms.

Understanding these regulatory circuits and social dynamics is critical for predicting how biofilm populations evolve, respond to stress, or resist antimicrobial interventions, particularly in engineered or clinical environments where flow, nutrients, and selective pressures vary.

#### 1.4.4. Mechanics, Hydrodynamics, and Biofilm Architecture

In complex environments, hydrodynamic forces are central to biofilm structure and function. The shear stress imposed by fluid flow governs both attachment and detachment dynamics, shaping the spatial organisation, biomass accumulation, and stability of biofilms (Stoodley et al., 1999) (Rusconi, Garren and Stocker, 2014). Even subtle variations in shear can drastically alter architectural outcomes: under low shear, biofilms often grow into tower-like, heterogeneous microcolonies with water channels; moderate shear may compact these structures into denser layers; while high shear not only thins the biofilm but can also generate streamer-like filaments that stretch between surfaces or obstacles in the flow path (Marra et al., 2025) (Pizzi et al., 2025). These streamers can cause clogging in filtration systems, turbulence-induced detachment, and accelerated downstream colonisation in industrial settings (Rusconi, Garren and Stocker, 2014).

Biofilms exhibit viscoelastic behaviour, meaning they possess both elastic (solid-like) and viscous (fluid-like) properties. When exposed to stress, such as laminar flow, pulsatile pressure, or vibrational forces, biofilms can deform, creep, or relax over time, depending on their matrix composition and hydration state (Towler et al., 2003). Such behaviour influences

detachment thresholds, streamer formation, and cell release patterns, which are key for understanding contamination in drinking water networks, medical devices, and bioreactors (Flemming et al., 2016).

Importantly, mechanical forces do not only act externally, but they also feedback into the biofilm's internal biology. Mechanosensing refers to the ability of bacterial cells to detect and respond to physical forces or mechanical cues in their environment. In the context of biofilms, this sensing enables bacteria to perceive surface stiffness, shear stress, and compression, which then influences gene expression and behavioural outcomes (Gordon and Wang, 2019) (Rodesney et al., 2017). For example, fluid shear has been shown to affect biofilm thickness, matrix production, and cellular differentiation, particularly in flow systems where mechanical stimuli fluctuate over time (Rusconi, Garren and Stocker, 2014). Moreover, mechanosensitive channels in the bacterial membrane can trigger ion fluxes or changes in membrane potential in response to tension or compression, further influencing cell fate decisions (Rodesney et al., 2017). In B. subtilis, surface contact and shear have been shown to modulate Spo0A phosphorylation, biasing the population toward matrix production or sporulation, depending on the local mechanical context (Wittig et al., 2025). These mechanical feedback loops allow biofilms to dynamically adapt their architecture, resilience, and dispersal behaviour, especially in engineered systems like pipelines, reactors, or medical devices where physical forces are both sustained and variable (Conrad, 2018).

Overall, mechanics and hydrodynamics act as both sculptors and signals in biofilm ecology. Their interplay governs not only the physical appearance of biofilms but also their evolutionary strategies, gene regulatory responses, and engineering outcomes.

#### 1.4.5. Dispersal, Detachment, and Lifecycle Transitions

Biofilm dispersal is not a terminal event but a dynamic and regulated phase of the biofilm lifecycle. Bacteria within a mature biofilm can exit the community either through active dispersal, driven by molecular signals and environmental cues, or through passive detachment, caused by mechanical forces such as shear stress, abrasion, or hydraulic flushing (Petrova and Sauer, 2016) (Rumbaugh and Sauer, 2020). This release of single cells, microcolonies, or biofilm fragments facilitates the colonisation of new surfaces and the reinitiation of biofilm development elsewhere, posing challenges in both clinical and industrial systems (Hall-Stoodley, Costerton and Stoodley, 2004).

Active dispersal is mediated by environmental triggers such as nutrient starvation, oxygen limitation, or the presence of nitric oxide, which acts as a dispersal signal in many Gramnegative bacteria (Barraud et al., 2006). In *B. subtilis*, D-amino acids released by aging biofilms can remodel the matrix and promote dispersal by weakening peptidoglycan crosslinks and triggering cell release (Kolodkin-Gal et al., 2010). These mechanisms are often tightly linked to quorum sensing and stress responses, coordinating dispersal with broader population-level decisions (Petrova and Sauer, 2016).

Passive detachment, in contrast, results from physical processes such as sloughing due to shear stress, bubbles, or fluid turbulence, which strip biofilms from surfaces and distribute cells downstream (Stoodley et al., 1999) (Rusconi, Garren and Stocker, 2014). Detached aggregates can remain highly tolerant to antimicrobials and are frequently implicated in recolonisation, biofilm regrowth, and secondary contamination in engineered water systems and filtration units (Sauer, 2022) (Bridier et al., 2015).

From an engineering perspective, dispersal represents both a vulnerability and a threat. It offers a point of intervention, such as promoting dispersal for cleaning, but also enables biofilms to spread, making source control, flow path design, and downstream barriers critical to biofilm management in pipelines, reactors, and medical devices (Rumbaugh and Sauer, 2020) (Bridier et al., 2015).

## 1.5. *Bacillus subtilis* as a Model for Biofilm Development and an Engineering Model

#### 1.5.1. Strain Diversity, Domestication, and Environmental Relevance

The biofilm-forming capabilities of *B. subtilis* are strongly influenced by strain background, particularly the contrast between wild isolates and laboratory-domesticated strains. Wild-type strains such as NCIB 3610 exhibit robust colony wrinkling, pellicle formation, and biofilm matrix production, reflecting their natural adaptability to complex environments (Branda et al., 2004) (McLoon et al., 2011). These wild strains retain intact regulatory systems for matrix gene expression, including pathways involving *SpoOA*, a master transcriptional regulator that integrates stress and quorum sensing signals to initiate biofilm formation and sporulation; *SinR*, a repressor of matrix gene expression that acts as a key switch between motility and sessility; and *DegU*, a response regulator that modulates expression of genes involved in exopolysaccharide production and surface adhesion (Kearns et al., 2005).

By contrast, commonly used domesticated strains, notably strain 168, derived from early auxotrophic mutants, often carry loss-of-function mutations in key biofilm regulatory loci. These include disruptions to *sfp*, affecting surfactin synthesis, or frameshifts in *eps* operons, leading to impaired matrix production (McLoon et al., 2011). While advantageous for laboratory growth and genetic manipulation, these mutations significantly attenuate the ability of domesticated strains to form structured multicellular communities, limiting their environmental relevance.

This distinction has serious implications for environmental and industrial microbiology. When studying biofilm-mediated processes such as plant root colonisation, biocontrol of phytopathogens, or biofilm-based surface coatings, the choice of strain directly affects the interpretation and translatability of findings (Bais, Fall and Vivanco, 2004) (Arnaouteli et al., 2021). Wild-type strains like NCIB 3610 display biofilm traits beneficial for rhizosphere competence, including motility, robust matrix secretion, and resistance to environmental stressors (Vlamakis et al., 2013). These features also position *B. subtilis* as a candidate for biosurface engineering, where its natural matrix components could be used for protective coatings or biomineralisation in built infrastructure.

Consequently, strain selection is not trivial: aligning model strain behaviour with the chemical, mechanical, and ecological conditions of real-world systems is essential for generating actionable insight.

#### 1.5.2. Matrix Architecture in *B. subtilis*

Biofilm formation in *B. subtilis* is a coordinated developmental process that relies on the secretion of a protective and adhesive matrix (Fig. 1.4). This matrix provides the mechanical integrity, cohesion, and environmental resistance required for collective survival. At the heart of this architecture are three principal components, each playing a unique role in shaping the physical and functional properties of the biofilm (Vlamakis et al., 2013) (Arnaouteli et al., 2021).

First, the EPS produced by the *epsA–O* operon forms a sticky, sugar-based scaffold that allows cells to adhere to one another and to surfaces. This polymer is essential for the development of complex colony morphology, including the wrinkled structures often observed in mature biofilms. Loss of EPS production results in flat, poorly structured biofilms, highlighting its critical role in architectural development (Branda et al., 2001) (Vlamakis et al., 2013)

(Arnaouteli et al., 2021). Secondly, the TasA amyloid fibres, encoded by the *tapA-sipW-tasA* operon, provide internal structural reinforcement. These protein fibres interweave through the matrix, stabilising the biofilm and promoting robustness under physical stress. The SipW protein is a signal peptidase that processes and facilitates the secretion of TasA, enabling its proper assembly into functional fibres. Without TasA, the biofilm loses cohesion and becomes mechanically unstable (Romero et al., 2010) (Arnaouteli et al., 2021). Third, the BsIA protein (previously known as YuaB) acts as a biofilm surface sealant. This hydrophobin-like protein self-assembles at the air—biofilm interface, forming a hydrophobic layer that repels water and enhances the biofilm's resistance to desiccation and external perturbation. BsIA gives *B. subtilis* biofilms their characteristic sheen and mechanical integrity, particularly in surface-exposed environments (Kobayashi and Iwano, 2012) (Arnaouteli et al., 2021).

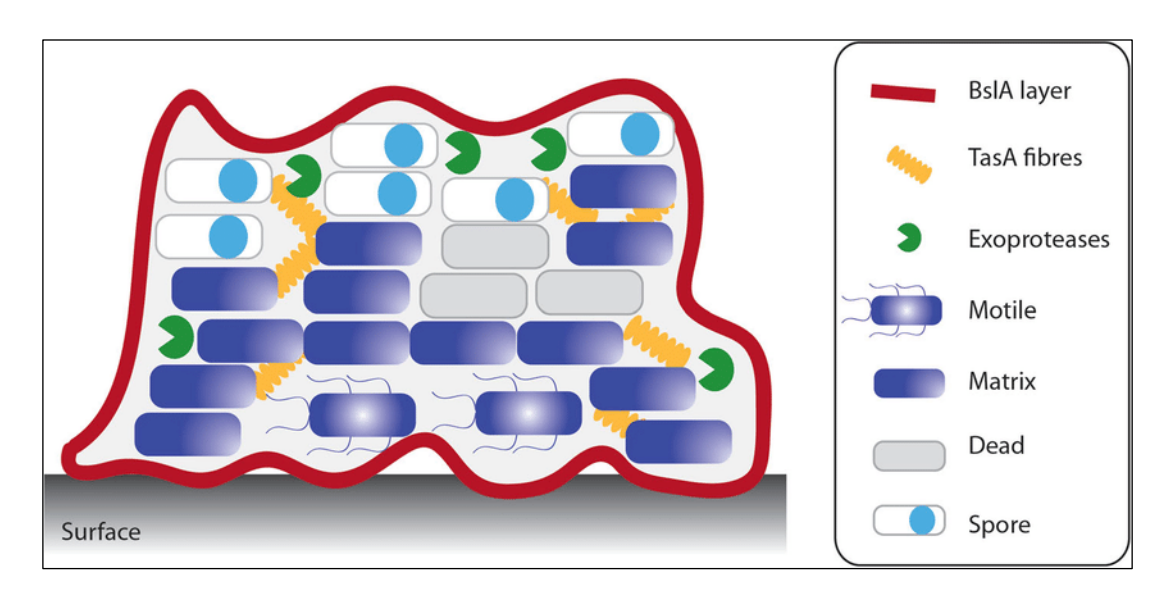


Figure 1.4. Schematic representation of the spatial organisation and functional specialisation within a *Bacillus subtilis* biofilm. The extracellular matrix is composed of a hydrophobic BsIA layer (red) and TasA amyloid fibres (yellow), with exoproteases (green) distributed throughout. Differentiated cell types include motile cells (blue with flagella), matrix-producing cells (dark blue), dead cells (grey), and spores (blue circles). This structural and functional heterogeneity underpins the stability, adaptability, and resilience of the biofilm community. From Hobley et al. (2015)

In addition to these core components, a variety of accessory factors modulate biofilm structure and mechanics. These include TapA, which anchors TasA fibres to the cell surface; cross-linking proteins that bridge EPS and TasA; and metal ion interactions that influence biofilm stiffness and maturation. Together, these elements create a composite matrix that is viscoelastic, chemically protective, and mechanically adaptive; all traits essential for biofilm survival in fluctuating natural and engineered environments (Vlamakis et al., 2013) (Arnaouteli et al., 2021).

#### 1.5.3. Genetic Regulatory Network Overview

Biofilm formation in *B. subtilis* is not a default state of growth, but a tightly regulated developmental decision (Fig. 1.5), shaped by environmental conditions, nutrient cues, population density, and stress. This transition from free-living motile cells to matrix-producing, surface-attached communities is orchestrated by a multilayered regulatory network that integrates internal and external signals to control gene expression, cellular differentiation, and community behaviour (Vlamakis et al., 2013) (Arnaouteli et al., 2021) (Milton et al., 2023).

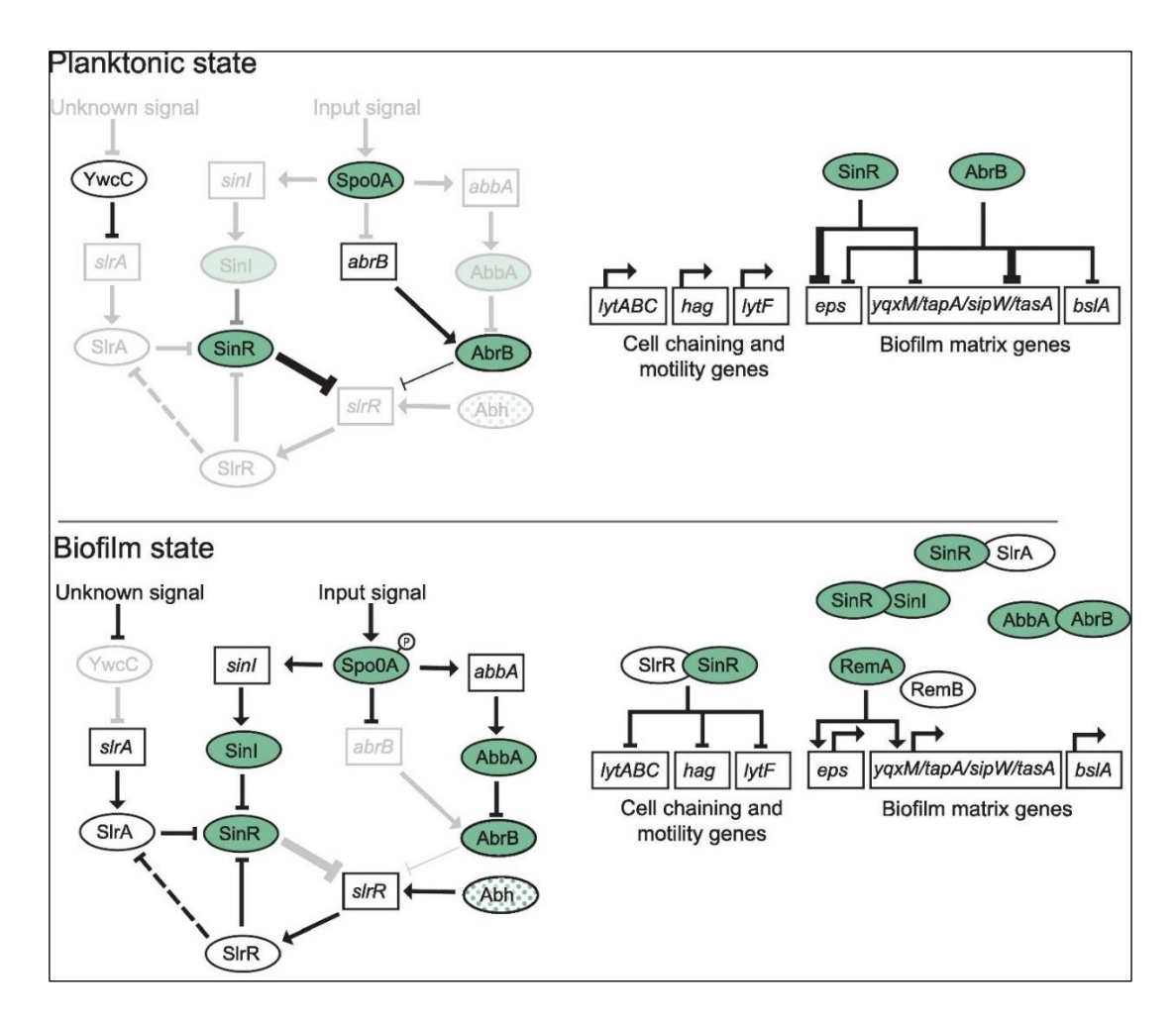


Figure 1.5. Simplified model of the *Bacillus subtilis* biofilm regulatory network showing transitions between planktonic and biofilm states. In the planktonic state (top), SinR and AbrB repress the expression of genes involved in extracellular matrix production (eps, yqxM/tapA/sipW/tasA, bslA) and cell chaining/motility (lytABC, hag, lytF). Activation of SpoOA through phosphorylation, along with input from other regulators (e.g., SinI, AbbA, SIrA, SIrR, RemA/B), shifts the network towards the biofilm state (bottom), relieving repression and promoting matrix synthesis, chaining, and motility modulation. From Milton and Cavanagh (2023)

At the heart of this network lies the SpoOA phosphorelay, a hierarchical signalling cascade that functions like a molecular decision-making circuit. Environmental stimuli, such as

nutrient limitation or cell density, are first detected by a suite of sensor kinases (KinA to KinE), which initiate a phosphotransfer relay via Spo0F and Spo0B, ultimately phosphorylating the master regulator Spo0A. The level of Spo0A~P (the phosphorylated form) acts as a rheostat: moderate levels activate genes involved in biofilm matrix production, while higher levels drive entry into sporulation, a dormant survival state (Palma et al., 2025) (Vlamakis et al., 2013).

Another pivotal node in this system is the Sinl/SinR/SlrR switch, which governs the expression of the structural genes that encode the biofilm matrix. SinR functions as a potent repressor of matrix operons (*epsA-O* and *tapA-sipW-tasA*), preventing biofilm development under favourable conditions. This repression is relieved when Sinl, a small protein antagonist, binds SinR and neutralises its activity (Chai et al., 2010). The regulatory process is further complicated by SlrR, which also binds SinR and helps repress motility genes, effectively flipping cells into a sessile, matrix-producing state (Chai et al., 2010). This multi-protein switch exhibits bistable behaviour, meaning that only a subset of cells in a genetically identical population activate matrix production at any given time, resulting in a heterogeneous community with distinct functional subgroups (Chai et al., 2010) (Vlamakis et al., 2013) (Milton et al., 2023).

*AbrB*, a global transition state regulator, further contributes to this network by repressing early stationary-phase genes under nutrient-rich conditions. As Spo0A~P levels rise, *AbrB* is repressed, removing this brake on matrix gene expression and linking nutritional stress to the commitment to biofilm formation (Strauch et al., 1990) (Vlamakis et al., 2013).

Additional layers of regulation involve other two-component systems, notably the DegS–DegU pair, which fine-tune surface behaviours, including motility, exoprotease secretion, and matrix elaboration. Phosphorylated DegU~P has been shown to repress motility and promote biofilm formation, although its effect is context-dependent and may vary between strains and growth conditions (Verhamme et al., 2007) (Arnaouteli et al., 2021).

Cell-cell communication is another essential input. The ComX-ComP/ComA quorum sensing pathway governs the development of genetic competence (the ability to uptake DNA from the environment) and indirectly regulates biofilm formation. The ComA response regulator activates genes for surfactin production, a lipopeptide biosurfactant that plays a dual role: it facilitates sliding motility and also acts as a signalling molecule. Surfactin induces potassium leakage from the membrane, which is detected by KinC, feeding back into the SpoOA

phosphorelay to stimulate matrix gene expression, a prime example of a self-generated cue linking quorum sensing to developmental choice (Lopez et al., 2009) (Vlamakis et al., 2013).

Alternative sigma factors (notably  $\sigma^A$ H,  $\sigma^B$ , and various extracytoplasmic function (ECF) sigma factors) further adjust the transcriptional response to environmental challenges such as oxidative stress, membrane damage, and nutrient limitation. These factors broaden the cell's regulatory toolbox and provide additional inputs into the matrix gene network (Helmann, 2016) (Arnaouteli et al., 2021).

A striking and recently uncovered layer of regulation is tied to DNA replication. The genes encoding SinR and SIrR are located at different positions on the chromosome. During active replication, the unequal gene dosage can temporarily skew the SinR/SIrR ratio, triggering pulsatile waves of matrix expression across the population. This dynamic tuning is thought to help maintain a consistent proportion of matrix-producing cells, balancing structure and flexibility in response to fluctuating nutrient levels (Milton et al., 2023).

Altogether, these interlinked pathways illustrate that *B. subtilis* biofilm formation is not just a stress response, but a developmental programme underpinned by finely tuned genetic logic, capable of producing complex, multicellular architectures in response to dynamic environmental signals.

#### 1.5.4. Phenotypic Differentiation and Developmental Progression

One of the most fascinating features of *B. subtilis* biofilms is their ability to differentiate into multiple, spatially organised cell types, despite being composed of genetically identical individuals. As the biofilm develops, it gives rise to distinct subpopulations with specialised roles that together sustain the structural and functional integrity of the community (Vlamakis et al., 2013).

At the leading edges of expanding colonies, motile cells remain active, facilitating surface exploration and colonisation of new territories (Vlamakis et al., 2013). In contrast, matrix-producing cells accumulate in regions where architectural scaffolding is needed, contributing to the thick wrinkles and raised ridges that define mature biofilm morphology (Arnaouteli et al., 2021). These structural features often emerge in response to nutrient gradients or oxygen limitation, reinforcing spatial differentiation via microenvironmental cues (Lopez, Vlamakis and Kolter, 2009).

A particularly remarkable morphological feature observed in B. subtilis biofilms is the emergence of Van Gogh bundles, defined as long, aligned chains of cells that form densely packed, fibre-like structures projecting outward from the colony surface. These bundles resemble thick painterly strokes, hence the evocative name introduced by van Gestel, Vlamakis and Kolter (2014). They are characteristic of robust and wrinkled colony morphologies seen in wild-type strains such as NCIB 3610 and represent a high level of spatiotemporal coordination among genetically identical cells. The formation of Van Gogh bundles depends on both extracellular matrix production and flagellum-driven motility, which together enable chains of cells to push, bend, and align under physical constraints. These structures are thought to aid in colony expansion and surface colonisation, while also reflecting internal mechanical tensions within the biofilm (van Gestel, Vlamakis and Kolter, 2014) (Vlamakis et al., 2013). Their development is tightly regulated by genetic switches involving SpoOA, SinR, and DegU, which control the transition from motility to matrixproducing states (Kearns et al., 2005) (Chai et al., 2010). The existence of Van Gogh bundles exemplifies how local gene regulation, physical forces, and collective behaviour converge to generate complex, emergent structures within bacterial communities.

As the biofilm matures, nutrient depletion and crowding trigger the emergence of sporulating cells, particularly in interior regions or along vertical ridges. Sporulation, a stress-resistant, dormant state, enables a subpopulation of cells to survive harsh conditions, ensuring long-term viability of the community (Arnaouteli et al., 2021). However, sporulation is not uniform or immediate. Some cells delay entering this state by producing toxins that eliminate or inhibit neighbouring cells, a form of microbial cannibalism that reallocates nutrients and controls population density (Lopez, Vlamakis and Kolter, 2009).

This complex division of labour is governed by bistability in gene expression, especially at the matrix genes, where some cells activate biofilm-related genes while others remain inactive. As shown by Chai et al. (2010), this bistable switch ensures that even genetically identical cells can adopt divergent fates under the same external conditions. Such bet-hedging strategies are especially relevant in fluctuating environments, such as water treatment systems, where physical stressors or chemical treatments may abruptly change the landscape. Under these conditions, phenotypic heterogeneity allows parts of the population to survive and repopulate (Milton et al., 2023).

Rather than being static structures, *B. subtilis* biofilms are dynamic developmental systems that allocate tasks through differentiation. They achieve resilience by spreading risk and maintaining diversity, using a sophisticated regulatory architecture that links gene expression to spatial structure and population dynamics.

### 1.5.5. Environmental and Engineering Cues Affecting *B. subtilis*Biofilms

The formation and structure of *B. subtilis* biofilms are highly responsive to environmental and physical cues, both in natural settings and engineered systems. Factors such as nutrient availability, ionic composition, surface properties, and fluid dynamics directly influence gene regulation pathways involved in matrix production and morphological development (Vlamakis et al., 2013). For instance, nutrient limitation is a well-known trigger that promotes entry into the biofilm lifestyle by activating stress response systems and initiating Spo0A-controlled developmental cascades (Vlamakis et al., 2013) (Arnaouteli et al., 2021). This aligns with conditions commonly encountered in environmental niches and industrial processes, where fluctuating resource levels select for resilient, multicellular strategies.

Divalent cations such as calcium and magnesium have been shown to enhance biofilm stability and cross-link matrix polymers, reinforcing biofilm integrity under stress. At the same time, the hydrophobicity of surfaces strongly modulates initial bacterial attachment and matrix gene expression, as cells respond to physical features of the substrate (Arnaouteli et al., 2021). These cues are especially important in designing materials for use in pipelines, reactors, and filtration systems where microbial colonisation can be either desirable or problematic.

Hydrodynamic shear (the mechanical force of flowing fluids) emerges as one of the most significant engineering parameters influencing biofilm architecture. Research suggests that moderate levels of shear can actually enhance extracellular polymeric substance (EPS) production in some *Bacillus* strains, possibly as an adaptive response to mechanical stress (Chang, Huang and Liu, 2020) (Portas et al., 2024). However, high shear stress can also thin biofilms, disrupt cellular cohesion, or promote detachment events, leading to downstream contamination and recolonisation (Rusconi et al., 2011) (Towler et al., 2003) (Portas et al., 2024).

In systems where biofilms grow at the air-liquid interface, such as in aeration basins or biofilm reactors, *B. subtilis* can produce a floating pellicle supported by BsIA, a hydrophobic protein that forms a protective film on the biofilm surface. These pellicles are highly relevant in wastewater treatment environments and open bioreactors (Arnaouteli et al., 2021). Conversely, in submerged flow systems, such as filtration channels or membrane units, biofilms can form streamer-like structures that stretch along flow lines. Biofilm streamers are filamentous extensions of microbial biomass that form under flow, particularly in narrow or complex geometries. In *B. subtilis* and other species, they arise from initial surface-attached colonies subjected to shear stress, elongating into viscoelastic structures that span channels or corners (Rusconi et al., 2010) (Rusconi et al., 2011). Streamers contribute to clogging, increased pressure drop, and downstream colonisation in industrial and clinical systems (Portas et al., 2024). Their formation reflects both mechanical forces and active matrix production, highlighting the interplay between hydrodynamics and biofilm development.

Ultimately, understanding how *B. subtilis* biofilms respond to these environmental and engineering cues is essential not only for controlling unwanted growth in industrial systems, but also for harnessing biofilms in beneficial contexts, such as biocontrol, water treatment, or biosurface coatings.

## 1.6. Biofilm Development in Dynamic Systems and Under Fluid Flow

Hydrodynamics profoundly influence biofilm initiation, architecture, mass transfer, and detachment in pipes, reactors, membranes, and open channels (Stoodley et al., 1999). This section synthesises conceptual advances and their engineering implications.

#### 1.6.1. Shear Regimes: Laminar, Transitional, Turbulent

In engineered systems such as pipelines, membrane bioreactors, and flow cells, biofilm formation is tightly regulated by the hydrodynamic conditions, particularly the wall shear stress (tw), which governs both the thickness of the nutrient boundary layer and the mechanical forces acting on the biofilm surface (Stoodley et al., 1999) (Rochex et al., 2008) (Paul et al., 2012) (Valladares Linares et al., 2016). The nature of flow, whether laminar, transitional, or turbulent, shapes not only the initial attachment of cells but also long-term architecture, mass transfer, and detachment dynamics (Stoodley et al., 1999) (Paul et al., 2012) (Valladares Linares et al., 2016).

P. aeruginosa biofilms subjected to increasing wall shear stress, whether in rotating systems or flow reactors, often become thinner and more compact, reflecting mechanical compression of the matrix and tighter cellular packing (Stoodley et al., 1999) (Paul et al., 2012) (Valladares Linares et al., 2016). Studies show that increasing wall shear stress generally reduces biofilm biomass and thickness, as seen in P. aeruginosa and Cobetia marina (Chun et al., 2022). Conversely, moderate or oscillatory shear regimes can enhance biofilm cohesion and growth, likely due to improved nutrient transport and mechanosensory responses (Tsagkari et al., 2022). Horn and Hempel's laboratory, (in Möhle et al., 2007), demonstrated that biofilm thickness in rotating-disc reactors increases under low-shear, high-substrate conditions (up to several hundred µm), whereas high shear conditions constrain biofilm height to about 100 µm, reinforcing the role of hydrodynamic forces in regulating architecture and detachment dynamics. In engineered systems, wall shear stress plays a dual role by enhancing nutrient transport to the biofilm surface while simultaneously exerting erosive forces that limit excessive growth. This interplay often leads to a sheardependent steady state, where moderate shear supports balanced biofilm development by improving substrate delivery without triggering detachment (Tsagkari et al., 2022). In contrast, high shear stress can compress the biofilm, reduce its thickness, or induce sloughing by exceeding the mechanical tolerance of the matrix (Duddu, Chopp and Moran, 2009). Experimental and computational studies support this model of dynamic equilibrium, demonstrating that shear modulates both biofilm architecture and cohesion by regulating the balance between biomass accumulation and mechanical erosion (Tsagkari et al., 2022) (Duddu, Chopp and Moran, 2009).

Studies investigating biofilms under continuous unidirectional flow, typically using microfluidic flow systems, have significantly shaped our understanding of how shear stress, nutrient delivery, and hydrodynamics influence biofilm development. In these systems, shear stress promotes streamlined biofilm architecture, often leading to the formation of mushroom-shaped microcolonies, as seen in *P. aeruginosa* (Klausen et al., 2003) (Karampatzakis et al., 2017). These structured biofilms develop steep nutrient and oxygen gradients, driving spatial differentiation into metabolically active and dormant zones (Stewart and Franklin, 2008).

A growing body of research has explored how *B. subtilis* biofilms respond to controlled unidirectional flow, revealing important insights into their structural adaptation and

development under shear. Wittig et al. (2025) used optical coherence tomography to monitor B. subtilis biofilms grown in straight millifluidic channels under a range of wall shear stresses (tw). They observed that biofilm growth was approximately linear over a 7-day period, with increasing shear correlating with reduced biofilm thickness and more compact, dense structures. Notably, slender vertical pillars formed on colony tops and served as anchoring points for streamers, illustrating how surface microstructures and fluid friction interact to shape morphology. Seručnik et al. (2024) developed a custom microfluidic bioreactor to grow B. subtilis biofilms continuously under low flow conditions (1  $\mu$ L/min) while carefully controlling oxygen levels. Their work emphasised the importance of aeration and flow geometry in determining both total biomass and spatial coverage, indicating that oxygen transfer, modulated by flow, is a limiting factor in biofilm development.

Together, these studies highlight that even modest shear can influence growth kinetics, morphological patterning (e.g. wrinkle formation), and detachment phenomena in *B. subtilis*. While unidirectional flow is known to influence *B. subtilis* biofilm morphology, overall biofilm morphology and molecular basis remain indirectly inferred. No single study has explicitly isolated unidirectional flow as a variable and quantified its direct impact on genetic expression. As a result, conclusions about gene regulation under flow conditions often rely on phenotypic proxies such as wrinkling or matrix abundance, rather than direct transcriptional evidence. This represents a critical gap in linking environmental flow regimes to molecular regulation in real-world settings.

While microfluidic devices offer precise control over flow dynamics, nutrient gradients, and oxygen availability, making them valuable for dissecting the spatial and temporal development of *B. subtilis* biofilms, they also present notable limitations when extrapolating findings to real-world systems. Most devices operate at microscale volumes and under idealised, laminar flow conditions, which do not fully capture the complexity of industrial, clinical, or environmental biofilm habitats. Real-world systems often involve turbulent or transitional flows, fluctuating shear stress, mixed-species communities, and irregular geometries that affect nutrient distribution, detachment, and biofilm resilience in ways not easily replicated in microchannels. Furthermore, the materials commonly used in microfluidics (e.g. PDMS) can adsorb small molecules or interfere with surface adhesion, potentially skewing microbial responses (van Meer et al., 2017) (Abouhagger et al., 2024).. Finally, the high degree of control and homogeneity in microfluidic platforms may mask

emergent behaviours that arise in larger, more heterogeneous environments. As such, while these systems are invaluable for hypothesis testing and mechanistic insights, complementary studies in meso- or full-scale reactors are essential for validating engineering relevance and scaling predictive models (Pousti et al., 2021).

#### 1.6.2. Secondary Flows, Fluid Friction, and Streamer Formation

Biofilm streamers are slender, filamentous extensions (Fig. 1.6), that form in flowing systems and can dramatically influence hydrodynamics and biofilm-related fouling. Even under laminar flow conditions, streamers can emerge when suspended cells or matrix fragments are trapped in low-shear regions created by obstacles, corners, or existing microcolonies (Rusconi et al., 2011). Studies using time-resolved fluorescence and confocal imaging have revealed that these streamers often originate from leaning pillar-shaped microcolonies that reach a friction-limited growth threshold. Once initiated, the streamers extend downstream, with their growth rate inversely correlated to wall shear stress, implying that excessive viscous drag suppresses vertical development while promoting horizontal elongation (Witting et al., 2025).

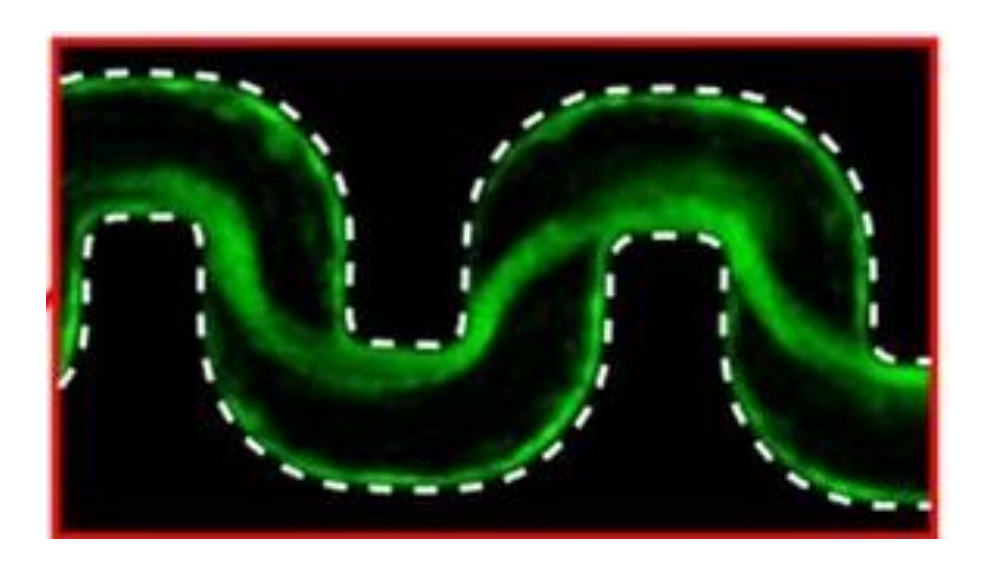


Figure 1.6. Fluorescent micrograph of a gfp-expressing *Pseudomonas aeruginosa* biofilm streamer formed within a curved channel of a microfluidic device. The streamer, composed of extracellular polymeric substances and cells, bridges across the channel and aligns with flow paths, ultimately capable of causing significant flow obstruction. White dashed lines indicate the channel walls. Adapted from Drescher et al. (2013)

Rusconi et al. (2011) also demonstrated that even minimal geometric asymmetries in flow channels can give rise to stable recirculation zones, allowing biofilm fragments or planktonic cells to become entrained and subsequently form streamers. This phenomenon is not

exclusive to engineered setups; similar streamer dynamics have been observed in porous filters, medical catheters, and environmental flow systems (Drescher et al., 2013) (Valiei et al., 2012). Critically, the formation of streamers leads to a marked increase in headloss (i.e., pressure drop) due to flow obstruction, and their rapid propagation can culminate in catastrophic clogging events. This makes them a major concern in both industrial and biomedical contexts, where they compromise flow efficiency, sterility, and system integrity (Stoodley et al., 1999) (Drescher et al., 2013).

### 1.6.3. Mass Transfer, Nutrient Limitation, and Chemical Conditioning Films

In flow-exposed environments, the delivery of nutrients, gases, and biocides to microbial cells is governed not only by bulk fluid properties but critically by the hydrodynamic boundary layer, defined as an interface where diffusion dominates over convection. This region forms at the biofilm-liquid interface and varies in thickness depending on flow velocity and shear stress. Under high shear, the boundary layer becomes thinner, facilitating greater flux of nutrients and disinfectants into the biofilm (Donlan, 2002). However, the increased mechanical stress can compromise the structural integrity of the biofilm or induce detachment (Stewart and Franklin, 2008) (Flemming et al., 2016). Conversely, low shear allows for stable growth and structural elaboration, but also limits diffusion rates, especially to interior or basal layers, which may result in oxygen or nutrient depletion. This can lead to the emergence of metabolically quiescent persister cells, which are more tolerant to antibiotics and environmental stressors (Stewart and Franklin, 2008).

In parallel, a less visible but equally critical component of surface colonisation is the rapid formation of chemical conditioning layers. These are composed of organic molecules, such as proteins, polysaccharides, and humic substances, that adsorb to the surface within minutes of contact with flowing water. Conditioning layers can significantly alter the surface energy and physicochemical properties of substrates, thereby influencing the subsequent attachment of microbial cells (Kreve, 2021) (Bhagwat, 2021) (Kim and Vrouwenvelder, 2019). In engineered water systems, such as drinking water pipes and filtration membranes, the presence of conditioning layers can attenuate the effectiveness of residual disinfectants. For instance, recent studies show that disinfectants such as chlorine or chloramine can be rapidly neutralised or decayed within these layers, creating microsites of reduced oxidative stress

that support microbial colonisation and biofilm initiation (Wang et al., 2021) (Chowdhury, 2019).

Together, these processes, boundary layer regulation, nutrient gradients, and conditioning layer dynamics establish the chemical landscape in which biofilms form and persist. Their interplay is crucial for engineers seeking to predict biofilm growth, optimise cleaning regimes, or design antifouling surfaces.

#### 1.7. Burden of Biofilms Across Sectors

Biofilms impose a massive and largely underappreciated economic burden, with recent multidisciplinary estimates suggesting a global impact in the trillions of US dollars annually (Fig. 7) (Cámara et al., 2022) (Highmore et al., 2022).

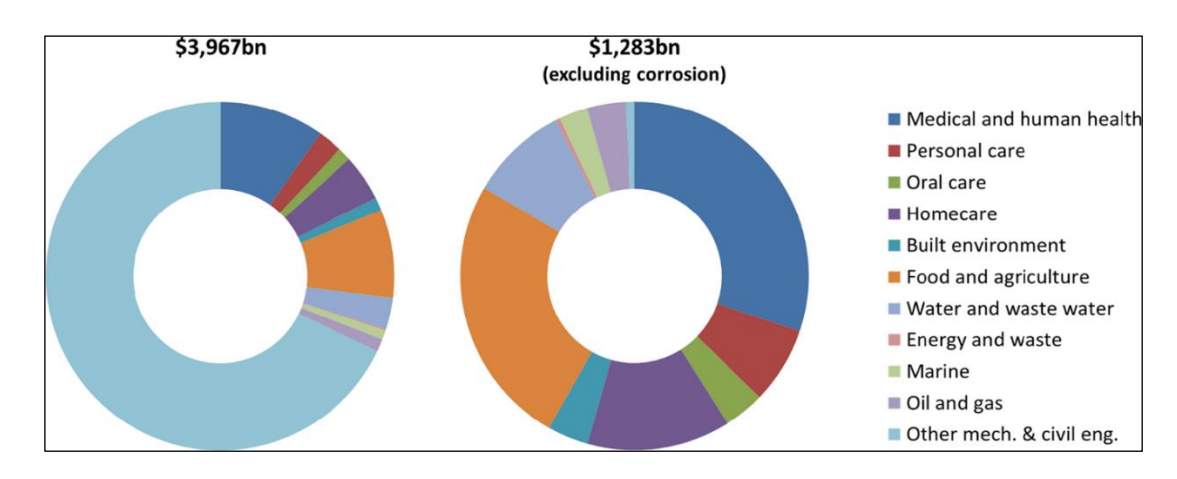


Figure 1.7. Estimated global economic impact of biofilms across major industrial sectors. The left chart represents the total estimated cost of biofilms, including corrosion (\$3,967 billion), while the right chart excludes corrosion-related costs (\$1,283 billion). Sectoral contributions include medical and human health, food and agriculture, built environment, water and wastewater, and others. Data adapted from Câmara et al. (2022).

The majority of the biofilm-related economic burden, approximately 69%, stems from corrosion, much of which is linked to microbiologically induced corrosion (MIC) impacting infrastructure and energy sectors worldwide (Kreve, 2023). Notably, MIC accounts for an estimated 20% of total corrosion costs globally, significantly contributing to maintenance and replacement expenses in marine and industrial pipelines (Pusparizkita et al., 2023) (Arroussi et al., 2023).

In the healthcare sector, central line-associated bloodstream infections (CLABSIs) impose a major economic burden. In the U.S., annual costs attributable to the five most common healthcare-associated infections, including CLABSIs, are estimated around US \$9.8 billion,

with catheter-related infections being the most expensive per case at US \$45,814 (Zimlichman et al., 2013). These infections result from microbial colonisation of catheters, leading to hospitalisation, costly treatments, and device replacement. For example, biofilms on urinary catheters, ventilators, and prosthetic devices contribute hundreds of millions more, including \$1 billion/year for catheter-associated urinary tract infections and \$920 million/year for ventilator-associated pneumonia (Cámara et al., 2022).

Marine biofouling presents another economic dimension: biofilm accumulation on ship hulls increases drag by up to 60%, often necessitating 10-40% more fuel consumption (Schultz et al., 2011). For example, a single U.S. Navy destroyer may incur US \$1.15 million additional fuel annually, with fleet-wide losses reaching US \$56 million per year (Schultz et al., 2011).

In the food sector, *Listeria monocytogenes* (*L. monocytogenes*) contamination of processing surfaces has led to high-profile product recalls. For example, one recall in the EU involving fresh produce incurred direct costs of approximately €30 million due to product removal and disposal (Cámara et al., 2022). Although comprehensive global data on biofilm-related recalls are limited, the economic impact of Listeria-linked food safety failures continues to be a major concern for the industry.

Overall, these costs, spanning healthcare, energy, transport, food safety, water systems, and agricultural sectors, make a compelling case for investing in biofilm research and more effective and sustainable antibiofilm strategies.

## 1.8. Biofilm Control Strategies in Industry: Conventional and Emerging Approaches

No single intervention suffices across industrial sectors due to the complex and context-dependent nature of biofilm formation. Control strategies must be tailored to the specific system, accounting for hydraulic conditions, surface materials, nutrient loads, and microbial composition (Flemming et al., 2016) (Bridier et al., 2015). In sectors such as food processing, healthcare, and water treatment, conventional approaches often involve the use of chemical biocides like chlorine, peracetic acid, or quaternary ammonium compounds, typically in combination with physical methods such as high-pressure flushing or scrubbing (Chowdhury et al., 2019) (Liu et al., 2024). However, the efficacy of such treatments is limited by the biofilm matrix, which can neutralise oxidising agents and hinder penetration into deeper layers (Bridier et al., 2011) (Stewart and Franklin, 2008). Novel strategies are especially

needed in complex environments where flow regimes, temperature, and surface roughness all affect biofilm formation and resilience.

#### 1.8.1. Chemical Biocides and Disinfectants

Oxidising agents such as chlorine, ozone, and peracetic acid are commonly used to disrupt microbial cells and degrade biofilm matrices, but their efficacy varies depending on the organic load and EPS reactivity (Flemming et al., 2016) (Oliveira et al., 2024). Periodic high-concentration slug dosing has been shown to outperform low-level continuous dosing in heavily fouled systems (Elbehiry et al., 2025). Non-oxidising biocides like glutaraldehyde, quaternary ammonium compounds, and isothiazolinones disrupt membrane integrity or protein function but are often diffusion-limited in dense biofilms (Flemming et al., 2016). To boost penetration, synergists such as ethylenediaminetetraacetic acid (EDTA) and surfactants are used, while enzymatic adjuvants like DNase or polysaccharide lyases target specific matrix components (Petrova and Sauer, 2016) (Pinto et al., 2020) (Oliveira et al., 2024). Regulatory approval for industrial or food-contact applications requires validated performance, minimal toxic residues, and sector-specific guidelines (EPA, 2024) (Khan et al., 2016) (Elbehiry et al., 2025).

## 1.8.2. Physical and Mechanical Interventions and Surface Modification and Coatings

High shear flushing, pigging, brushing, and abrasive cleaning physically remove biofilm layers; effectiveness depends on access to surfaces and material compatibility (Flemming et al., 2016). Heat, steam treatment, ultraviolet (UV) irradiation, ultrasound, and pulsed electric fields complement chemical control by damaging cells and biofilm structure (Piyasena, Mohareb and McKellar, 2003) (Calero Preciado et al., 2022). Hydrodynamic management, including maintaining velocities above deposition thresholds and minimizing dead legs, is a preventive strategy in piping networks, as stagnant zones resist removal and act as reservoirs for biofilm regrowth (Simunič et al., 2020) (Calero Preciado et al., 2022).

Non-stick surfaces with low surface energy, such as fluoropolymers and silicone-based materials, reduce initial microbial adhesion by minimizing surface-microbe interactions (Campoccia, Montanaro and Arciola, 2013). Antimicrobial-release coatings incorporating silver, copper, or quaternary ammonium compounds actively kill microbes through ion release or membrane disruption (Singha, Locklin and Handa, 2016) (Marzullo, Gruttadauria

and D'Anna, 2024). Contact-active surfaces, including polymer brushes and surfaces functionalised with cationic groups, kill microbes upon contact without leaching agents (Salta et al., 2013). Zwitterionic and hydrophilic coatings resist biofouling by forming hydration layers that block protein adsorption and microbial attachment (Jiang and Cao, 2010). In marine contexts, self-polishing coatings reduce drag and biofouling through gradual surface erosion (Li, 2023). However, longevity, leachate toxicity, mechanical wear, and regulatory approval remain practical constraints across applications (Campoccia, Montanaro and Arciola, 2013) (Marzullo, Gruttadauria and D'Anna, 2024).

#### 1.8.3. Biological and Ecological Controls

Competitive exclusion and probiotics involve applying benign biofilm formers, such as *B. subtilis* biocontrol strains, to occupy niches on plant roots or surfaces, where they protect plants by forming stable biofilms and producing antimicrobials like surfactin (Bais, Fall and Vivanco, 2004) (Arnaouteli et al., 2021). Enlisting bacteriophages and phage-derived enzymes allows targeting of specific pathogens within biofilms; though efficacy may be reduced due to diffusion barriers, these agents can act synergistically with biocides to improve eradication (Chan and Abedon, 2012). Predatory bacteria like *Bdellovibrio* have shown experimental promise in biofilm control due to their ability to prey on Gram-negative pathogens and disrupt EPS structures (Bratanis et al., 2020) (Tang et al., 2025). Engineered microbial consortia, which are designed to perform distributed functions such as mutualistic interactions or population control, offer potential for targeted biofilm removal, though their application remains primarily theoretical (Duncker, Holmes and You, 2021).

#### 1.8.4. Matrix-Targeting Enzymes and Disassembly Signals

Enzymatic treatments such as DNase I, dispersin B, proteases (e.g. trypsin), and glycosidases effectively degrade biofilm matrix components like eDNA, polysaccharides, and structural proteins, thereby weakening cohesion and enhancing biocide access (Fleming and Rumbaugh, 2018) (Kaplan, 2009). The timing of application is crucial, as younger biofilms are more susceptible to enzymatic disruption, while mature biofilms often require combined strategies. For instance, pre-treatment with matrix-degrading enzymes followed by biocides or antibiotics has been shown to significantly improve efficacy in disrupting mature biofilms compared to monotherapy (Xavier et al., 2005) (Fleming and Rumbaugh, 2017). Additionally, D-amino acids and nitric oxide donors can induce dispersal mechanisms by interfering with

biofilm signalling and matrix stability, although these effects are often species- and context-dependent (Barraud et al., 2006) (Kolodkin-Gal et al., 2010).

#### 1.8.5. Monitoring, Sensing, and Control Loops

Monitoring technologies such as biofilm potential sensors, ATP-based detection, and optical coherence tomography (OCT) imaging provide real-time insight into biofilm development on surfaces (Fish, Osborn and Boxall, 2016) (Oliveira et al., 2024). These tools support adaptive control strategies by enabling responsive biocide dosing based on early detection of microbial activity or structural growth. Data-driven feedback loops reduce chemical overuse and improve treatment precision, particularly in dynamic systems like drinking water or industrial cooling networks (Calero Preciado et al., 2023). Advanced computational tools, including digital twins that couple hydraulic simulations with biofilm growth models, are being explored to simulate and predict biofilm behaviour under varying flow and treatment conditions (Zlatanović, van der Hoek and Vreeburg, 2017). These integrated frameworks offer promising avenues for proactive biofilm management and system optimisation.

#### 1.9. Ginkgo biloba: a Potential Natural Antibiofilm Agent

Interest in plant-derived antibiofilm compounds has grown in response to increasing concern over microbial resistance to chemical biocides, regulatory pressure to minimise disinfection by-product (DBP) formation, and public demand for safer, environmentally friendly interventions, particularly in food and healthcare settings (Lee et al., 2014) (Khan et al., 2016). Several phytochemicals, including flavonoids, terpenoids, and phenolic acids, have demonstrated the ability to disrupt quorum sensing, inhibit biofilm matrix production, or promote dispersal across a range of bacterial species (Esposito et al., 2022). *Ginkgo biloba*, widely used in traditional medicine, has been shown to contain ginkgolic acids and flavonol glycosides with antimicrobial and antibiofilm activity, particularly against Gram-positive organisms such as *S. aureus*/MRSA and the Gram-negative *E. coli* (Lee et al., 2014) (Wang et al., 2021).

#### 1.9.1. Compound Classes from *Ginkgo biloba*

Ginkgo biloba produces a wide range of secondary metabolites with demonstrated antibiofilm potential. Among these, ginkgolic acids, a class of alkyl phenols with varying chain lengths, have been isolated from leaves and fruit extracts. Their antibiofilm activity is

influenced by hydrophobic tail length, which affects membrane interactions and cellular uptake (Wang et al., 2021). Crude *Ginkgo biloba* extracts (GbE), obtained using solvents such as ethanol, methanol, or petroleum ether, contain diverse mixtures of flavonoids, terpenoids, and ginkgolic acids. These solvent systems significantly influence the extract's composition and corresponding antimicrobial efficacy (Cui et al., 2020) (Biernacka et al., 2023). *Ginkgo biloba* exocarp extracts (GBEE), derived from the outer fruit flesh, are particularly rich in lipophilic compounds and have demonstrated inhibitory effects on biofilms formed by MRSA and *Staphylococcus haemolyticus* (*S. haemolyticus*) in vitro (Wang et al., 2021). In addition, polysaccharide fractions such as GBSPII-1, isolated from *Ginkgo biloba* seeds or leaves, have shown antioxidant and biofilm-inhibiting properties against *S. aureus*, potentially through interference with oxidative stress pathways or extracellular matrix formation (Jiang et al., 2021).

#### 1.9.2. Spectrum of Activity Against Priority and Foodborne Organisms

In a study by Lee et al. (2014), the screening of 560 phytochemicals identified ginkgolic acids as potent inhibitors of *E. coli* O157:H7 biofilm formation across multiple surfaces, with significant effects observed at low concentrations (5  $\mu$ g/mL) that had minimal impact on planktonic growth. Crude GbE at 100  $\mu$ g/mL also effectively suppressed biofilm formation and downregulated the expression of fimbrial and curli genes. Notably, cross-inhibition was observed against *S. aureus* strains as well, suggesting broader antibiofilm potential.

Crude GbE, applied at approximately 75 µg/mL, significantly reduced biofilm formation by *Salmonella* and *L. monocytogenes* isolates from poultry across different surface materials and temperature conditions. The antibiofilm activity was particularly notable for certain *Salmonella* serotypes, where reduced motility appeared to play a role. In contrast, *L. monocytogenes* showed more variable responses, indicating species- and strain-specific mechanisms (Wu et al., 2016).

In a study by Wang et al. (2021), GBEE demonstrated bacteriostatic activity against *S. haemolyticus* and MRSA clinical strains at low minimum inhibitory concentration (MIC) values in the microgram per millilitre range. In addition to inhibiting planktonic growth, GBEE disrupted preformed biofilms. Transcriptomic analysis of treated cells revealed modulation of gene expression associated with cell envelope integrity and biofilm formation, suggesting a multi-target mode of action.

#### 1.9.3. Mechanistic Insights

The antibiofilm activity of *Ginkgo biloba* extracts appears to result from multiple, often strain-specific and preparation-dependent mechanisms. In *E. coli* O157:H7, ginkgolic acids have been shown to downregulate genes responsible for surface adhesion, including curli and fimbrial components, leading to reduced biofilm formation without significantly affecting planktonic growth (Lee et al., 2014). In *Salmonella* poultry isolates, *Ginkgo biloba* extracts impaired motility, notably swimming and swarming behaviours, which are essential for surface colonisation and early biofilm establishment (Wu et al., 2016). Against *S. aureus* and MRSA, GBEE disrupted cell membrane integrity and ion homeostasis, accompanied by transcriptomic changes in envelope and biofilm-related gene expression (Wang et al., 2021). Furthermore, antioxidant components of *Ginkgo biloba* may mitigate oxidative stress, indirectly modulating redox-sensitive regulatory systems involved in matrix production and dispersal (Di Meo et al., 2020). The mechanistic breadth of these effects likely reflects the composite nature of solvent-derived extracts, highlighting the need for fractionation and chemical profiling to pinpoint active constituents and modes of action.

### 1.9.4. Limitations of Static Models in Evaluating *Ginkgo biloba*Antibiofilm Efficacy

While *Ginkgo biloba* extracts have shown promising antibiofilm effects against pathogens like *S. aureus* and *Salmonella* in static in vitro models, a major limitation of these studies is their lack of relevance to real-world conditions. Most experiments are conducted on polystyrene plates or static glass surfaces, which fail to replicate the dynamic shear, nutrient gradients, and oxygen diffusion present in industrial, medical, or environmental flow systems. Biofilm structure and susceptibility to antimicrobials are strongly influenced by fluid dynamics, with shear stress modulating matrix density, cell physiology, and agent penetration (Stoodley et al., 1999) (Petrova and Sauer, 2016) (Oliveira et al., 2024). Despite this, few studies incorporate flow-based models, such as flow cells or microfluidic devices, when evaluating plant-derived antibiofilm agents. This omission limits the translational potential of *Ginkgo biloba*-based interventions, underscoring the need for experimental systems that more accurately reflect the physical realities of target applications.

#### 1.10. Knowledge Gaps and Research Opportunities

#### 1.10.1. Genotype and Environment Interactions

Microbial domestication, defined as the adaptation of strains to laboratory conditions, can profoundly alter biofilm-related traits. In B. subtilis, repeated passaging under nutrient-rich, static environments often selects for genetic variants that suppress features important in natural settings, such as motility, complex surface architecture, and robust matrix production (Kearns et al., 2005) (McLoon et al., 2011). Genomic comparisons between wild-type environmental strains (e.g., NCIB3610) and domesticated laboratory derivatives (e.g., strain 168) have revealed multiple changes, including point mutations in regulatory genes, loss of plasmids, and inactivation of biosynthetic pathways (McLoon et al., 2011). These mutations reshape key regulatory circuits, including the Spo0A phosphorelay, SinR/SinI module, DegS/DegU system, and other transcriptional regulators that coordinate developmental decisions and matrix production (Vlamakis et al., 2013). Emerging findings suggest that chromosomal positioning and replication dynamics may also influence spatial expression patterns of biofilm genes, adding an additional layer of complexity (Wu, Kong and Liu, 2024). To better understand biofilm regulation in real-world environments, biofilm traits should be mapped across relevant environmental conditions, such as flow, metal exposure, and chemical disinfection, using strains that retain ecological regulatory integrity.

#### 1.10.2. Linking Gene Regulation to Biofilm Mechanics and Detachment

Despite extensive advances in biofilm research, understanding how bacterial gene expression directly influences the physical behaviour of biofilms remains a key challenge. In particular, there is a lack of quantitative data linking which genes are active (e.g. those involved in matrix production, motility, sporulation, or stress responses) to how biofilms behave mechanically, such as how strong they are, how they deform, and how they break under fluid flow.

Studies of *B. subtilis* have mapped out a complex network of regulators, such as Spo0A, SinR/SinI, DegU, AbrB, and RemA, that control the production of the biofilm matrix and transitions between cell states (Vlamakis et al., 2013) (Diethmaier et al., 2011) (Verhamme et al., 2007). However, few experiments have tracked these gene networks under realistic mechanical forces, like those found in pipes, medical devices, or flowing water systems.

Recent studies on flow dynamics and streamer formation (thin filamentous biofilm structures) show that the rate at which biofilms accumulate and the frequency at which

streamers form are strongly influenced by the intensity of fluid shear (Rusconi et al., 2010) (Kurz et al., 2022). Higher shear often suppresses matrix production or detaches biofilm fragments, yet the exact gene expression responses driving this mechanical adaptation remain largely uncharacterised.

Emerging research suggests that bacteria may be able to sense and respond to rhythmic or pulsed flow conditions, potentially allowing us to "reprogram" biofilm behaviour by adjusting fluid forces (Wei and Yang, 2023). This opens new possibilities: if we can map how mechanical stress shapes gene expression in real time, we may be able to shift biofilms into weaker, more easily removable states. Realising this will require new experimental approaches that combine genetic tools (e.g. RNA-seq, fluorescent reporters) with physical measurements (e.g. biofilm density) under carefully controlled flow conditions.

Bridging this gap would greatly enhance predictive biofilm models used in medicine, industry, and environmental management, allowing for the design of surfaces, flows, and treatments that exploit biofilm vulnerability rather than just reacting to their presence.

### 1.10.3. Natural Product Translation Under Realistic Conditions: *Ginkgo biloba*

Natural compounds derived from plants have shown promising effects in laboratory tests for preventing bacterial biofilms. However, these tests are often carried out under simple conditions that do not reflect real-life scenarios, such as flowing water, industrial pipelines, or medical equipment.

Ginkgo biloba offers a good example of this gap. Extracts from Ginkgo leaves, seeds, and fruit have been shown to reduce biofilm formation by *E. coli* O157:H7, *S. aureus* and MRSA, not by killing the bacteria outright, but by turning off genes involved in extracellular matrix formation (Lee et al., 2014) (Wang et al., 2022). Other studies have shown that *Ginkgo* extracts can reduce motility-related biofilm formation in *Salmonella* and *Listeria* strains (Wu et al., 2016).

However, the vast majority of these studies have relied on static in vitro models, such as microtiter plate biofilm assays, which lack the physical and hydrodynamic complexity of real-world environments. These simplified systems do not account for key variables such as shear stress, nutrient flux, or surface renewal, all of which critically influence biofilm architecture, dispersal dynamics, and antimicrobial tolerance (Stoodley et al., 1999) (Purevdorj et al.,

2002) (Kurz et al., 2022). In contrast, industrial, clinical, and natural systems are governed by continuous or intermittent flow regimes, where fluid dynamics modulate biofilm development, mechanical properties, and susceptibility to treatment interventions (Rusconi and Stocker, 2015) (Fish, Osborn and Boxall, 2016). Moreover, studies rarely report whether the plant compounds remain stable or effective under conditions such as water shear stress, disinfectant exposure, or long-term contact with different materials.

To date, no peer-reviewed study has tested *Ginkgo biloba* extracts in flow systems against *B. subtilis*, nor have researchers evaluated how well these natural products perform when embedded in surfaces or exposed to continuous flow. Bridging this gap is essential to move plant-based antibiofilm strategies from promising ideas to practical, industrial or clinical tools.

#### 1.11. Thesis Overview

This thesis investigates the structural and molecular responses of *B. subtilis* biofilms to environmental stressors, with a focus on two key factors: exposure to *Ginkgo biloba* leaf extract (GBLE), a plant-derived compound with reported antibiofilm activity, and the influence of fluid flow dynamics, including unidirectional and bidirectional regimes. Despite growing interest in natural antimicrobials, the mechanisms by which phytochemicals like GBLE impact biofilm development, especially under realistic flow conditions, remain poorly understood.

To address this, the thesis combines traditional microbiology, fluorescent microscopy, quantitative image analysis, and gene expression profiling (RT-qPCR and RNA-Seq) across a series of four interconnected research chapters. In addition, these experiments use *B. subtilis* JWV042, a wild-type derivative of NCIB3610 that retains the genetic capacity for robust, architecturally complex biofilm formation. Its constitutive green fluorescent protein (GFP) expression enables direct, non-invasive visualisation by fluorescence and confocal microscopy, making it well-suited for studying structural and molecular responses to mechanical and chemical stressors.

Each chapter targets a different scale of analysis, from early static inhibition to structural adaptation under continuous flow, and ultimately to transcriptomic responses under complex mechanical and chemical stress. Collectively, these studies aim to deepen the

understanding of biofilm plasticity, explore the role of mechanical forces in shaping bacterial multicellularity, and evaluate the potential of GBLE as a sustainable antibiofilm intervention.

# 1.11.1. Chapter 2: Investigating the Antibiofilm and Antimicrobial Activity of *Ginkgo biloba* Leaf Extract Against *Bacillus subtilis* Static Biofilms

This research chapter addresses the limited understanding of how GBLE affect biofilm architecture and differentiation beyond human-associated pathogens. While prior studies have reported antibacterial or antibiofilm activity of *Ginkgo* seed and exocarp extracts, most have focused on a narrow range of clinical strains using endpoint assays with minimal structural resolution. In contrast, this study investigates the effects of GBLE, a chemically distinct fraction, on the model organism *B. subtilis* JWV042, using an integrated workflow combining quantitative and qualitative biofilm assays and fluorescence imaging. By distinguishing growth inhibition from biofilm-specific responses and visualising structural and matrix-level changes, this chapter provides novel insight into how *B. subtilis* adapts to phytochemical stress and reveals the potential of GBLE as a natural antibiofilm agent.

# 1.11.2. Chapter 3: Fluid Flow-Induced Morphological Adaptations in Bacillus subtilis Biofilms and Their Inhibition by *Ginkgo biloba* Leaf Extract

Building on the findings of Chapter 2, this research chapter addresses the limited understanding of how mature biofilms develop under continuous flow, a condition highly relevant to industrial systems, yet underexplored at the macroscale. Most prior studies have focused on early-stage microcolony formation using microfluidic devices, offering limited insight into the full 3D architecture or differentiated cell types of mature biofilms. This chapter overcomes those constraints by using GFP-tagged *B. subtilis* JWV042 within flow cell reactors, enabling high-resolution confocal imaging of intact, macroscale biofilms exposed to shear stress. The study reveals novel structural adaptations, including the formation of Van Gogh ropes, twisting assemblies of aligned cell chains, and a previously uncharacterised ECM-rich attachment layer, suggesting a refinement of existing biofilm development models. Furthermore, the antibiofilm effects of GBLE were assessed under flow for the first time, revealing disruption of biofilm integrity, reduced biofilm biomass and suppression of multicellular organisation. These findings not only expand understanding of *B. subtilis* 

architecture under hydrodynamic forces but also highlight GBLE's potential in managing biofilms in real-world flow environments, although further research is needed.

# 1.11.3. Chapter 4: Structural Adaptation of *Bacillus subtilis* Biofilms to Bidirectional Flow and the Disruptive Effect of *Ginkgo biloba* Leaf Extract

This research chapter investigates how changes in flow direction influence the development, architecture, and mechanical adaptation of *B. subtilis* biofilms, an understudied yet industrially relevant parameter. While biofilm responses to shear and flow velocity have been widely explored, the effects of true bidirectional flow remain largely uncharacterised. This study addresses this gap by comparing biofilms grown under unidirectional and bidirectional flow in flow cell systems, revealing distinct structural features such as elevated folds containing underlying channels and increased porosity and biomass exclusive to bidirectional regimes. Using confocal microscopy and image analysis, the work shows that flow reversal drives the emergence of higher-order architecture, likely enhancing resilience to fluctuating mechanical stress. Furthermore, the antibiofilm efficacy of GBLE was confirmed under these conditions, building on previous findings and demonstrating a disruptive effect on biofilm morphology, reduced biomass and cohesion. These results provide new insight into how *B. subtilis* biofilms respond to dynamic hydrodynamic forces and support the use of GBLE as a potential sustainable control strategy in flow-variable environments.

# 1.11.4. Chapter 5: Gene Expression Rewiring and Biofilm Morphogenesis in *Bacillus subtilis* Exposed to *Ginkgo biloba* Leaf Extract and Fluid Flow

This research chapter investigates the molecular mechanisms underlying *B. subtilis* biofilm responses to both GBLE and dynamic flow regimes, addressing a critical gap in our understanding of how environmental and phytochemical cues shape biofilm gene expression. While earlier chapters focused on morphological adaptations, this study uses RT-qPCR and RNA-Seq to examine how matrix production, stress response, motility, and developmental pathways are transcriptionally regulated under static, unidirectional, and bidirectional flow and how GBLE modulates gene expression. Findings reveal that GBLE consistently suppresses core biofilm and sporulation genes across conditions, while simultaneously inducing oxidative stress and survival-associated transcripts. Bidirectional flow, in particular, elicits broad transcriptional activation and promotes structural

complexity, suggesting a synergistic role of flow direction in biofilm development. By integrating molecular and structural data, this chapter advances a systems-level view of how *B. subtilis* adapts to physical and chemical pressures and highlights the *B. subtilis* bacterial adaptations.

#### 1.12. References

Abouhagger, A., Celiešiūtė-Germanienė, R., Bakute, N., Stirke, A. and Melo, W.C.M.A. (2024) Electrochemical biosensors on microfluidic chips as promising tools to study microbial biofilms: a review. *Frontiers in Cellular and Infection Microbiology*. Vol.14, p.1419570.

Arnaouteli, S., Matthews, C., Hodgkinson, J.T., Hilton, S.H., Hasan, M. and Stanley-Wall, N.R. (2021) Biofilm formation in *Bacillus subtilis*: A review of environmental signals and regulatory pathways. *FEMS Microbiology Reviews*. Vol.45(6), p.064.

Arnaouteli, S., Bamford, N.C., Stanley-Wall, N.R. and Kovács, Á.T. (2021) Bacillus subtilis biofilm formation and social interactions. *Nature Reviews Microbiology*. Vol.19(9), pp. 600–614.

Arroussi, M., Zhao, J., Bai, C., Zhang, S., Xia, Z., Jia, Q., Yang, K. and Yang, R. (2023) Evaluation of inhibition effect on microbiologically influenced corrosion of Ti-5Cu alloy against marine *Bacillus vietnamensis* biofilm. *Bioelectrochemistry*. Vol.149(108265).

ASTM International (2021) ASTM E2871-21: Standard test method for evaluating disinfectant efficacy against Pseudomonas aeruginosa biofilms grown in CDC biofilm reactor using Single Tube Methodology.

Barraud, N., Hassett, D.J., Hwang, S.-H., Rice, S.A. and Kjelleberg, S. (2006) Involvement of nitric oxide in biofilm dispersal of *Pseudomonas aeruginosa*. *Journal of Bacteriology*. Vol.188(21), pp.7344–7353.

Bais, H.P., Fall, R. and Vivanco, J.M. (2004) Biocontrol of *Bacillus subtilis* against infection of *Arabidopsis* roots by *Pseudomonas syringae* is facilitated by biofilm formation and surfactin production. *Plant Physiology*. Vol.134(1), pp.307–319.

Beech, I.B. and Sunner, J.A. (2004) Biocorrosion: towards understanding interactions between biofilms and metals. *Current Opinion in Biotechnology*. Vol.15(3), pp. 181–186.

Bhagwat, G. (2021) Understanding the Fundamental Basis for Biofilm–Surface Interactions. *Frontiers in Microbiology*.

Biernacka, P., Adamska, I. and Felisiak, K. (2023) The potential of *Ginkgo biloba* as a source of biologically active compounds: a review of the recent literature and patents. *Molecules*. Vol.28(10), p.3993.

Bjarnsholt, T., Moser, C., Jensen, P.Ø., Hoiby, N. and Tolker-Nielsen, T. (2022) The in vivo biofilm. *Trends in Microbiology*. Vol.30(12), pp. 1074–1083.

Boles, B.R. and Horswill, A.R. (2008) Agr-mediated dispersal of *Staphylococcus aureus* biofilms. *PLoS Pathogens*. Vol.4(4), e1000052.

Branda, S.S., González-Pedrajo, B., Losick, R. and Kolter, R. (2001) Fruiting body formation by *Bacillus subtilis*. *Proceedings of the National Academy of Sciences USA*. Vol.98(4), pp.11621–11627.

Branda, S.S., González-Pedrajo, B., Losick, R. and Kolter, R. (2004) Genes involved in formation of structured multicellular communities by Bacillus subtilis. *Journal of Bacteriology*. Vol.186(12), pp. 3970–3979.

Bratanis, E., Andersson, T., Lood, R. and Bukowska-Faniband, E. (2020) Biotechnological potential of *Bdellovibrio* and like organisms and their secreted enzymes. *Frontiers in Microbiology*. Vol.11, p. 662.

Bridier, A., Briandet, R., Thomas, V. and Dubois-Brissonnet, F. (2011) Resistance of bacterial biofilms to disinfectants: a review. *Biofouling*. Vol.27(9), pp. 1017–1032.

Bridier, A., Sanchez-Vizuete, P., Guilbaud, M., Piard, J.-C., Naitali, M. and Briandet, R. (2015) Biofilm-associated persistence of food-borne pathogens. *Food Microbiology*. Vol.45 (Part B), pp.167–178.

Calero Preciado, C., Soria-Carrasco, V., Boxall, J. and Douterelo, I. (2023) Climate change and management of biofilms within drinking water distribution systems. *Science of the Total Environment*. Vol.887, p.163864.

Cámara, M., Green, W., MacPhee, C.E., Rakowska, P.D., Raval, R., Richardson, M.C., Slater-Jefferies, J., Steventon, K. and Webb, J.S. (2022) Economic significance of biofilms: a multidisciplinary and cross-sectoral challenge. *NPJ Biofilms and Microbiomes*. Vol.8(1), p.42.

Campoccia, D., Montanaro, L. and Arciola, C.R. (2013) A review of the biomaterials technologies for infection-resistant surfaces. *Biomaterials*. Vol.34(34), pp.8533–8554.

Chai, L., Zaburdaev, V. and Kolter, R. (2024) How bacteria actively use passive physics to make biofilms. *Proceedings of the National Academy of Sciences*. Vol.121(40), e2403842121.

Chai, Y., Norman, T., Kolter, R. and Losick, R. (2010) An epigenetic switch governing daughter cell separation in *Bacillus subtilis*. *Genes & Development*. Vol.24(8), pp.754–765.

Chambers, L.D., Stokes, K.R., Walsh, F.C. and Wood, R.J.K. (2021) 'Modern approaches to marine antifouling coatings. *Surface and Coatings Technology*. Vol.201(6), pp. 3642–3652.

Shen-Jie Chang, P., Huang, X. and Liu, Y. (2020) The influence of hydrodynamic shear force on adhesion morphology and biofilm conformation of *Bacillus* sp. on stainless steel by a flow cell. *Journal of Industrial Microbiology & Biotechnology*. Vol.47(10–11).

Chowdhury, D., Rahman, A., Hu, H., Jensen, S.O., Deva, A.K. and Vickery, K. (2019) Effect of disinfectant formulation and organic soil on the efficacy of oxidizing disinfectants against biofilms. *Journal of Hospital Infection*. Vol.103(1), pp.e33–e41.

Chun, A.F.M., Tolker-Nielsen, T., Ragas, P.C., Mattick, J.S. and Stoodley, P. (2022) Early biofilm and streamer formation is mediated by wall shear stress and surface wettability. *MicrobiologyOpen*. Vol.e1310.

Cohn, F. (1877) 'Ueber Bakterien', Beiträge zur Biologie der Pflanzen, 2(2), pp. 249–276.

Colvin, K.M., Irie, Y., Tart, C.S., Urbano, R., Whitney, J.C., Ryder, C., Howell, P.L. and Parsek, M.R. (2011) The Pel polysaccharide can serve a structural and protective role in *Pseudomonas aeruginosa* biofilms. *PLoS Pathogens*. Vol.7(1), e1001264.

Colvin, K.M., Irie, Y., Tart, C.S., Urbano, R., Whitney, J.C., Ryder, C., Howell, P.L., Wozniak, D.J. and Parsek, M.R. (2012) The Pel and Psl polysaccharides provide *Pseudomonas aeruginosa* structural redundancy within the biofilm matrix. *Environmental Microbiology*. Vol.14(8), pp.1913–1928.

Conrad, J.C. (2018) Consequences and implications for bacteria and biofilms. *Annual Review of Biophysics*. Vol.47, pp.353–371.

Costerton, J.W., Geesey, G.G. and Cheng, K.J. (1978) How bacteria stick. *Scientific American*. Vol.238(1), pp. 86–95.

Costerton, J.W., Lewandowski, Z., Caldwell, D.E., Korber, D.R. and Lappin-Scott, H.M. (1995) Microbial biofilms. *Annual Review of Microbiology*. Vol.49, pp. 711–745.

Costerton, J.W., Stewart, P.S. and Greenberg, E.P. (1999) Bacterial biofilms: a common cause of persistent infections. *Science*. Vol.284(5418), pp. 1318–1322.

Cue, D., Lei, M.G. and Lee, C.Y. (2012) Genetic regulation of the intercellular adhesion (icaADBC) locus in *Staphylococcus aureus*. *Journal of Bacteriology*. Vol.194(16), pp. 4529–4538.

Cui, N., Zhang, L., Quan, M. and Xu, J. (2020) Profile of the main bioactive compounds and *in vitro* biological activity of different solvent extracts from *Ginkgo biloba* exocarp. *RSC Advances*. Vol.10(73), pp.45105–45111.

Davies, D. (2003) Understanding biofilm resistance to antibacterial agents. *Nature Reviews Drug Discovery*. Vol.2(2), pp.114–122.

de Kreuk, M.K., Pronk, M. and van Loosdrecht, M.C.M. (2005) Formation of aerobic granules and conversion processes in an aerobic granular sludge reactor at moderate and low temperatures. *Water Research*. Vol.39 (18), pp.4476-84.

Di Meo, F., Cuciniello, R., Margarucci, S., Bergamo, P., Petillo, O., Peluso, G., Filosa, S. and Crispi, S. (2020) Ginkgo biloba prevents oxidative stress-induced apoptosis blocking p53 activation in neuroblastoma cells. *Antioxidants*. Vol.9(4), p.279.

Diethmaier, C., Pietack, N., Gunka, K., Wrede, C., Lehnik-Habrink, M., Herzberg, C., Hübner, S. and Stülke, J. (2011) A novel factor controlling bistability in *Bacillus subtilis*: the YmdB protein affects flagellin expression and biofilm formation. *Journal of Bacteriology*. Vol.193(21), pp.5997–6007.

Donlan, R.M. (2001) Biofilm formation: a clinically relevant microbiological process. *Clinical Infectious Diseases*. Vol.33(8), pp. 1387–1392.

Donlan, R.M., (2002) Biofilms: microbial life on surfaces. *Emerging Infectious Diseases*. Vol.8(9), pp.881–890.

Donlan, R.M. and Costerton, J.W. (2002) Biofilms: survival mechanisms of clinically relevant microorganisms. *Clinical Microbiology Reviews*. Vol.15(2), pp. 167–193.

Drescher, K., Shen, Y., Bassler, B.L. and Stone, H.A. (2013) Biofilm streamers cause catastrophic disruption of flow with consequences for environmental and medical systems. *Proceedings of the National Academy of Sciences USA*. Vol.110(11), pp.4345–4350.

Duddu, R., Chopp, D.L. and Moran, B. (2009) A two-dimensional continuum model of biofilm growth incorporating fluid flow and shear stress—based detachment. *Biotechnology and Bioengineering*. Vol.103(1), pp.92–104.

Duncker, K.E., Holmes, Z.A. and You, L. (2021) Engineered microbial consortia: strategies and applications. *Microbial Cell Factories*. Vol.20, Article 211.

Elbehiry, A., Osama, M., Khaled, M., Al-Sanie, E., Ahmad, S., Yafet, M., Abdelkhalek, N. and Mohamed, Z. (2025) Emerging technologies and integrated strategies for controlling foodborne pathogens in fresh produce. *Microorganisms*. Vol.13(7), Article 1447.

EPA (2024) Biofilm test guidance for antimicrobial products. United States Environmental Protection Agency.

EPA (2024) Finalized Test Methods for Measuring Disinfectant Residues on Hard Surfaces. U.S. Environmental Protection Agency. Available at: <a href="https://www.epa.gov/pesticides">https://www.epa.gov/pesticides</a>.

Esposito, M.M., Osman, M., and Pintado, M.E. (2022) The use of natural methods to control foodborne biofilms. *Pathogens*. Vol.12(1), p.45.

Fish, K.E., Osborn, A.M. and Boxall, J.B. (2016) Characterising and understanding the impact of microbial biofilms and the extracellular polymeric substance (EPS) matrix in drinking water distribution systems. *Environmental Science: Water Research & Technology*. Vol.2(6), pp.614–630.

Flemming, H.C. (2002) Biofouling in water systems—cases, causes and countermeasures. *Applied Microbiology and Biotechnology*. Vol.59(6), pp. 629–640.

Flemming, H.C., Neu, T.R. and Wozniak, D.J. (2007) The EPS matrix: the "house of biofilm cells". *Journal of Bacteriology*. Vol.189(22), pp. 7945–7947.

Flemming, H.C. and Wingender, J. (2010) The biofilm matrix. *Nature Reviews Microbiology*. Vol.8(9), pp. 623–633.

Flemming, H.C., Wingender, J., Szewzyk, U., Steinberg, P., Rice, S.A. and Kjelleberg, S. (2016) Biofilms: an emergent form of bacterial life. *Nature Reviews Microbiology*. Vol.14(9), pp. 563–575.

Fleming, D. and Rumbaugh, K.P. (2017) Approaches to Dispersing Medical Biofilms. *Microorganisms*. Vol.5(2), p.15.

Flemming, H. C. and Wuertz, S. (2019) Bacteria and archaea on Earth and their abundance in biofilms. *Nature Reviews Microbiology*. Vol.17(4), pp. 247–260.

Gbejuade, H.O., Lovering, A.M. and Webb, J.C. (2015) The role of microbial biofilms in prosthetic joint infections. *Acta Orthopaedica*. Vol.86(2), pp. 147–158.

Gordon, V.D. and Wang, L. (2019) Bacterial mechanosensing: the force will be with you, always. *Journal of Cell Science*. Vol.132, jcs227694.

Ha, D.G. and O'Toole, G.A. (2015) c-di-GMP and its effects on biofilm formation and dispersion in *Pseudomonas aeruginosa*. *Environmental Microbiology*. Vol.18(7), pp.1786–1796.

Hall-Stoodley, L., Costerton, J.W. and Stoodley, P. (2004) Bacterial biofilms: from the natural environment to infectious diseases. *Nature Reviews Microbiology*. Vol.2(2), pp. 95–108.

Helmann, J.D. (2016) Bacillus subtilis extracytoplasmic function (ECF) sigma factors and defense of the cell envelope. *Current Opinion in Microbiology*. Vol.30, pp.122–132.

Herzberg, M. and Elimelech, M. (2007) Biofouling of reverse osmosis membranes: Role of biofilm-enhanced osmotic pressure. *Journal of Membrane Science*. Vol.295(1–2), pp. 11–20.

Highmore, C.J., Melaugh, G., Morris, R.J., Parker, J., Direito, S.O.L., Romero, M. and Gilmore, B.F. (2022) Translational challenges and opportunities in biofilm science: a BRIEF for the future. *NPJ Biofilms and Microbiomes*. Vol.8(1), 68.

Hobley, L., Harkins, C., Macphee, C. and Stanley-Wall, N.R. (2015) Giving structure to the biofilm matrix: an overview of individual strategies and emerging common themes. *FEMS Microbiology Reviews*. Vol.39(5), pp. 649–669.

Hoek, E.M.V. (2022) Reverse osmosis membrane biofouling: causes, consequences, and control strategies across water types. *npj Clean Water*. Vol.1(1), Article 6.

Høiby, N., Bjarnsholt, T., Givskov, M., Molin, S. and Ciofu, O. (2010) Antibiotic resistance of bacterial biofilms. *International Journal of Antimicrobial Agents*. Vol.35(4), pp. 322–332.

Høiby, N., Bjarnsholt, T., Moser, C., Bassi, G.L., Coenye, T., Donelli, G., Hall-Stoodley, L., Hola, V., Imbert, C., Kirketerp-Møller, K., Lebeaux, D., Oliver, A., Ullmann, A.J. and Williams, C. (2015) ESCMID guideline for the diagnosis and treatment of biofilm infections 2014. *Clinical Microbiology and Infection*. Vol.21(S1), pp. S1–S25.

Horn, H., Reiff, H. and Morgenroth, E. (2003) Simulation of growth and detachment in biofilm systems under defined hydrodynamic conditions. *Biotechnology and Bioengineering*. Vol.81(5), pp.607–617.

Horswill, A.R., Stoodley, P., Stewart, P.S. and Parsek, M.R. (2007) The effect of the chemical microenvironment on the structure and function of biofilms. *Analytical and Bioanalytical Chemistry*. Vol.387(2), pp.371–380.

Jennings, L.K., Storek, K.M., Ledvina, H.E., Coulon, C., Marmont, L.S., Sadovskaya, I., Secor, P.R., Tseng, B.S., Scian, M., Filloux, A., Wozniak, D.J., Parsek, M.R. and Lee, V.T. (2021) *Pseudomonas aeruginosa* aggregates in cystic fibrosis airway mimic long-term infection. *Cell Reports*. Vol.35(4), 109113.

Jiang, H., Luan, Z., Fan, Z., Wu, X., Xu Z., Zhou T. and Wang H. (2021) Antibacterial, antibiofilm, and antioxidant activity of polysaccharides obtained from fresh sarcotesta of *Ginkgo biloba*. *Antibiotics*. Vol.10(8), p.986.

Jiang, S. and Cao, Z. (2010) Ultralow-fouling, functionalizable, and hydrolyzable zwitterionic materials and their derivatives for biological applications. *Advanced Materials*. Vol.22(9), pp.920–932.

Kaplan, J.B. (2009) Therapeutic potential of biofilm-dispersing enzymes. *International Journal of Artificial Organs*. Vol.32(9), pp.545–554.

Karampatzakis, A., Rose, C., Hubbell, R., and Grunwald, M. (2017) Probing the internal micromechanical properties of *Pseudomonas aeruginosa* biofilms. *npj Biofilms and Microbiomes*. Vol.3, Article 28.

Karatan, E. and Watnick, P. (2009) Signals, regulatory networks, and materials that build and break bacterial biofilms. *Microbiology and Molecular Biology Reviews*. Vol.73(2), pp. 310–347.

Karygianni, L., Busscher, H.J., van der Mei, H.C. and Sharma, P.K. (2020) Insights into the role of extracellular DNA and proteins in bacterial biofilm mechanics and structure. *Frontiers in Microbiology*. Vol.11, Article 813.

Kearns, D.B., Chu, F., Losick, R. and Kolter, R. (2005) A master regulator of biofilm formation by *Bacillus subtilis*. *Molecular Microbiology*. Vol.55(3), pp.739–749.

Khan, I., Khan, J., Miskeen, S., Tango, C.N., Park, Y.S. and Oh, D.H. (2016) Prevalence and control of Listeria monocytogenes in the food industry – a review. *Czech Journal of Food Sciences*. Vol.34(6), pp.469–487

Kiedrowski, M.R., Malone, C.L., Johnston, M.D., Scott, R.M. and Smeltzer, M.S. (2011) Nuclease modulates biofilm formation in community-associated methicillin-resistant *Staphylococcus aureus. PLOS ONE*. Vol.6(11), e26714.

Kim, L.H. and Vrouwenvelder, J.S. (2019) Insignificant Impact of Chemotactic Responses of *Pseudomonas aeruginosa* on the Bacterial Attachment to Organic Pre-Conditioned RO Membranes. Vol.9(12), p.162.

Klapper, I. and Dockery, J. (2010) Mathematical description of microbial biofilms. *SIAM Review*. Vol.52(2), pp. 221–265.

Klausen, M., Heydorn, A., Ragas, P., Lappin-Scott, H.M., Kjelleberg, S. and Molin, S. (2003) Biofilm formation by *Pseudomonas aeruginosa* wild type, flagella and type IV pili mutants. *Molecular Microbiology*. Vol.48(6), pp.1511–1524.

Kobayashi, K. and Iwano, M. (2012) BsIA (YuaB) forms a hydrophobic layer on the surface of *Bacillus subtilis* biofilms. *Molecular Microbiology*. Vol.85(1), pp.51–66.

Kolenbrander, P.E., Palmer, R.J., Periasamy, S. and Jakubovics, N.S. (2010) Oral multispecies biofilm development and the key role of cell–cell distance. *Nature Reviews Microbiology*. Vol.8(7), pp. 471–480.

Kolodkin-Gal, I., Romero, D., Cao, S., Clardy, J., Kolter, R. and Losick, R. (2010) D-Amino acids trigger biofilm disassembly. *Science*. Vol.328(5978), pp.627–629.

Kovács, Á.T. and Kuipers, O.P. (2011) Identification and functionality of different Bacillus subtilis biofilm matrix components. *Molecular Microbiology*. Vol.83(4), pp. 792–803.

Kragh, K.N., Hutchison, J.B., Melaugh, G., Rodesney, C., Colvin, K.M., Campagna, S.R., Sauer, K., Harley, B.A.C., and Bjarnsholt, T. (2016) Role of multicellular aggregates in biofilm formation. *mBIO*. Vol.7(2): e00237-16.

Kragh, K.N., Alhede, M., Jensen, P.Ø., Moser, C. and Bjarnsholt, T. (2023) The biofilm matrix: A sticky framework for microbial life. *Nature Reviews Microbiology*. Vol.21(4), pp. 247–260.

Kragh, K.N., Tolker-Nielsen, T., Lichtenberg, M. and Bjarnsholt, T. (2023) The non-attached biofilm aggregate. *Communications Biology*. Vol.6(1), p. 898.

Kreve, S. (2021) Bacterial adhesion to biomaterials: What regulates this? *Frontiers in Cellular and Infection Microbiology*.

Kurz, D.L., Secchi, E., Carrillo, F.J., Bourg, I.C., Stocker, R. and Jimenez-Martinez, J. (2022) Competition between growth and shear stress drives intermittency in preferential flow paths in porous medium biofilms. *Proceedings of the National Academy of Sciences of the United States of America*. Vol.119(30), p.e2122202119.

LaPointe, G., Wilson, T., Tarrah, A. and Gagnon, M. (2025) Microbial Community Tracking from Dairy Farm to Factory: Insights on Biofilm Management for Enhanced Food Safety and Quality. *Journal of Dairy Science*. [preprint].

Latorre, A.A., Martínez-Ramírez, M.A., Silva, L.M., González-Ramírez, M. and del Río-García, C. (2022) Multispecies biofilm presence in dairy milking equipment hoses: implications for pathogenic persistence and resistance. *Frontiers in Veterinary Science*. Vol.Article 969455.

Lawrence, J.R., Korber, D.R., Hoyle, B.D., Costerton, J.W. and Caldwell, D.E. (1991) Optical sectioning of microbial biofilms. *Journal of Bacteriology*. Vol.173(20), pp. 6558–6567.

Lee, J.H., Kim, Y.G., Cho, H.S., Kim, S.I., Lee, J. (2014) Plant flavonoids inhibit *Escherichia coli* 0157:H7 biofilm formation and virulence. *Food Microbiology*. Vol.40, pp. 56–65.

Li, L. (2023) Progress in marine antifouling coatings: current status and eco-friendly strategies. *Coatings*. Vol.13(11), p.1893.

Liu, G., Smith, C., O'Connor, K. and Douterelo, I. (2024) Microbial community dynamics in drinking water systems and their influence on disinfection by-products and water quality. *Water Research*. Vol.247, 120867.

Lopez, D., Fischbach, M.A., Chu, F., Losick, R. and Kolter, R. (2009) Structurally diverse natural products that cause potassium leakage trigger multicellularity in *Bacillus subtilis*. *Proceedings of the National Academy of Sciences USA*. Vol.106(1), pp.280–285.

Lopez, D., Vlamakis, H. and Kolter, R. (2009) Generation of multiple cell types in *Bacillus subtilis*. *FEMS Microbiology Reviews*. Vol.33(1), pp. 152–163.

Marra, D., Moreno, Rizzo, S. and Caserta, S. (2025) Microfluidics unveils role of gravity and shear stress on *Pseudomonas fluorescens* motility and biofilm growth. *NPJ Biofilms and Microbiomes*. [preprint].

Marzullo, P., Gruttadauria, M. and D'Anna, F. (2024) Quaternary ammonium salts-based materials: A review on environmental toxicity, anti-fouling mechanisms and applications in marine and water treatment industries. *Biomolecules*. Vol.14(8), p.957.

Mazaheri, T., Cervantes-Huamán, B.R.H., Bermúdez-Capdevila, M., Ripolles-Avila, C. and Rodríguez-Jerez, J.J. (2021) *Listeria monocytogenes* biofilms in the food industry: Is the current hygiene program sufficient to combat the persistence of the pathogen?' *Foods*. Vol.10(6), p.1416.

McLoon, A.L., Guttenplan, S.B., Kearns, D.B., Kolter, R. and Losick, R. (2011) Tracing the domestication of a biofilm-forming bacterium. *Journal of Bacteriology*. Vol.193(7), pp. 2027–2034.

Melaugh, G., Hutchison, J., Kragh, K.N., Irie, Y., Roberts, A., Bjarnsholt, T., Diggle, S.P., Gordon, V.D. and Allen, R.J. (2016) Shaping the growth behaviour of biofilms initiated from bacterial aggregates. *PLoS ONE*. Vol.11(3), e0149683.

Milton, M.E. and Cavanagh, J. (2023) The biofilm regulatory network from Bacillus subtilis: A structure—function analysis. Journal of Molecular Biology. Vol.435(3), 167923.

Milton, M.E., Cavanagh, J., Lochhead, A., Smith, R. and Smith, L. (2023) The biofilm regulatory network from *Bacillus subtilis*: master regulators, signal integration, and architecture. *Journal of Molecular Biology*. Vol.435(20), pp.167900.

Möhle, R.B., Langemann, T., Haesner, M., Augustin, W., Scholl, S., Neu, T.R., Hempel, D.C. and Horn, H. (2007) Structure and shear strength of microbial biofilms as determined with confocal laser scanning microscopy and fluid dynamic gauging using a novel rotating disc biofilm reactor. *Biotechnology and Bioengineering*. Vol.98(4), pp.747–755.

Nadell, C.D., Xavier, J.B. and Foster, K.R. (2010) The sociobiology of biofilms. *FEMS Microbiology Reviews*. Vol.33(1), pp. 206–224.

Nadell, C.D., Drescher, K. and Foster, K.R. (2016) Spatial structure, cooperation and competition in biofilms. *Nature Reviews Microbiology*. Vol.14(9), pp. 589–600.

Neu, T.R. and Lawrence, J.R. (2010) Investigation of microbial biofilm structure by laser scanning microscopy. *Advances in Biochemical Engineering/Biotechnology*. Vol.146, pp. 1–51.

Ng, W.-L. and Bassler, B.L. (2009) Bacterial quorum-sensing network architectures. *Annual Review of Genetics*. Vol.43, pp.197–222.

Oliveira, I.M., Gomes, I.B., Simões, L.C. and Simões, M. (2024) A review of research advances on disinfection strategies for biofilm control in drinking water distribution systems. *Water Research*. Vol.253, p.121273.

Oliveira, N.M., Niehus, R. and Foster, K.R. (2014) Evolutionary limits to cooperation in microbial communities. *Proceedings of the National Academy of Sciences USA*. Vol.111, pp.17941–17946.

Oliveira, N.M., Martinez-Garcia, E. and Foster, K.R. (2015) Why do bacteria form biofilms?. *Current Biology*. Vol.25(13), pp. 593–596.

Otto, M. (2013) Staphylococcal infections: mechanisms of biofilm maturation and detachment as critical determinants of pathogenicity. *Annual Review of Medicine*. Vol.64, pp.175–188.

Palma, C.S.D., Igoshin, O.A., Fujita, M. and Losick, R. (2025) Changes in Spo0A~P pulsing frequency control biofilm matrix deactivation and sporulation thresholds in *Bacillus subtilis*. *PLOS Computational Biology*. Vol.21(4), pp.e1013263.

Parsek, M.R. and Greenberg, E.P. (2005) Sociomicrobiology: the connections between quorum sensing and biofilms. *Trends in Microbiology*. Vol.13(1), pp.27–33.

Paul, E., Ochoa, J.C., Pechaud, Y., Liu, Y. and Liné, A. (2012) Effect of shear stress and growth conditions on detachment and physical properties of biofilms. *Water Research*. Vol.46(17), pp.5499–5508.

Percival, S.L., Suleman, L., Vuotto, C. and Donelli, G. (2015) Healthcare-associated infections, medical devices and biofilms: risk, tolerance and control. *Journal of Medical Microbiology*. Vol.64(4), pp. 323–334.

Peterson, B.W., Busscher, H.J., van der Mei, H.C. and Sharma, P.K. (2013) A distinguishable role of extracellular DNA in the viscoelastic relaxation of biofilms. *mBio*. Vol.4(4), e00103-13.

Petrova, O.E. and Sauer, K. (2012) Sticky Situations: Key components that control bacterial surface attachment. *Journal of Bacteriology*. Vol.194(10), pp. 2413–2430.

Peschel, A. and Otto, M. (2013) Phenol-Soluble Modulins and staphylococcal infection. *Nature Reviews Microbiology*. Vol.11(10), pp.667–673.

Picioreanu, C., van Loosdrecht, M.C.M. and Heijnen, J.J. (2001) Two-dimensional model of biofilm detachment caused by internal stress from liquid flow. *Biotechnology and Bioengineering*. Vol.72(2), pp.205–218.

Pinto, R.M., Soares, F.A., Reis, S., Nunes, C., and Van Dijck, P. (2020) Innovative strategies toward the disassembly of the EPS matrix in bacterial biofilms. *Frontiers in Microbiology*. Vol.11, article 952.

Piyasena, P., Mohareb, E. and McKellar, R.C. (2003) Inactivation of microbes using ultrasound: a review. *International Journal of Food Microbiology*. Vol.87(3), pp.207–216.

Portas, A., Tessier, B., Basset, J.-M. and Mullineaux, L. (2024) Shear stress regulates biomass, EPS production and community structure in marine microbial biofilms. *Environmental Microbiome*. Vol.19, 47.

Pousti, M., Zarabadi, M.P., Abbaszadeh Amirdehi, M., Paquet-Mercier, F. and Greener, J. (2019) Microfluidic bioanalytical flow cells for biofilm studies: a review. *Analyst*. Vol.144, pp.68–86.

Purevdorj, B., Costerton, J.W. and Stoodley, P. (2002) Influence of hydrodynamics and cell signaling on the structure and behavior of *Pseudomonas aeruginosa* biofilms. *Applied and Environmental Microbiology*. Vol.68(9), pp.4457–4464.

Pusparizkita, Y.M., Aslan, C., Schmahl, W.W., Devianto, H., Harimawan, A., Setiadi, T., Ng, Y.J., Bayuseno, A.P. and Show, P.L. (2023) Microbiologically influenced corrosion of the ST-37 carbon steel tank by *Bacillus licheniformis* present in biodiesel blends. *Biomass and Bioenergy*. Vol.168, Article 106653.

Rodríguez-López, P., Rodríguez-Herrera, J.J., Vázquez-Sánchez, D., López Cabo, M. and Prado, M. (2019) Current knowledge on Listeria monocytogenes biofilms in food-related environments: Incidence, resistance to biocides, ecology and biocontrol. *Foods*. Vol.8(11), p. 395.

Rittmann, B.E. and McCarty, P.L. (2001) Environmental Biotechnology: Principles and Applications. New York: McGraw-Hill.

Rochex, A., Godon, J.J., Bernet, N. and Escudié, R. (2008) Role of shear stress on composition, diversity and dynamics of biofilm bacterial communities. *Water Research*. Vol.42(6-7), pp.4915–4922.

Rodesney, C.A., Roman, B., Dhamani, N., Cooley, B.J., Mishra, M., Pine, D.J. and Goulian, M. (2017) Mechanosensing of shear by Pseudomonas aeruginosa stimulates biofilm development. *Proceedings of the National Academy of Sciences USA*. Vol.114(23), pp.12362–12367.

Romero, D., Aguilar, C., Losick, R. and Kolter, R. (2010) Amyloid fibers provide structural integrity to *Bacillus subtilis* biofilms. *Proceedings of the National Academy of Sciences*. Vol.107(5), pp. 2230–2234.

Rumbaugh, K.P. and Sauer, K. (2020) Biofilm dispersion. *Nature Reviews Microbiology*. Vol.18(10), pp. 571–586.

Rusconi, R., Lecuyer, S., Guglielmini, L. and Stone, H.A. (2010) Laminar flow around corners triggers the formation of biofilm streamers. *Journal of the Royal Society Interface*. Vol.7(50), pp. 1293–1299.

Rusconi, R., Lecuyer, S., Guglielmini, L. and Stone, H.A. (2011) Secondary flow as a mechanism for the formation of biofilm streamers. *Biophysical Journal*. Vol.100(6), pp.1392–1399.

Rusconi, R., Garren, M. and Stocker, R. (2014) Microfluidics expanding the frontiers of microbial ecology. *Annual Review of Biophysics*. Vol.43, pp. 65–91.

Rusconi, R. and Stocker, R. (2015) Microbes in flow. *Current Opinion in Microbiology*. Vol.25, pp.1–8.

Salta, M., Wharton, J.A., Blache, Y., Stokes, K.R. and Briand, J.F. (2013) Marine biofilms on artificial surfaces: structure and dynamics. *Environmental Microbiology*. Vol.15(11), pp.2879–2893.

Sanderson, J.B. (1871) Report on the cholera epidemic of 1866 in England. Appendix 1: Microscopic examination of the intestinal mucous membrane in cholera. London: Her Majesty's Stationery Office.

Sauer, K. and Camper, A.K. (2001) Characterization of phenotypic changes in *Pseudomonas putida* in response to surface-associated growth. *Journal of Bacteriology*. Vol.183(22), pp. 6579–6589.

Sauer, K., Stoodley, P., Goeres, D.M., Hall-Stoodley, L., Burmølle, M., Stewart, P.S. and Bjarnsholt, T. (2022) The biofilm life cycle: expanding the conceptual model of biofilm formation. Nature Reviews Microbiology. Vol.20, pp. 608–620.

Schultz, M.P., Bendick, J.A., Holm, E.R. and Hertel, W.M. (2011) Economic impact of biofouling on a naval surface ship. *Biofouling*. Vol.27(1), pp. 87–98.

Schwartz, K., Syed, A.K., Stephenson, R.E., Rickard, A.H. and Boles, B.R. (2012) Functional amyloids composed of phenol-soluble modulins stabilize Staphylococcus aureus biofilms. *PLOS Pathogens*. Vol.8(8), e1002744.

Seručnik, M., Dogsa, I., Zadravec, L.J., Mandic-Mulec, I., Žnidaršič-Plazl, P. and Gáspár, A. (2024) Development of a microbioreactor for *Bacillus subtilis* biofilm cultivation. *Micromachines*. Vol.15(8), p.1037.

Simunič, U., Pipp, P., Dular, M. and Stopar, D. (2020) The limitations of hydrodynamic removal of biofilms from the dead-ends in a model drinking water distribution system. *Water Research*. Vol.1(170), p. 115838.

Singha, P., Locklin, J. and Handa, H. (2016) A review of the recent advances in antimicrobial coatings for urinary catheters. *Acta Biomaterialia*. Vol.50, pp.20–40.

Stewart, P.S. and Franklin, M.J. (2008) Physiological heterogeneity in biofilms. *Nature Reviews Microbiology*. Vol.6(3), pp. 199–210.

Stoodley, P., Lewandowski, Z., Boyle, J.D. and Lappin-Scott, H.M. (1999) Structural deformation of bacterial biofilms caused by short-term fluctuations in fluid shear: an in situ investigation of biofilm rheology. *Biotechnology and Bioengineering*. Vol.65(1), pp. 83–92.

Stoodley, P., Sauer, K., Davies, D.G. and Costerton, J.W. (2002) Biofilms as complex differentiated communities. *Annual Review of Microbiology*. Vol.56, pp. 187–209.

Strauch, M.A., Webb, V., Spiegelman, G.B., Burbulys, D. and Hoch, J.A. (1990) Spo0A is a direct transcriptional repressor of the transition-state regulator AbrB in *Bacillus subtilis*. *Proceedings of the National Academy of Sciences USA*. Vol.87(10), pp.4129–4133.

Tang, Y., Chen, Y., Qi, Y.-D., Yan, H.-Y., Peng, W.-A., Wang, Y.-Q., Huang, Q.-X., Liu, X.-H., Ye, J.-J., Yu, Y., Zhang, X.-Z. and Huang, C. (2025) Engineered *Bdellovibrio bacteriovorus* enhances antibiotic penetration and biofilm eradication. *Journal of Controlled Release*. Vol.380, pp.283–296.

Towler, B.W., Rupp, C.J., Cunningham, A.L.B. and Stoodley, P. (2003) Viscoelastic properties of a mixed culture biofilm from rheometer creep analysis. *Biofouling*. Vol.19(5), pp.279–285.

Tsagkari, E., Connelly, S., Liu, Z., McBride, A. and Sloan, W.T. (2022) The role of shear dynamics in biofilm formation. *npj Biofilms and Microbiomes*. Vol.8(1), Article 33.

Valiei, A., Kumar, A., Mukherjee, P.P., Liu, Y. and Thundat, T. (2012) A web of streamers: biofilm formation in a porous microfluidic device. *Lab on a Chip*. Vol.12(24), pp.5133–5137.

Valladares Linares, R., Wexler, A. D., Bucs, S., Dreszer, C., Zwijnenburg, A., Flemming, H.-C., Kruithof, J. C. and Vrouwenvelder, J. S. (2015) Compaction and relaxation of biofilms. *Desalination and Water Treatment*. Vol.57(28), pp.12902–12914.

van Gestel, J., Vlamakis, H. and Kolter, R. (2014) From cell differentiation to cell collectives: *Bacillus subtilis* uses division of labor to migrate. *PLoS Biology*. Vol.12(4), e1001891.

van Meer, B.J.G., de Moggio, R., Zhuang, Z., Rana, A., Smith, L. and Ten Haken, B. (2017) Small molecule absorption by PDMS in the context of drug assays. *Lab on a Chip*. Vol.16(19), pp.3232–3240.

Verhamme, D.T., Kiley, T.B. and Stanley-Wall, N.R. (2007) DegU co-ordinates multicellular behaviour exhibited by *Bacillus subtilis*. *Molecular Microbiology*. Vol.65(2), pp.554–568.

Vlamakis, H., Aguilar, C., Losick, R. and Kolter, R. (2008) Control of cell fate by the formation of an architecturally complex bacterial community. *Genes & Development*. Vol.22(7), pp.945–953.

Vlamakis, H., Aguilar, C., Losick, R. and Kolter, R. (2013) Sticking together: building a biofilm the *Bacillus subtilis* way. *Journal of Bacteriology*. Vol.195(6), pp. 1173–1179.

Walters, M.C., Roe, F., Bugnicourt, A., Franklin, M.J. and Stewart, P.S. (2003) Contributions of antibiotic penetration, oxygen limitation, and low metabolic activity to tolerance of *Pseudomonas aeruginosa* biofilms to ciprofloxacin and tobramycin. *Antimicrobial Agents and Chemotherapy*. Vol.47(1), pp. 317–323.

Wang, B., Wei, P.-W., Wan, S., Yao, Y., Song, C.-R., Song, P.-P., Xu, G.-B., Hu, Z.-Q., Zeng, Z., Wang, C. and Liu, H.-M. (2021) *Ginkgo biloba* exocarp extracts inhibit *S. aureus* and MRSA by disrupting biofilms and affecting gene expression. *Journal of Ethnopharmacology*. Vol.271, p.113895.

Wang, Z., Li, L., Ariss, R.W., Coburn, K.M., Behbahani, M., Xue, Z. and Seo, Y. (2021) The role of biofilms on the formation and decay of disinfection by-products in chlor(am)inated water distribution systems. *Science of the Total Environment*. Vol.753, p.141606.

Wanner, O., Morgenroth, E., Eberl, H., Noguera, D., Rittmann, B.E., Van Loosdrecht, M.C.M. and Yuan, Z. (2006) Mathematical Modeling of Biofilms. London: IWA Publishing.

Webster, S.S., Harrison, J.J., Fulcher, N.B., Yarrington, C.D., and O'Toole, G.A. (2022) Type IV pili tip-signaling drives surface sensing and c-di-GMP induction in *Pseudomonas aeruginosa*. *Journal of Bacteriology*. Vol.204(15), e00084-22.

Wei, G. and Yang, J.Q. (2023) Microfluidic investigation of the impacts of flow fluctuations on the development of *Pseudomonas putida* biofilms. *NPJ Biofilms and Microbiomes*. Vol.9(73).

Whitchurch, C.B., Tolker-Nielsen, T., Ragas, P.C. and Mattick, J.S. (2002) Extracellular DNA required for bacterial biofilm formation. *Science*. Vol.295(5559), pp.1487–1487.

Whiteley, M., Bangera, M.G., Bumgarner, R.E., Parsek, M.R., Teitzel, G.M., Lory, S. and Greenberg, E.P. (2001) Gene expression in *Pseudomonas aeruginosa* biofilms. *Nature*. Vol.413(6858), pp. 860–864.

Wittig, C., Wagner, M., Vallon, R., Crouzier, T., van der Wijngaart, W., Horn, H. and Bagheri, S. (2025) The role of fluid friction in streamer formation and biofilm growth. *npj Biofilms and Microbiomes*. Vol.11(1), Article 17.

Wu, V.C.H., Kim, B., Balasubramaniam, V.M., Hsueh, Y.H. and Zhang, H. (2016) Strategies and challenges for control of *Listeria monocytogenes* in food processing environments. *Journal of Food Protection*. Vol.79(3), pp.387–398.

Wu, R., Kong, L.-X. and Liu, F. (2024) Regulation of biofilm gene expression by DNA replication in *Bacillus subtilis*. *Journal of Cellular and Molecular Medicine*. Vol.28(12), p.e18481.

Xavier, J.B., Picioreanu, C., Rani, S.A., van Loosdrecht, M.C. and Stewart, P.S. (2005) Biofilm-control strategies based on enzymic disruption of the extracellular polymeric substance matrix—a modelling study. *Microbiology*. Vol.151(12), pp.3817—3832.

Zhang, R., Lin, H., Wang, Z., Xu, Y., Chen, X. and Li, P. (2025) Research progress on antimicrobial biomaterials. *Macromolecular Bioscience*. [preprint].

Zimlichman, E., Henderson, D., Tamir, O., Franz, C., Song, P., Yamin, C.K., Keohane, C., Denham, C.R. and Bates, D.W. (2013) Health care—associated infections: a meta-analysis of costs and financial impact on the US health care system. *JAMA Internal Medicine*. Vol.173(22), pp.2039–2046.

Zlatanović, L., van der Hoek, J.P. and Vreeburg, J.H.G. (2017) An experimental study on the influence of water stagnation and temperature change on water quality in a full-scale domestic drinking water system. *Water Research*. Vol.123, pp.761–772.

# 2. Investigating the Antibiofilm and Antimicrobial Activity of *Ginkgo biloba* Leaf Extract Against *Bacillus subtilis* Static Biofilms

#### 2.1. Abstract

Biofilm development is fundamental for bacterial resilience. Biofilms represent a problem across clinical and environmental settings, due to their resistance to antimicrobials. In this study, the antibiofilm effect of *Gingko biloba* leaf extract (GBLE) is investigated in static *gfp*-expressing *Bacillus subtilis* (*B. subtilis*) JWV042 pellicle biofilms.

Using standard microbiological techniques, fluorescent imaging and molecular techniques, it was possible to study the behaviour of *B. subtilis* biofilms at different concentrations of GBLE. Results show that the extract has an antibiofilm activity rather than bactericidal, inhibiting biofilm formation but having a smaller impact on bacterial growth. A concentration-dependent biofilm inhibitory effect was observed for both agar and static biofilms. Impacts on biofilm morphology are also observed, as findings suggest cellular differentiation occurrence in response to GBLE. Confocal laser scanning microscopy reveals a concentration-dependent effect on static biofilm development and morphology, resulting in highly organized filaments. Fluorescent microscopy also shows localized fluorescence in the centre of the bacterial cells, indicating that GBLE is inducing intracellular changes. Biofilm matrix and amyloids production microscopic analysis revealed an increase in amyloid production and the presence of cell types specialized in amyloid production.

This study indicates the mechanisms employed by *B. subtilis* JWV042 to overcome challenging environmental conditions, including cellular differentiation and increased extracellular matrix components production, which allow the biofilm to persist in adverse environmental conditions. Additionally, findings highlight the potential of GBLE for biofilm control.

#### 2.2. Introduction

At present, biofilms in industrial settings are usually treated with disinfectants. Disinfectants used for cleaning include quaternary ammonium compounds, hypochlorites, aldehydes, amphoteric compounds and phenolics. The main classes of disinfectants used in healthcare and industry have remained largely unchanged for decades, relying on quaternary

ammonium compounds, hypochlorites, aldehydes, amphoteric compounds, and phenolics (Maillard, 2005). With the emergence of antimicrobial resistance and the lack of novel antimicrobial compounds, the use of plant-derived antimicrobials is becoming more widespread (Khameneh et al., 2019).

Gingko biloba is a tree belonging to the Gingkoaceae family, native to Eastern Asia. It dates back to 200 million years ago and it has been widely used in Traditional Chinese Medicine (TCM). Many parts of this tree, such as leaves and seeds, are used for the treatment of a variety of diseases, including lung, heart and memory-associated disorders (Chassagne et al., 2019) (Isah, 2015) (Mahady, 2001). Gingko biloba extracts have also gained interest due to their antibacterial and antibiofilm effect. For example, Chassagne et al. (2019) have demonstrated the effectiveness of Gingko biloba seeds against common skin pathogens Cutibacterium acnes (C. acnes), Staphylococcus aureus (S. aureus) and Streptococcus pyogenes (S. pyogenes). In their study, researchers extracted compounds from different Ginkgo biloba components, such as seed coats, immature seeds, branches, and kernels, using a range of different solvents. These were tested against clinically relevant skin pathogens and out of 27 extracts, 18 exhibited growth inhibitory effects against at least one bacterial strain, with immature seeds and seed coats showing the strongest activity. Anti-biofilm activity was also observed, mainly on S. aureus, and one extract inhibited C. acnes biofilms. Chemical analysis of their extracts revealed that Ginkgolic acid C15:1 was the most potent antibacterial compound, strongly correlating with the inhibitory activity of ethanol-based extracts. However, this compound also demonstrated notable cytotoxicity toward human keratinocyte cell lines, raising concerns about its potential for safe topical application. Despite its potency, the therapeutic index of most extracts remained modest, with the exception of those from immature seeds and seed coats (Chassagne et al., 2019).

Other studies have shown the ability of *Gingko Biloba* extracts in inhibiting *S. aureus* and methicillin-resistant *S. aureus* (MRSA) biofilms (Wang et al., 2021). Wang et al. (2021) assessed the antibacterial and antibiofilm properties of *Ginkgo biloba* exocarp extract and their findings showed potent antibacterial activity, with minimum inhibitory concentrations (MICs) of 4  $\mu$ g/mL and minimum bactericidal concentrations (MBCs) of 8  $\mu$ g/mL against *S. aureus* and MRSA. Importantly, their *Ginkgo biloba* extract also exhibited strong antibiofilm activity, inhibiting the formation of MRSA and *S. aureus* biofilms in a concentration-dependent manner. At a higher concentration (12  $\mu$ g/mL), the extract was also effective in

disrupting mature biofilms, highlighting the strong potential of *Ginkgo biloba* as a plant-based antibiofilm agent (Wang et al., 2021).

Wang et al. (2021) highlighted how the expression of biofilm-associated genes in *S. aureus* was affected by the presence of *Ginkgo biloba* exocarp extracts in the medium. At the molecular level, real-time PCR revealed that *Ginkgo biloba* exocarp extracts influenced the expression of biofilm-regulatory and virulence-associated genes in MRSA. Interestingly, *Ginkgo biloba* exocarp extracts downregulated the expression of master regulators of biofilm development, as well as a gene associated with toxin production (Wang et al., 2021). Additionally, *Ginkgo biloba* exocarp extracts suppressed the synthesis of staphyloxanthin, a molecule that contributes to MRSA's resistance to oxidative stress and host immune responses (Wang et al., 2021). The findings of this study indicate the promising potential for *Ginkgo biloba* exocarp extracts as a natural antibacterial and antibiofilm agent.

Many other plant extracts, *Coptis chinensis*, *Scutellaria baicalensis*, have exhibited antimicrobial properties against bacteria including *E. coli*, *S. aureus* and *Micrococcus luteus* (*M. luteus*) (Muluye et al., 2014) (Leach et al., 2011) (Zhao, Chen and Martin, 2016).

Enterohemorrhagic E. coli O157:H7 (EHEC) is a common cause of disease in humans, as the bacteria can colonise and form biofilms in the large intestine (Lee et al., 2014). EHEC can also develop biofilms on plants as well as glass and various abiotic surfaces (Lee et al., 2014). EHEC is also a major foodborne pathogen. In a screen of 560 plant-derived compounds Lee et al. (2014) concluded that Ginkgolic acid C15:1 is of the most effective inhibitors of EHEC biofilm formation, with >90% reduction at 5 µg/mL. Interestingly, this antibiofilm effect occurred without inhibiting bacterial growth, reducing the risk of promoting antibiotic resistance (Lee et al., 2014). Both Ginkgolic acids C15:1 and C17:1, along with the whole Ginkgo biloba extract, significantly inhibited biofilm formation on polystyrene, nylon, and glass surfaces. Confocal microscopy and SEM revealed that this inhibition was accompanied by a marked reduction in fimbriae production, a key structural component of EHEC biofilms (Lee et al., 2014). While Lee et al. (2014) established proof-of-concept that Ginkgo-derived compounds can disrupt EHEC biofilm development on abiotic surfaces, that work was limited to a Gram-negative enteric pathogen under laboratory conditions and did not examine environmentally and industrially relevant Gram-positive model organisms and biofilm formers such as Bacillus subtilis (B. subtilis). The present study addresses these gaps by testing Ginkgo biloba leaf extract (GBLE) across growth and biofilm assays in B. subtilis, examining colony morphology, microscopic structure, and amyloid-associated matrix signals using fluorescence-based approaches.

Bacillus spp. frequently colonize food-processing and agricultural equipment, and their resistant spores and matrix-embedded cells can survive routine sanitation, developing recurrent biofilms in dairy and other food systems (Galié et al., 2018) (Ostrov et al., 2019). B. subtilis is a Gram-positive microorganism commonly found in plants and soils and being a highly characterised model organism for microbiological study, a wide range of genetic and molecular techniques are available (Arnaouteli et al., 2021). Because B. subtilis is a non-pathogenic, soil- and plant-associated species that forms architecturally complex biofilms and is a well-established genetic model system, it provides a powerful model for developing and evaluating biofilm control strategies relevant to industrial systems (Arnaouteli et al., 2021) (Dogša et al., 2024).

*B. subtilis* cells can form at least three types of biofilms *in vitro*, including surface-attached biofilms submerged in a medium (Arnaouteli et al., 2021). Beyond its diverse biofilm morphotypes, *B. subtilis* populations readily specialise into motile, matrix-producing, sporulating, competent and other specialized subpopulations in response to external signals such as nutrient limitation, surface/oxygen gradients, and plant-derived molecules encountered on roots, making the species a powerful readout for how environmental cues drive bacterial cell-fate decisions. (Dogša et al., 2024) (Beauregard et al., 2013) (Kuchina et al., 2011) (Vlamakis et al., 2013).

The lack of knowledge of biofilm development in non-laboratory environments along with the lack of novel antimicrobials must push for a broader screen of potential antimicrobial compounds that are also able to inhibit and control biofilm development in a sustainable and environmentally friendly manner. There is an increasing demand for non-toxic antibacterial and antimicrobial agents in industrial disinfection, particularly in food processing, agriculture, and water treatment, where microbial contamination and biofilm formation affect both public health and operational safety (Jones, 2021) (Liu et al., 2021). Traditional chemical disinfectants such as chlorine compounds, quaternary ammonium salts, and oxidizing agents, although effective, often pose significant risks (Carrascosa et al., 2021) (Zhang et al., 2021) (Ng, 2025). Their widespread and repeated use can lead to the release of hazardous residues into the environment, leading to soil contamination and water systems (Bondarczuk et al., 2016) (Dai et al., 2020). These chemical residues can disrupt microbial communities, reduce

soil fertility, and negatively impact aquatic ecosystems (Zhang et al., 2021) (Dai et al., 2020). Furthermore, persistent antimicrobial chemicals can accumulate through the food chain, threatening higher organisms and contributing to long-term ecological imbalances (Martínez, 2009). Additionally, environmental exposure to sublethal concentrations of these agents may promote antimicrobial resistance (AMR) in environmental microbial communities, which can ultimately spread to pathogens (Baquero et al., 2008) (Singer et al., 2016). Therefore, there is a need to develop and implement biodegradable, plant-derived antimicrobial and antibiofilm alternatives that are effective and safe for both humans and the environment.

Although *Ginkgo biloba*-derived compounds have shown antibiofilm or antibacterial activity against several clinically oriented targets, such as *E. coli* O157:H7, *S. aureus*/MRSA, and common skin pathogens (Lee et al., 2014) (Wang et al., 2021) (Chassagne et al., 2019), the published studies are limited in scope. Most have examined seed or exocarp extracts, focused on a small set of human-associated bacteria, and relied primarily on planktonic MIC/MBC determinations or bulk/end-point biofilm biomass assays with relatively coarse structural readouts. Consequently, little is known about how *Ginkgo*-derived materials influence biofilm architecture, matrix organization, or cellular differentiation in other bacterial species.

In the present study, *Ginkgo biloba* leaf extract (GBLE), chemically distinct from the seed/exocarp fractions previously investigated, was evaluated for its antibiofilm effects on *B. subtilis*. We deliberately combine complementary scales of analysis: planktonic growth curves to distinguish growth inhibition from biofilm-specific effects; microtiter dish biofilm assays to quantify early biofilm formation across a concentration gradient; colony agar biofilms to assess surface architecture and macroscopic morphology; and fluorescence microscopy of static biofilms, including an extracellular matrix (ECM)-associated amyloid probe (EbbaBiolight 680), to visualize structural responses and potential shifts in matrix component distribution. To our knowledge, this integrated workflow has not previously been applied to *Ginkgo* extracts, nor has *B. subtilis* been investigated in this context.

The findings of this study contribute to the knowledge in understanding how bacteria modulate their physiology to overcome challenging environments, in this case the presence of GBLE. Furthermore, this work further highlights the potential of this natural compound for microbiological control.

## 2.3. Materials and Methods

# 2.3.1. Bacterial Strain, Culture Conditions and Growth Curves Measurements

*Gfp*-expressing *Bacillus subtilis* (JWV042 strain, Hbs-GFP endogenous localization, cat amyE::Phbs-hbs-gfp, cat marker) colonies on agar were obtained from Strathclyde Institute of SIPBS Pharmacy and Biomedical Sciences (SIPBS). A flask containing 150 mL of Luria-Bertani (LB) broth (Sigma-Aldrich) was inoculated with a colony from the plate and incubated overnight at 37°C. The cultures were supplemented with 5  $\mu$ g/mL chloramphenicol to ensure selection of *gfp* mutants. Glycerol stocks were made from the culture and stored at -80°C. The stocks were then used for the rest of this study.

GBLE powder was obtained from Wuhan ReCedar Biotechnology Co., Ltd (Wuhan, China). The extract was resuspended in RNAse-free water to make working solutions and was added to the culture media accordingly.

Prior each experiment, *B. subtilis* JWV042 was cultured in LB broth overnight at  $37^{\circ}$ C in a shaking incubator at 150 rpm. The OD<sub>600</sub> of the inoculum was measured prior inoculation in each experiment and was adjusted to 0.3. All experiments were carried out in triplicates on separate occasions, using freshly prepared cultures each time to ensure biological replication, unless stated otherwise. All bacterial cultures, including static and agar biofilms, were grown using LB media, supplemented with 5  $\mu$ g/mL chloramphenicol. All materials and reagent were sterile at the time of use and sample preparations was carried out in biological safety cabinets.

# 2.3.2. Impact of GBLE on Bacterial Planktonic Growth

In order to investigate the effect of the effect of GBLE on bacterial planktonic growth, growth curves were generated. A 96-well polystyrene microtiter plate was prepared with 150  $\mu$ L inocula containing increasing concentrations of GBLE, specifically 0, 50, 75, 100, 150, 175, 200, 300, 400, 500 and 600  $\mu$ g/mL, up to 8 replicates. Plates were incubated for 24 hours at 37°C and OD<sub>600</sub> measurements were automatically taken using a microplate spectrophotometer (BioTek). Measurements were taken for 24 hours at 30 minutes intervals.

# 2.3.3. Impact of GBLE on Static Biofilm Formation and Adhesion

Static biofilms were grown in 96-well polystyrene plates at different GBLE concentrations to investigate biofilm formation and bacterial adhesion. A *B. subtilis* culture was previously grown overnight and it was diluted 1:100 for the inoculum. Different inocula were prepared with different GBLE concentrations, namely 0, 50, 75, 100, 150, 175, 200, 300, 400, 500 and  $600 \,\mu\text{g/mL}$ .

150  $\mu L$  of inoculum was added in each well up to ten replicates. The 96-well plates were incubated overnight at 37°C and after incubation, unbound cells were discarded and the plates were washed several times by gently submerging them in a tub of water. Individual wells were stained with 185  $\mu L$  of 0.1% Crystal Violet and rinsed again after 10-15 minutes of incubation at room temperature. Once dry, 185  $\mu L$  of 30% acetic acid was added to each well to solubilize the crystal violet stain. Following 10-15 minutes of incubation, the 185  $\mu L$  solubilized Crystal Violet in each well was transferred to a new 96-well polystyrene plate. To quantify the amount of biofilm, the absorbance of each well was quantified using a plate reader (Epoch – BioTek Gen5) at 550 nm, using acetic acid as the blank.

# 2.3.4. Impact of GLBE Concentration on Bacterial Colony Morphology and Motility

Plastic petri dishes (Thermo Fisher Scientific) containing 0.3% or 0.6% (w/v) agar and graded concentrations of GBLE (0, 50, 75, 100, 150, 175, 200, 300, 400, 500, 600 μg/mL) were stab-inoculated with an overnight *B. subtilis* culture to assay motility. The 0.3% agar condition supports swimming, a largely single-cell, flagella-mediated movement through the aqueous phase within soft agar, whereas 0.6% agar promotes swarming, a coordinated multicellular surface translocation that often requires surfactant production. These behaviours were assessed because motility strongly influences initial surface colonization and the transition to biofilm development; changes in swimming or swarming under GBLE exposure help distinguish direct antibiofilm effects from upstream impacts on bacterial movement. Furthermore, agar plates also revealed macroscopic phenotypic changes in presence of different concentrations of GBLE. Plates were incubated at 37°C and pictures were taken after 24 and 48 hours of incubation.

# 2.3.5. Confocal Laser Scanning Microscopy

Gfp-expressing B. subtilis JWV042 static biofilms were cultured in sterile 6-well flat bottom polystyrene plates (Sigma-Aldrich) as stated in "Protocol I – Labelling of surface biofilms using EbbaBiolight" (EbbaBiotech.com) with minor modifications. Briefly, two sterile glass coverslip ( $22 \times 22$  mm, Thickness No. 1.5, VWR) were placed inside each well balanced against the walls on the well. Each well was inoculated with 1:100 diluted bacterial culture in LB broth supplemented with different concentrations of GBLE (0, 50, 75, 100, 200, 300, 400 and 500  $\mu$ g/mL). Plates were incubated for 48 hours at 37°C in static conditions.

Following incubation, *B. subtilis* static biofilms were attached to the glass coverslips. For imagining, the glass coverslips were removed from each well and after wiping the backside with 70% ethanol, they were placed on microscope slides ready for imaging.

In order to investigate extracellular matrix components (ECM) synthesis and intracellular and extracellular amyloid protein production in response to GBLE, a set of static biofilms were stained using EbbaBiolight 680. When using this dye, static biofilms were cultured as stated above, with the addition of the dye (1:1000 dilution) to the well.

Biofilm imaging was performed using a Leica Microsystems TCS SP5 confocal laser scanning microscope (Leica Microsystems, Germany) equipped with a motorised stage and high-numerical aperture (N. A.) objectives. The *gfp*-expressing *B. subtilis* JWV042 strain was excited using an argon laser at 488 nm, and emission was collected between 500–550 nm. In addition, samples stained with EbbaBiolight 680 were excited at 530 nm, and fluorescence emission was detected at 680 nm. High-resolution images were acquired with a 63 x /1.40 N. A. oil-immersion Plan-Apochromat objective ( $\approx 630 \text{ x}$  overall optical magnification through the eyepieces). Laser power and detector gain were kept constant across samples to allow comparative quantification. All image acquisition was carried out at room temperature using Leica LAS AF software.

#### 2.4. Results

# 2.4.1. Impact of GBLE on Bacterial Planktonic Growth

The effect of GBLE on bacterial cell replication of *B. subtilis* JVW042 was investigated by measuring the optical density of bacterial cultures over a 24 hour period. As seen in Fig. 2.2-2.7, bacterial replication displayed a concentration-dependent delay in the development of the log phase, with higher concentrations of GLBE causing longer delays in log phase

development. GBLE also seemed to accelerate cell death at concentrations between 50  $\mu$ g/mL and 300  $\mu$ g/mL, while it seemed to prolong the stationary phase for concentrations above 300  $\mu$ g/mL. These trends are summarised in Fig. 2.1.

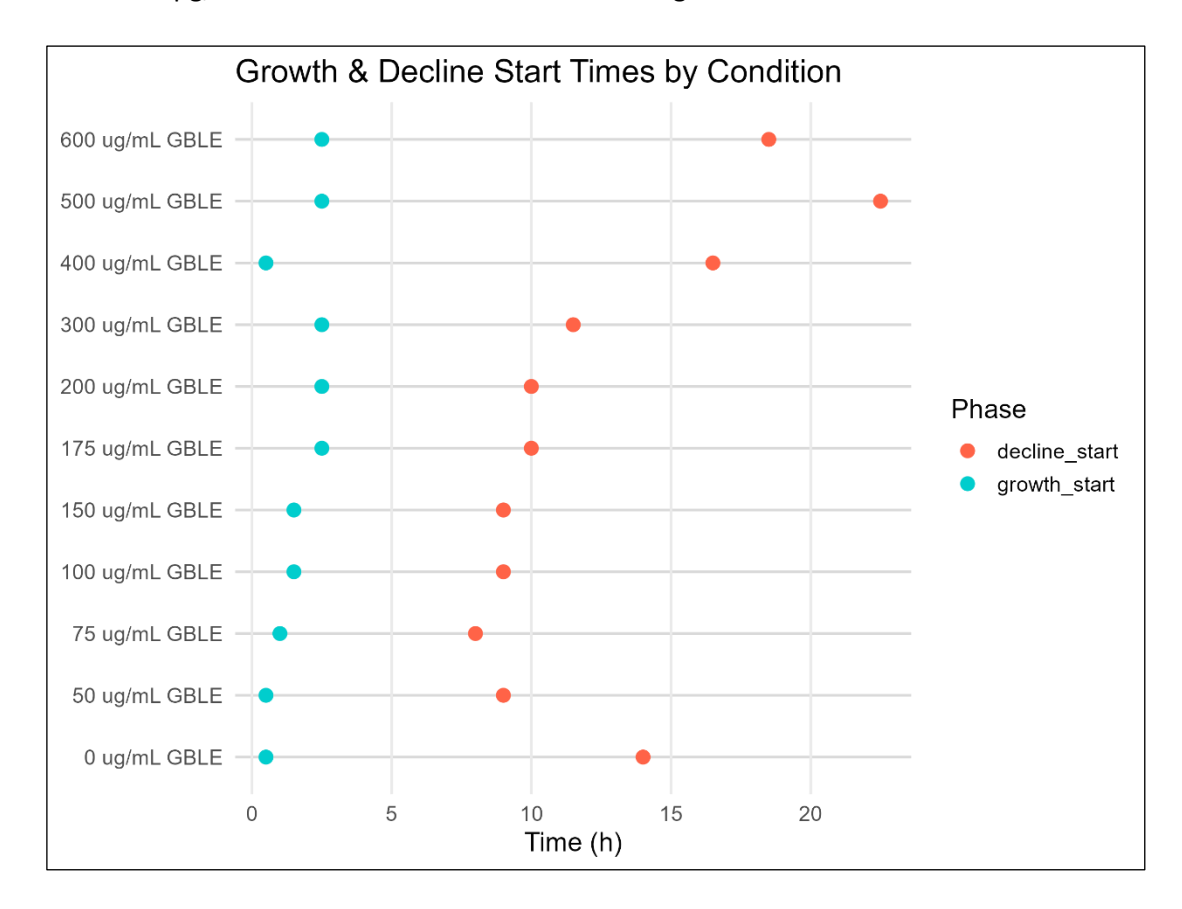


Figure 2.1. Growth (teal) and decline (salmon) start times from smoothed OD curves of cultures grown with increasing GBLE. Growth = first sustained  $\uparrow$ ; Decline = first sustained  $\downarrow$  after peak. Time in hours post-inoculation.

Although GBLE does affect cell growth, it does not seem to have a direct antibacterial effect on *B. subtilis* planktonic cultures, rather it seems to have a time-dependent bacteriostatic effect, as it is slowing bacterial proliferation without causing immediate cell death.

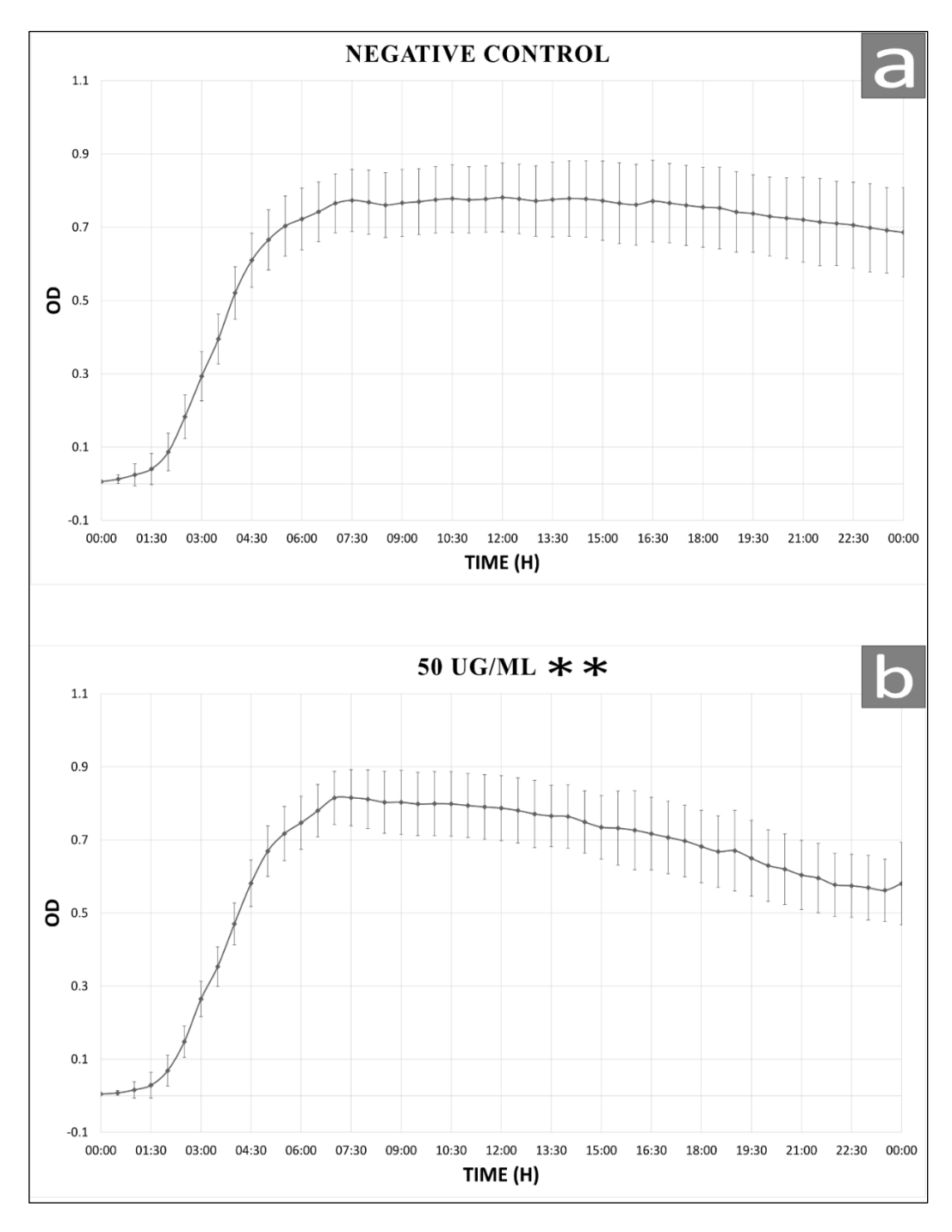


Figure 2.2. Bacillus subtilis planktonic growth curves at 0 and 50  $\mu$ g/mL Ginkgo biloba Leaf Extract, a and b respectively. The values were acquired every 30 minutes throughout a period of 24 hours. All data are presented as means  $\pm$  STDV and n = 8. \*P < 0.05, \*\*P < 0.005, \*\*\*P < 0.001 vs Negative Control.

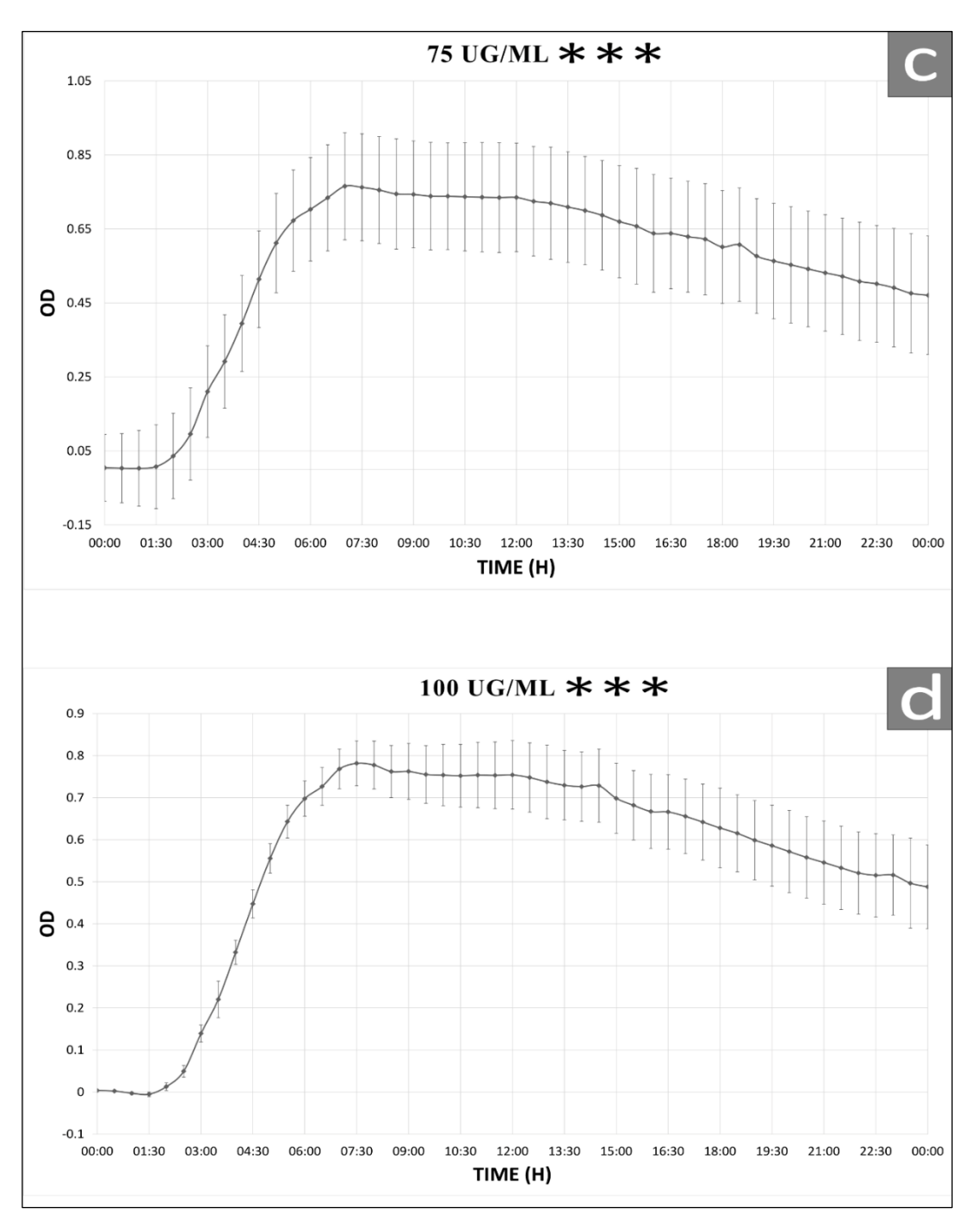


Figure 2.3. Bacillus subtilis planktonic growth curves at 75 and 100  $\mu$ g/mL Ginkgo biloba Leaf Extract, c and d respectively. The values were acquired every 30 minutes throughout a period of 24 hours. All data are presented as means  $\pm$  STDV and n = 8. \*P < 0.05, \*\*P < 0.005, \*\*\*P < 0.001 vs Negative Control.

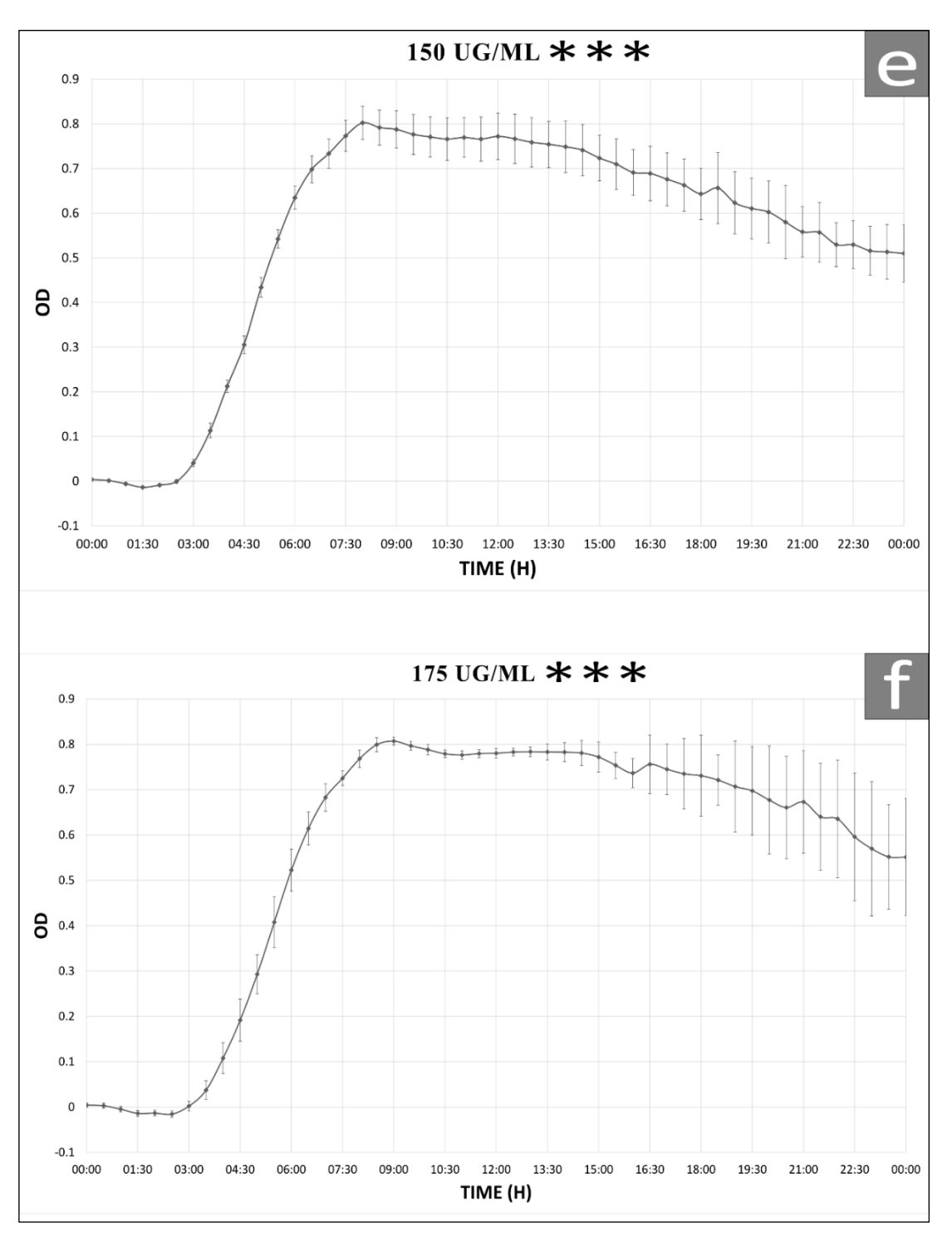


Figure 2.4. Bacillus subtilis planktonic growth curves at 150 and 175  $\mu$ g/mL Ginkgo biloba Leaf Extract, e and f respectively. The values were acquired every 30 minutes throughout a period of 24 hours. All data are presented as means  $\pm$  STDV and n = 8. \*P < 0.05, \*\*P < 0.005, \*\*\*P < 0.001 vs Negative Control.

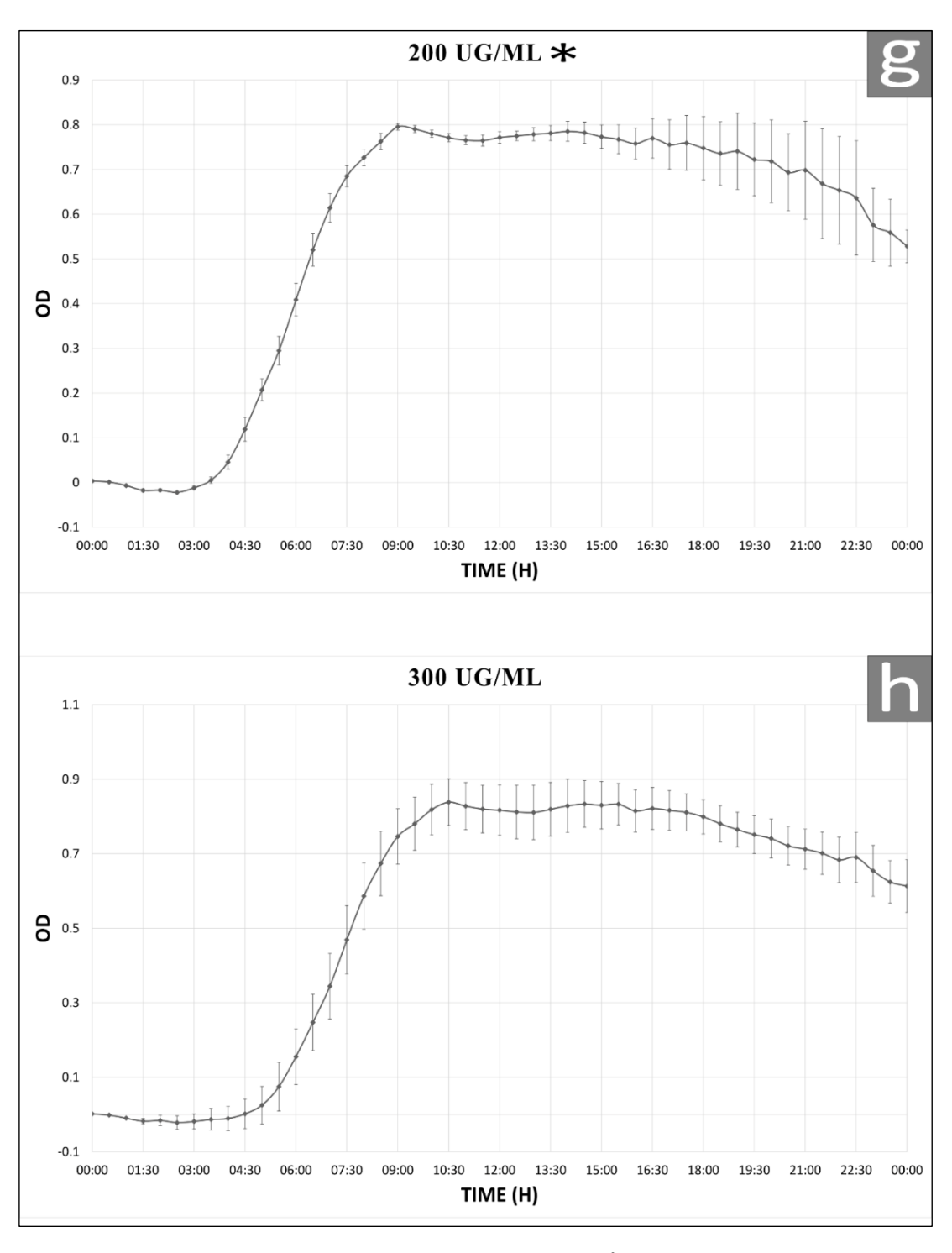


Figure 2.5. Bacillus subtilis planktonic growth curves at 200 and 300  $\mu$ g/mL Ginkgo biloba Leaf Extract, g and h respectively. The values were acquired every 30 minutes throughout a period of 24 hours. All data are presented as means  $\pm$  STDV and n = 8. \*P < 0.05, \*\*P < 0.005, \*\*P < 0.001 vs Negative Control.

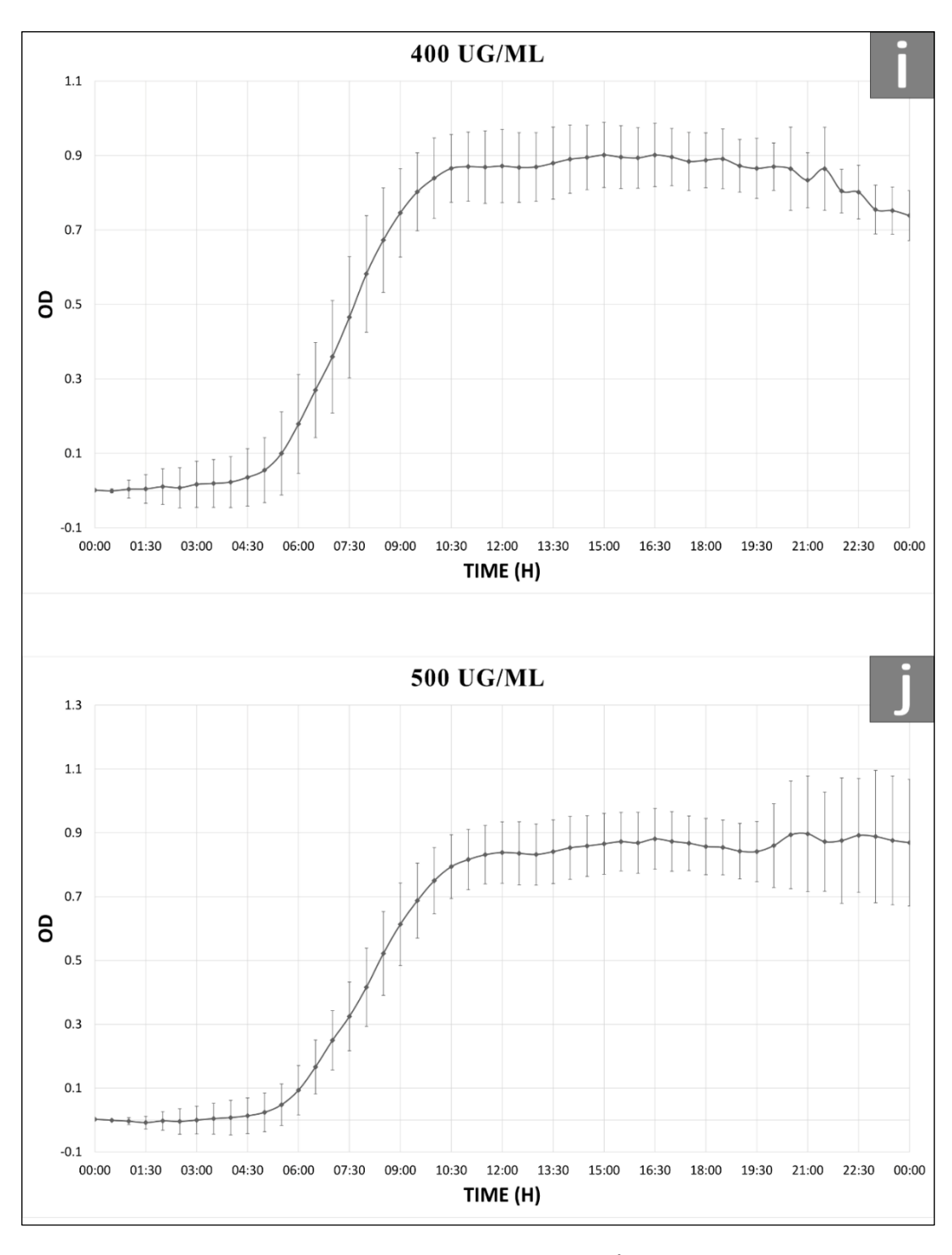


Figure 2.6. Bacillus subtilis planktonic growth curves at 400 and 500  $\mu$ g/mL Ginkgo biloba Leaf Extract, i and j respectively. The values were acquired every 30 minutes throughout a period of 24 hours. All data are presented as means  $\pm$  STDV and n = 8. \*P < 0.05, \*\*P < 0.005, \*\*P < 0.001 vs Negative Control.

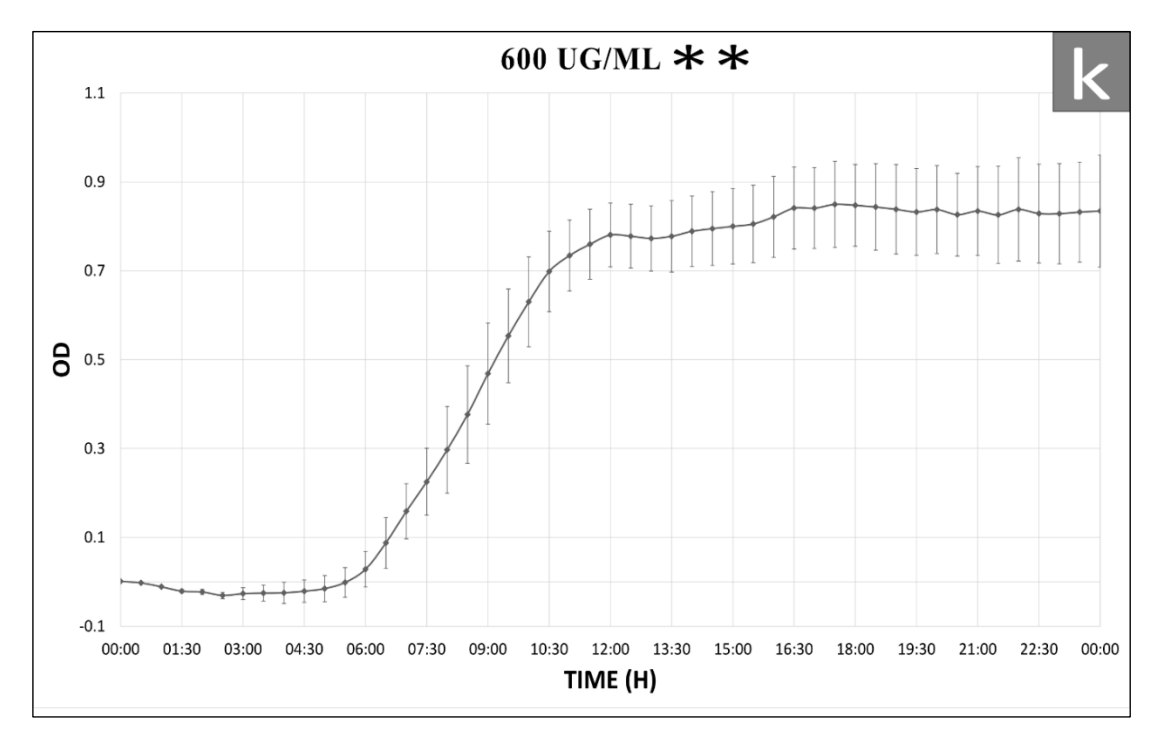


Figure 2.7. Bacillus subtilis planktonic growth curves at  $600 \,\mu\text{g/mL}$  Ginkgo biloba Leaf Extract, (k). The values were acquired every 30 minutes throughout a period of 24 hours. All data are presented as means  $\pm$  STDV and n = 8. \*P < 0.05, \*\*P < 0.005, \*\*P < 0.001 vs Negative Control.

# 2.4.2. Microtiter Dish Biofilm Assay

To investigate overall biofilm formation and attachment at different *Ginkgo biloba* concentrations, a microtiter dish biofilm assay was performed. In this assay, the amount of Crystal Violet stain, which indicates the amount of biofilm present, is quantified using spectrophotometry. As shown in Fig. 2.8, biofilm formation and attachment increased in concentrations up to 100 ug/mL of *Ginkgo biloba* compared to the control, followed by a concentration-dependent decrease in overall biofilm formation and surface attachment at concentrations of 150  $\mu$ g/mL and above, compared to the control.

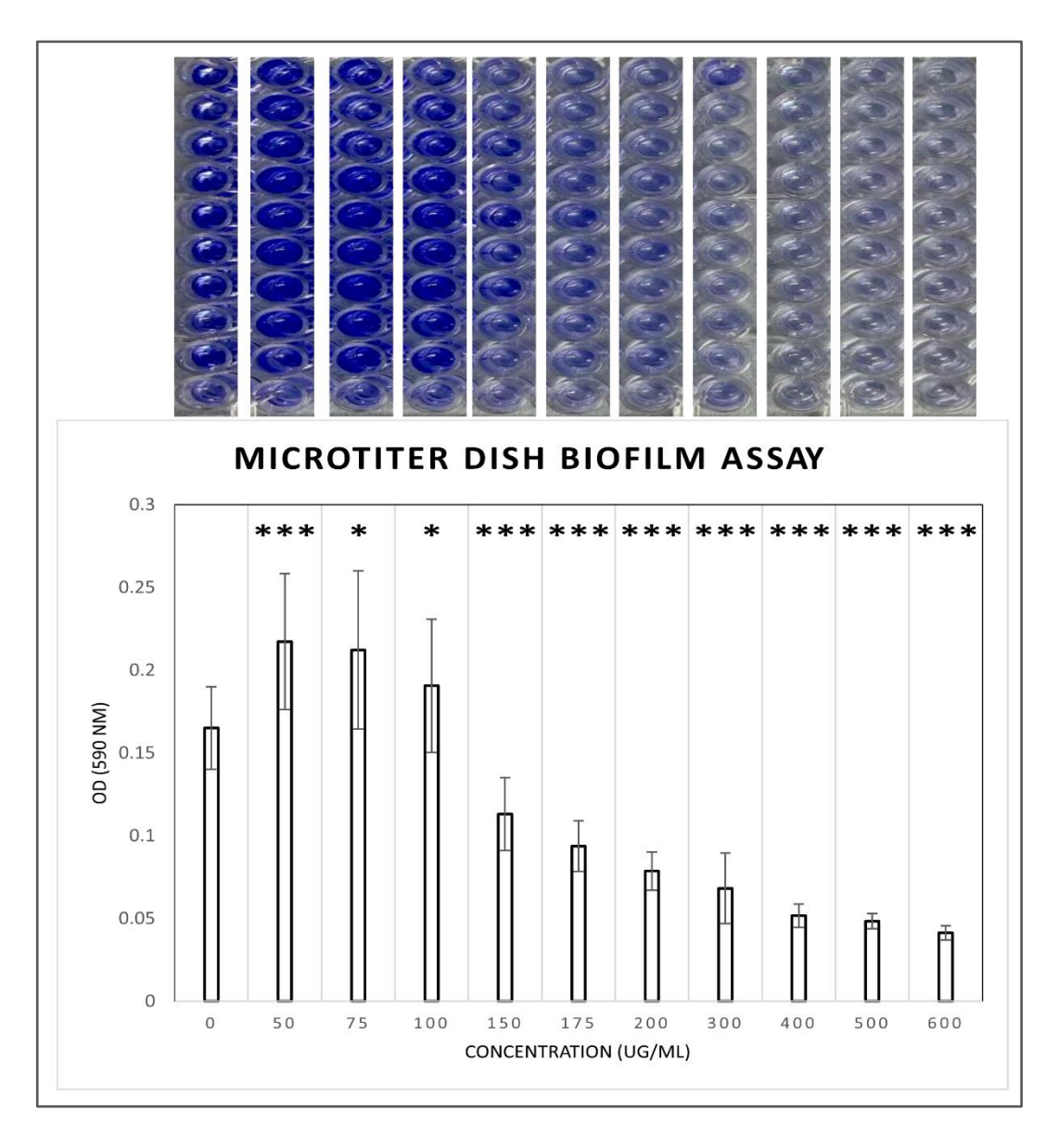


Figure 2.8. Histogram showing the mean value of optical density (590 mm), in relation to increasing concentrations of *Ginkgo biloba* leaf extract. All values are represented as mean values  $\pm$  STDV and n = 8. \*P < 0.05, \*\*P < 0.005, \*\*P < 0.001 vs Negative Control.

# 2.4.3. Bacterial Colony Morphology and Motility Assay

The effect of different concentrations of GBLE on bacterial colony morphology and motility was investigated by growing *B. subtilis* cultures at different agar concentrations on petri dishes (Fig. 2.9-2.20). Plates were imaged after 24 and 48 hours.

#### 2.4.3.1. Swimming Motility

0.3% agar plates were inoculated with overnight *B. subtilis* culture in order to study swimming motility and GBLE (Fig. 2.9-2.14). GBLE seemed to promote this type of motility in most GBLE concentrations in *B. subtilis*. This can be seen as early as after 24 hours of

incubation, where the control reaches an average of 29 mm colony diameter (Fig. 2.9a), while the cultures supplemented with GBLE spread much further and rapidly saturate the petri dish (Fig. 2.9b, c, d, Fig. 2.10 and Fig. 2.11).

GBLE appeared to influence biofilm morphology depending on the concentration. Filaments and punctiform colonies can be seen at relatively higher concentrations but do not appear at lower concentrations. Unlike most plates, the culture grown at 400  $\mu$ g/mL (Fig. 2.11i) only showed decreased swimming motility, and also developed a combination of filamentous structures and punctiform colonies (Fig. 2.11i and 2.11i1, Arrows), also seen at 300 and 500  $\mu$ g/mL (48 hours incubation) (Fig. 2.13h, i). In contrast, lobe formation at the edge of the biofilm can be seen at lower concentrations. For example, lobe development can be seen at 75  $\mu$ g/mL (Fig. 2.9c1) as well as minor filament formation at 100 and 200  $\mu$ g/mL (Fig. 2.9d, Fig. 2.10g), indicating the occurrence of different types of bacterial differentiation depending on GBLE concentration.

GBLE seemed to promote swimming motility in most concentrations; this effect appears to be concentration-dependent, as some cultures present a decrease in this type of motility. The extract also significantly influenced agar biofilm morphology, resulting in lobe and filament formation as well as punctiform colonies.

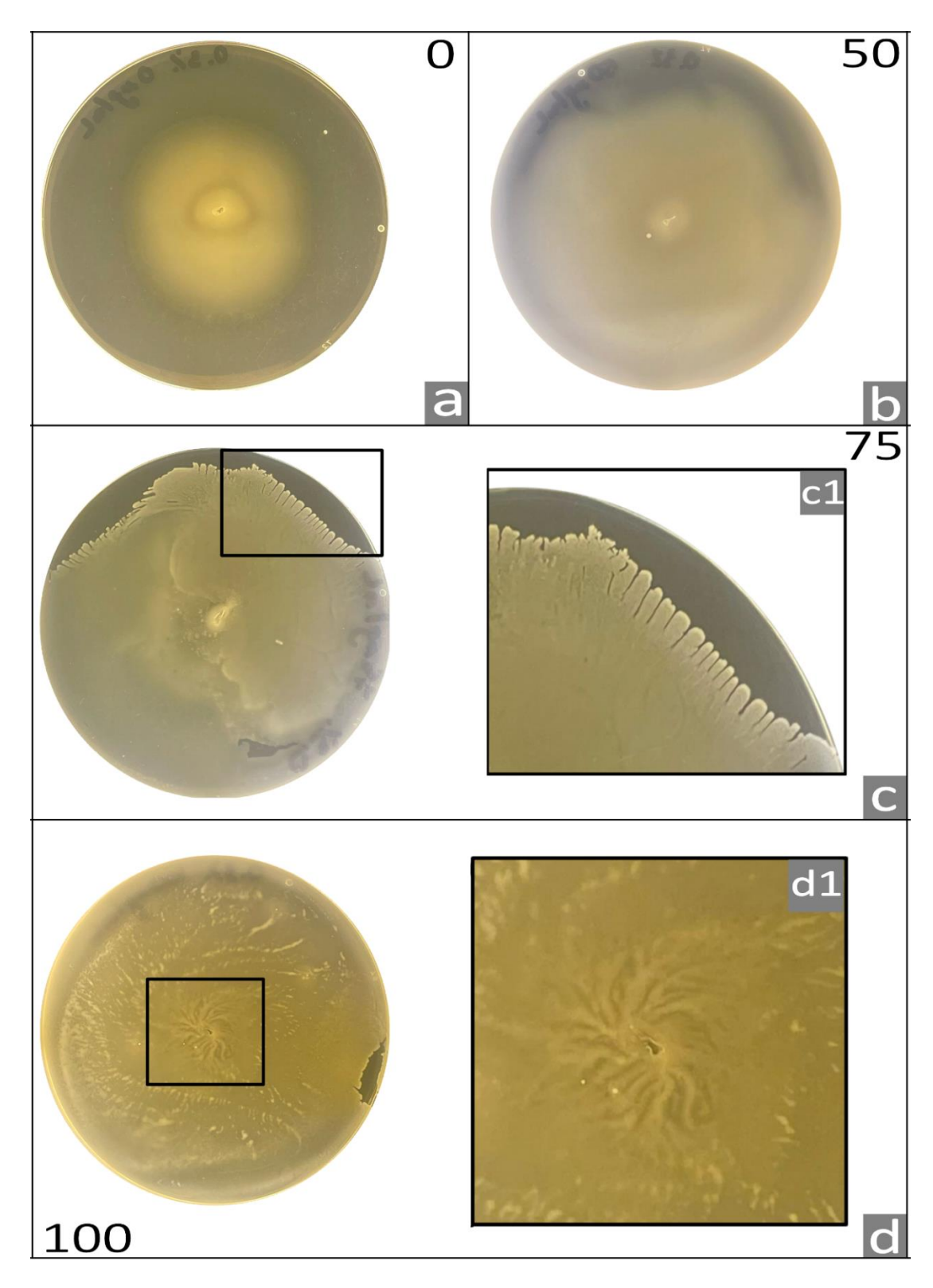


Figure 2.9. Pictures of 0.3% LB agar petri dishes containing increasing concentrations of GBLE and inoculated with *B. subtilis* culture to test swimming motility. Pictures were taken after 24 hours of incubation at 37°C. a) Negative control, with 0  $\mu$ g/mL GBLE. b) B. subtilis culture at 50  $\mu$ g/mL GBLE. c) Lobe formation at the edge of the agar biofilm in response to 75  $\mu$ g/mL GBLE (c1). d) Swimming motility patterns (d1) of B. subtilis supplemented with 100  $\mu$ g/mL GBLE.

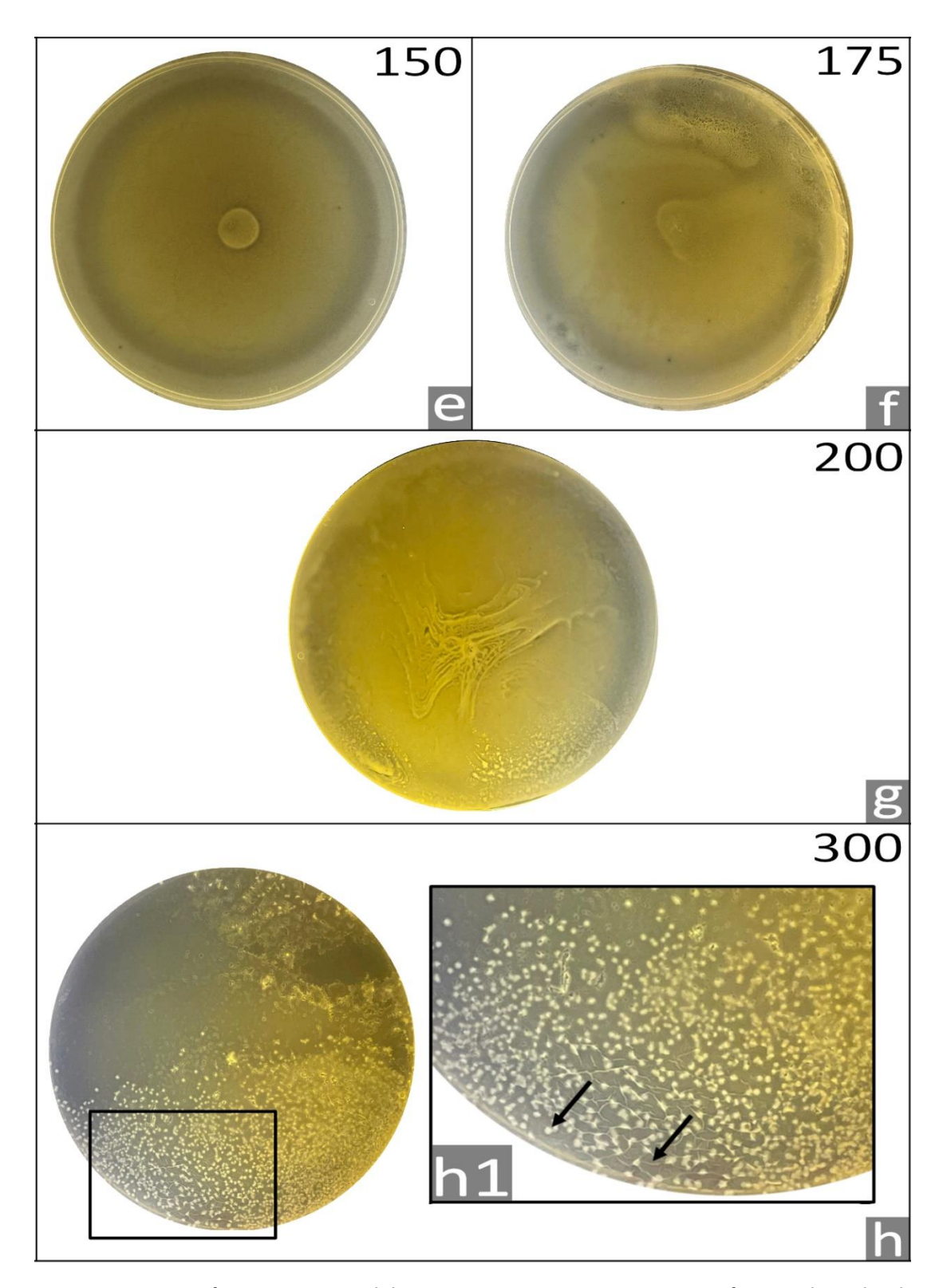


Figure 2.10. Pictures of 0.3% LB agar petri dishes containing increasing concentrations of GBLE and inoculated with *B. subtilis* culture to test swimming motility. Pictures were taken after 24 hours of incubation at 37°C. e) B. subtilis culture at 150  $\mu$ g/mL GBLE. f) B. subtilis culture at 175  $\mu$ g/mL GBLE. g) Swimming motility patterns of B. subtilis supplemented with 200  $\mu$ g/mL GBLE. h) Combination of filamentous and punctiform colonies (h1) at 300 GBLE (arrows).

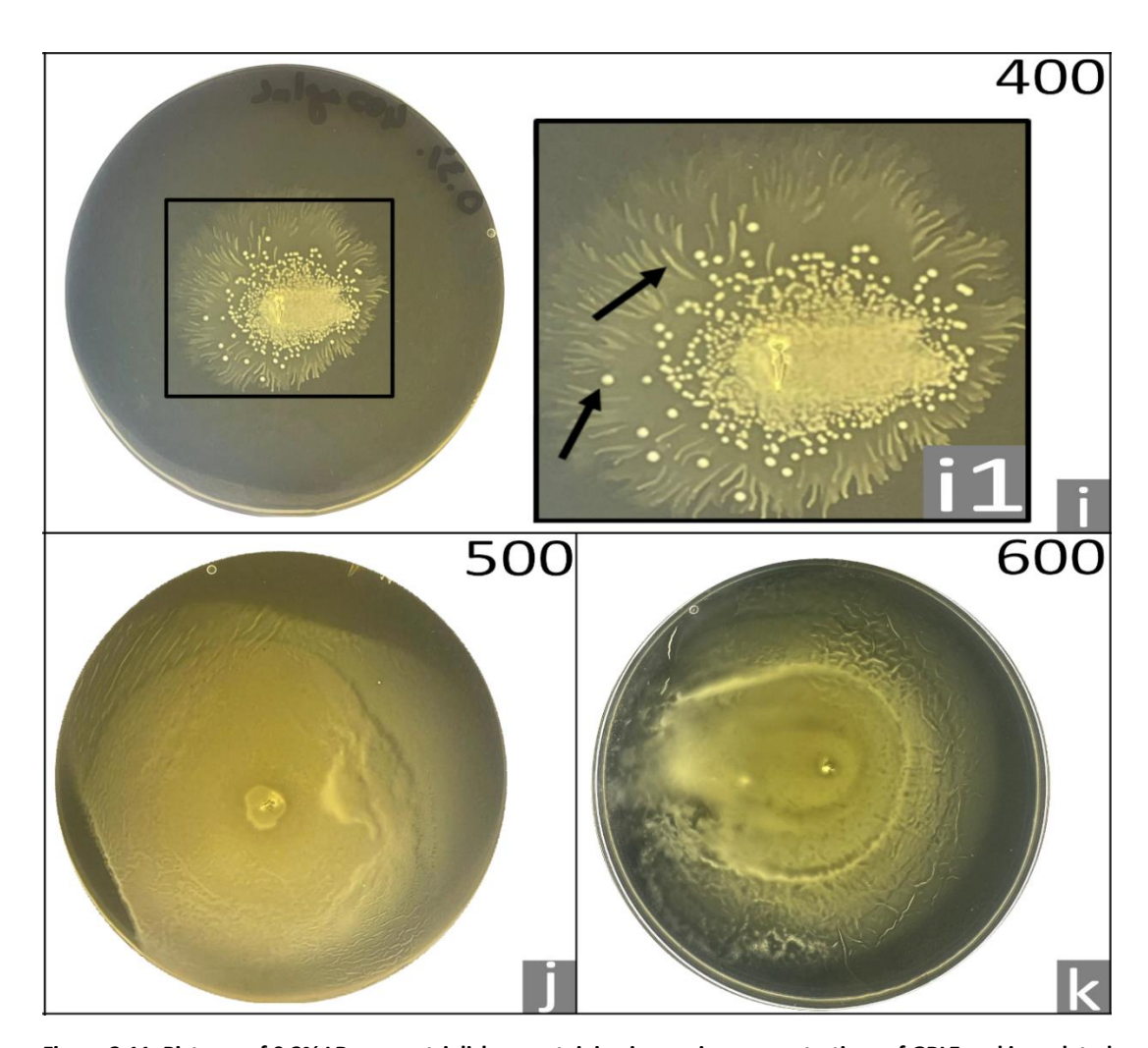


Figure 2.11. Pictures of 0.3% LB agar petri dishes containing increasing concentrations of GBLE and inoculated with *B. subtilis* culture to test swimming motility. Pictures were taken after 24 hours of incubation at 37°C. i) Combination of filamentous and punctiform colonies (i1) at 400  $\mu$ g/mL GBLE (arrows). j) and k) *B. subtilis* culture at 500 and 600  $\mu$ g/mL GBLE, respectively.

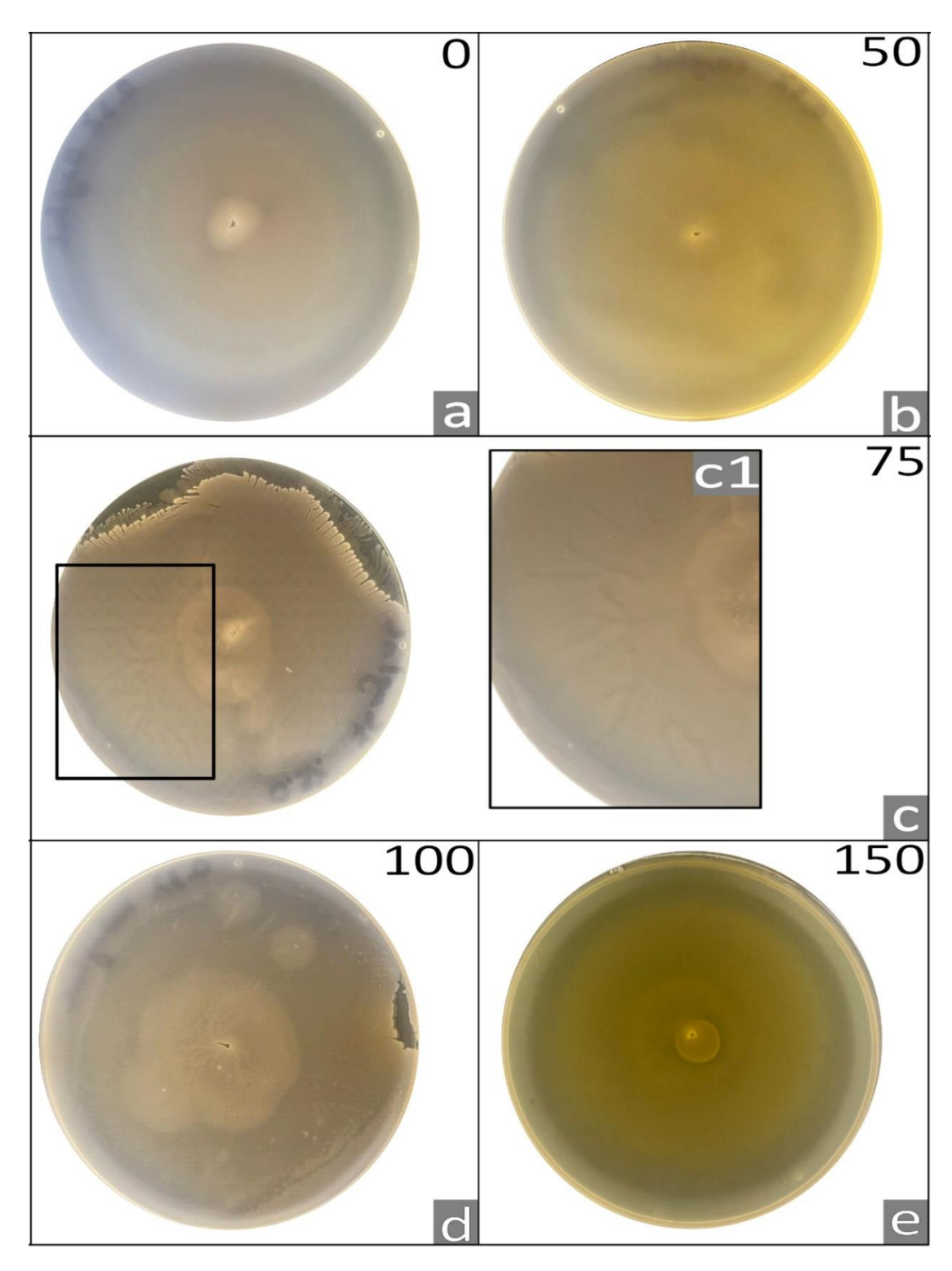


Figure 2.12. Pictures of 0.3% LB agar petri dishes containing increasing concentrations of GBLE and inoculated with *B. subtilis* culture to test swimming motility. Pictures were taken after 48 hours of incubation at 37°C. a) Negative control, with 0  $\mu$ g/mL GBLE and b) with 50  $\mu$ g/mL GBLE. c) Lobe formation and branching (c1) within the agar biofilm at 75  $\mu$ g/mL GBLE after 48 hours of incubation. d) and f) Swimming motility patterns of *B. subtilis* supplemented with 100 and 150  $\mu$ g/mL GBLE, respectively.

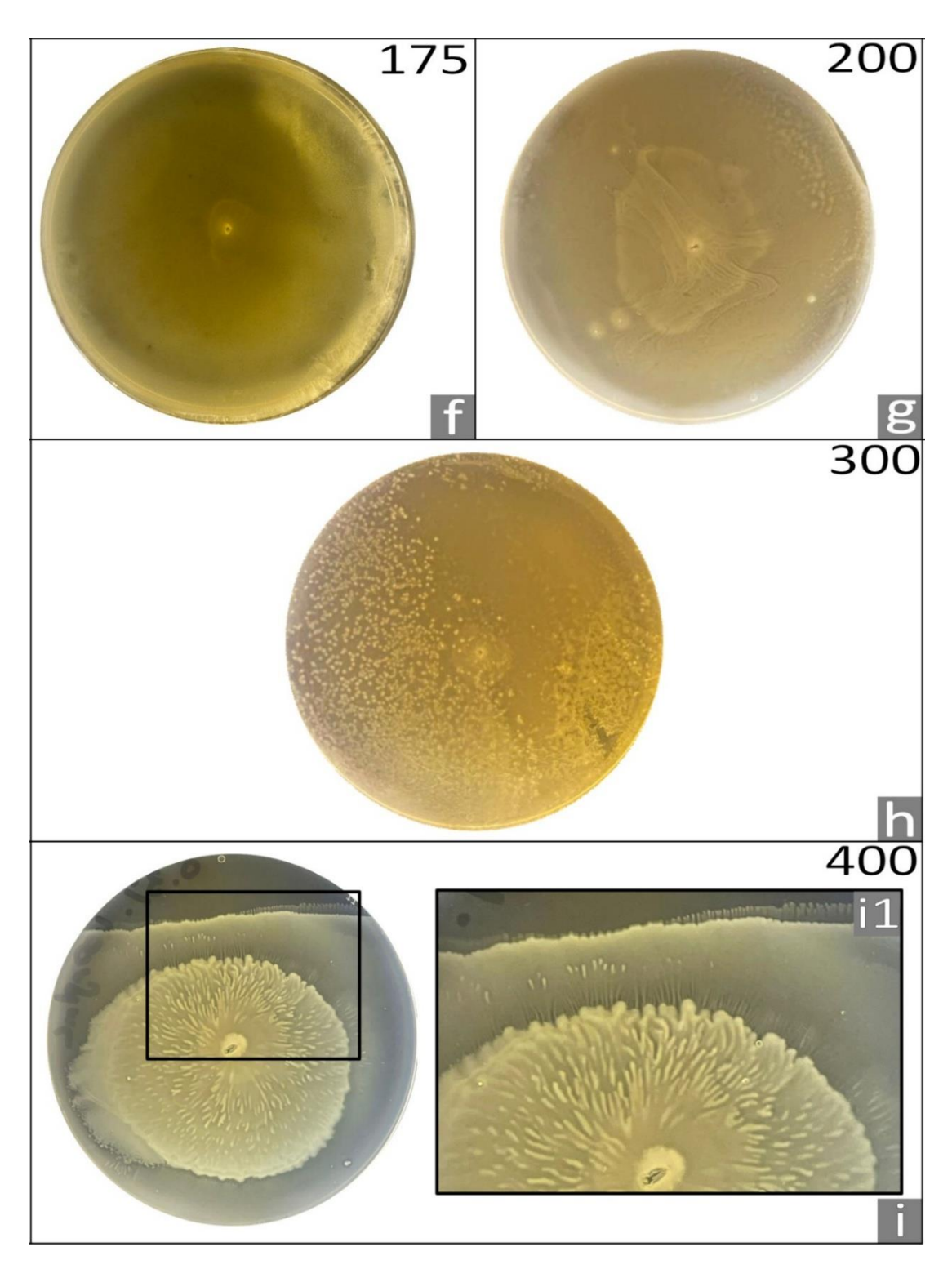


Figure 2.13. Pictures of 0.3% LB agar petri dishes containing increasing concentrations of GBLE and inoculated with *B. subtilis* culture to test swimming motility. Pictures were taken after 48 hours of incubation at 37°C. f) and g) Swimming motility patterns of *B. subtilis* supplemented with 175 and 200  $\mu$ g/mL GBLE, respectively. h) *B. subtilis* showing punctiform colonies at 300  $\mu$ g/mL GBLE. i) *B. subtilis* at 400  $\mu$ g/mL GBLE showing filamentous branching and lobe formation (i1).

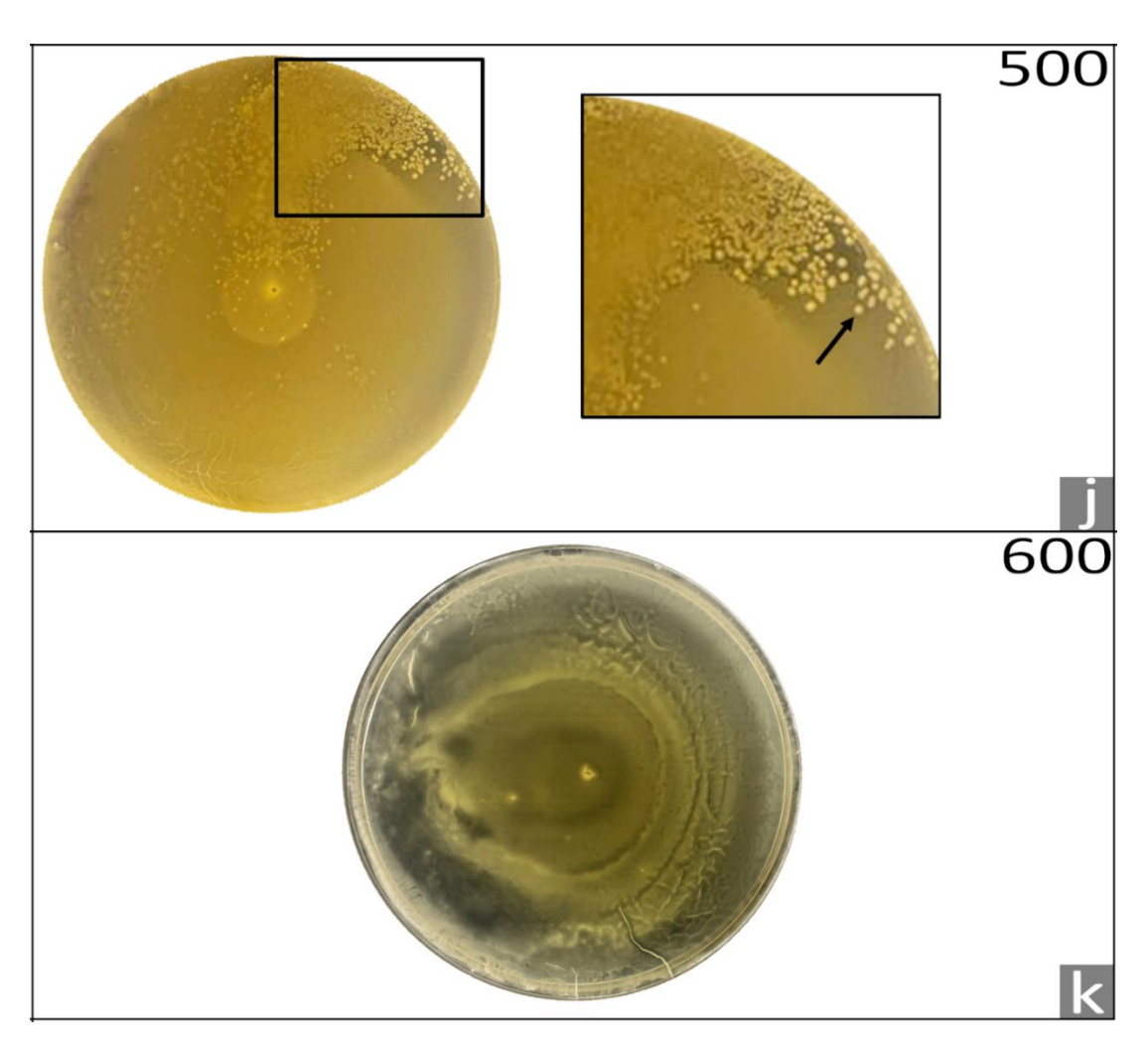


Figure 2.14. Pictures of 0.3% LB agar petri dishes containing increasing concentrations of GBLE and inoculated with B. subtilis culture to test swimming motility. Pictures were taken after 48 hours of incubation at 37°C. j) Punctiform colonies seen at 500  $\mu$ g/mL GBLE after 48 hours of incubation. k) Swimming motility patterns of B. subtilis supplemented with 600  $\mu$ g/mL GBLE following 48 hours of incubation.

#### 2.4.3.2. Swarming Motility

0.6% agar plates were inoculated with overnight *B. subtilis* culture in order to study swarming motility and GBLE (Fig. 2.15-2.20). When analysing 0.6% agar plates, GBLE seemed to significantly modulate biofilm morphology, starting from concentrations as low as 50  $\mu$ g/mL (Fig 2.15). While the control biofilm displays classic morphology, with a circular shape and an entire margin (Fig 2.15a), agar biofilms grown in the presence of GBLE show lobate margins and irregular forms (e.g. Fig 2.15b-d) (Refer to Appendix S1 for Colony Morphology guide). This is exemplified in the biofilm grown at 75  $\mu$ g/mL after 48 hours of incubation (Fig. 2.18c). The biofilm is extremely different from the negative control, and bacterial cells seem to achieve colony expansion using that phenotype. This occurs up to 100  $\mu$ g/mL. Once GBLE concentration surpasses 100  $\mu$ g/mL, the biofilm architecture changes drastically. At

specifically 150  $\mu$ g/mL (Fig. 2.16e1) and above, bacterial cells begin to grow in filamentous form or chains from a circular colony, to achieve motility. This phenomenon becomes more apparent when agar biofilms are grown at 300 and 600  $\mu$ g/mL GBLE, where mutation events can be seen as the bacterial colony evolves into filamentous form, after 48 hours of incubation (Fig. 2.19h1, Fig. 2.20k1, 2, 3).

However, this does not occur at 400 and 500  $\mu$ g/mL (Fig. 2.17i, j). At these concentrations, there are no mutation events or cellular differentiation and the agar biofilm remains relatively small. Interestingly, the culture grown at 400  $\mu$ g/mL has decreased dimensions compared to the control, indicating a strong concentration-dependent effect.

The presence of GBLE was seen to have a significant effect on colony morphology in all samples. While the negative control colonies displayed a circular form with an entire margin and overall smooth surface, GBLE induced the development of irregular lobate colonies, with the presence of punctiform and filamentous colonies, indicating that GBLE might induce cellular differentiation. All colonies displayed a flat elevation, with colony size varying depending on the concentration of GBLE.

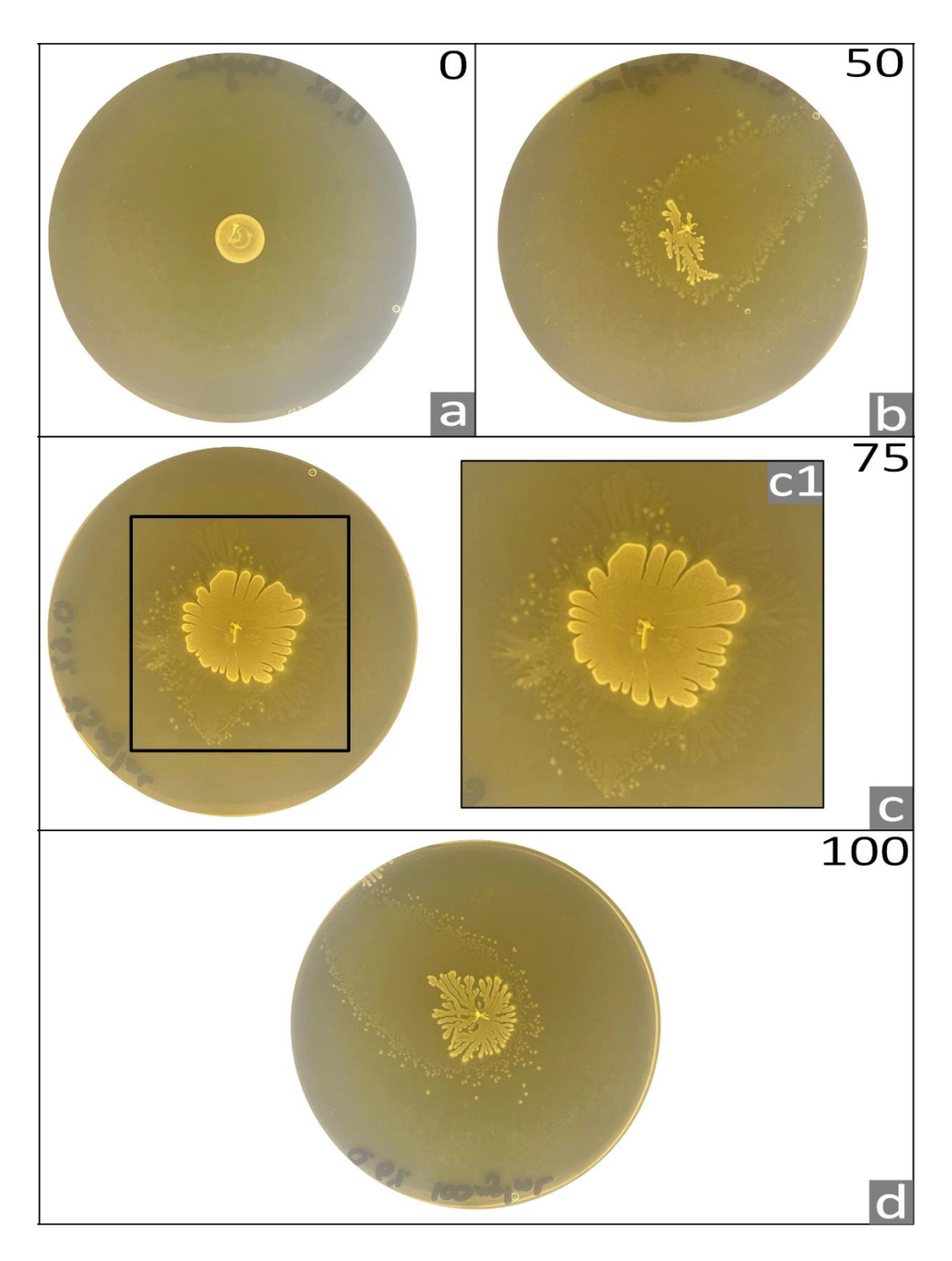


Figure 2.15. Pictures of 0.6% agar petri dishes containing increasing concentrations of GBLE and inoculated with *B. subtilis* culture. Pictures were taken after 24 hours of incubation at 37°C. a) Negative control, with 0  $\mu$ g/mL GBLE. b) and c) Ray and lobe (c1) development in combination with punctiform colonies, in response to 50 and 75  $\mu$ g/mL GBLE, respectively. d) Ray development after 24 hours of incubation at 100  $\mu$ g/mL GBLE.

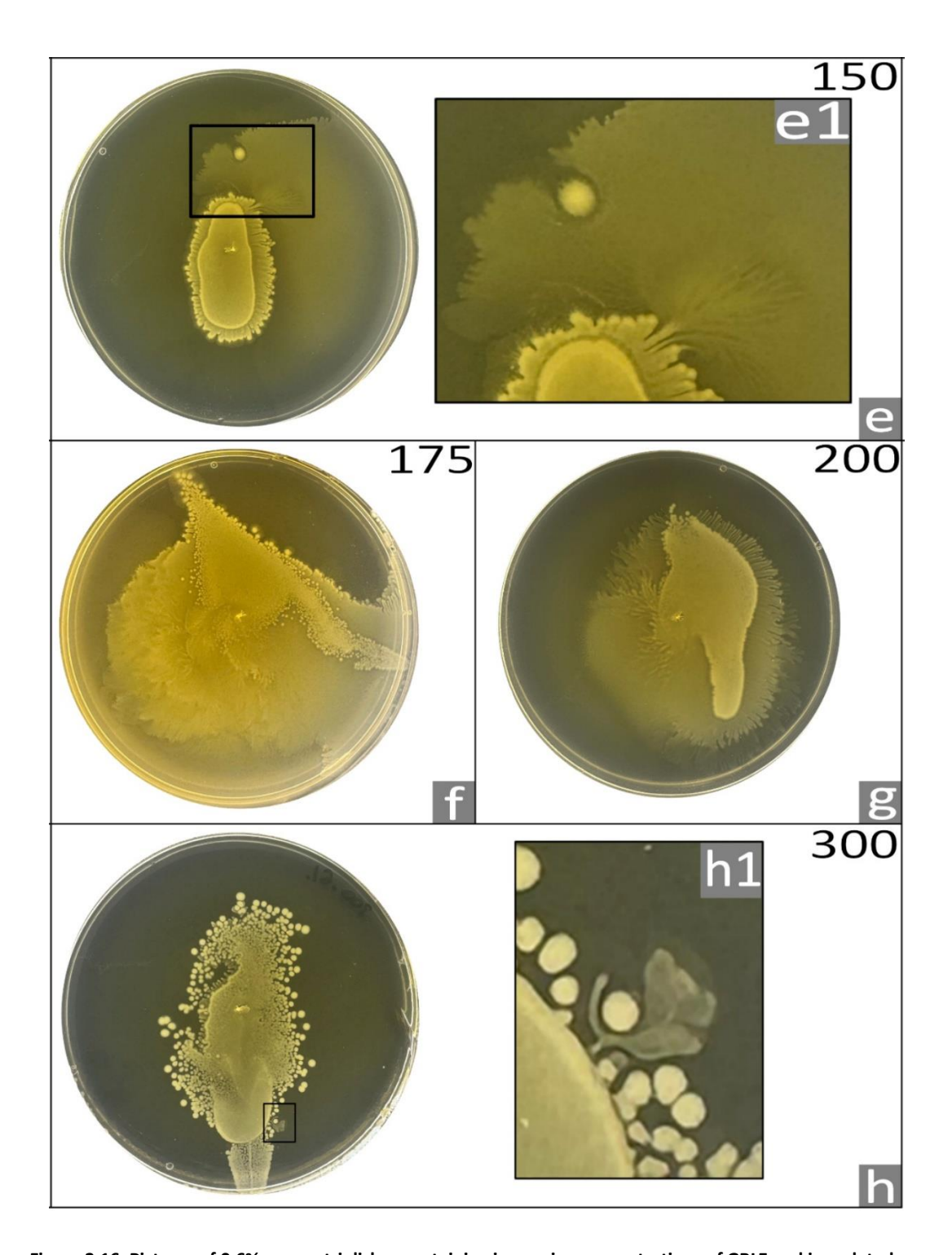


Figure 2.16. Pictures of 0.6% agar petri dishes containing increasing concentrations of GBLE and inoculated with *B. subtilis* culture. Pictures were taken after 24 hours of incubation at 37°C. e) Lobe development and cellular differentiation (e1) at 150  $\mu$ g/mL GBLE. f) and g) B. subtilis swarming motility at 175 and 200  $\mu$ g/mL GBLE, respectively. h) Cellular differentiation (h1) at 300  $\mu$ g/mL GBLE.

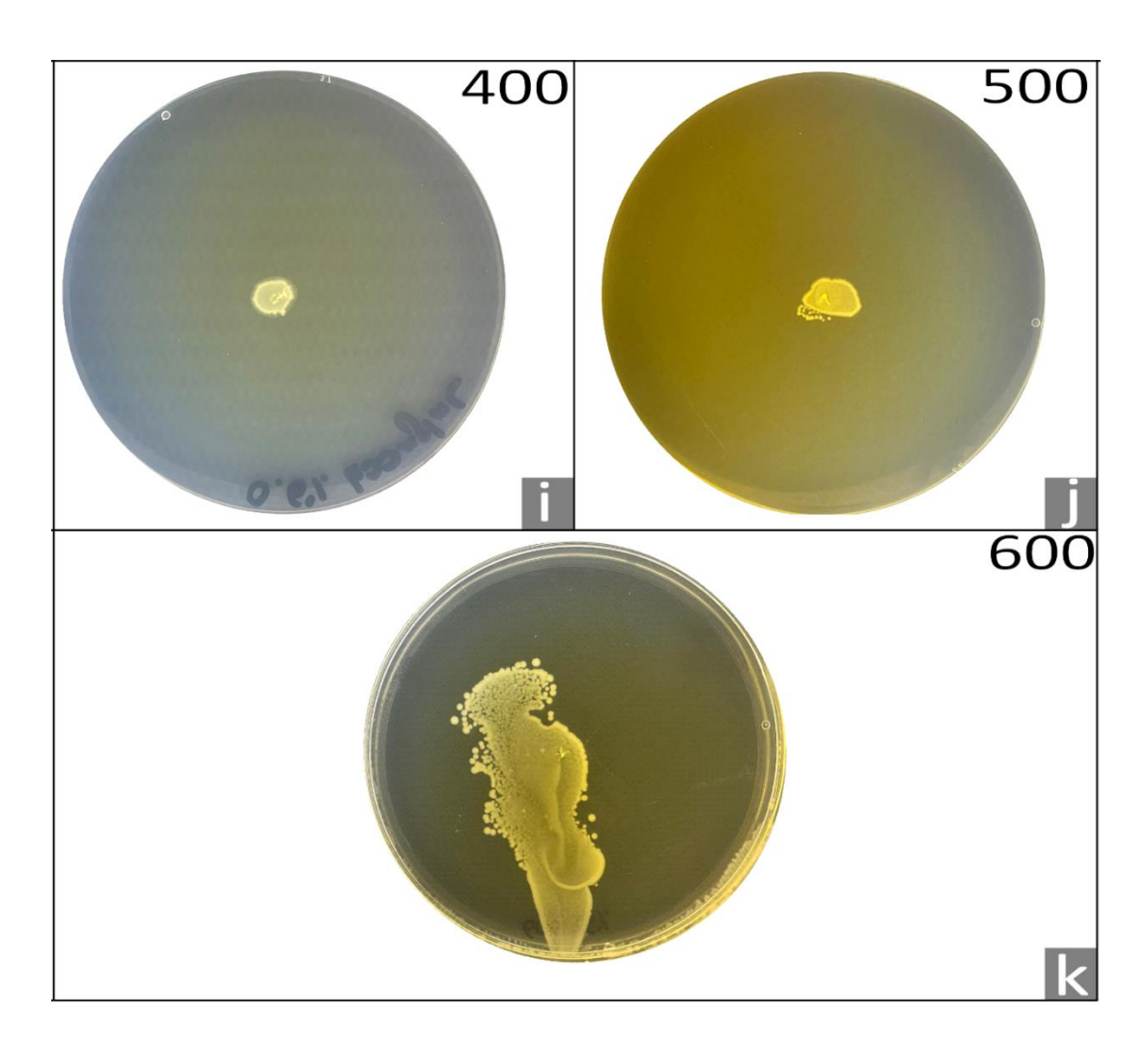


Figure 2.17. Pictures of 0.6% agar petri dishes containing increasing concentrations of GBLE and inoculated with *B. subtilis* culture. Pictures were taken after 24 hours of incubation at 37°C. i) and j) *B. subtilis* showing limited swarming 75  $\mu$ g/mL GBLE. k) Swarming motility of *B. subtilis* at 600  $\mu$ g/mL GBLE along with punctiform colonies.

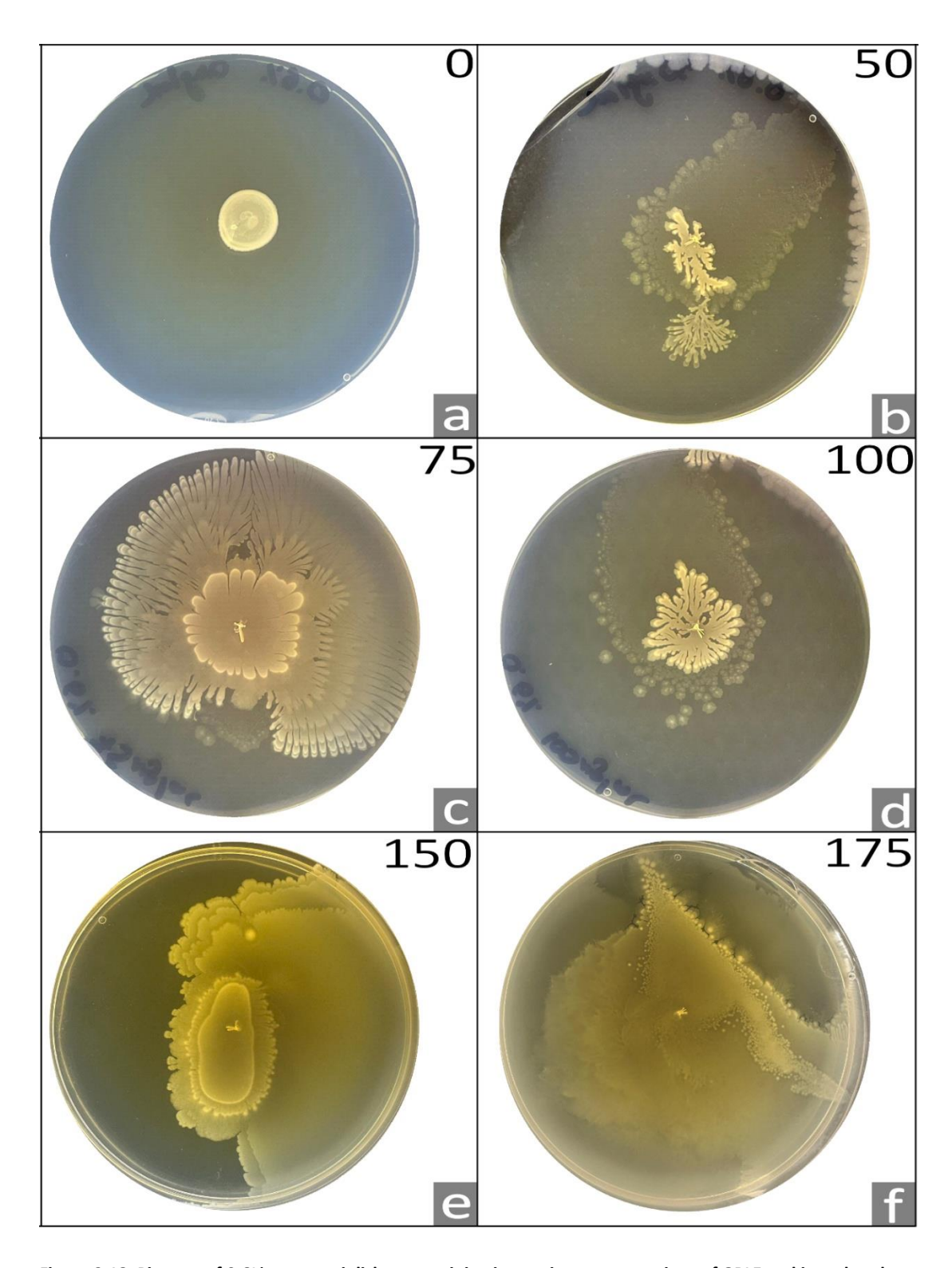


Figure 2.18. Pictures of 0.6% agar petri dishes containing increasing concentrations of GBLE and inoculated with *B. subtilis* culture. Pictures were taken after 48 hours of incubation at 37°C. a) Negative control at 0,  $\mu$ g/mL GBLE. b) c) and d) Extensive ray, lobe and petal development in response to 50, 75 and 100  $\mu$ g/mL GBLE, respectively. e) f) Further colony spread and morphological differentiation at 150 and 175  $\mu$ g/mL GBLE, respectively.

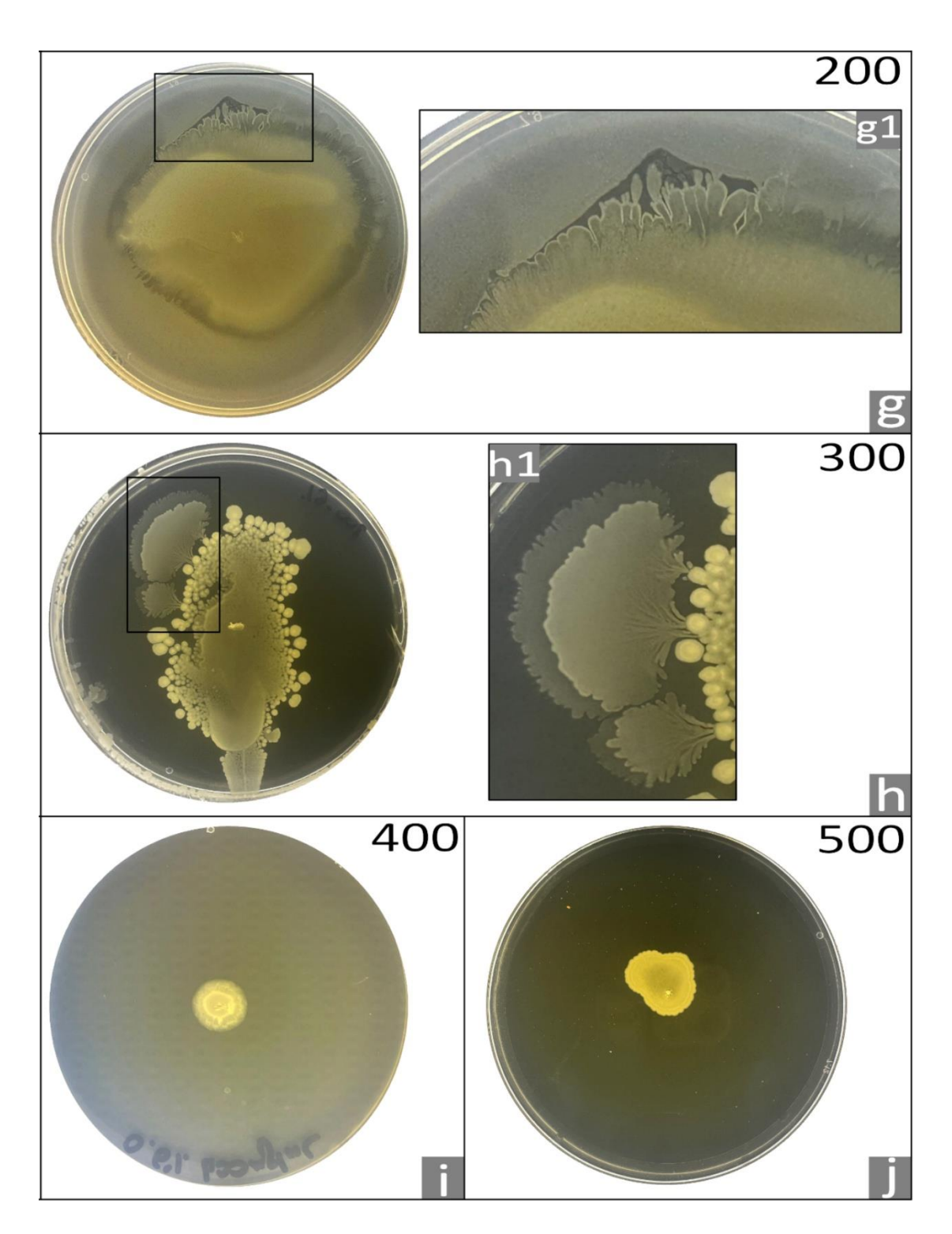


Figure 2.19. Pictures of 0.6% agar petri dishes containing increasing concentrations of GBLE and inoculated with *B. subtilis* culture. Pictures were taken after 48 hours of incubation at 37°C. g) Lobe and petal development as well as cellular differentiation at 200  $\mu$ g/mL GBLE. h) Strong cellular differentiation (h1) at 300  $\mu$ g/mL GBLE; bacterial cells mutate to ray morphology. i) j) Limited colony spread at 400 and 500  $\mu$ g/mL GBLE, respectively.

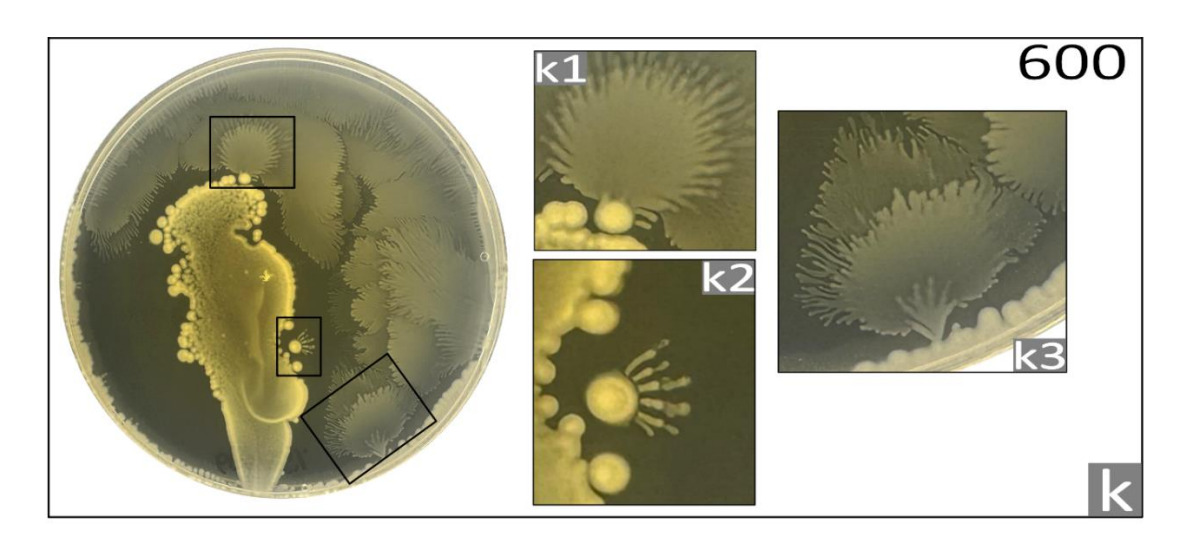


Figure 2.20. Picture of 0.6% agar petri dishes containing 600 μg/mL GBLE and inoculated with *B. subtilis* culture (k). Picture was taken after 48 hours of incubation at 37°C. Multiple cellular differentiation points (k1, k2, k3)) as bacterial cells mutate to ray morphology.

## 2.4.4. Confocal Laser Scanning Microscopy

In order to understand the impact of GBLE on biofilm morphology in greater detail, static biofilms were grown under various GBLE concentrations and imaged using confocal laser scanning microscopy (CLSM) (Fig. 2.21-2.28). Results show that the extract GBLE structurally affects biofilm architecture. GBLE exposure increased the emergence of Van Gogh bundles. These are defined as filamentous, looped bundles of aligned matrix-producing *B. subtilis* cell chains that propel colony spreading (van Gestel et al., 2015).

As seen in the negative control (Fig. 2.20), when GBLE is absent, the biofilm shows its standard morphology, with bacterial cells encased in extracellular matrix and minimal Van Gogh bundle formation. Once GBLE is added, the standard biofilm morphology shifts to a more filamentous architecture. Long chains of *B. subtilis* cells appear, forming highly organised networks of Van Gogh bundles. In addition to the formation of Van Gogh bundles, there was a general decrease in ECM fluorescence compared to the control, in response to GBLE. Furthermore, the presence of GBLE results in the formation of bacterial aggregates within the biofilms (Fig. 2.22b, 2.24c, 2.24d, 2.25a, 2.25d and 2.27c).

Interestingly, while the concentration of GBLE increases, two different cell types appear. This is apparent at 100  $\mu$ g/mL (Fig. 2.23a, c, d), as some cells show increased fluorescence compared to the rest. The biofilm shows a combination of elongated rod-shaped cells and cells showing a more round shape, suggesting that GBLE is triggering biochemical changes of the bacterial cell.

In addition, at higher concentrations, specifically 400 and 500  $\mu$ g/mL (Fig. 2.26d, 2.27b and 2.27c), a change in intracellular fluorescence can be seen. Under normal conditions, the *gfp* protein is constitutively expressed throughout the whole bacterial cells, as it is bound to DNA histone proteins. This can be clearly seen in the negative control. At high concentrations of GBLE, *gfp* becomes localised within the nucleoid of the bacterial cells, resulting in the fluorescent signal concentrated in the middle of the cell in circular shape.

#### 2.4.4.1. Negative Control

The following micrograph (Fig. 2.21) displays the structural organization of B. subtilis biofilms formed under negative control conditions (0  $\mu g/mL$ ). Cells exhibit characteristic arrangements typical of wild-type B. subtilis biofilm morphology, with no visible disruption or detachment. The absence of treatment allows for the natural development of standard biofilm architecture, showcasing the integrity of matrix components.

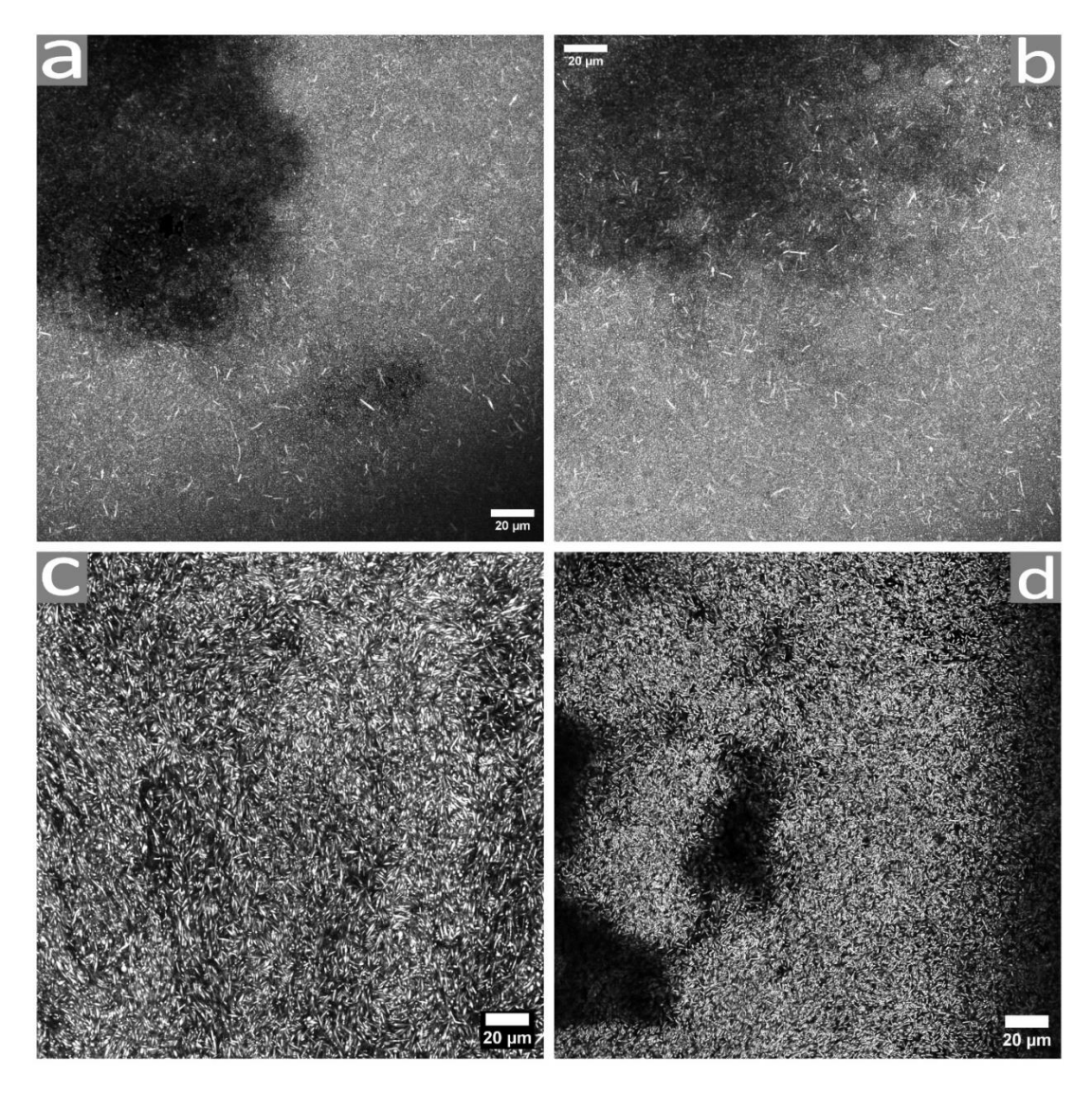


Figure 2.21. Fluorescent images of *gfp*-expressing *B. subtilis* biofilms, grown without GBLE. Cells were imaged to assess baseline biofilm architecture in the absence of treatment. indicating robust biofilm formation and preserved extracellular matrix integrity. Biofilms were grown for 72 hours, incubated at 37° in LB medium. Images acquired using SP5 Leica (630X magnification), Scale bars = 20 µm.

## 2.4.4.2. 50 μg/mL *Ginkgo biloba* Leaf Extract

The images below reveal the impact of 50  $\mu$ g/mL GBLE on *B. subtilis* biofilm architecture (Fig. 2.22). Compared to the untreated control, the biofilm displays tightly packed Van Gogh bundles. The biofilm remains dense and cell chains start to appear (Fig. 2.22d).

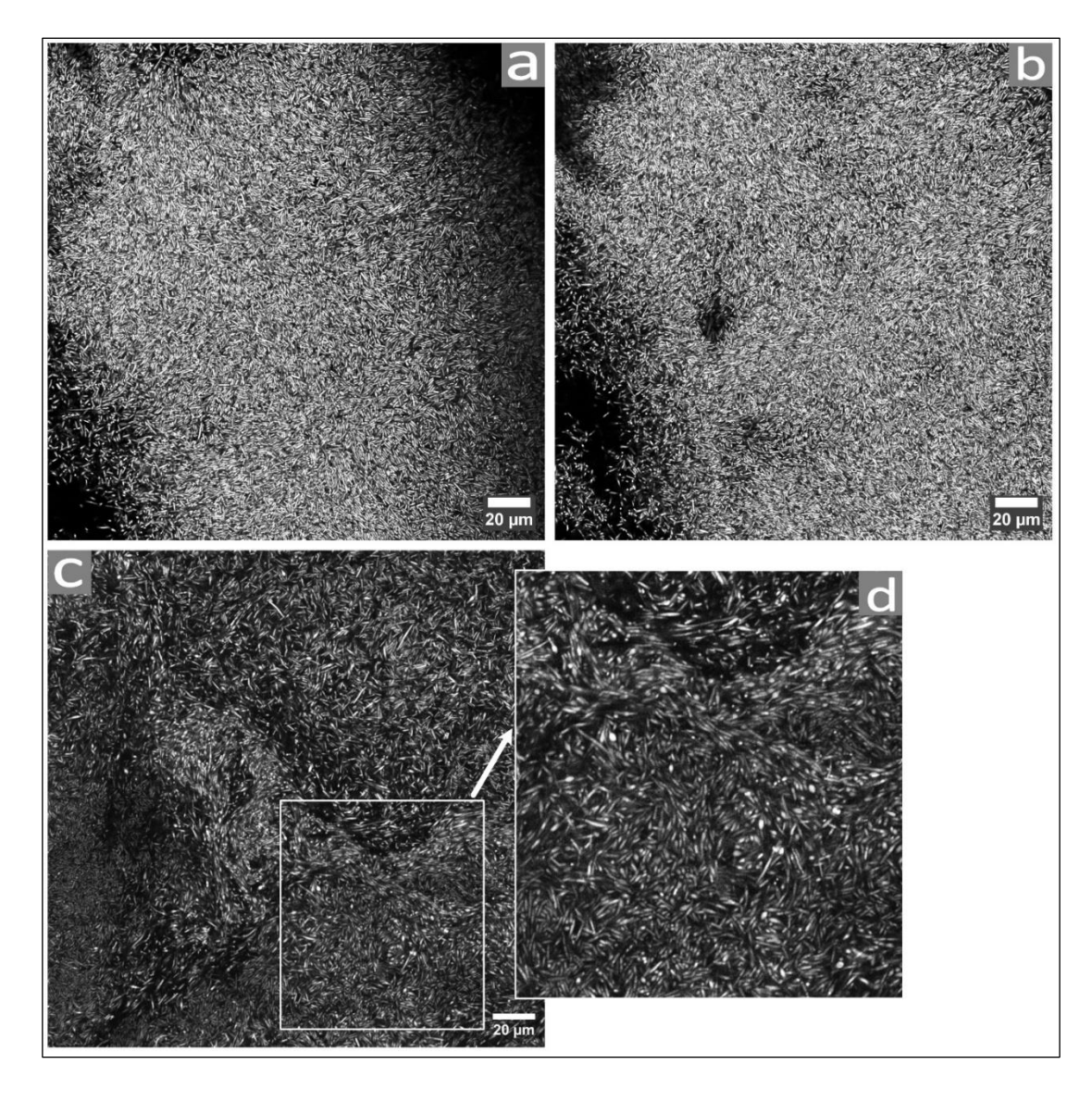


Figure 2.22. Fluorescent images of *gfp*-expressing *B. subtilis* biofilms, grown with 50  $\mu$ g/mL GBLE. The biofilm structure is still maintained, presenting increased chaining formation (d), indicating a response to GBLE. Biofilms were grown for 72 hours, incubated at 37° in LB medium. Images acquired using SP5 Leica (630X magnification), Scale bars = 20  $\mu$ m.

#### 2.4.4.3. 75 μg/mL *Ginkgo biloba* Leaf Extract

Treatment with 75  $\mu$ g/mL GBLE significantly alters *B. subtilis* biofilm morphology (Fig. 2.23). The micrographs show pronounced structural disintegration, with large voids in the biofilm matrix and a clear reduction in cell clustering. Cells are sparsely distributed and appear detached from the biofilm core and also show changes in intracellular fluorescence (Fig. 2.23d, arrow). Similarly to 50  $\mu$ g/mL GBLE, Van Gogh bundles appear (Fig. 2.23d). These features suggest a dose-dependent effect of GBLE on biofilm integrity and cellular cohesion.

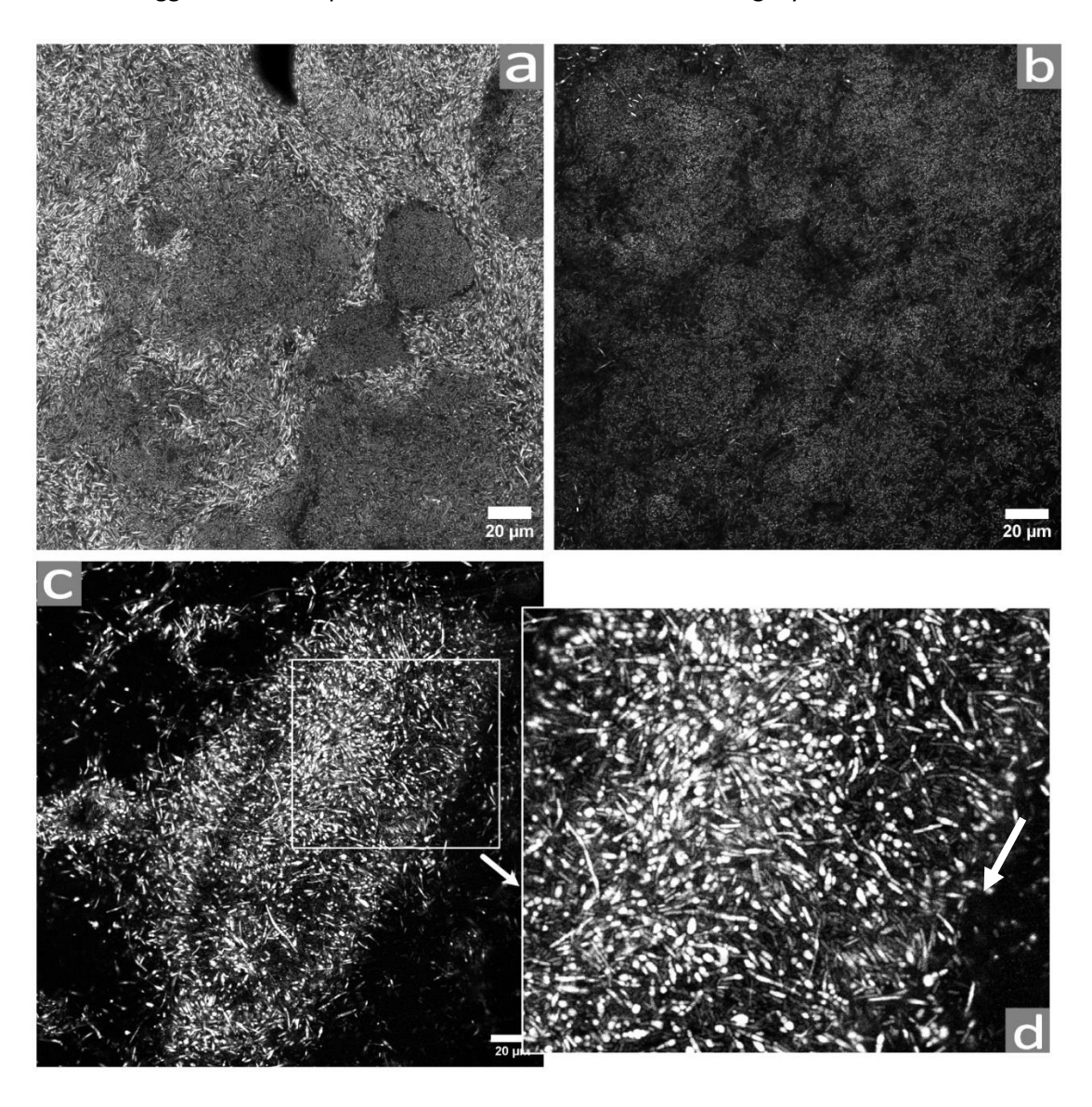


Figure 2.23. Fluorescent images of *gfp*-expressing *B. subtilis* biofilms, grown with 75  $\mu$ g/mL GBLE. The biofilm structure is partially maintained, showing chaining formation (d) as well as gaps in the matrix, indicating a response to GBLE. Biofilm cells show change in shape and fluorescence (d, arrow). Biofilms were grown for 72 hours, incubated at 37° in LB medium. Images acquired using SP5 Leica (630X magnification), Scale bars = 20  $\mu$ m.

#### 2.4.4.4. 100 μg/mL Ginkgo biloba Leaf Extract

At 100 µg/mL, GBLE exerts a profound effect on *B. subtilis* biofilms (Fig. 2.24). The micrographs display extensive changes of the biofilm network, with reduced cohesion and abnormal filamentous structures. Long chains of *B. subtilis* cells appear, forming highly organised networks of Van Gogh bundles. Instead of uniform coverage, the biofilm appears patchy, with loose aggregates and increased extracellular voids, exhibiting long cell chains and changes in cell shape (Fig. 2.24a). Fig. 2.24c and 2.24d show intertwined Van Gogh bundles, wrapped in an unorganised manner.

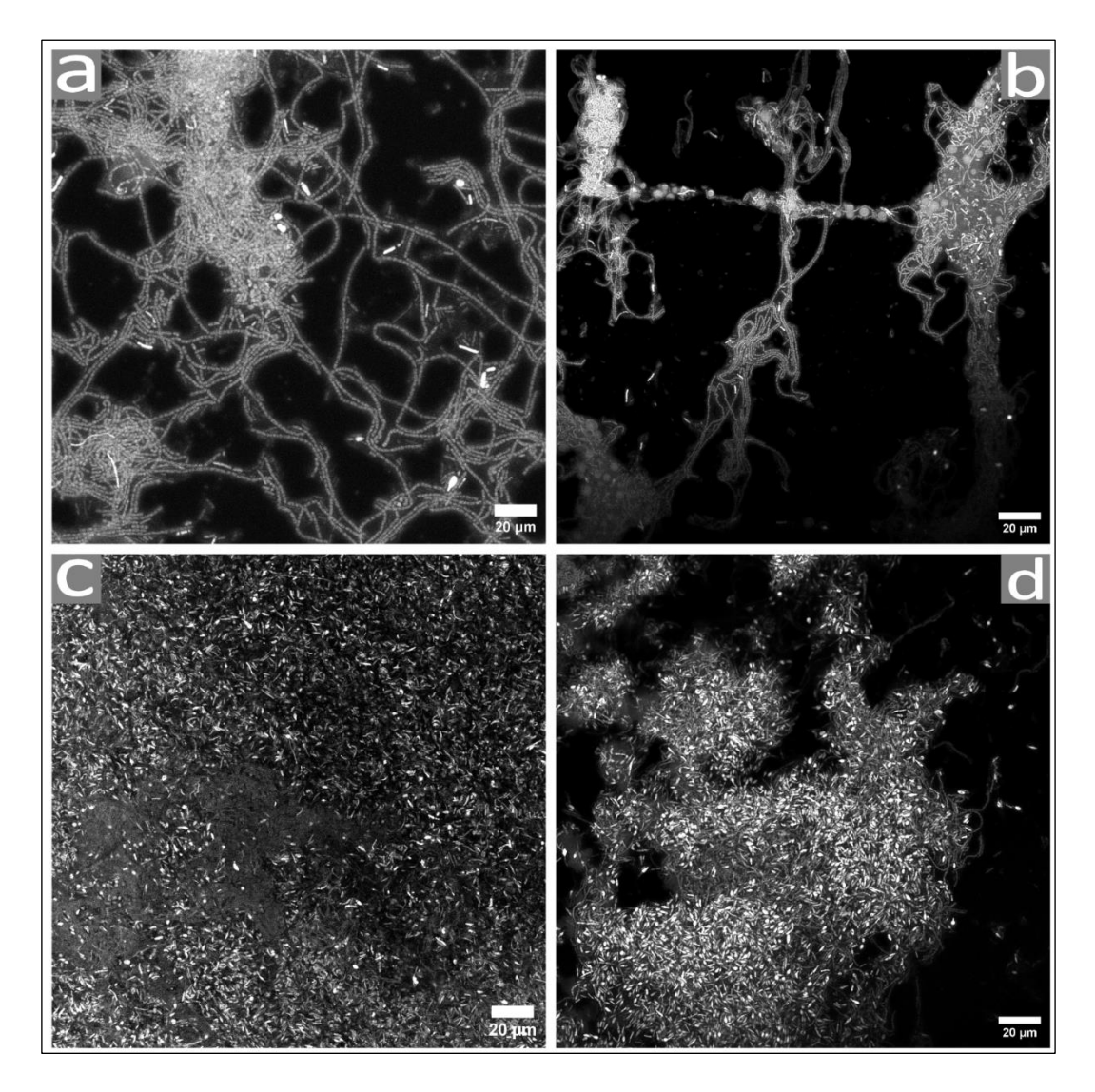


Figure 2.24. Microscopy images of *gfp*-expressing *Bacillus subtilis* biofilms treated with 100 μg/mL GBLE. Biofilms display severe disorganization, cellular clusters, and filamentous structures (Van Gogh bundles). Biofilms were grown for 72 hours, incubated at 37° in LB medium. Images acquired using SP5 Leica (630X magnification), Scale bars = 20 μm.

# 2.4.4.5. 200 μg/mL *Ginkgo biloba* Leaf Extract

Exposure to 200  $\mu$ g/mL GBLE results in pronounced disruption of *B. subtilis* biofilm formation (Fig. 2.25). The images show sparse, scattered cell clusters and reduced surface coverage, with cells forming compact microcolonies rather than extended chains or interconnected networks (Fig. 2.25 c, d). The biofilm appears highly fragmented, with large regions devoid of biomass, indicating strong inhibition of both initial attachment and biofilm maturation processes at this concentration.

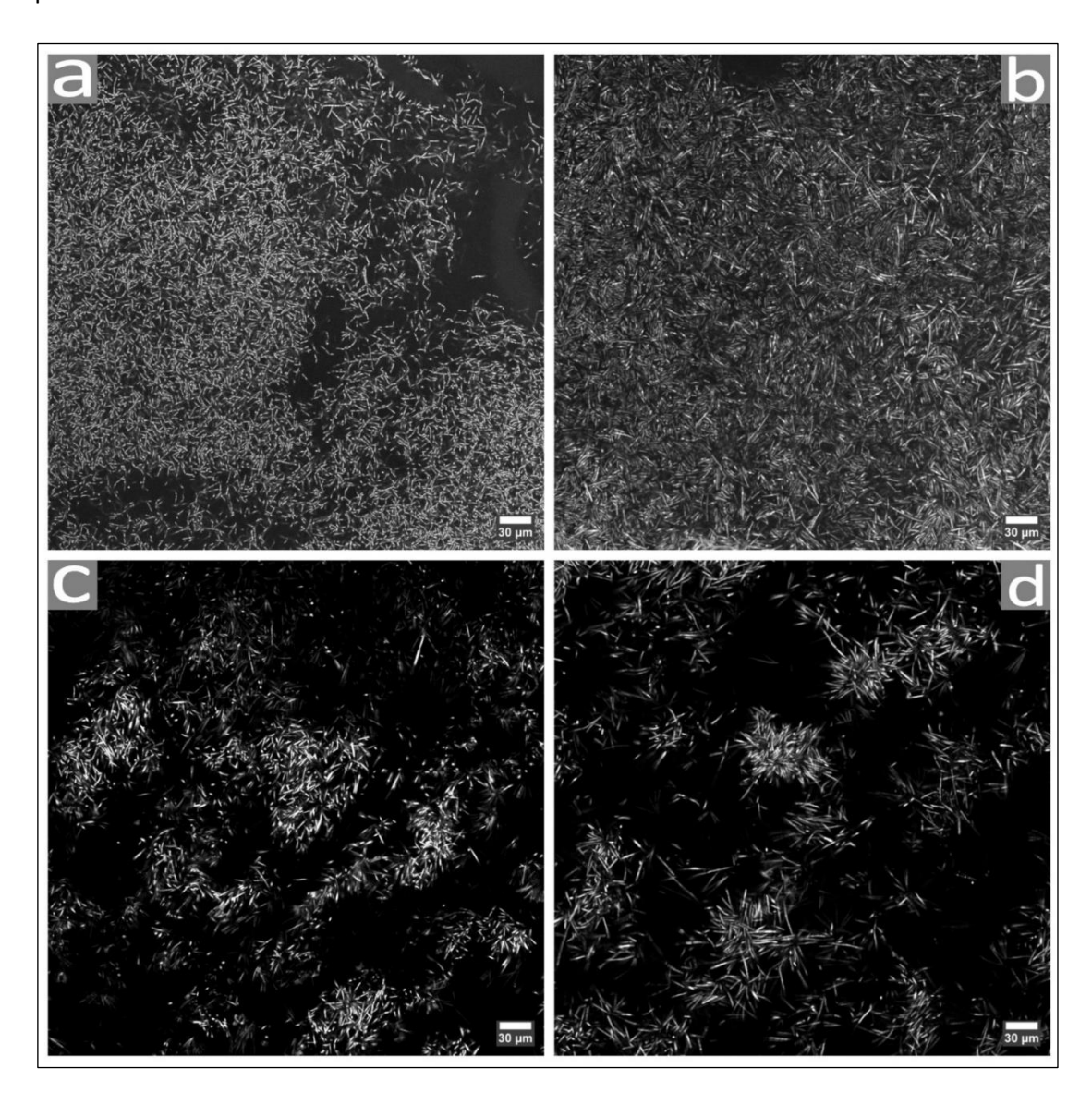


Figure 2.25. Microscopy images of *gfp*-expressing *Bacillus subtilis* biofilms treated with 200 μg/mL GBLE. High-dose treatment leads to severe biofilm inhibition, evident by the scattered microcolonies, minimal surface coverage, and disrupted cellular organization. Biofilms were grown for 72 hours, incubated at 37° in LB medium. Images acquired using SP5 Leica (630X magnification), Scale bars = 20 μm.

# 2.4.4.6. 300 μg/mL *Ginkgo biloba* Leaf Extract

Treatment with 300  $\mu$ g/mL GBLE leads to drastic changes in biofilm morphology in *B. subtilis* (Fig. 2.26). The biofilm architecture is heavily compromised, with large voids and irregular, crater-like gaps forming across the surface. Remaining cells accumulate at the biofilm periphery or in isolated dense clusters, while the central regions are devoid of biomass.

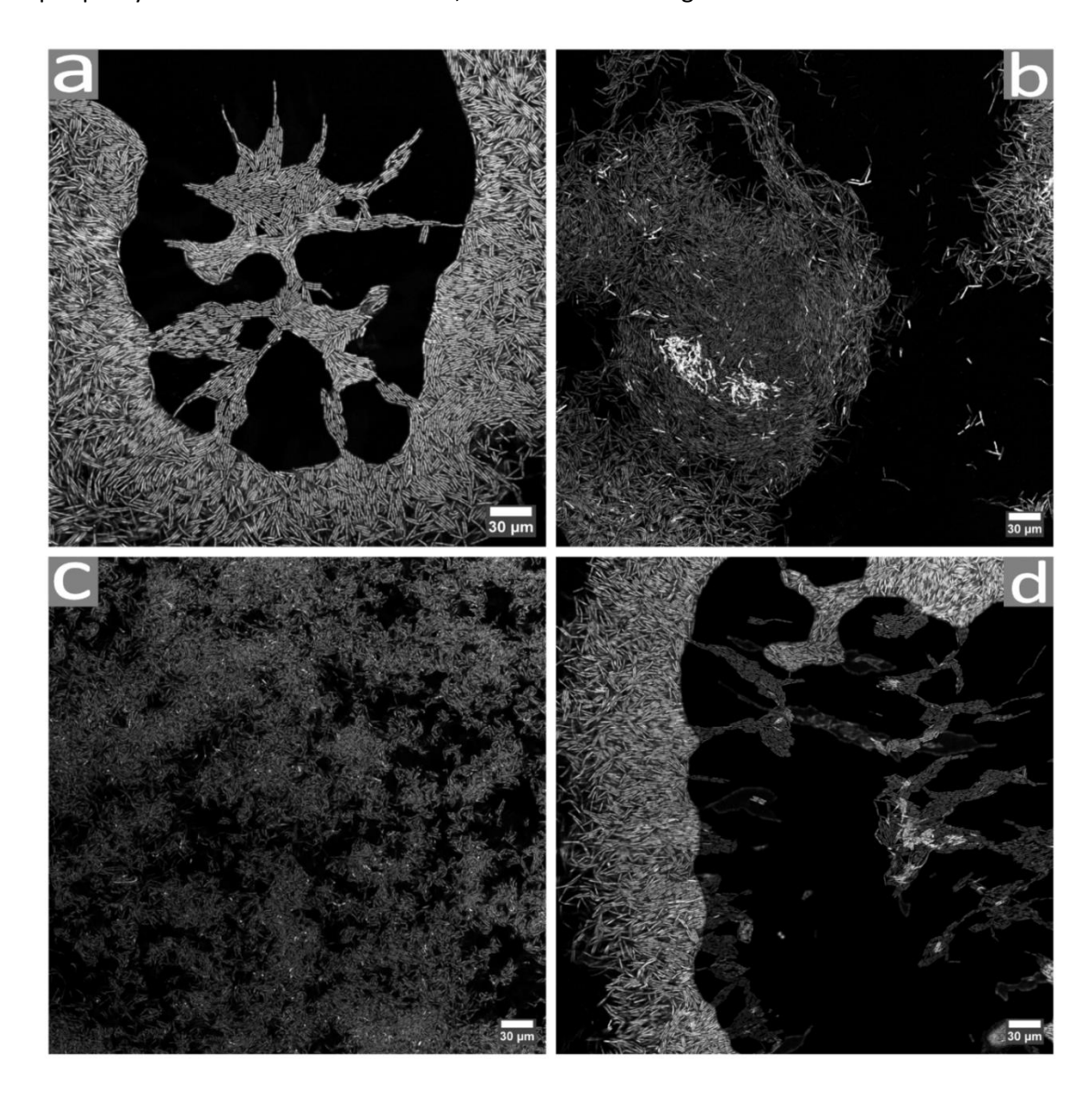


Figure 2.26. Microscopy images of *gfp*-expressing *Bacillus subtilis* biofilms treated with 300  $\mu$ g/mL GBLE. The biofilm is severely disrupted, with extensive clearing zones, fragmented cellular regions, a response to the extract's strong antibiofilm activity at high concentration. Biofilms were grown for 72 hours, incubated at 37° in LB medium. Images acquired using SP5 Leica (630X magnification), Scale bars = 20  $\mu$ m.

# 2.4.4.7. 400 μg/mL *Ginkgo biloba* Leaf Extract

Biofilms treated with 400  $\mu$ g/mL GBLE exhibit heterogeneous structural effects (Fig. 2.27). While some regions shows moderate biofilm disruption and cell dispersal (Fig. 2.27a, d), the remaining areas display dense cellular filaments (Fig. 2.27c, arrow) and relatively preserved architecture (Fig. 2.27b). Interestingly, GBLE is also affecting intracellular fluorescence (Fig. 2.27d), as short cell chains show circular fluorescent dots.

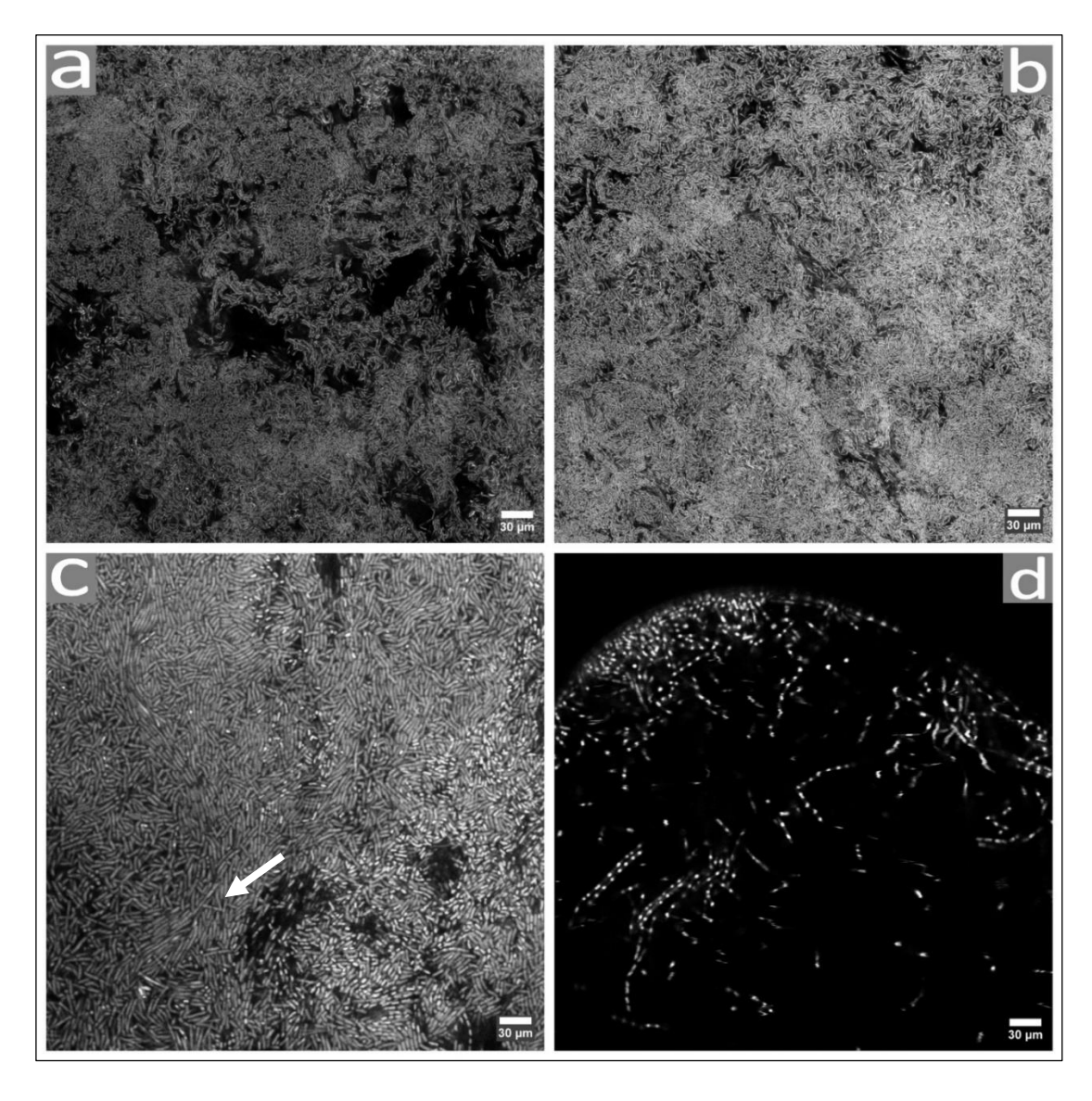


Figure 2.27. Microscopy images of gfp-expressing Bacillus subtilis biofilms treated with 400  $\mu$ g/mL GBLE. Three of the four regions maintain dense biofilm structures, while presenting increased cell chains (arrow) and matrix gaps. One image shows significant disruption with sparse cell distribution and intracellular DNA condensation (d). Biofilms were grown for 72 hours, incubated at 37° in LB medium. Images acquired using SP5 Leica (630X magnification), Scale bars = 30  $\mu$ m.

#### 2.4.4.8. 500 μg/mL Ginkgo biloba Leaf Extract

At 500  $\mu$ g/mL, GBLE induces moderate and regionally variable effects on *B. subtilis* biofilms. While some regions maintain a moderately dense, cohesive biofilm structure with visible chains and clusters of cells (Fig. 2.28a), others show more isolated bacterial aggregates and lower cell density. However, biofilm density at this concentration is still lower than the negative control. In addition, GBLE seems to, again, induce changes in intracellular fluorescence, as cell show localised fluorescence in the middle of the rod-shaped cell (Fig. 2.28b, c).

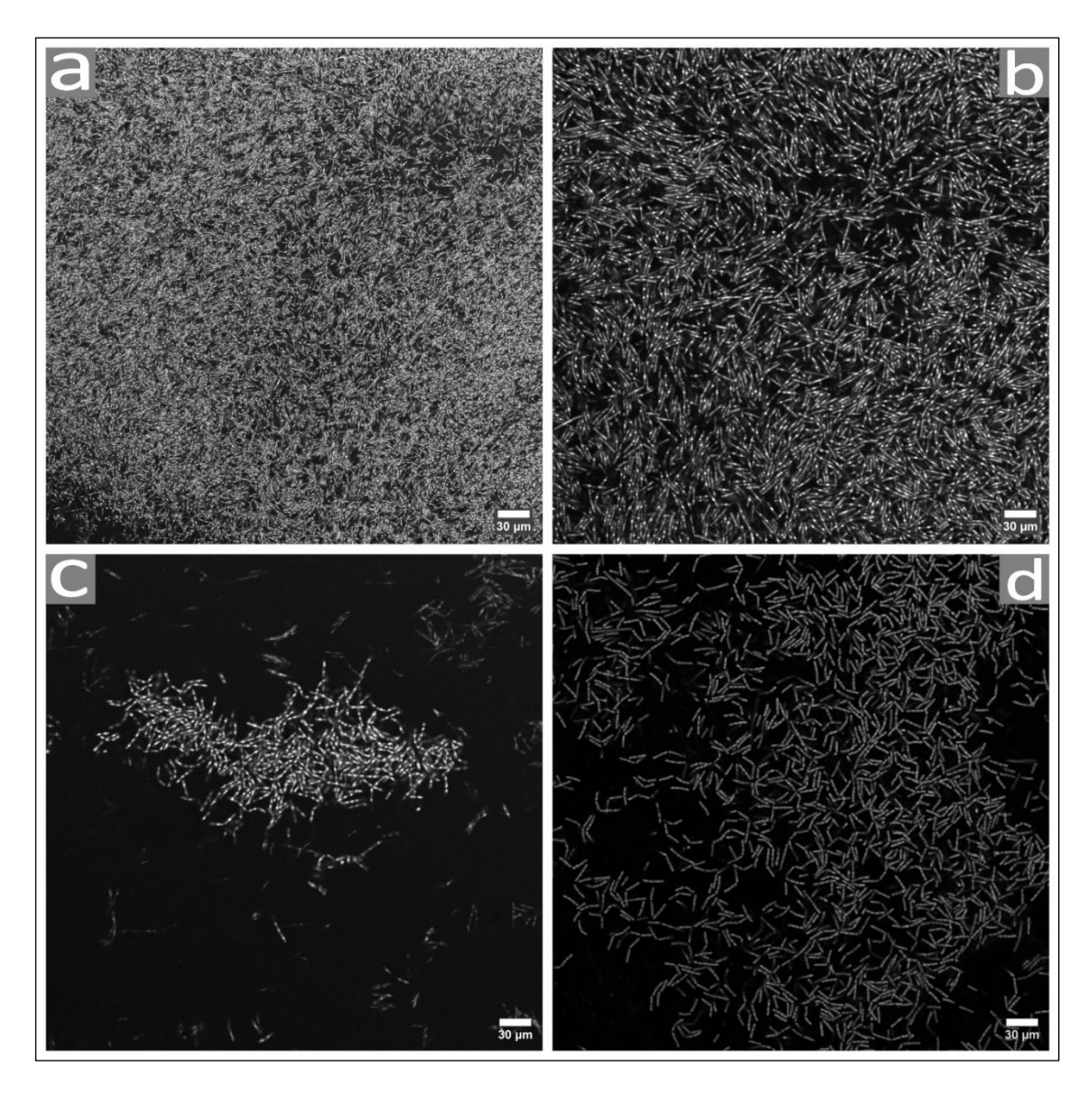


Figure 2.28. Microscopy images of gfp-expressing Bacillus subtilis biofilms treated with 500  $\mu g/mL$  GBLE. Biofilm architecture is affected, showing scattered cell clusters (c, d) and mild matrix disruption (a, b). Biofilms were grown for 72 hours, incubated at 37° in LB medium. Images acquired using SP5 Leica (630X magnification), Scale bars = 30  $\mu m$ .

#### 2.4.4.9. Amyloid fibre TasA in response to *Ginkgo biloba* Leaf Extract

To further investigate how GBLE influences extracellular matrix synthesis and bacterial amyloid fibre production, EbbaBiolight 680 stain was used on B. subtilis static biofilms and imaged using CLSM (Fig. 2.29-2.30). This stain binds to extracellular and intracellular amyloid fibres and specific ECM components such as curli,  $\beta$ -glucans and chitins. In the case of B. subtilis, the stain binds to amyloid fibre TasA.

The negative control biofilms exhibited a dense, cohesive layer of bacterial cells, uniformly distributed across the surface (Fig. 2.29a–d). Fluorescence staining with EbbaBiolight 680 revealed localized TasA production, showed by the bright magenta signals embedded within the cyan bacterial cells. In particular, Fig. 2.29a shows minimal TasA accumulation, while Fig. 2.29b shows more pronounced TasA accumulation, showing the formation of structurally complex aggregates associated with higher TasA expression. These results indicate the natural presence and spatial variability of TasA-rich regions within mature, untreated biofilms, serving as a functional baseline for comparison with GBLE-treated conditions.

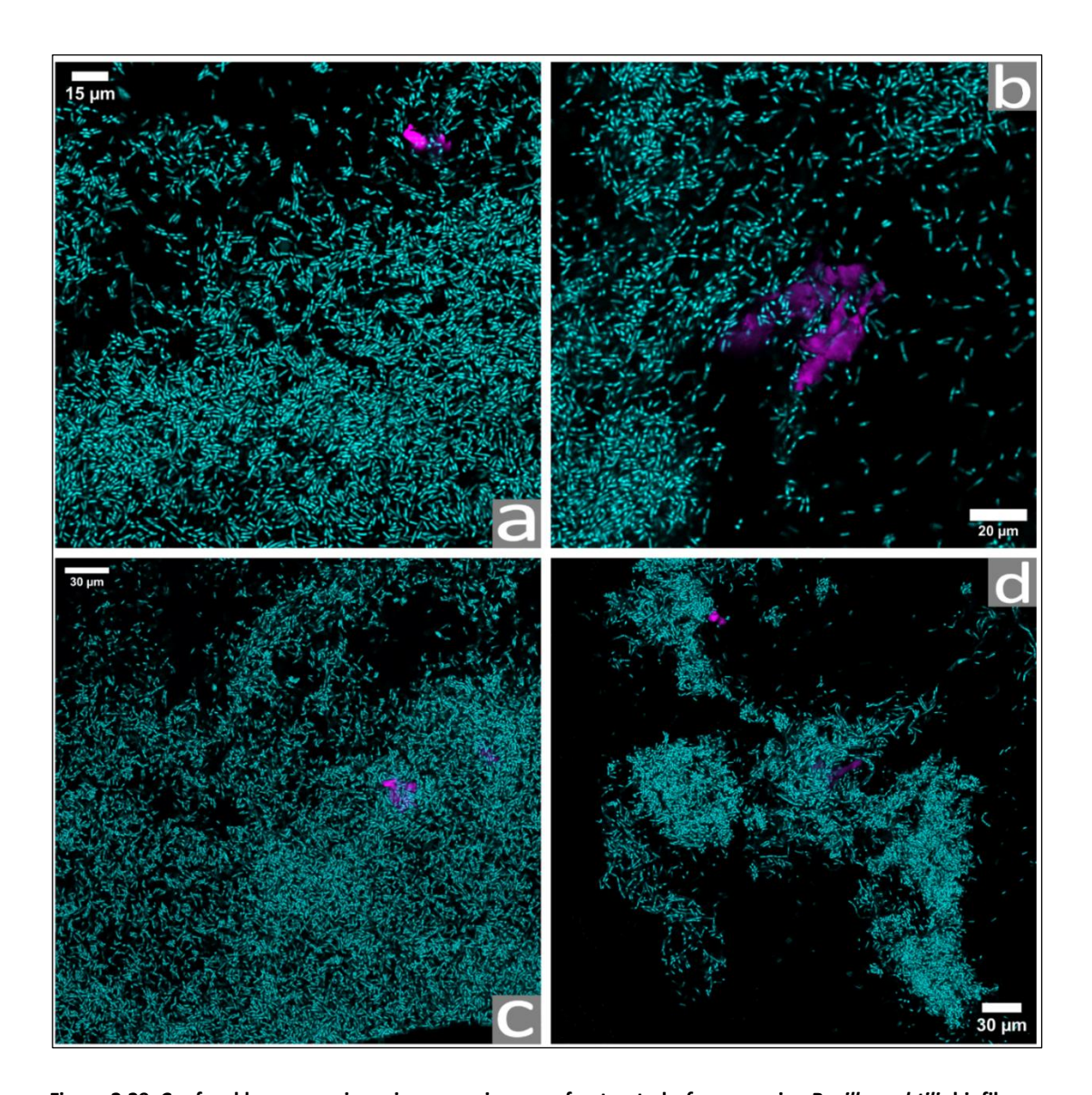


Figure 2.29. Confocal laser scanning microscopy images of untreated *gfp*-expressing *Bacillus subtilis* biofilms stained with EbbaBiolight 680. Cyan fluorescence marks bacterial cells, and magenta highlights TasA amyloid fibres. (a–c) Biofilms exhibit dense, uniform cell coverage with minimal localized TasA-rich regions. Image d shows particularly pronounced TasA accumulation associated with aggregated structures. Images acquired using SP5 Leica (630X magnification), Scale bars = 15–30 μm.

Unlike the negative control, *B. subtilis* biofilms supplemented with 100  $\mu$ g/mL GBLE showed significant changes in both biofilm architecture and TasA fibre distribution (Fig. 2.30). When GBLE is present at 100  $\mu$ g/mL, bacterial density is reduced and spatial heterogeneity increases. Notably, TasA signal was significantly more intense in several areas, often appearing in diffuse or aggregated clusters. Fig. 2.30a shows TasA intertwined within the biofilm, while Fig. 2.30b and 2.30c show scattered bacterial aggregates embedded in diffuse amyloids. Interestingly, TasA seems to be binding to either the cellular surface or the intracellular cytoplasm, as some cells fully fluoresce in magenta (Fig. 2.30d, arrows). These

findings suggest that GBLE at 100  $\mu$ g/mL disrupts cellular cohesion while simultaneously promoting TasA expression or stability, potentially as a bacterial stress response.

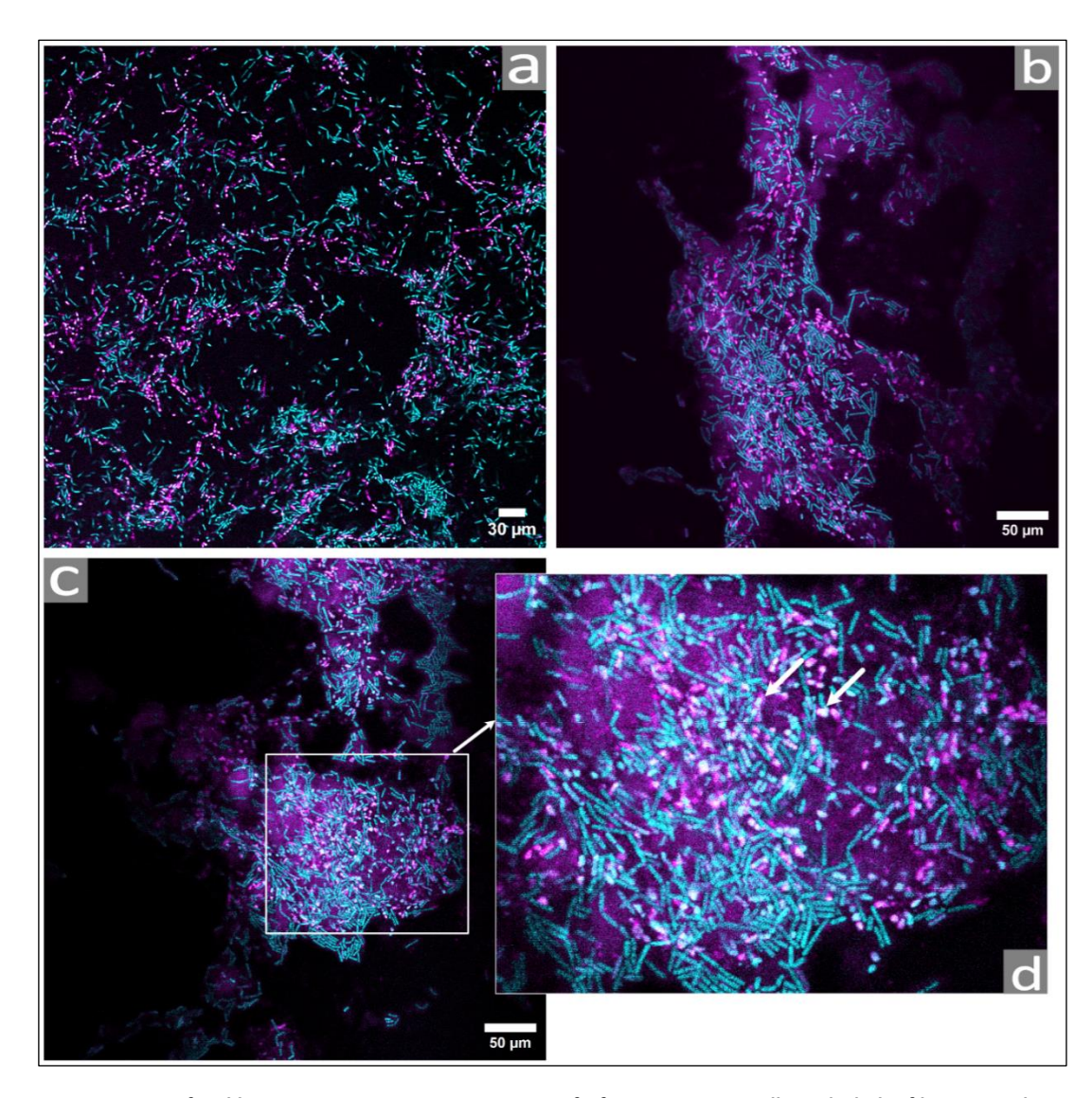


Figure 2.30. Confocal laser scanning microscopy images of *gfp*-expressing *Bacillus subtilis* biofilms treated with 100  $\mu$ g/mL GBLE and stained with EbbaBiolight 680. Cyan indicates bacterial cells; magenta indicates TasA amyloid fibres. GBLE-treated biofilms show disrupted architecture and widespread TasA accumulation (a) and around biofilm gaps (b-c), relative to the untreated control. TasA appears bound to the cellular surface or intracellularly, as some cells exhibit dua fluorescence (d). Images acquired using SP5 Leica (630X magnification) Scale bars: (a) 50  $\mu$ m; (b-c) 30  $\mu$ m; (d) 20  $\mu$ m.

## 2.5. Discussion

The formation of biofilms significantly increases the resilience of bacteria in a wide range of settings, including industrial, domestic, clinical and natural environmental settings (Flemming et al., 2016) (Liu et al., 2024) (Abdallah et al., 2014) (Otter et al., 2023). Biofilms are aggregates of microorganisms which often display increased resistance to antimicrobials (Mah and O'Toole, 2001) and become problematic once they start growing and persisting within industrial equipment and surfaces, leading to equipment decay and product contamination (Simões et al., 2010) (Abdallah et al., 2014), or inside indwelling medical devices, resulting in chronic infections (Donlan and Costerton, 2002) (Otter et al., 2023) (Liu et al., 2024). In order to be eradicated, chemical biocides, such as bleach, are usually used in the industry (Simões et al., 2010) (Otter et al., 2023) (Abdallah et al., 2014), while antibiotics are widely used for the treatment of biofilm-associated chronic infections (Donlan and Costerton, 2002) (Liu et al., 2024).

This study aims is investigate biofilm development in response to GBLE and to understand the potential antibiofilm activity of the extract. This is the first study investigating GBLE on *B. subtilis*, an environmentally relevant biofilm former.

# 2.5.1. Impact of GBLE on Planktonic Growth

Firstly, bacterial growth curves were generated from a 24 hour growth period, using *gfp*-expressing *B. subtilis* JWV042. As seen in Fig. 2.1-2.7, GBLE seems to have an effect on planktonic bacterial growth. In a concentration-dependent manner, GBLE delayed the development of the exponential phase and therefore, the growth curves show a more prolonged lag phase. It is widely known that during lag phase, the bacterial cells need time to adapt to the new environment (Rolfe et al., 2012), therefore the exponential phase delay seen in the presence of GBLE can be associated with the need of the bacterial cells to adapt to a new challenging environment. This effect was also described by Zhang et al., (2018); in their study, GBLE delayed the exponential growth phase of *Shewanella putrefaciens* (*S. putrefaciens*) and *Saprophytic staphylococcus* (*S. saprophyticus*). While a delay in exponential growth due to GBLE is observed, the growth curves also show a decrease in the length of the stationary phase, and therefore a quicker cell death, in response to GBLE. During the death phase, the number of nonviable bacterial cells exceeds the number of viable cells, hence why there is a steady decline in the growth curve. Although *B. subtilis* cells reach a higher bacterial

cell density when GBLE is present, this is followed by a shorter stationary phase and a steep decline phase, meaning that bacterial cells are dying at a faster rate compared to the negative control. This becomes particularly noticeable at 75, 100, 150, 175 and 200 µg/mL (Fig. 2.1). Several mechanisms may explain this effect. GBLE contains bioactive compounds such as ginkgolic acids and flavonoids that exert strong antibacterial effects. Experimental studies have shown that GBLE can disrupt bacterial growth by interfering with key cellular processes, including DNA replication, RNA transcription, protein synthesis, and cell division (Hua et al., 2017). In addition, crude leaf extracts have demonstrated broad-spectrum inhibitory activity against both Gram-positive and Gram-negative bacteria, with low minimum inhibitory concentrations reported for several species (Sati and Joshi, 2011), thereby stopping bacterial proliferation. In addition, disruption of iron homeostasis has been proposed as another mode of antibacterial action, as ginkgolic acid C15:1 demonstrates enhanced inhibition of Grampositive pathogens, such as Enterococcus faecalis (E. faecalis) and S. aureus, when iron assimilation is impaired, potentially via Fur regulatory pathways (Wen et al., 2022). These combined effects likely underlie the observed shorter stationary phase and steep decline in bacterial viability of *B. subtilis* planktonic cultures at concentrations  $\geq$  75 µg/mL GBLE.

The impact of GLBE on cell growth have been observed in other species of bacteria A study investigating the antimicrobial effect of *G. biloba* seed exocarp extract in *S. aureus* and MRSA highlighted a concentration-dependent bactericidal activity of this compound (Wang et al., 2021), meaning that the extract killed more bacteria as its concentration increased. *G. biloba* seed exocarp extract was also studied by Wang et al. (2021), who tested the extract against thirteen clinical isolates. Their findings showed that the seed extract inhibited the bacterial growth of all Gram positive bacteria investigated, but only two of the nine Gram negative bacteria, as well as the biofilm development of *Streptococcus haemolyticus* (*S. haemolyticus*) (Wang et al., 2021). While their investigation resulted in the inhibition of the growth of *Staphylococcus epidermidis* (*S. epidermidis*), *S. haemolyticus*, *E. faecium*, *Acinetobacter baumannii* (*A. baumannii*) and *Stenotrophomonas maltophilia* (*S. maltophilia*), this effect is not seen when GBLE is supplemented to *B. subtilis* cultures, in relation to this present study. This could indicate differences in potencies of *G. biloba* tree components, as the various studies use extracts obtained from different tree parts, or it more likely suggests a different effect of the extracts depending on the bacteria tested.

Another study by Lee et al. (2014) investigated the effect of *G. biloba* extract and Ginkgolic acid C15:1 against EHEC. The compounds investigated had no effect on bacterial growth. The non-uniform response of *G. biloba* extracts to planktonic growth is also attributed to the heterogeneity of the plant. Climatic and growth conditions of the plant influence the flavonoid and terpene content of the extracts, resulting in the difference in the results seen (Kulić et al., 2022).

## 2.5.2. Impact of GBLE on Agar Colony Biofilms

Although the literature shows different results when it comes to planktonic growth, studies seem to agree on the antibiofilm effect of G. biloba extracts. In order to investigate the antibiofilm effect of GBLE on B. subtilis JWV042, a microtiter dish assay was performed (Fig. 2.8). As seen in Fig. 2.8, GBLE inhibited biofilm development and attachment at  $\geq$  150 µg/mL, compared to the control. While it does not have an apparent effect on B. subtilis planktonic growth (apart from delayed lag phase and increase death rate), GBLE shows a concentrationdependent antibiofilm effect, suggesting that the extract modulates biofilm development independently from bacterial growth. Similar effects have been reported in S, aureus and E. coli, where Ginkgo biloba extracts inhibited the expression of critical biofilm-associated genes. Specifically, the extract downregulated key biofilm-associated genes, disrupting matrix production and stress adaptation (Wang et al., 2021). In E. coli, Ginkgolic acids were shown to inhibit csqA, csqB, and csqD, which encode curli fimbriae involved in surface attachment and matrix fibre formation (Lee et al., 2014). Furthermore, Ginkgo extracts triggered the disruption of quorum sensing pathways and a reduction of the release of extracellular DNA by repressing autolysis-related genes, leading to the impairment of biofilm maturation (Wang et al., 2021). These mechanisms are consistent with the observed reduction in B. subtilis biofilm mass, suggesting that GBLE may disrupt matrix production, interfere with cell adhesion, and suppress early biofilm development without necessarily inhibiting planktonic growth.

While the results of this present study are consistent with the previously published literature, this study is the first to focus on *B. subtilis*, an environmentally relevant model organism and biofilm former; whereas the focus of the scientific community is on clinical isolates, neglecting environmental isolates.

Due to the fact that motility and biofilm development are connected, *B. subtilis* agar biofilms were grown at different agar and GBLE concentrations, to investigate if GBLE had any effect on swimming and swarming motility. Interestingly, GBLE promoted swimming motility in *B. subtilis* JWV042 (Fig. 2.9-2.11); different results were seen for swarming motility depending on the concentration of GBLE (Fig. 2.15-2.17). In addition to a change in motility, GBLE seems to promote cellular differentiation in *B. subtilis*, leading to the development of filaments (Fig. 2.10h.1, 2.11i.1, 2.13i.1) and lobes (Fig. 2.9c.1, 2.13i.1, 2.15c.1, 2.15d, 2.18b, 2.18c, 2.18d, 2.19g.1), and triggering mutation events (Fig. 2.16e.1, 2.16h.1, 2.19h.1, 2.20k.1, 2.20k.2 and 2.20k.3). The mutants seem to be able to spread across the plate easily, compared to their mother colony, as seen in Fig. 2.20k, in which the filamentous mutant is able to saturate the plate anchoring itself to the plastic petri dish wall, at 600 μg/mL.

The increase of swimming motility in *B. subtilis* upon GBLE exposure may indicate an adaptive response to environmental stress, conferring enhanced competitive and survival advantages. The increase in colony expansion is beneficial as it leads to a more effective colonization of new territory, access to fresh nutrients, and escape from antimicrobial hotspots (Kearns, 2010). Similarly, the observed increase in swimming motility in *B. subtilis* at various GBLE concentrations suggests that individual cells are actively moving to locate more favourable microenvironments (Guttenplan et al., 2013). Swimming and surface spreading not only support dispersal but may also reduce the energetic cost of maintaining biofilm architecture under stress (Kearns, 2010) (Katharios-Lanwermeyer and O'Toole, 2022). In addition, motility is often inversely regulated with biofilm formation, and increased motility may signal a phenotypic shift away from the biofilm lifestyle toward a more exploratory, planktonic state, better suited for survival under stress (Chai et al., 2011). This behaviour suggests that GBLE not only disrupts biofilm stability but may actively promote microbial differentiation and evolutionary adaptation, by inducing a stress response.

An increased swimming motility in response to GBLE has also been reported by Lee et al., (2014), as well as a reduction in swarming motility on EHEC. A decreased swarming motility of *B. subtilis* in this study can be seen at 400 and 500  $\mu$ g/mL, indicating that the concentration-dependent antibiofilm effect might be associated with a change in the swarming motility pattern (Lee et al., 2014) and the mutation events.

Although at different concentrations, the antibiofilm activity of *G. biloba* extracts remains clear and consistent within the literature, this effect is biofilm specific as it occurs

independently from planktonic growth. This is seen in this present study, investigating the effect of GBLE on *B. subtilis*, and by Lee et al. (2014), who reported a similar outcome when they tested GBLE on *E. coli*.

# 2.5.3. Impact of GBLE on static Biofilms

To further elucidate the effect of GBLE on *B. subtilis* biofilms, *gfp*-expressing *B. subtilis* static biofilms were grown in 6 wells plates on microscope coverslips and imaged using confocal microscopy. Results show a drastic change in biofilm architecture following the addition of GBLE (Fig. 2.21-2.28), with the appearance of bacterial aggregates and chains, also known as Van Gogh bundles. Distinctive Van Gogh bundles can be clearly seen at 100 μg/mL (Fig. 2.24a and 2.24b) and more densely packed bundles can also be seen at higher concentrations (Fig. 2.27c, arrow). Van Gogh bundles have been characterised in a study carried out by van Gestel, Vlamakis and Kolter (2015), as they defined this cellular conformation as organised single-cell chains that push themselves out of the colony edge and therefore, contribute to colony expansion, in the context of sliding motility on agar surface. In the following images (Fig. 2.31), we see Van Gogh bundle formation within static biofilms in response to GBLE (Fig. 2.31B). However, the Van Gogh bundles developed in response to GBLE show structural differences compared to the ones described by van Gestel, Vlamakis and Kolter (2015) (Fig. 2.31A).

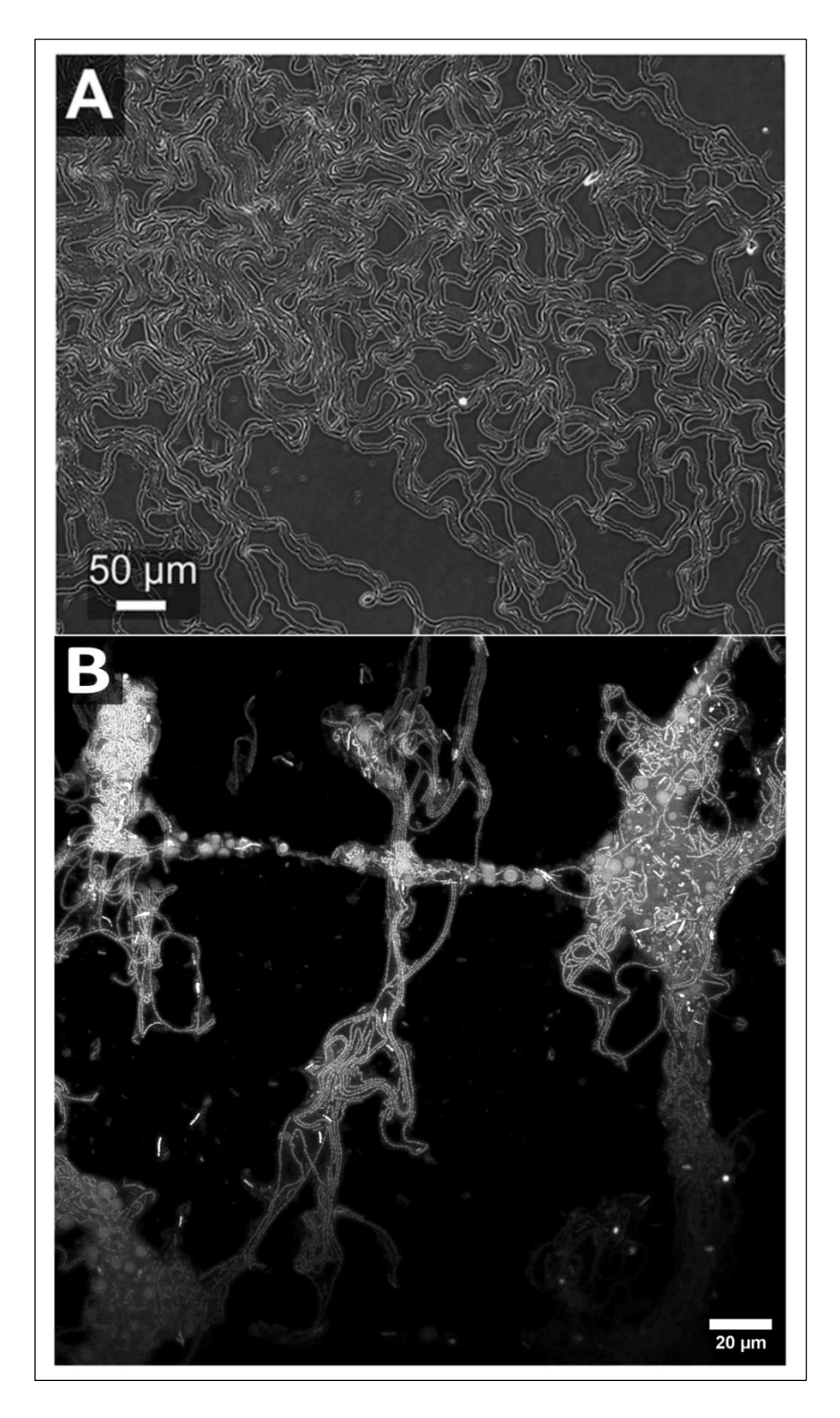


Figure 2.31. A) Van Gogh bundles characterised by van Gestel, Vlamakis and Kolter (2015) on agar plates at the edge of *Bacillus subtilis* colonies. B) Van Gogh bundles seen in this present study, in *B. subtilis* JWV042 static biofilms in response to 100  $\mu$ g/mL GBLE (Image acquired using Leica SP5, 630x Magnification).

While the Van Gogh bundles on agar characterized by van Gestel et al. (2015) display an organised structure (Fig. 2.31A), the Van Gogh bundles seen in the static biofilms in response

to GBLE (Fig. 2.31B) show a disorganised architecture compared to Fig. 2.31A, with bundles intertwined between each other, as well as the presence of circular structures. Additionally, while the agar bundles show uniform bacterial cells (van Gestel et al., 2015), static bundles in the presence of GLBE show the presence of different cell types, which appear less elongated and more of a round shape, compared to the traditional B. subtilis rod shape (Fig. 2.23d, arrow). In a study carried out by Zhang et al. (2018), results showed that GBLE affected the integrity of the cell membrane, leading to cell lysis. Furthermore, GBLE also influenced membrane permeability, which triggered a change in the shape of bacterial cells as well as intracellular organelles (Zhang et al., 2018). This is consistent with the change in the rodshape in B. subtilis cells seen here. Moreover, as seen in Fig. 2.27d, 2.28b and 2.28c, GBLE influences intracellular structures, resulting in DNA condensation in the nucleoid, indicating that GBLE also modulates DNA production. A number of studies have already highlighted the ability of G. biloba extracts to influence expression of genes related to biofilm development, eDNA release and cell-surface proteins (Wang et al., 2021) (Lee et al., 2014). Nucleoid condensation in bacteria is a common structural response to environmental and physiological stress and can arise through several, often overlapping mechanisms (Ohniwa et al., 2006) (de Vries, 2010) (Hołówka and Zakrzewska-Czerwińska, 2020). Increased production or activity of nucleoid-associated proteins (NAPs) can compact DNA under starvation, oxidative, or antibiotic stress (Ohniwa et al., 2006) (Hołówka and Zakrzewska-Czerwińska, 2020), and post-translational modification of HBsu in Bacillus subtilis (e.g., lysine acetylation) has been shown to regulate both DNA compaction and sporulation, as well as survival after antibiotic exposure (Luu et al., 2022). Changes in DNA topology mediated by topoisomerases (including DNA gyrase) also influence the degree of nucleoid packing (Ohniwa et al., 2006) (de Vries, 2010), and small molecules, including some plant-derived phenolics, can interfere with these enzymes and/or bind DNA directly (Khameneh et al., 2019).

Along with Van Gogh bundles, bacterial aggregates also appear (Fig. 2.25c and 2.25d), which do not form in the negative control (Fig. 2.21). Autoaggregates are usually a protective form that the bacterial cells adopt to protect themselves from environmental stresses, specifically nutrient depletion and oxidative stress (Trunk, Khalil and Leo, 2018) (Dogsa, Kostanjšek and Stopar, 2023), suggesting that GBLE is inducing nutrient starvation and/or oxidative stress. GBLE may induce nutrient starvation in bacteria by disrupting cell membrane integrity, a mechanism commonly observed with plant-derived phenolics, resulting in impaired uptake

of essential nutrients and ions and eventual cell death (Bouarab-Chibane et al., 2019) (Lobiuc et al., 2023). In addition, as *B. subtilis* utilises eDNA as a scaffold for autoaggregation (Dogsa, Kostanjšek and Stopar, 2023), it is possible that the eDNA released by cell lysis due to GBLE is promoting aggregate formation, assuming that in this study, GBLE is indeed triggering cell lysis.

# 2.5.4. Impact of GBLE on TasA Amyloid Fibres

To understand the synthesis of extracellular matrix components and amyloid fibres, qfpexpressing B. subtilis static biofilms were supplemented with EbbaBiolight 680 dye and grown on microscope coverslips. This dye binds to extracellular and intracellular amyloids and some glucans found within the ECM. B. subtilis biofilms supplemented with EbbaBiolight 680 were then imaged using confocal laser microscopy (Fig. 2.29-2.30). The first thing that strikes the eye is the presence of more bound EbbaBiolight 680 stain when GBLE is present, as more magenta fluorescence can be seen (Fig. 2.30b-c). This indicates an increase in the production of bacterial amyloid fibres, also known as protein TasA in the case of B. subtilis biofilms. As the TasA protein folds into a fibrous network, which interlinks cells within a biofilm (Romero et al., 2010), GBLE seems to promote TasA amyloid fibre synthesis at relatively lower concentrations (Fig. 2.30). This does not happen in the same structural conformation in the control (Fig. 2.29). TasA protein in its amyloid form appears to function as a rigid scaffolding network within the biofilm, upon which more flexible ECM components are localised (Cámara-Almirón et al., 2020). TasA amyloid fibres are resistant to denaturation and degradation and they confer structural integrity and robustness to the biofilm. They are also employed as a survival mechanism to environmental stimuli during biofilm development (Cámara-Almirón et al., 2020).

Referred to as functional amyloid fibres due to their biological roles, bacterial amyloids have multiple purposes within the biofilm. In addition to being structural components of the ECM, functional amyloids were also found to be involved in cellular detoxification (Taglialegna, Lasa and Valle, 2016). In *B. subtilis*, TasA fibres are also involved in cell-to-cell interactions within the biofilms. They aid bacterial cells in surface adhesion as well as in raising aerial projections in biofilms (Romero et al., 2010). Interestingly, amyloids were found to be prevalent in biofilms found in natural environments (Larsen et al., 2007). In non-laboratory environments, bacterial biofilms have to withstand numerous environmental stresses and therefore, a more robust structure is needed. An increased synthesis of TasA in response to

GBLE found here suggests that the presence of GBLE is creating a challenging environment for *B. subtilis* and that the bacterial cells have to adopt a multicellular biofilm form which requires an increased production of the TasA amyloid fibre in order to survive.

TasA is synthesised in the cytoplasm in a soluble globular nonamyloid state and it is hypothesised to fold into structured amyloid fibres on the cell wall, depending on the surrounding environmental conditions (Álvarez-Mena et al., 2020). Due to their versatility, functional amyloid fibres are used by microorganisms to efficiently adapt to unexpected changes in the environment. Previous studies have indicated the ability of *Gingko biloba* extracts to inhibit ECM synthesis by downregulating biofilm-associated gene expression of *S. aureus,* MRSA and *E. coli* (Wang et al., 2021) (Lee et al., 2014). Additionally, Lee et al. (2014) highlighted how Ginkgolic acids repressed *E. coli* genes responsible for curli synthesis, an amyloid protein produced by *E. coli* during biofilm development. This suggests that *G. biloba* affects bacterial amyloid production, which is also seen *B. subtilis* JWV042 biofilms stained with EbbaBiolight 680.

Specifically to *B. subtilis* JWV042, low concentrations of GBLE result in the formation of larger biofilms on agar and it is highly probable that the larger agar biofilms are associated with an increase in production of TasA, also seen in static biofilms. The agar biofilms also present more complex filamentous structures, consistent with the Van Gogh bundles observed in the static biofilms. TasA is also associated with motility. The amyloid protein has been found to act as a signal molecule which keeps a subpopulation of cells motile within the biofilm (Álvarez-Mena et al., 2020). Specifically, TasA plays a role in sliding motility and studies have highlighted that the protein upregulates motility genes in biofilms (Arnaouteli et al., 2021), which might explain why, in this present study, *B. subtilis* agar biofilms show increased motility on agar.

In addition to being bound to TasA fibres in the ECM, EbbaBiolight 680 was also bound to the cell surface of some bacterial cells, indicating the presence of subpopulations. These bacterial cells showed both cyan and magenta fluorescence, in the middle of the cell and on parts of the bacterial cell surface, respectively (Fig. 2.30d, arrows). This indicates the presence of amyloid structures on the cell wall of a subpopulation within the biofilm. Within the subpopulation that presents both fluorescent signals, bacterial cells seem to have two distinct shapes, the classic *B. subtilis* vegetative cells rod shape and cells that present a rounder and smaller shape (Fig. 2.30d, arrows). A number of studies have indicated the

presence of amyloid-like fibres TasA in the spore coat of various bacterial species, including B. subtilis (Stöver and Driks, 1999) (Bauer et al., 1999). Considering the size and shape of the round subpopulation of B. subtilis cells as well as the presence of TasA on their surface, it is possible to assume that this subpopulation might be B. subtilis spores. This hypothesis further indicates that GBLE is promoting cellular differentiation within B. subtilis biofilms when present at relatively low concentrations. This is further supported by the presence of a subpopulation of rod-shape vegetative cells, which show dual fluorescence (Fig. 2.30d, arrows). Additionally to being part of the ECM, TasA fibres are also attached to the cell surface, and this happens through the TapA protein, which modulates the amyloid fibres polymerization. TapA has been recently defined as a functional amyloid, due to its ability to self-polymerize into amyloid form in vitro (Álvarez-Mena et al., 2020). The assembly of unfolded TasA into mature amyloid TasA seems to happen on the cell wall, and this process is catalysed by TapA (Diehl et al., 2018). Unfolded TapA and TasA proteins are moved from the cytoplasm to the cell wall through the general secretory pathway SipW, where TapA anchors itself to the cell membrane and amyloid fibre formation occurs (Romero et al., 2010) (Hobley et al., 2013). Unfolded TasA proteins assume the cross-β sheet structural conformation and extend like appendages from the bacterial cell. TapA was found to not only modulate fibre assembly of TasA, but it is also incorporated in the fibre structure at low levels. 1:100 (Romero et al., 2011) (El Mammeri et al., 2019).

Recent studies have highlighted the dual role of the TasA protein, which is essential for both ECM formation and the regulation of cell membrane dynamics. Amyloid proteins adhere to functional components of the cell membrane and specifically in *B. subtilis*, TasA is found attached to the lipids of detergent-resistant membrane loci (Cámara-Almirón et al., 2020). Due to the protective and stabilising effect that TasA has on the cellular membrane, it is possible that *B. subtilis* cells are also upregulating membrane anchored TasA proteins to counteract possible stress induced by the presence of GBLE. Bacteria possess a complex stress response machinery, which also includes changes in the cell membrane composition, a process referred to as cell envelope stress responses (CESRs). During CESRs, bacteria are able to modify membrane lipids and proteins to confer resistance against membrane-active compounds (Willdigg and Helmann., 2021). In order to withstand cell membrane disturbance, some bacterial cells differentiate into a subpopulation with increased amount of TasA bound to the cell surface. Cámara-Almirón et al. (2020) speculate that *B. subtilis* cells can control the quantity of TasA bound to the cell membrane to adjust membrane dynamics to allow for

an improved stress response to challenging environmental changes. This hypothesis is further supported by the findings of this present study, which suggest that *B. subtilis* JWV042 cells differentiate into multiple subpopulations, including cells with increased amounts of membrane TasA, indicating that bacterial cells can modulate cell membrane biochemical composition depending on the environmental conditions.

#### 2.6. Conclusion

This chapter provides the first systematic evaluation of a *Ginkgo biloba* leaf extract (GBLE) against the model biofilm former *Bacillus subtilis* using a multi-scale experimental pipeline spanning planktonic growth assays, microtiter biofilm quantification, agar-based motility/biofilm tests, and high-resolution confocal imaging of static biofilms stained with the ECM/amyloid probe EbbaBiolight 680.

GBLE delayed entry into exponential growth and shortened stationary-phase survival at ≥75 µg/mL, yet inhibited surface attachment and early biofilm accumulation in microtiter assays at ≥150 µg/mL, indicating biofilm-specific effects partially uncoupled from bulk growth inhibition. On semi-solid media GBLE enhanced swimming while altering swarming in a concentration-dependent manner and promoted pronounced colony differentiation, including filaments, lobed sectoring, emergent mutant lineages with increased spreading, and putative spore-like subpopulations. Microscopy of air-liquid interface biofilms revealed dose-responsive remodelling of community architecture: GBLE induced Van Gogh-like multicellular bundles, stress-associated aggregates, and nucleoid condensation consistent with physiological stress responses. EbbaBiolight 680 staining further showed elevated and spatially redistributed amyloid signal, suggesting increased TasA fibre production, membrane-associated TasA, and links to motility and envelope stress adaptation. Importantly, antibiofilm activity was observed at concentrations that did not proportionally suppress planktonic growth across much of the tested range, pointing to opportunities for selective biofilm targeting with potentially lower selection for resistance. Together these findings show that GBLE does more than reduce biomass: it rewires developmental trajectories, motility and biofilm trade-offs, and matrix organization in B. subtilis. From an applications standpoint, plant-derived formulations such as GBLE may be leveraged to weaken or redirect biofilms, but their concentration-dependent capacity to provoke adaptive multicellular behaviours argues for mechanism-informed dosing and combination strategies.

#### 2.7. References

Abdallah, M., Benoliel, C., Drider, D., Dhulster, P. and Chihib, N. E. (2014) Biofilm formation and persistence on abiotic surfaces in the context of food and medical environments. Archives of Microbiology. Vol. 196(7), pp. 453–472.

Álvarez-Mena, A., Muñoz-Pinedo, C., Fernández-Tresguerres, M.E., Alonso, C., Sánchez-Quesada, J., Otzen, D.E., Cortajarena, A.L. and Caro, E. (2020) Environmental regulation of amyloid formation by Bacillus subtilis TasA. mBio. Vol. 11(1), e02254-19.

Arnaouteli, S., Bamford, N.C., Stanley-Wall, N.R. & Kovács, Á.T. (2021) Bacillus subtilis biofilm formation and social interactions. Nature Reviews Microbiology. Vol. 19(9), pp. 600–614.

Baquero, F., Martínez, J.L. and Cantón, R. (2008) Antibiotics and antibiotic resistance in water environments. Current Opinion in Biotechnology. Vol. 19(3), pp.260–265.

Bauer, T., Little, S. and Driks, A. (1999) Functional regions of the Bacillus subtilis spore coat morphogenetic protein CotE. Journal of Bacteriology. Vol. 181(22), pp. 7043–7051

Beauregard, P.B., Chai, Y., Vlamakis, H., Losick, R. and Kolter, R. (2013) Bacillus subtilis biofilm induction by plant polysaccharides. Proceedings of the National Academy of Sciences of the United States of America. Vol. 110(17), pp. E1621–E1630.

Bondarczuk, K., Markowicz, A. and Piotrowska-Seget, Z. (2016) The urgent need for risk assessment on the antibiotic resistance spread via sewage sludge land application. Environment International. Vol. 87, pp.49–55.

Bouarab-Chibane, L., Forquet, V., Lantéri, P., Clément, Y., Léonard-Akkari, L., Oulahal, N., Degraeve, P. and Bordes, C. (2019) Antibacterial properties of polyphenols: Characterization and QSAR (quantitative structure—activity relationship) models. Frontiers in Microbiology. Vol. 10, Article 829.

Cámara-Almirón, J., Navarro, Y., Díaz-Martínez, M.E., Magno-Pérez-Bryan, M.C., Molina-Santiago, C., Pearson, J.R., de Vicente, A., Pérez-García, A. and Romero, D. (2020) Dual functionality of the amyloid protein TasA in Bacillus subtilis. Frontiers in Microbiology. Vol. 11, Article 602.

Carrascosa, C., Raheem, D., Ramos, F., Saraiva, A. and Raposo, A. (2021) Microbial biofilms in the food industry - A comprehensive review. International Journal of Environmental Research and Public Health. Vol. 18(4), Article 2014.

Chai, Y., Norman, T., Kolter, R. and Losick, R. (2011) An epigenetic switch governing daughter cell separation in Bacillus subtilis. Molecular Microbiology. Vol. 80(3), pp. 486–496.

Chassagne, F., Huang, X., Lyles, J.T. and Quave, C.L. (2019) Validation of a 16th Century Traditional Chinese Medicine use of Ginkgo biloba as a topical antimicrobial. Frontiers in Microbiology. Vol. 10, Article 775.

Dai, Z., Sevillano-Romero, M., Balboa, S., Sánchez, D., Martínez, J.L. and González-Zorn, B. (2020) Disinfection exhibits systematic impacts on the drinking water microbiome. Microbiome. Vol. 8, Article 59.

de Vries, R. (2010) DNA condensation in bacteria: Interplay between macromolecular crowding and nucleoid proteins. Biochimie. Vol. 92(12), pp. 1715–1721.

Diehl, A., Roske, Y., Ball, L., Chowdhury, A., Hiller, M., Molière, N., Kramer, R., Stöppler, D., Worth, C.L., Schmidt, A., Cremer, N., Erdmann, N., Lopez, D., Stephanowitz, H., Krause, E., Stülke, J., Bremer, E., Daniel, R., Bange, G., Becher, D. and Turgay, K. (2018) Structural changes of TasA in biofilm formation of Bacillus subtilis. Proceedings of the National Academy of Sciences of the United States of America. Vol. 115(13), pp. 3237–3242.

Dogša, I., Kostanjšek, R. and Stopar, D. (2023) eDNA provides a scaffold for autoaggregation of Bacillus subtilis in bacterioplankton suspension. Microorganisms. Vol. 11(2), Article 332.

Dogša, I., Bellich, B., Blaznik, M., Lagatolla, C., Ravenscroft, N., Rizzo, R., Stopar, D. and Cescutti, P. (2024) Bacillus subtilis EpsA O: a novel exopolysaccharide structure acting as an efficient adhesive in biofilms. NPJ Biofilms and Microbiomes. Vol. 10(1), Article 98.

Donlan, R.M. and Costerton, J.W. (2002) Biofilms: survival mechanisms of clinically relevant microorganisms. Clinical Microbiology Reviews. Vol.15(2), pp. 167–193.

El Mammeri, N., Hierrezuelo, J., Tolchard, J., Bertoncini, C.W., Cascella, R., Cross, S.J., Rosengarten, A.S., Shimanovich, U., Li, J., Shen, Y., Radford, S.E., Mezzenga, R., Knowles, T.P.J., MacPhee, C.E., Caruso, M.M. and Perrett, S. (2019) Molecular architecture of bacterial amyloids in Bacillus subtilis biofilms. Frontiers in Microbiology. Vol. 10, Article 2626.

Flemming, H.-C., Wingender, J., Szewzyk, U., Steinberg, P., Rice, S.A. and Kjelleberg, S. (2016) Biofilms: an emergent form of bacterial life. Nature Reviews Microbiology. Vol. 14(9), pp. 563–575.

Galié, S., García-Gutiérrez, C., Miguélez, E.M., Villar, C.J. and Lombó, F. (2018) Biofilms in the food industry: Health aspects and control methods. Frontiers in Microbiology. Vol. 9, Article 898.

Guttenplan, S.B. and Kearns, D.B. (2013) Regulation of flagellar motility during biofilm formation. Nature Reviews Microbiology. Vol. 11(5), pp. 338–348.

Hobley, L., Ostrowski, A., Rao, F.V., Bromley, K.M., Porter, M., Prescott, A.R., MacPhee, C.E., van Aalten, D.M.F. and Stanley-Wall, N.R. (2013) BslA is a self-assembling bacterial hydrophobin that coats the Bacillus subtilis biofilm. Proceedings of the National Academy of Sciences of the United States of America. Vol. 110(33), pp. 13600–13605.

Hołówka, J. and Zakrzewska-Czerwińska, J. (2020) Nucleoid-associated proteins: The small organizers that help bacteria adapt to stress. Frontiers in Microbiology. Vol. 11, Article 590.

Hua, Z., Wu, C., Fan, G., Tang, Z. and Cao, F. (2017) The antibacterial activity and mechanism of ginkgolic acid C15:1. BMC Biotechnology. Vol. 17(1), Article 5.

Isah, T. (2015) Rethinking Ginkgo biloba L.: Medicinal uses and conservation. Pharmacognosy Reviews. Vol. 9(18), pp.140–148.

Jones, I.A. (2021) Biocide use in the antimicrobial era: a review. Molecules. Vol. 26(8), Article 2276.

Katharios-Lanwermeyer, S. and O'Toole, G.A. (2022) Biofilm maintenance as an active process: Evidence that biofilms work hard to stay put. Journal of Bacteriology. Vol. 204, e0058721.

Kearns, D.B. (2010) A field guide to bacterial swarming motility. Nature Reviews Microbiology. Vol. 8(9), pp. 634–644.

Khameneh, B., Iranshahy, M., Soheili, V. and Fazly Bazzaz, B.S. (2019) Review on plant antimicrobials: a mechanistic viewpoint. Antimicrobial Resistance & Infection Control. Vol. 8, Article 118.

Kuchina, A., Espinar, L., Çağatay, T., Balbin, A.O., Zhang, F., Alvarado, A., García Ojalvo, J. and Süel, G.M. (2011) Temporal competition between differentiation programs determines cell fate choice. Molecular Systems Biology. Vol. 7, Article 557.

Kulić, Ž., Lehner, M.D. and Dietz, G.P.H. (2022) Ginkgo biloba leaf extract EGb 761® as a paragon of the product by process concept. Frontiers in Pharmacology. Vol. 13, Article 1007746.

Larsen, P., Nielsen, J.L., Dueholm, M.S., Wetzel, R., Otzen, D. and Nielsen, P.H. (2007) Amyloid adhesins are abundant in natural biofilms. Environmental Microbiology. Vol. 9(12), pp. 3077–3090.

Leach, F.S. (2011) Anti-microbial properties of Scutellaria baicalensis and Coptis chinensis, two traditional Chinese medicines. Bioscience Horizons: The International Journal of Student Research. Vol. 4(2), pp.119–127.

Lee, J.-H., Kim, Y.-G., Ryu, S.Y., Cho, M.H., and Lee, J. (2014) Ginkgolic acids C15:1 and C17:1 and Ginkgo biloba extract inhibit Escherichia coli O157:H7 and Staphylococcus aureus biofilm formation. International Journal of Food Microbiology. Vol. 174, pp.47–55.

Liu, C., Sun, D., Liu, J., Zhu, J. and Liu, W. (2021) Recent advances and perspectives in efforts to reduce the production and application cost of microbial flocculants. Bioresources and Bioprocessing. Vol. 8, Article 51.

Liu, H.Y., Prentice, E.L. & Webber, M.A. (2024) Mechanisms of antimicrobial resistance in biofilms. NPJ Antimicrobials and Resistance. Liu, H.Y., Prentice, E.L. & Webber, M.A. (2024) Mechanisms of antimicrobial resistance in biofilms. NPJ Antimicrobials and Resistance, 2(1), 27. Vol. 2(1), 27.

Lobiuc, A., Pavăl, N-E., Mangalagiu, I.I., Gheorghiță, R., Teliban, G-C., Amăriucăi-Mantu, D. and Stoleru, V. (2023) Future antimicrobials: Natural and functionalized phenolics. Molecules. Vol. 28(3), Article 1114.

Luu, J., Mott, C. M., Schreiber, O. R., Giovinco, H. M., Betchen, M. & Carabetta, V. J. (2022) Ne-Lysine acetylation of the histone-like protein HBsu regulates the process of sporulation

and affects the resistance properties of Bacillus subtilis spores. Frontiers in Microbiology. Vol. 12, Article 782815.

Mah, T.F.C. and O'Toole, G.A. (2001) Mechanisms of biofilm resistance to antimicrobial agents. Trends in Microbiology. Vol. 9(1), pp.34–39.

Mahady, G.B. (2001) Ginkgo Biloba: A Review of Quality, Safety, and Efficacy. Nutrition in Clinical Care. Vol. 4(3), pp.140–147.

Maillard, J.Y. (2005) Antimicrobial biocides in the healthcare environment: efficacy, usage, policies, and perceived problems. Therapeutics and Clinical Risk Management. Vol. 1(4), pp.307–320.

Martínez, J.L. (2009) Environmental pollution by antibiotics and by antibiotic resistance determinants. Environmental Pollution. Vol. 157(11), pp.2893–2902.

Muluye, R.A., Bian, Y. and Alemu, P.N. (2014) Anti-inflammatory and antimicrobial effects of heat-clearing Chinese herbs: A current review. Journal of Traditional and Complementary Medicine. Vol. 4(2), pp.93–98.

Ng, M.K. (2025) Clinical and environmental harms of quaternary ammonium compounds. Journal of Hazardous Materials Advances. Vol. 15, Article 100343.

Ohniwa, R.L., Morikawa, K. and Kim, J. (2006) Nucleoid architecture and dynamics in Escherichia coli. Microbiology. Vol. 152(4), pp. 1119–1131.

Ostrov, I., Paz, T. and Shemesh, M. (2019) Robust biofilm-forming Bacillus isolates from the dairy environment demonstrate an enhanced resistance to cleaning-in-place procedures. Foods. Vol. 8(4), Article 134.

Otter, J.A., Yezli, S., Perl, T.M., Barbut, F., French, G.L. and Vickery, K. (2023) Biofilms on medical instruments and surfaces: do they interfere with cleaning and disinfection? American Journal of Infection Control. Vol. 51(12), pp. 1554–1563.

Rolfe, M.D., Rice, C.J., Lucchini, S., Pin, C., Thompson, A., Cameron, A.D.S., Alston, M., Stringer, M.F., Betts, R.P., Baranyi, J., Peck, M.W. and Hinton, J.C.D. (2012) Lag phase is a distinct growth phase that prepares bacteria for exponential growth. BMC Microbiology. Vol. 12, Article 102.

Romero, D., Aguilar, C., Losick, R. and Kolter, R. (2010) Amyloid fibers provide structural integrity to Bacillus subtilis biofilms. Proceedings of the National Academy of Sciences of the United States of America. Vol. 107(5), pp. 2230–2234.

Romero, D., Vlamakis, H., Losick, R. and Kolter, R. (2011) An accessory protein required for anchoring and assembly of amyloid fibres in Bacillus subtilis biofilms. Proceedings of the National Academy of Sciences of the United States of America. Vol. 108(52), pp. 20627–20632.

Sati, S.C. and Joshi, S. (2011) Antibacterial activities of Ginkgo biloba L. leaf extracts. The Scientific World Journal. Vol. 2011, Article 545421.

Simões, M., Simões, L.C. and Vieira, M.J. (2010) A review of current and emergent biofilm control strategies. LWT – Food Science and Technology. Vol. 43(4), pp.573–583.

Singer, A.C., Shaw, H., Rhodes, V. and Hart, A. (2016) Review of antimicrobial resistance in the environment and its relevance to environmental regulators. Frontiers in Microbiology. Vol. 7, Article 1728.

Stöver, A.G. and Driks, A. (1999) Secretion, localization, and antibacterial activity of TasA, a Bacillus subtilis spore-associated protein. Journal of Bacteriology. Vol. 181(1), pp. 166–173.

Taglialegna, A., Lasa, I. and Valle, J. (2016) Amyloid structures as biofilm matrix scaffolds. Journal of Bacteriology. Vol. 198(19), pp. 2579–2588.

Trunk, T., Khalil, H.S. and Leo, J.C. (2018) Bacterial autoaggregation. AIMS Microbiology. Vol. 4(1), pp. 140–164.

van Gestel, J., Vlamakis, H. and Kolter, R. (2015) From cell differentiation to cell collectives: Bacillus subtilis uses division of labor to migrate. PLoS Biology. Vol. 13(4), Article e1002141.

Vlamakis, H., Aguilar, C., Losick, R. and Kolter, R. (2008) Control of cell fate by the formation of an architecturally complex bacterial community. Genes & Development. Vol. 22(7), pp. 945–953.

Wang, B., Wei, P.-W., Wan, S., Yao, Y., Song, C.-R., Song, P.-P., Xu, G.-B., Hu, Z.-Q., Zeng, Z., Wang, C. and Liu, H.-M. (2021) Ginkgo biloba exocarp extracts inhibit S. aureus and MRSA by disrupting biofilms and affecting gene expression. Journal of Ethnopharmacology. Vol. 271, Article 113895.

Wen, Z., Zhao, Y., Gong, Z., Tang, Y., Xiong, Y., Chen, J., Chen, C., Zhang, Y., Liu, S., Zheng, J., Li, D., Deng, Q., and Yu, Z. (2022) The mechanism of action of ginkgolic acid (15:1) against Gram-positive bacteria involves crosstalk with iron homeostasis. Microbiology Spectrum. Vol. 10(1), e00991 21.

Willdigg, J.R. and Helmann, J.D. (2021) Bacterial membrane composition and its modulation in response to stress. Frontiers in Molecular Biosciences. Vol. 8, Article 634438.

Zhang, N., Lan, W., Wang, Q., Sun, X. and Xie, J. (2018) Antibacterial mechanism of Ginkgo biloba leaf extract when applied to Shewanella putrefaciens and Saprophytic staphylococcus. Aquaculture and Fisheries. Vol. 3(4), pp.163–169.

Zhang, Z., Hou, D., Wang, Y., Wang, C., Yang, Y. and Mao, D. (2021) Residual chlorine disrupts microbial communities and enhances antibiotic resistance gene dissemination in freshwater ecosystems. Journal of Hazardous Materials. Vol. 403, Article 123606.

Zhao, Q., Chen, X.Y. and Martin, C. (2016) Scutellaria baicalensis, the golden herb from the garden of Chinese medicinal plants. Science Bulletin (Beijing). Vol. 61(18), pp.1391–1398.

# 2.8. Appendix

#### 1. **S1.** Colony morphology description guide.

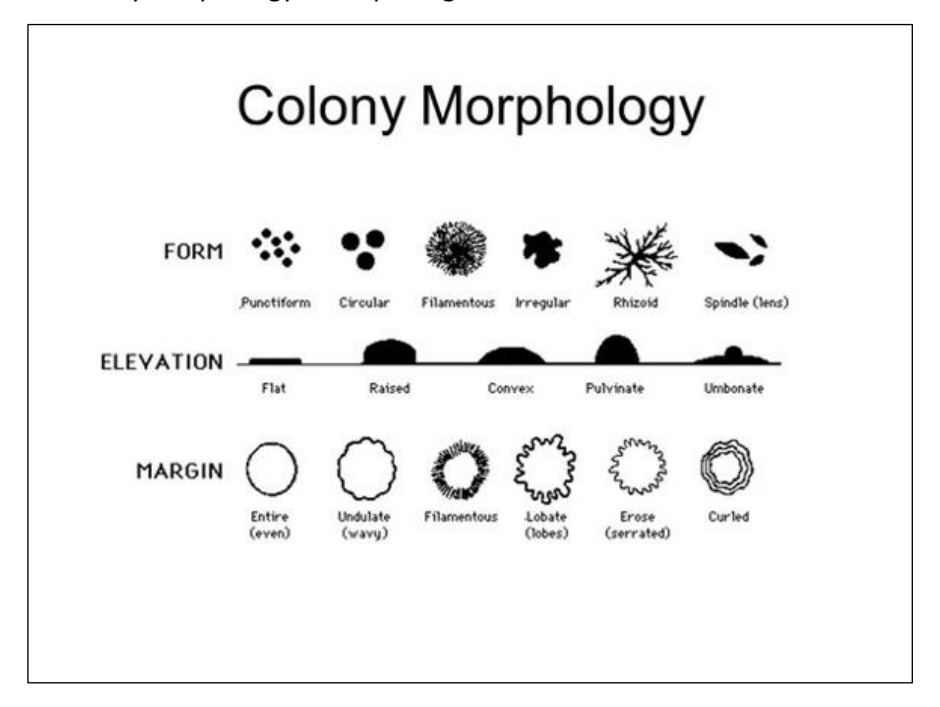


Figure S.2.32. Standard descriptive terms for bacterial colony morphology. Schematic shows common variation in (top) colony form (punctiform, circular, filamentous, irregular, rhizoid, spindle), (middle) elevation (flat, raised, convex, pulvinate, umbonate), and (bottom) margin (entire/smooth, undulate/wavy, filamentous, lobate/lobed, erose/serrated, curled). Adapted from Breakwell, Woolverton, MacDonald, Smith and Robison, "Colony Morphology Protocol," American Society for Microbiology, 2016. (Breakwell et al., 2016).

# 3. Fluid Flow-Induced Morphological Adaptations in Bacillus subtilis Biofilms and Their Inhibition by Ginkgo biloba Leaf Extract

# 3.1. Abstract

Biofilms pose significant challenges across industrial sectors, particularly in flow systems, where their persistence leads to contamination, spoilage, and equipment degradation. This chapter investigates how continuous fluid flow shapes the morphology and structural adaptation of *Bacillus subtilis* (*B. subtilis*) biofilms, and evaluates the antibiofilm efficacy of *Ginkgo biloba* leaf extract (GBLE) under such conditions. Using GFP-tagged *B. subtilis* JWV042 and confocal laser scanning microscopy (CLSM), biofilms grown under flow demonstrated distinct architectural features, including the formation of Van Gogh bundles and spore aggregates. For the first time, multiple Van Gogh bundles were also observed to align and twist into rope-like structures, referred to as Van Gogh ropes, representing a higher-order level of biofilm organization. These structures likely confer mechanical stability, enabling resistance against shear forces.

Furthermore, this study is the first to identify an attachment foundation layer composed of extracellular matrix (ECM) and Van Gogh bundles in *B. subtilis* flow biofilms, suggesting an additional developmental stage beyond the traditional five-step biofilm model.

Moreover, GBLE supplementation at increasing concentrations disrupted biofilm morphology, reduced biomass, and interfered with Van Gogh bundle organisation, indicating a concentration-dependent inhibitory effect. These findings highlight the plasticity of *B. subtilis* in adapting to mechanical stress through multicellular differentiation, and suggest that GBLE may hold potential as a candidate for sustainable antibiofilm strategies in flow systems, though further validation in applied settings is needed.

#### 3.2. Introduction

Bacterial contamination usually occurs in the form of biofilm growth, which can develop in virtually any environment (Costerton et al., 1995) (Flemming et al., 2016). Pumped fluid flow systems are widely used in a variety of industry sectors, including food and drink processing, agriculture, dairy processing, and oil and gas (Simões et al., 2010) (Flemming et al., 2016).

Unless heat sterilised, these systems are prone to bacterial and biofilm contamination due to the biofilm's resistant nature (Donlan, 2002) (Bridier et al., 2011). Biofilms represent a significant challenge in these settings, leading to product contamination and equipment deterioration (Hall-Stoodley et al., 2004) (Bridier et al., 2015). In food and drink processing, bacteria dislodged from biofilms can contaminate products, posing risks to public health and reducing shelf life (Carpentier and Cerf, 2011). While it is difficult to quantify bacterial contamination specifically due to biofilms, their role in industrial contamination is globally recognised (Simões et al., 2010) (Flemming et al., 2016).

In the food and drink industry, bacterial contamination of food products not only leads to public health concerns, but also shortens shelf life of the products. Listeria monocytogenes is a pathogenic bacteria which can form biofilms on stainless steel and conveyor belts and it causes recurrent contamination in dairy and meat processing plants (Latorre et al., 2010) (Carpentier and Cerf, 2011). Food products contaminated with Shiga toxin-producing Escherichia coli (STEC) resulted in significant morbidity: in one national outbreak in England, involving pre-packed sandwiches, 49% of cases were hospitalized (UKHSA, 2024). Every year, foodborne illnesses affect an estimated 600 million people worldwide, posing significant public health and economic burdens (WHO, 2023). The Food Standards Agency reports that food-borne diseases (FDBs) cost the NHS around £9bn, in addition to causing morbidity and mortality among the population. Microbial contamination of food products also cause of food waste, which results in substantial economic loss (Karanth et al., 2023). Food waste and spoilage not only cause financial losses, but are also a major issue concerning sustainability and food security (Karanth et al., 2023). According to a reported published by the United Nations Environment Program (UNEP), approximately 17% of food made in 2019 was disposed of. Tackling food waste and spoilage is important also in the context of the Sustainable Development Goals established by the United Nations, namely the Responsible Consumption and Production goal (Karanth et al., 2023). Biofilms are a major contributor to food spoilage and loss across various sectors of the food industry. In the dairy sector, Pseudomonas fluorescens (P. fluorescens) forms biofilms on equipment surfaces, secreting enzymes that degrade milk quality and reduce shelf life (Marchand et al., 2012). Similarly, Listeria monocytogenes forms persistent biofilms in meat-processing environments, leading to recurrent contamination of products despite routine sanitation (Carpentier and Cerf, 2011). In the fresh produce industry, biofilm-forming pathogens such as Salmonella enterica and Escherichia coli (E. coli) O157:H7 resist conventional washing, contributing to postharvest losses (Jahid and Ha, 2012). The seafood industry also suffers from biofilm-related spoilage, as surface-attached bacteria lead to texture degradation and off-odours in processed fish (Simões et al., 2010). Because of the recognized role of biofilms in food waste and loss, there is a need of developing effective and ecofriendly biofilm control strategies, also driven by the pressure to achieve a more sustainable world.

Not limited to food and drink processing facilities, biofilms represent a problem also in the oil and gas industry. Oil and gas mining and transportation rely on pipelines made of carbon steel, which is ideal due to its low cost and exceptional mechanical properties (Khan, Hussain and Djavanroodi, 2021). Despite the advantages of carbon steel, this material is also quite susceptible to microbially-induced corrosion (MIC), which increases risks in terms of facility operability, as well as of environmental contamination (Khan, Hussain and Djavanroodi, 2021). The global economic burden of microbiologically influenced corrosion (MIC) is estimated to be between US \$300 and 500 billion annually, representing a major share of the overall corrosion-related losses, which exceed US \$2.5 trillion per year worldwide (NACE International, 2013) (Springer, 2024), a number which spans across multiple different industries. Biofilms play a central role in MIC as they create microenvironments on metal surfaces that promote localized corrosion (Little et al., 2008). Within these biofilms, microbial communities change the surrounding chemistry by producing corrosive metabolic byproducts. These activities lead to pitting, crevice corrosion, and other forms of metal degradation (Beech and Sunner, 2004) (Kip and van Veen, 2015). Biofilms also provide a protective matrix that shields the microbial community from biocides and environmental stresses, allowing corrosion processes to persist even under cleaning or treatment protocols (Flemming et al., 2016) (Little et al., 2008). Thus, in many industrial settings, such as oil pipelines, maritime infrastructure, and water systems, MIC is synonymous with biofilminduced corrosion (Beech and Sunner, 2004) (Little et al., 2020).

Biofilm control strategies are categorized in physical and chemical eradication. Industries usually rely on chemical disinfection to eradicate biofilms, as these compounds are usually less costly and easier to use. In the food industry, chemicals including hydrogen peroxide, sodium hypochlorite and quaternary ammonium compounds are commonly used for bacterial disinfection. These compounds are effective against early biofilms, however, do not work when the biofilm is mature (Corcoran et al., 2014) (Fu et al., 2021). Additionally, the use of this disinfectants requires the strict adherence to cleaning protocols and the use of a vast

quantity of water for rinsing. It is also important to highlight that majority of the disinfectant used for biofilm eradication were tested on planktonic cultures and therefore, might not be as effective on biofilms, especially because bacteria, even the same bacterial strain, behave completely differently when growing in biofilm form compared to planktonic (Coughlan et al., 2016). In the context of sustainability, the harsh chemicals used for disinfection are then rinsed with water and disposed of the sewage systems, therefore have a significant impact on the ecosystem and biodiversity. Wastewater produced by cleaning and disinfection practices is contaminated with compounds such as soluble organic materials, phosphates and many more, which can then end up in the environment (Pascual, Llorca and Canut, 2007). This has detrimental effects on the ecosystem. Within the range of disinfectants available for biofilm control, there is a lack of ecofriendly alternatives that can be used at industrial levels. As a result, there is a pressing need to find an effective antibiofilm agent which is also sustainable and safe for use in food, drink and dairy processing.

In order to be able to achieve complete control of biofilm growth, it is necessary to first, fully understand how biofilms grow in the environments which are susceptible to biofilm contamination. The primary focus of this study is to investigate the morphology of biofilms grown under a flow regime. Bacteria and microorganisms in general are known for their ability to adapt to various environmental stresses, reasons why they are excellent at persisting even in the harshest environments. The ability of bacteria to survive under different conditions is, in part, due to their capability to switch to biofilm form.

Flow systems are widely used in a variety of sectors and they represent an optimal environment for biofilm growth. Because of the flow of fluid, a biofilm under flow will be subjected to a constant delivery of nutrients as well as a removal of waste metabolites, conditions that are advantageous to the biofilm. A number of studies have investigated biofilm development under flow regimes. A majority of these utilise microfluidic devices for their experimental investigation and the bacterial strains used are the commonly studied *Pseudomonas aeruginosa* (*P. aeruginosa*), *P. fluorescens*, *E. coli* and also *Vibrio cholera* (*V. cholera*), the causative agent of water-borne infectious disease cholera (Rusconi and Stocker, 2015) (Martínez-García et al., 2014) (Pearce et al., 2019) (Recupido et al., 2020). Fluid flow forces have been found to impact bacterial attachment and detachment, quorum sensing, ECM synthesis and overall behaviour and transcriptome of biofilms (Recupido et al., 2020) (Kurz et al., 2022). In addition, different flow regimes also result in the development of

biofilms with different morphological characteristics (Recupido et al., 2020). For example, under a slow fluid flow, P. fluorescens forms biofilms with column-like architecture, due to the nutrient concentration gradient caused by flow. Studies investigating the effect of fluid flow on V. cholera, mainly using microfluidics and mathematical models, found that flow forces induced spatial heterogeneity in biofilms, inducing spatial mixing of bacterial subpopulation (Martínez-García et al., 2018). Spatial heterogeneity is also given by the shear gradient created within the flow channels (Rusconi and Stocker, 2015). Additionally, Pearce et al. (2019) used a mathematical model to describe how shear forces induce verticalization of V. cholera bacterial cells, concluding that nematically aligned growth is the main factor of flow biofilm structure. Biofilms under flow have also shown distinct structures, specific to microfluidic devices, referred to as streamers. These are surface-associated filamentous arrangements that were found to connect corners of microfluidic chambers. Streamer formation has been investigated mainly in *P. aeruginosa* (Secchi et al., 2022) with few studies also addressing streamers made Bacillus subtilis (B. subtilis) (Zhang et al., 2022) and Staphylococcus aureus (S. aureus) (Kim et al., 2014). Despite the valuable findings of these studies, only a limited number of microorganisms have been investigated and the studies are limited to the use of microfluidic chambers and mathematical models, thus focusing on biofilm formation at microcolony scale. As such, they provide limited insight into the full 3D structure or biomass of mature biofilms as they would develop in larger-scale or real-world flow systems.

This present study addresses the need for a better understanding of macroscale biofilm architecture and uses *B. subtilis*, a model organism whose biofilms' macroscale architecture remains widely underexplored under flow. To address these gaps, this study employed *gfp*-expressing *B. subtilis* grown under continuous fluid flow within flow cells, enabling direct visualization of how shear forces shape biofilm architecture. Unlike microfluidic systems, flow cells allow the development of more mature, macroscale biofilms while still being compatible with high-resolution imaging. By using confocal laser scanning microscopy (CLSM) across a broad range of magnifications, it was possible to examine the entire architecture of the biofilm, from its overall 3D structure to single-cell morphology, without disrupting its natural arrangement. This approach overcomes limitations in earlier work by enabling both microscale and bulk-scale analysis of *B. subtilis* biofilms under realistic flow conditions, providing novel insights into how this species responds structurally to shear stress.

In the recent years, B. subtilis has become a model organism for biofilm studies, due its versatility and ability to differentiate in subpopulations with different roles within the biofilm. A number of B. subtilis cell types have been described in the context of biofilms. When growing in biofilm form and upon genetic signalling, bacteria need to divide labour in order to successfully grow and overcome challenging environmental conditions. B. subtilis is especially useful in studying bacterial differentiation, as the bacterial community is able to relatively quickly develop into distinct cell types (Vlamakis et al., 2013) (van Gestel et al., 2015) (Dragoš et al., 2018). In colony agar biofilms, B. subtilis cells seem to be able to differentiate into five subpopulations, and each cell type has different properties. B. subtilis biofilms require the cooperation of motile cells, surfactin-, protease- and matrix-producing cells and spores. For colony biofilm expansion, matrix- and surfactin-producing cells work together as chains of cells, referred to as Van Gogh bundles (van Gestel et al., 2015). Van Gogh bundles are seen at the edge of colony agar biofilms and expand using sliding motility. While matrix-producing cells secrete EPS, surfactin-producers synthesise surfactin, which aids expansion as it decreases surface tension. Cellular differentiation in B. subtilis biofilms was also seen in response to Gingko biloba leaf extract (GBLE), as the described in the result section in chapter I. In that study, GBLE affected the morphology of both colony agar biofilms and static biofilms, inducing the formation of Van Gogh bundles on agar plates and in static biofilms. More interestingly, GBLE triggered multiple mutation events on agar biofilms and cellular differentiation in static biofilms. B. subtilis cell types have only been investigated in colony agar biofilms, and the impact of other environmental conditions, including flow forces, on B. subtilis cell differentiation has not been studied.

Plant-based and natural compounds are becoming of more interest for their antimicrobial and antibiofilm activity, as they are sustainable and can potentially have no detrimental impact on the ecosystem (Singh et al., 2017) (Borges et al., 2016). While *Ginko Biloba* has been shown to have notable impacts on *B. subtilis* biofilms under static conditions (as shown in research chapter 2), the impact of *Ginko Biloba* under flow conditions is not known. This is pertinent as flow systems are particularly relevant to a wide range of industrial systems. In this study, the herbal extract *Gingko biloba* leaf extract (GBLE) was tested for its antibiofilm activity on *B. subtilis* flow cell biofilms. CLSM was used to visualise *gfp*-expressing *B. subtilis* biofilms grown within flow cell and due to the nature of the flow system set up, it was possible to image the biofilms without disturbance arising from manual handling.

#### 3.3. Materials and Methods

#### 3.3.1. Bacterial strain and Culture Conditions

Gfp-expressing Bacillus subtilis (JWV042 strain, Hbs-GFP endogenous localization, cat amyE::Phbs-hbs-gfp, cat marker) colonies on agar were obtained from Strathclyde Institute of Pharmacy and Biomedical Sciences (SIPBS). A flask containing 150 mL of Luria-Bertani (LB) broth (Sigma-Aldrich) was inoculated with a colony from the plate and incubated overnight at 37°C. The culture was supplemented with 5 μg/mL chloramphenicol to ensure selection of gfp mutants. Glycerol stocks were made from the culture and stored at -80°C. The stocks were then used for the rest of this study.

Gingko biloba leaf extract (GBLE) powder was obtained from Wuhan ReCedar Biotechnology Co., Ltd (Wuhan, China). The extract was resuspended in RNAse-free water to make working solutions and was added to the culture media accordingly.

Prior each experiment, *B. subtilis* JWV042 was cultured in LB broth overnight at  $37^{\circ}$ C in a shaking incubator at 150 rpm. The OD<sub>600</sub> of the inoculum was measured prior inoculation in each experiment and was adjusted to 0.3. All experiments were carried out in triplicates on separate occasions, using freshly prepared cultures each time to ensure biological replication, unless stated otherwise. All bacterial cultures and flow cell biofilms were grown using LB media, supplemented with 5  $\mu$ g/mL chloramphenicol. All materials and reagent were sterile at the time of use and sample preparations was carried out in biological safety cabinets.

#### 3.3.2. Fluid Flow System Design and Imaging

In order to study biofilm development under fluid flow and GBLE, a flow system which allowed for the development and microscopical imaging of bacterial biofilm was developed (Fig. 3.1).

Inlet media for the flow system was prepared in a 4L polycarbonate bottle (IBI Scientific) and autoclaved to achieve sterility. Subsequently, the inlet media was supplemented with 0, 75 or 400  $\mu$ g/mL GBLE suspension. These experiments were carried out separately. From the inlet media bottle, silicone tubing was connected to a sterile plastic drip chamber, to avoid inlet media contamination from the inoculum, and then it was placed through a pump channel. Non autoclavable silicone tubing was sterilised through a series of washes. The

tubing was first soaked overnight in 1%(w/v) Virkon solution and dried. Then, sodium hypochlorite was injected into the tubing using a sterile syringe, and this was followed by isopropyl alcohol (70%) wash. To achieve a continuous fluid flow, a peristaltic pump was used (VWR, PP4000 Series), at a set flow rate of 40 mL/h. Going through the peristaltic pump, the attached convertible flow tubing was then to cell IBI CFCAS0003). The flow cell is where the biofilm developed. Because of the presence of glass coverslips on the top and bottom of the cell, it was possible to image the biofilm using confocal fluorescent microscopy. From the flow cell, waste was collected in a second 4L polycarbonate bottle (IBI Scientific).

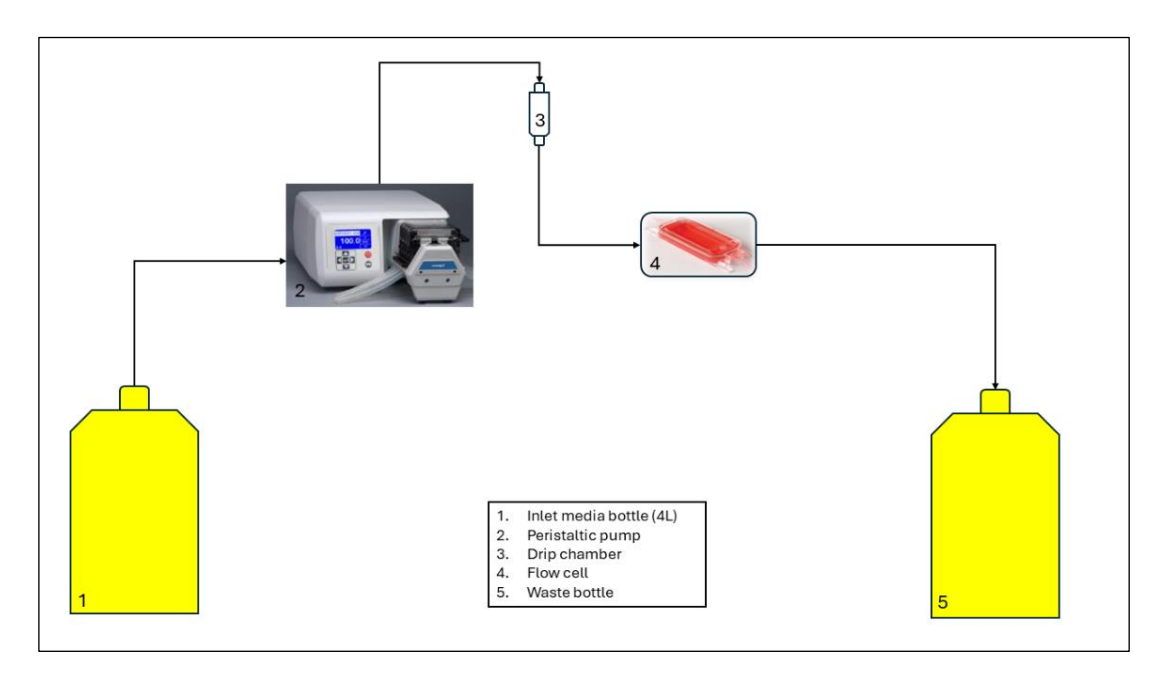


Figure 3.1. Schematic of the fluid flow set up used to grow biofilms under a fluid flow.

The flow system was run for a period of time of 1 hour and the outlet media was collected in a beaker. RPM value was then adjusted to a flow rate of 40 mL/h. After pausing the flow, inoculation of the system was achieved via injecting 150  $\mu$ L of overnight *B. subtilis* liquid culture (OD<sub>600</sub> = 0.3). Following inoculation, the flow was restarted 1 hour post inoculation. A desk lamp placed directly above the flow cell was used to achieve a warmer temperature for bacterial growth for the duration of the run. The system was run for a total of 48 hours.

The flow cell used in this study consists of a rectangular plastic chamber with an integrated glass coverslip that serves as the imaging surface (Fig. 3.2). Fluid enters through the inlet port (1) and exits through the outlet port (2), enabling a continuous flow across the chamber. The built-in glass coverslip (3) provides an optically clear base for high-resolution microscopy of

biofilms formed under controlled flow conditions. Fig. 3.2.A illustrates the three-dimensional structure of the flow cell, while fig. 3.2.B shows a simplified two-dimensional top-down view of the chamber and flow path.

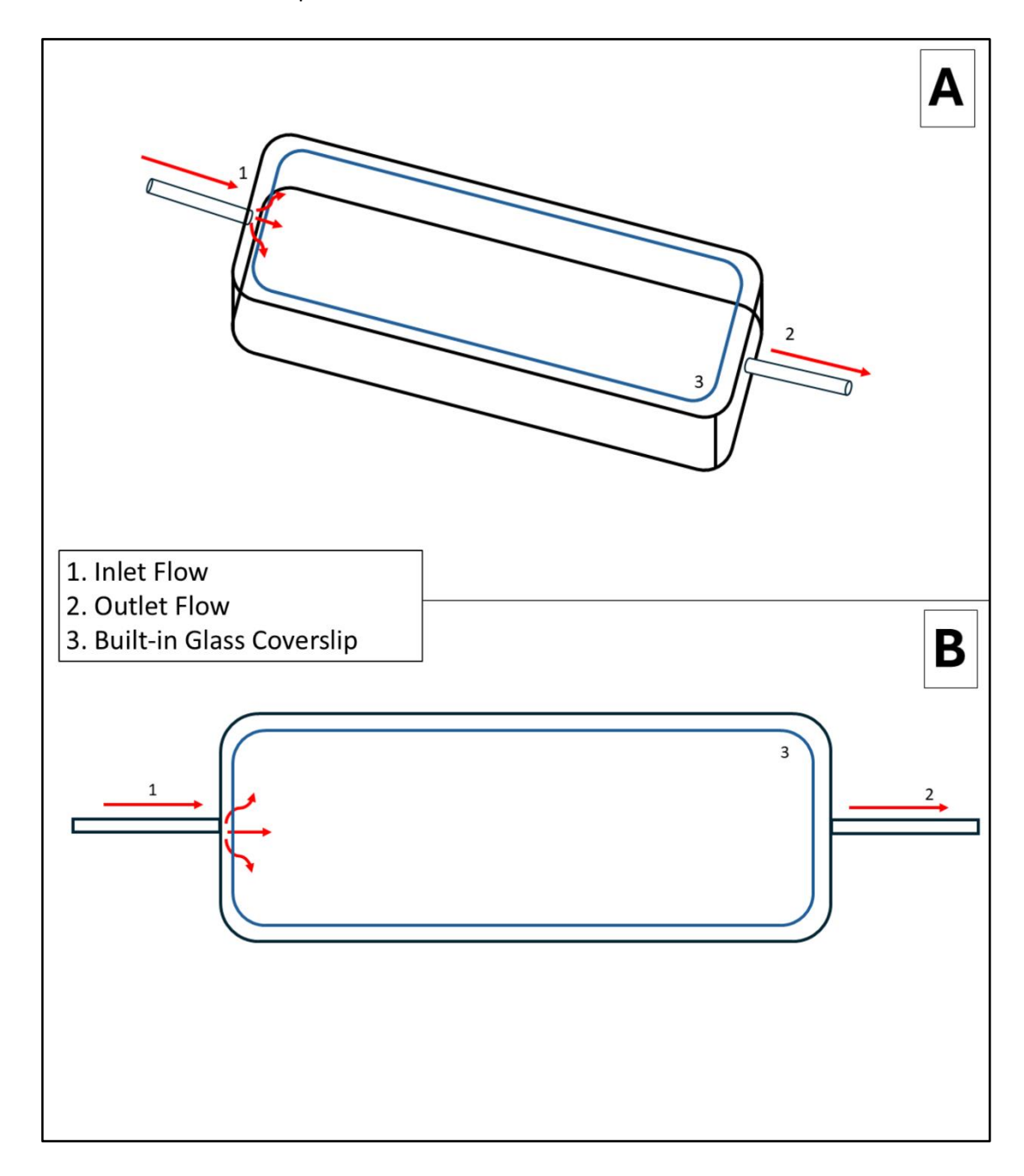


Figure 3.2 Flow cell schematic used for biofilm cultivation under controlled flow. (A) Three-dimensional schematic highlighting the inlet flow (1), outlet flow (2), and built-in glass coverslip (3). (B) Two-dimensional top-down schematic showing the flow path across the chamber. The integrated glass coverslip enables direct microscopic observation of biofilm growth on the chamber surface.

After the 48 hours, the flow was stopped and the tubing was clamped at either side of the flow cell, in proximity to the chamber. The tubing was cut at either side of the flow chamber

using a sterile scalpel. In order to image the biofilm adhered to the internal surface of the flow cell, the media inside was aspirated using a sterile plastic syringe.

Biofilm imaging was performed using a Leica TCS SP5 confocal laser scanning microscope (Leica Microsystems, Germany) equipped with a motorised stage. For whole-chamber biofilm imaging in the flow-cell, a 4x/0.10 numerical aperture (N. A.) HI PLAN PH 0 air objective ( $\approx 40\times$  overall optical magnification through the eyepieces) was used to capture the overall biofilm structure across the chamber. The *gfp*-expressing *B. subtilis* JWV042 strain was excited using an argon laser at 488 nm, and emission was collected between 500–550 nm. For finer structural details, the zoom function within the Leica LAS AF software was applied while maintaining the 4 x objective. Laser power and detector gain were kept constant across all samples to allow comparative quantification. All image acquisition was carried out at room temperature using Leica LAS AF software.

In order to minimise disruption to the morphology of the biofilm, the whole flow cell was placed under the objective lens.

#### 3.4. Results

# 3.4.1. Effect of flow on biofilm morphology

In order to investigate the effect of fluid flow on biofilm development and morphology, *gfp*-expressing *B. subtilis* biofilms were grown under a continuous flow of 40 mL/h. Biofilms formed inside the walls of the flow chamber and fluorescent imaging was possible due to the thin glass coverslips that make up the top and bottom wall of the flow cell.

Using a confocal laser scanner microscope, fluorescent images were acquired from within the flow cell.

Results show a drastic change in the morphology of an immersed biofilm developed under a continuous flow of media, compared to a static biofilm (Fig. 3.3). Unlike *B. subtilis* static biofilms, which displays standard biofilm morphology and no Van Gogh bundles, biofilms under flow appear as large dense structures composed of a cohesive network of interwoven and tightly packed filaments (Fig. 3.3a, b, c), suggestive of a "cloud like" general morphology. Single celled filaments (Van Gogh bundles) are seen extending from the edge of the biofilms (Fig. 3.3c and 3.3d (arrows), 3.3e). These biofilms, similarly to static and agar biofilms seen in chapter 2, develops in a three dimensional structure with an undulated surface and organised

"aerial" projections towards the inner part of the flow cell (Fig. 3.3a, Arrow), as indicated by changes in the fluorescent signal. In several regions, the filaments are arranged around central voids, creating ring-like or channel-like structures (Fig. 3.3c)

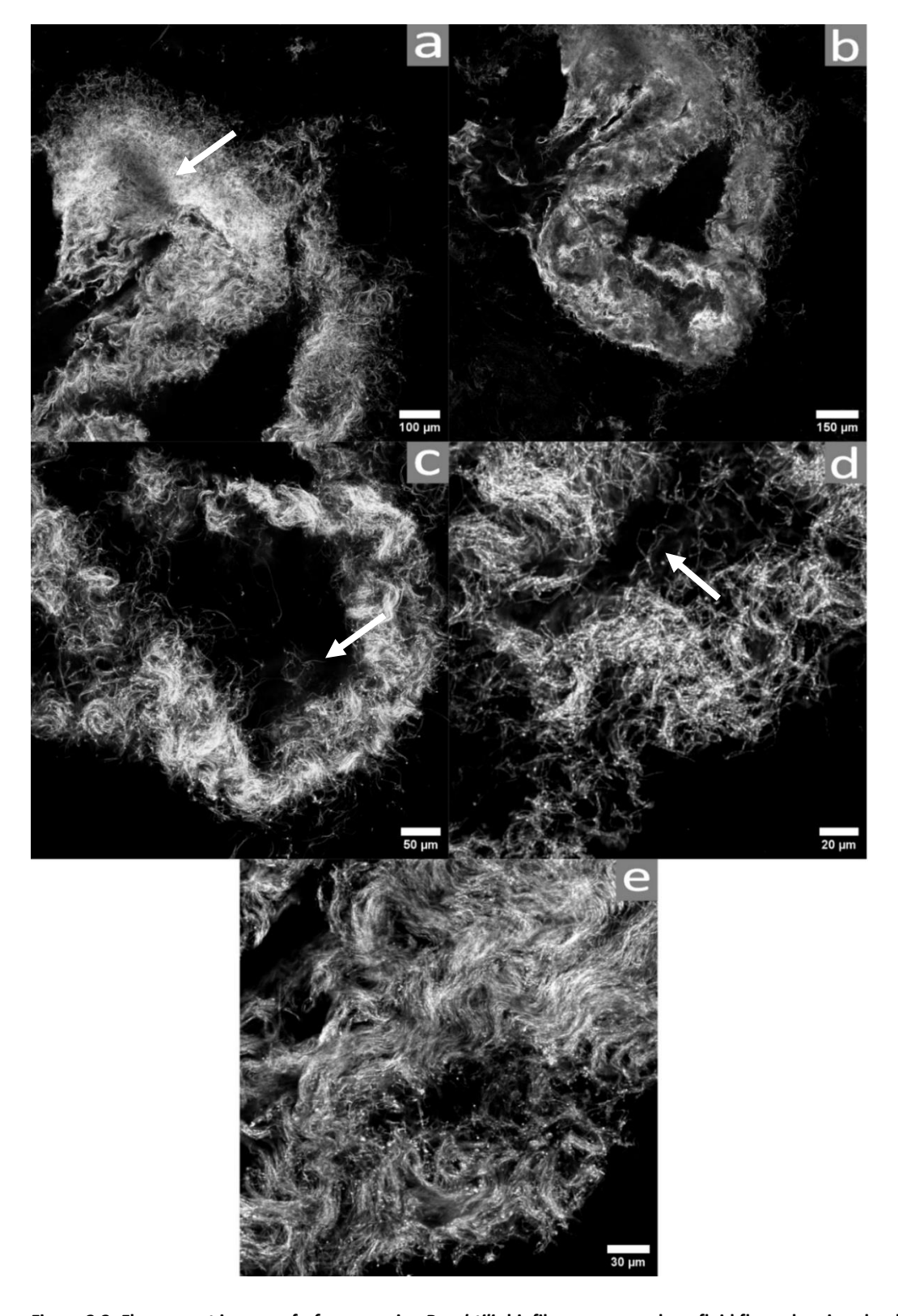


Figure 3.3. Fluorescent images of *gfp*-expressing *B. subtilis* biofilms grown under a fluid flow, showing cloudand wave-like morphology (a-b). Changes in fluorescent signal indicate three dimensionality (a, arrow). c) d) e) Higher magnification images showing undulated patterns, with arrows (c and d) highlighting emerging Van Gogh bundles. Biofilms were grown within flow cells under a continuous flow of LB media at room temperature, for 48 hours. Entire flow cells were imaged using Leica SP5 (40x magnification).

Under flow, biofilms showed different degrees of complexity across sections of the flow cell. Fig. 3.4 illustrates the extensive filamentous structuring of the biofilm across various regions and magnifications. The biofilms in Fig. 3.4 appear less dense compared to the cloud biofilms in figure 3.3, which show a more three-dimensional morphology. In contrast, the biofilms in Fig. 3.4 display a more organised structure, as the bundles are closely aligned adjacent to each other in a two-dimensional arrangement with parallel orientation of the bacterial filaments within each bundle. These aligned filaments exhibit a coordinated directional growth pattern (Fig. 3.4a, d); the filaments also border dark voids (Fig. 3.4a, arrows), which are frequently observed throughout the biofilm. Small fluorescent dots (Fig. 3.4b, arrow) and aggregates (Fig. 3.4c, arrow) can also be seen.

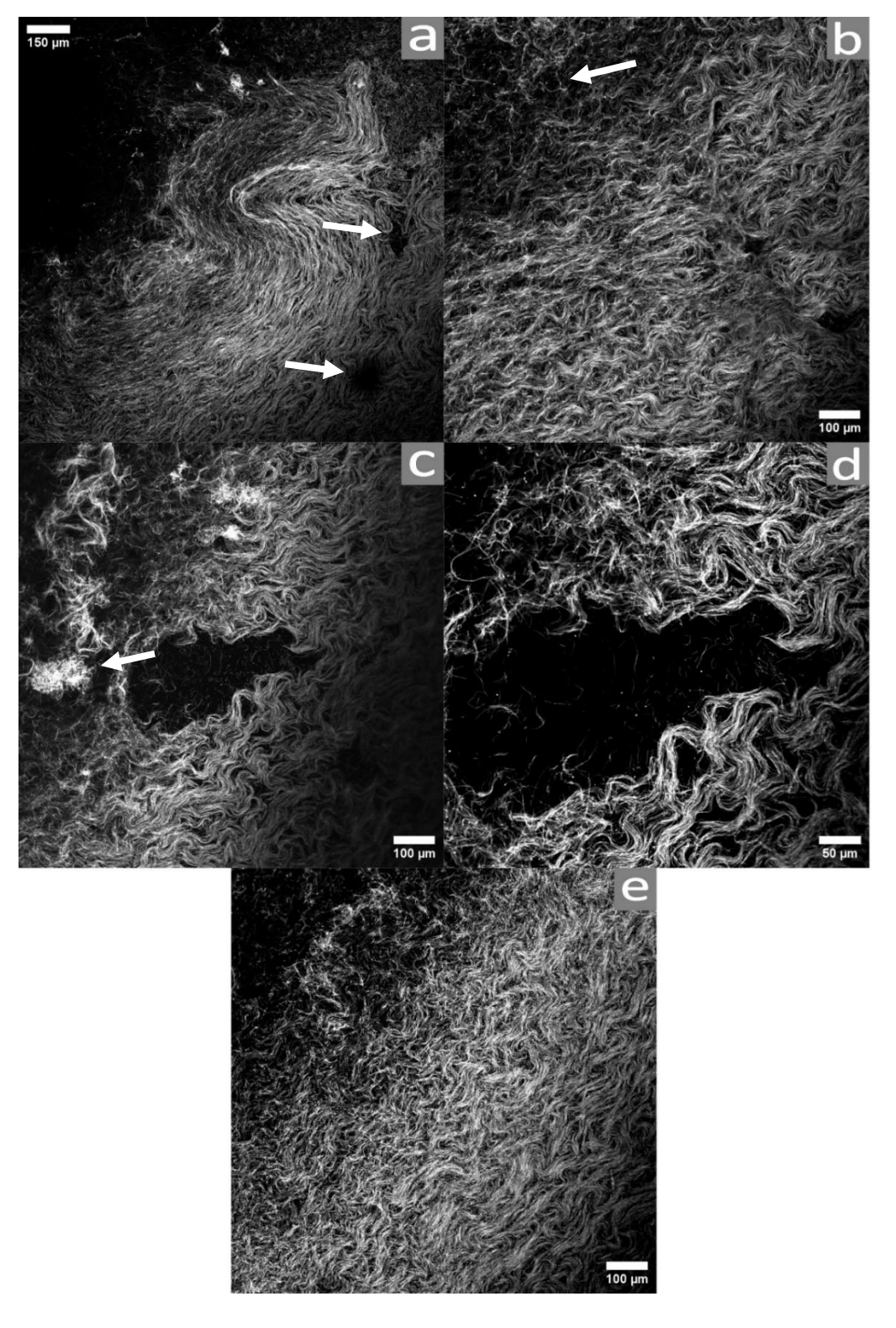


Figure 3.4. Fluorescent images of *gfp*-expressing *B. subtilis* biofilms grown under a fluid flow, showing multiple Van Gogh bundles aligned. Areas of void can be seen within the aligned Van Gogh bundles (a, arrows). Small fluorescent dots appear (b, arrow) and aggregates (c, arrow). Biofilms were grown within flow cells under a continuous flow of LB media at room temperature, for 48 hours. Entire flow cells were imaged using Leica SP5 (40x magnification).

## 3.4.1.1. Continuous Flow Induced the Development of Aggregates and Rope-like Structures

To further understand the aggregate-like structures observed within the flow cell biofilm, fluorescent microscope images coupled with light transmission images were taken. As seen in Fig. 3.5, these structures appear as part of the biofilm, intertwined with the Van Gogh bundles. Filaments of bacterial cells seem to go through the aggregates, which in turn seem to be formed by small round objects. Based on the observed size and morphology of the structures within the aggregates, they are most likely consistent with *B. subtilis* endospores.

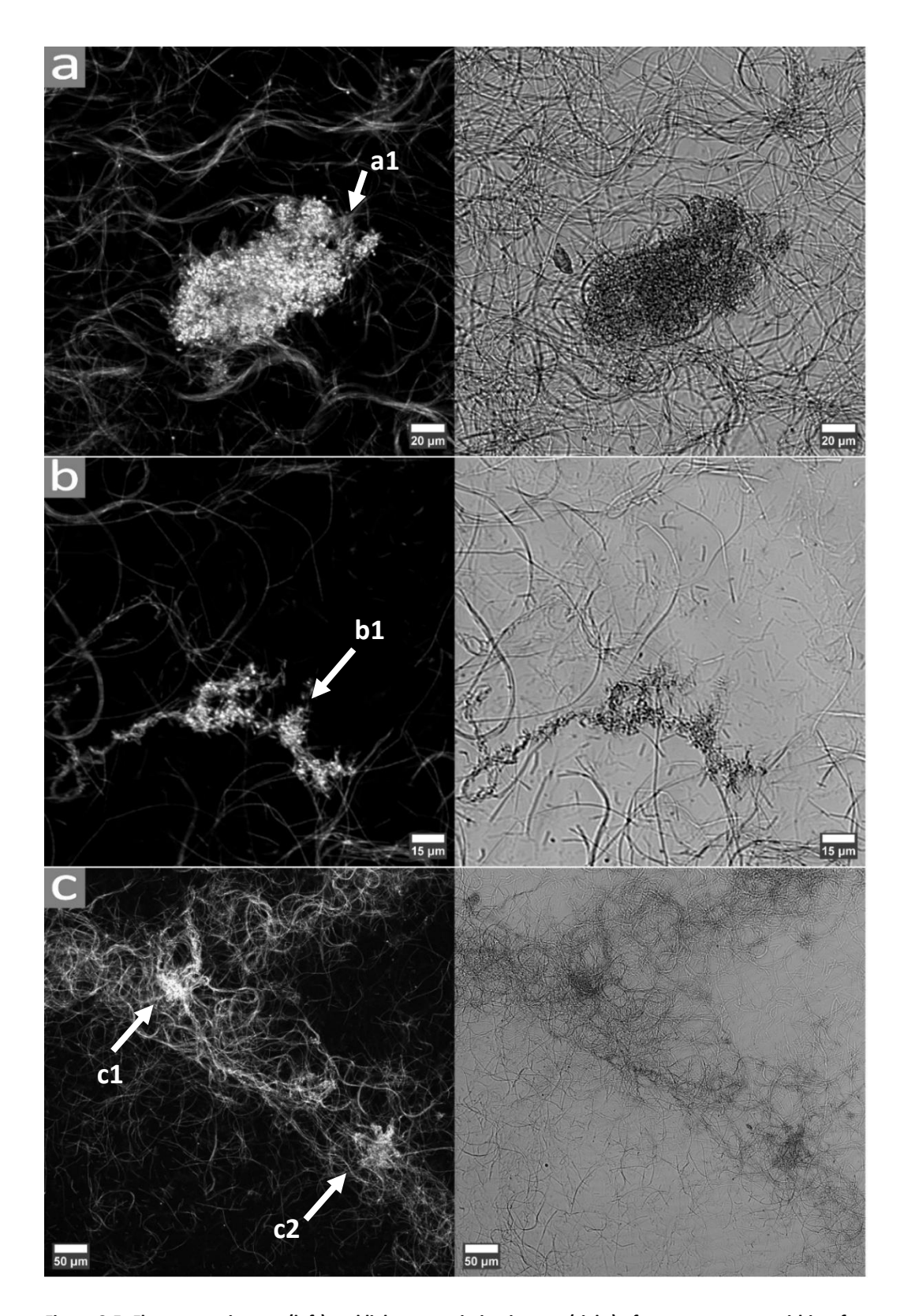


Figure 3.5. Fluorescent images (left) and light transmission images (right) of aggregates seen within *gfp*-expressing *B. subtilis* biofilms grown under a pumped fluid flow. Based on the observed size and morphology of the aggregates, they are most likely made of *B. subtilis* endospores. Aggregates are labelled with arrows and corresponding letter/number combination. Biofilms were grown within flow cells under a continuous flow of LB media at room temperature, for 48 hours. Entire flow cells were imaged using Leica SP5 (40x magnification).

Quantitative image analysis revealed heterogeneity in the size of individual aggregates formed under continuous unidirectional flow. As shown in Fig. 3.6, aggregate areas varied substantially across the four observed structures. The largest aggregate (a) exhibited a surface area exceeding 6,600  $\mu$ m<sup>2</sup>, whereas the smallest (b) measured just under 1,400  $\mu$ m<sup>2</sup>. Aggregates c1 and c2 displayed intermediate values (approximately 4,700  $\mu$ m<sup>2</sup> and 4,200  $\mu$ m<sup>2</sup>, respectively).

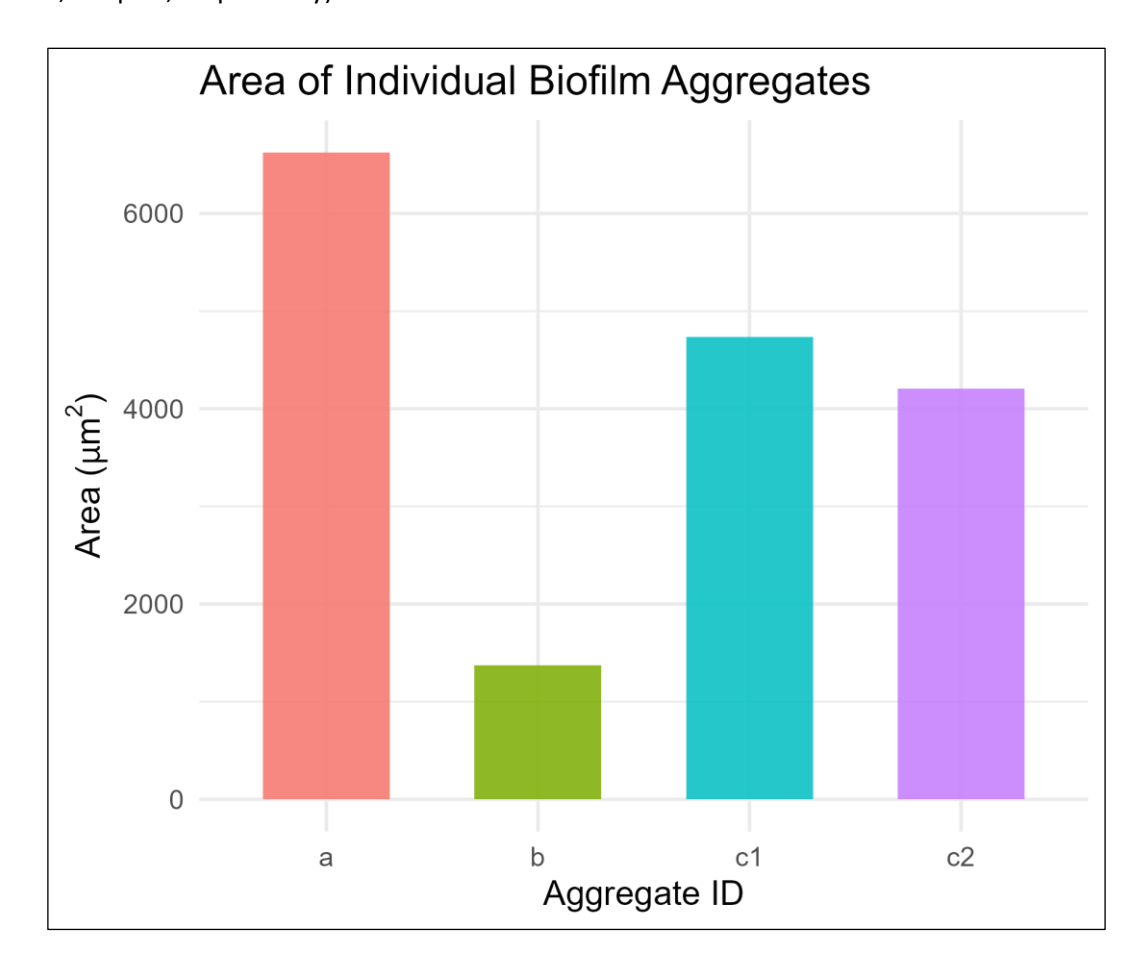


Figure 3.6. Barplot showing the surface area ( $\mu$ m<sup>2</sup>) of individual *Bacillus subtilis* biofilm aggregates formed under continuous unidirectional flow. Each bar represents a single aggregate (n = 1 per ID), with measurements obtained via quantitative image analysis.

The longitudinal dimension of biofilm aggregates formed under unidirectional flow also demonstrated considerable variability. As shown in Fig. 3.7, aggregate lengths ranged from approximately 87  $\mu$ m to 138  $\mu$ m. The longest aggregate (ID: b) reached nearly 138  $\mu$ m, while the shortest (ID: c2) measured just under 87  $\mu$ m. Aggregates a and c1 were similar in size, with lengths around 124  $\mu$ m and 118  $\mu$ m, respectively.

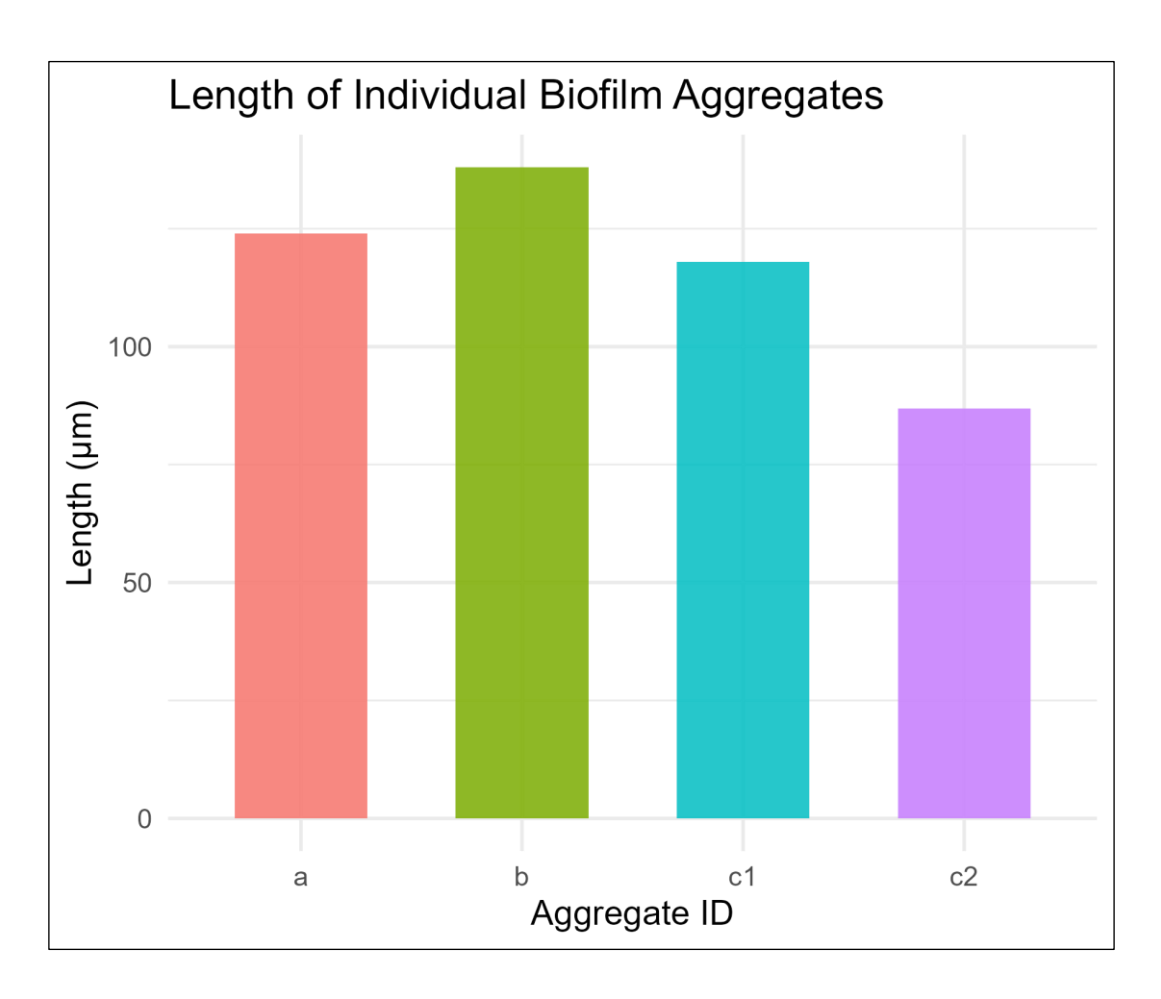


Figure 3.7. Barplot showing the length ( $\mu$ m) of individual *Bacillus subtilis* biofilm aggregates developed under continuous unidirectional flow. Each bar represents a single aggregate (n = 1 per ID), with measurements derived from image-based analysis.

The presence of a continuous flow also induced the formation of rope-like structures (Fig. 3.8 and 3.9). The rope-like structures, which will be referred to as Van Gogh ropes, are made of multiple Van Gogh bundles wrapped around each other like a rope, hence the name. Van Gogh ropes are specific to immersed biofilm under continuous fluid flow and have not been documented before. The ropes form from a simple twisting of filaments in an analogous way to wool yarn or agricultural twine.

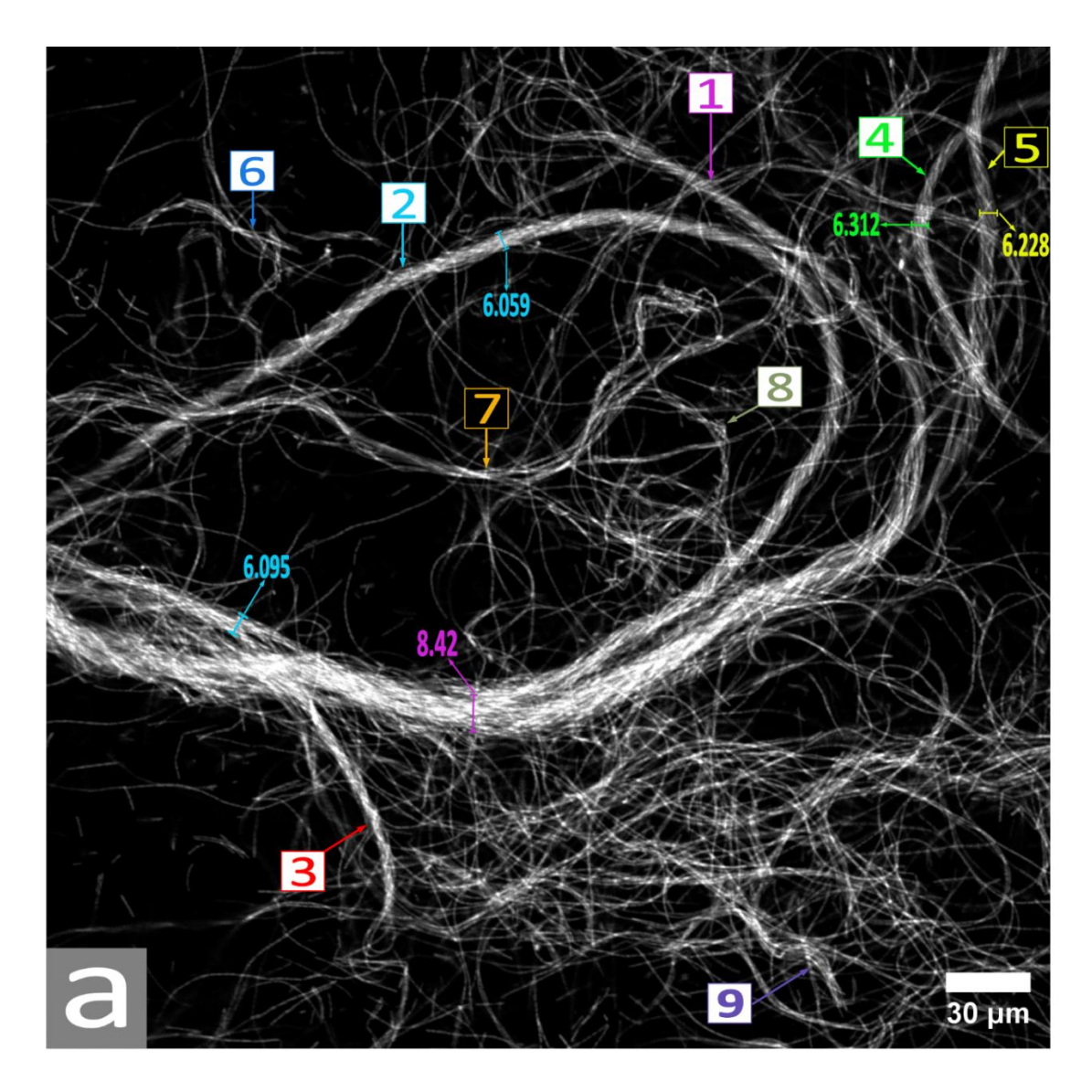


Figure 3.8. Fluorescent image of rope-like structure seen within *gfp*-expressing *B. subtilis* biofilm grown under a pumped flow of fluid. The image shows a multitude of *B. subtilis* cell chains, or Van Gogh bundles, tightly aligned in the form of a rope. Using ImageJ (FiJi), ropes were detected, numbered (1-9) and their width was measured. The image contains the maximum width of the main ropes in a colour coded manner. *B. subtilis* biofilms under flow were grown within flow cells under a continuous flow of LB media at room temperature, for 48 hours. Entire flow cells were imaged using Leica SP5 (40x magnification).

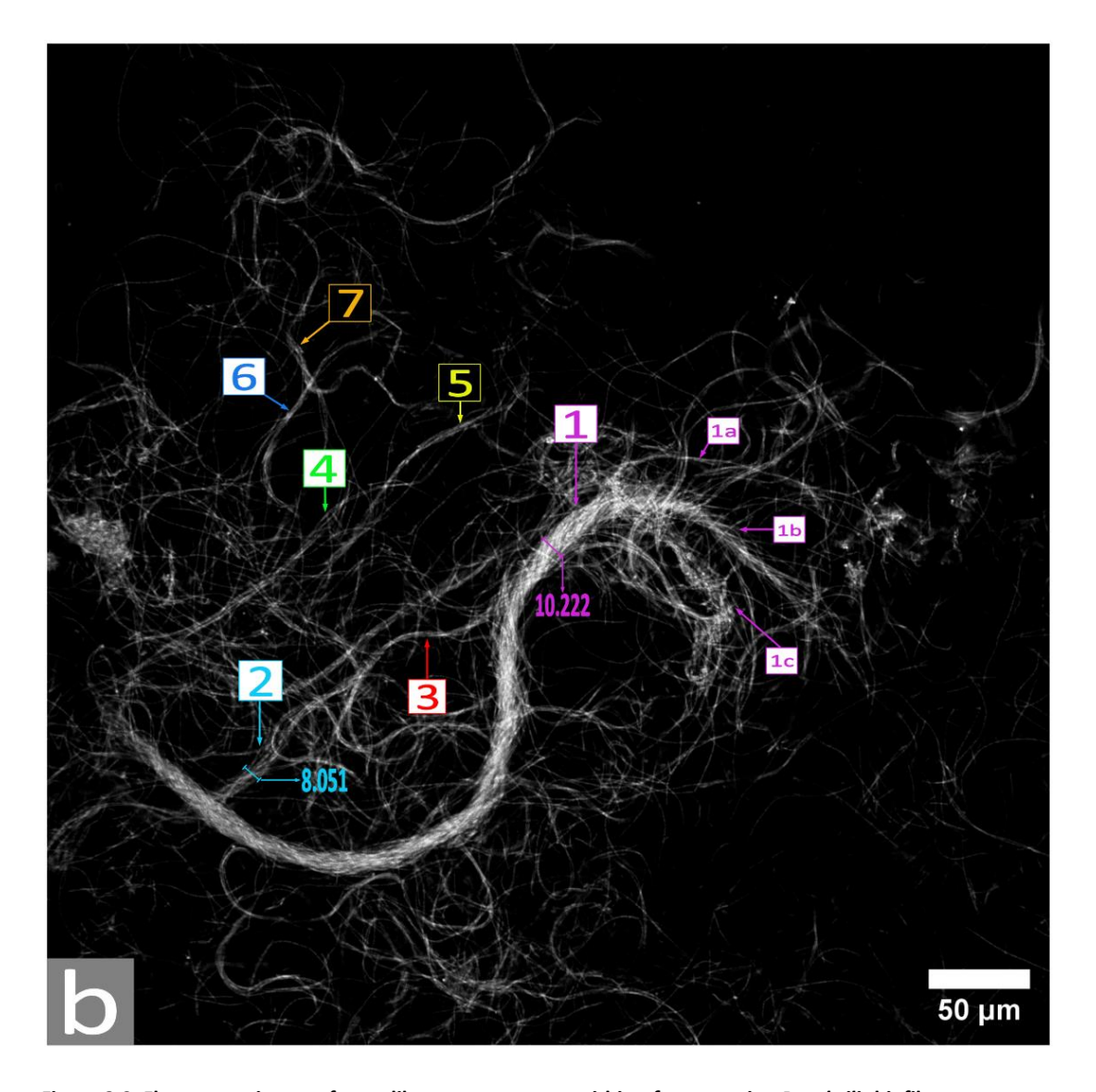


Figure 3.9. Fluorescent image of rope-like structures seen within *gfp*-expressing *B. subtilis* biofilm grown under a pumped flow of fluid. The image shows a multitude of *B. subtilis* cell chains, or Van Gogh bundles, tightly aligned in the form of a rope. Using ImageJ (FiJi), ropes were detected, numbered (1-7) and their width was measured. The main rope, rope 1, ramified into three other ropes (1a, 1b and 1c). The image contains the maximum width of the main ropes in a colour coded manner. *B. subtilis* biofilms under flow were grown within flow cells under a continuous flow of LB media at room temperature, for 48 hours. Entire flow cells were imaged using Leica SP5 (40x magnification).

Rope-like structures formed by *B. subtilis* under unidirectional flow were manually traced and their dimensions recorded. Rope lengths ranged from 64.1  $\mu$ m to 634.1  $\mu$ m, with rope 7.2 (Fig. 3.8, rope 2) being the longest (Fig. 3.10A). Average rope widths varied from 5.075  $\mu$ m to 9.479  $\mu$ m, with rope 8.1c exhibiting the thickest structure (Fig. 3.10B). While some of the longest ropes also had relatively high average widths (e.g., ropes 8.1 and 7.1), the overall relationship between length and width appeared weak (Fig. 3.10C), suggesting that rope thickness is not linearly dependent on rope extension.

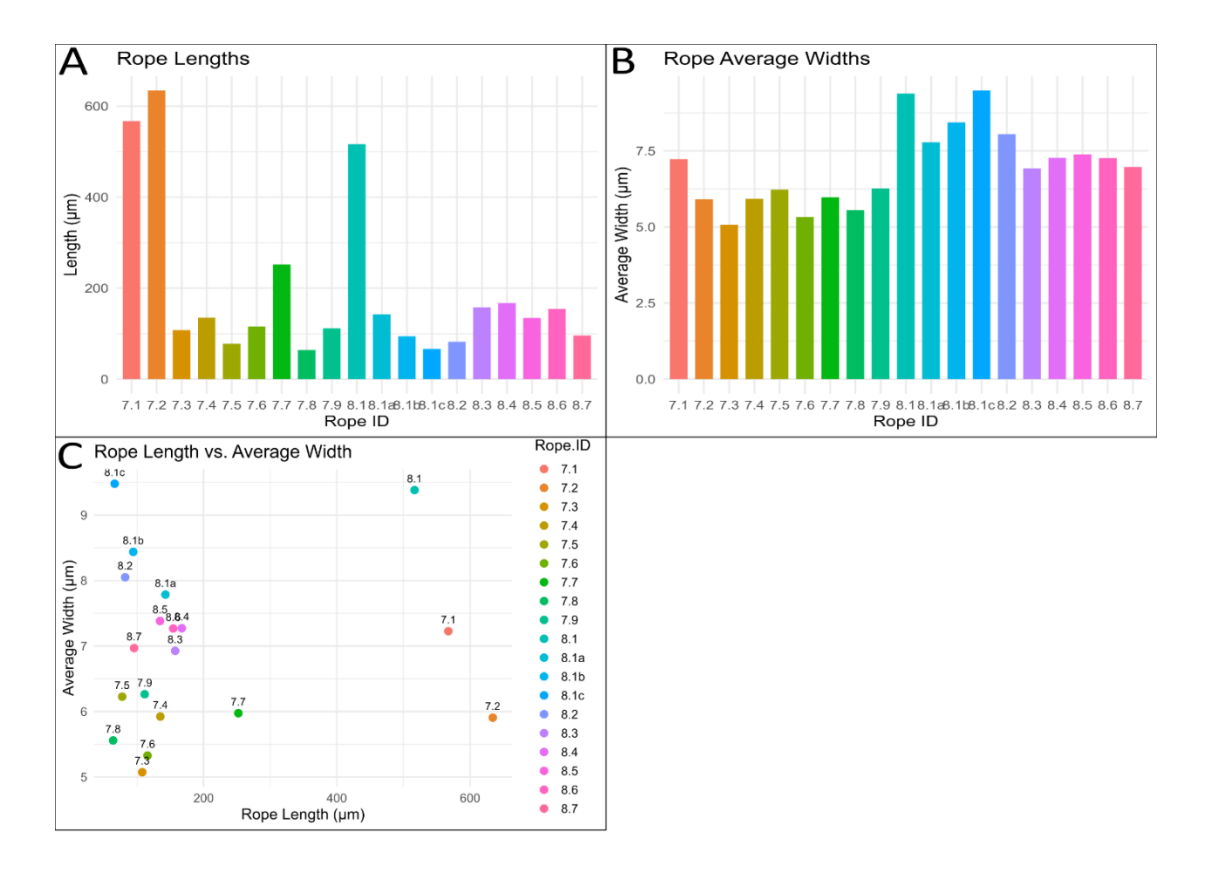


Figure 3.10. Rope dimensions and correlation between rope length and average width. (A) Individual rope lengths (in  $\mu$ m) measured from CLSM images of *B. subtilis* biofilms grown under unidirectional flow. (B) Average width (in  $\mu$ m) of each rope segment, calculated along its axis. (C) Scatter plot showing the relationship between rope length and average width. Each point is annotated by rope ID, with colour representing individual rope identity. While some longer ropes (e.g., 7.1, 7.2, 7.9) exhibit moderate to high widths, shorter ropes show a wide range of widths, indicating that rope thickness is not strictly dependent on rope length. Rope ID reflects figure (7 or 8) and rope number.

The term "twist angle" refers to how much the singular Van Gogh bundles in the biofilm spiral around themselves in the rope, similar to the twist in a rope or a braided cord, and is measured as the degree of rotation of each singular bundle around their own longitudinal axis (Goriely and Neukirch, 2006).

Twist angle measurements were conducted on a subset of ropes where individual filamentous chains could be clearly distinguished in CLSM images. Fig. 3.11 illustrates the distribution of twist angles across five such ropes. Median twist angles ranged from approximately 21.5° in rope 7.1 to ~26.5° in ropes 7.2 and 7.4, indicating a moderate helical winding of the cellular filaments. While ropes 7.1 and 7.5 showed relatively narrow distributions with low variance, ropes 7.2, 7.4, and 8.1 exhibited broader interquartile ranges and multiple outliers, suggesting heterogeneity in filament arrangement within these structures. Twist angle data were not collected for all ropes, as in several cases the internal filament organization was not sufficiently resolved to permit accurate measurement.

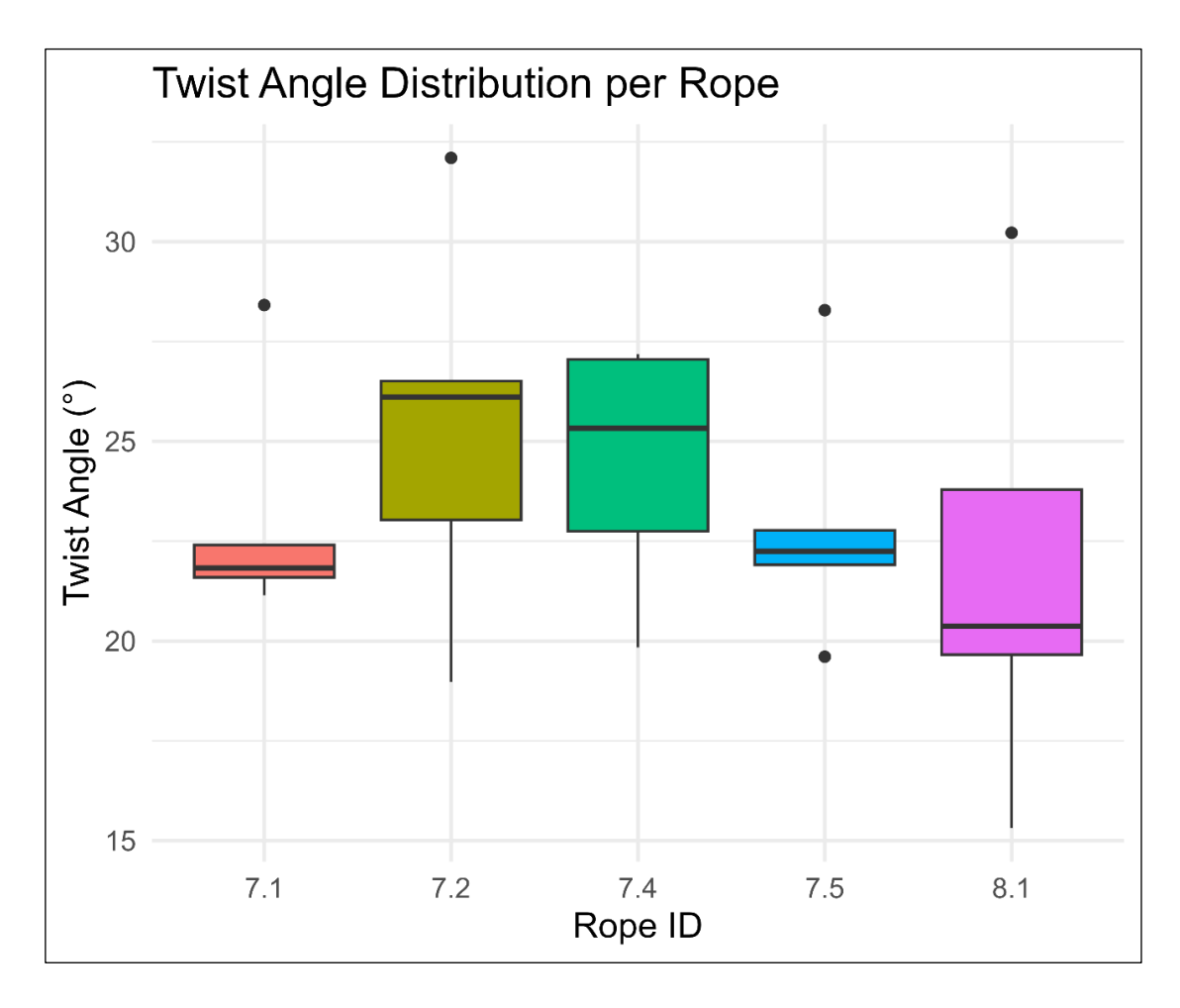


Figure 3.11. Twist angle distribution of selected *B. subtilis* biofilm ropes under unidirectional flow. Boxplots represent the measured twist angles (in degrees) for five ropes where individual helical filaments were clearly resolvable in CLSM images. Each box indicates the interquartile range (IQR), with the horizontal line showing the median and whiskers extending to 1.5× IQR. Outliers are plotted as individual points. Twist angle measurement was not possible for all ropes due to the lack of visible filament resolution in some regions.

Overall, the presence of a continuous flow triggered significant changes in biofilm morphology compared to static biofilms grown under static conditions. For comparison, Fig. 3.12 illustrates biofilms grown here under flow (Fig 3.12a and b), with static biofilms (Fig 3.12c and d).

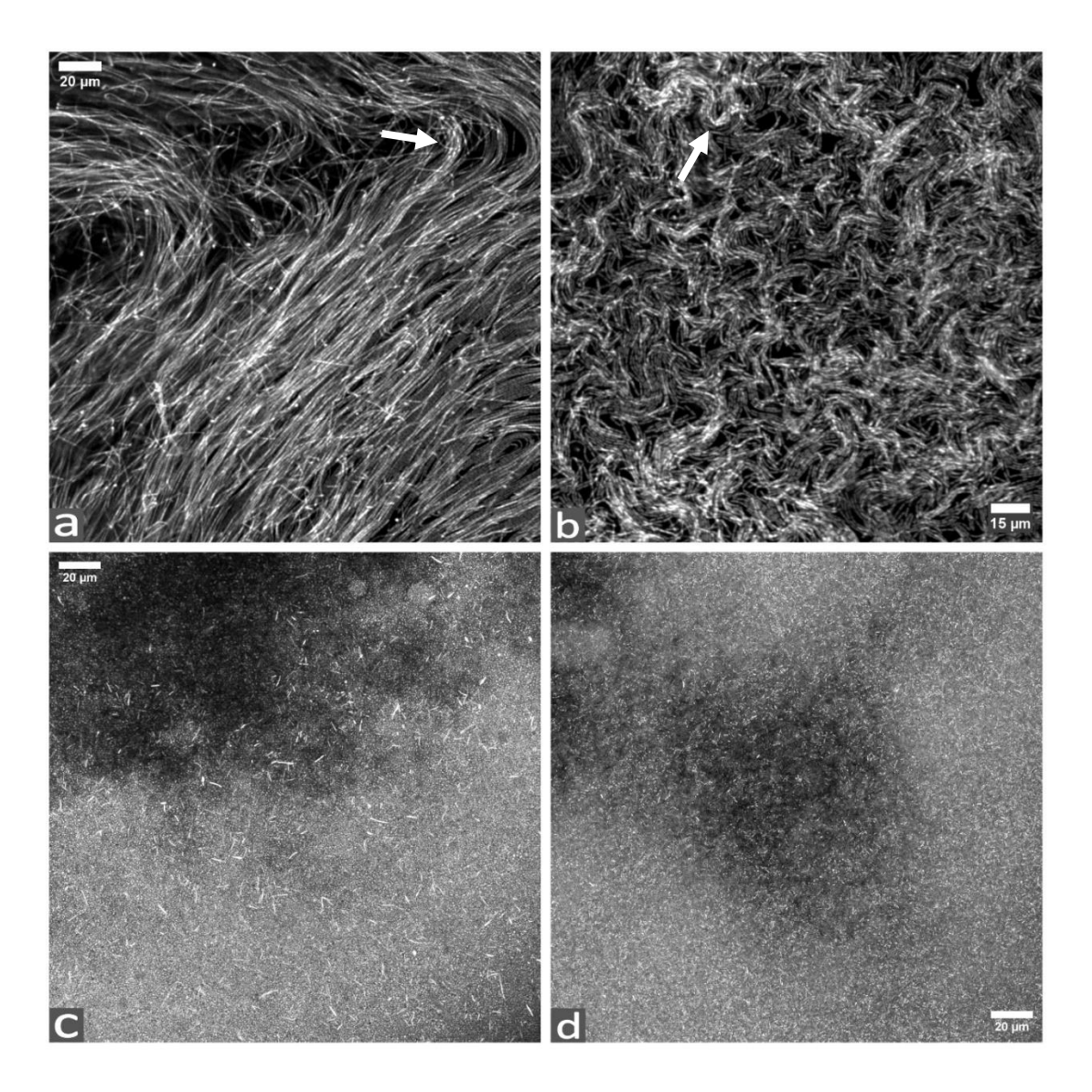


Figure 3.12. Fluorescent images of *gfp*-expressing *B. subtilis* biofilms grown under a fluid flow (a, b) and *B. subtilis* static biofilms (c, d). Flow cell biofilms were grown under a continuous flow of LB media at room temperature, for 48 hours. Static biofilms were grown in LB media on glass microscope coverslips. Images of the Static biofilms are from the previous study. Entire flow cells and static biofilms were imaged using Leica SP5 (40x magnification).

#### 3.4.1.2. Biofilm Attachment under Continuous Flow

In order to further understand biofilm development within a flow cell environment, CLSM images of a biofilm attached to the wall of the flow cell were taken. Fig. 3.13a depicts a *B. subtilis* biofilm that was found attached to the side of the flow cell.

The biofilm here was again composed of Van Gogh bundles forming wave-like patterns, which combined together to form a larger stem-like structure (Fig. 3.13). The tip (far end) of this structure attached itself to the flow cell wall via Van Gogh bundles (Fig. 3.13b). In addition, there seems to be a foundation network on the flow cell wall (Fig. 3.13b). This foundation network is also seen directly under the main body of the biofilm, which is composed of a mixture of ropes, Van Gogh bundles and round fluorescent objects in Fig. 3.13d and 3.13e (arrows). A further example of the attachment layer with a stem extending into the liquid media is shown in Fig. 3.13c.

Interestingly, a thin layer of ECM appears on the flow cell wall (Fig. 3.13d, green arrow), likely to be the biofilm's conditioning layer, a protein- or polymer-rich surface coating that forms rapidly upon contact with a substrate, facilitating initial microbial adhesion and biofilm development (Bos et al., 1999).

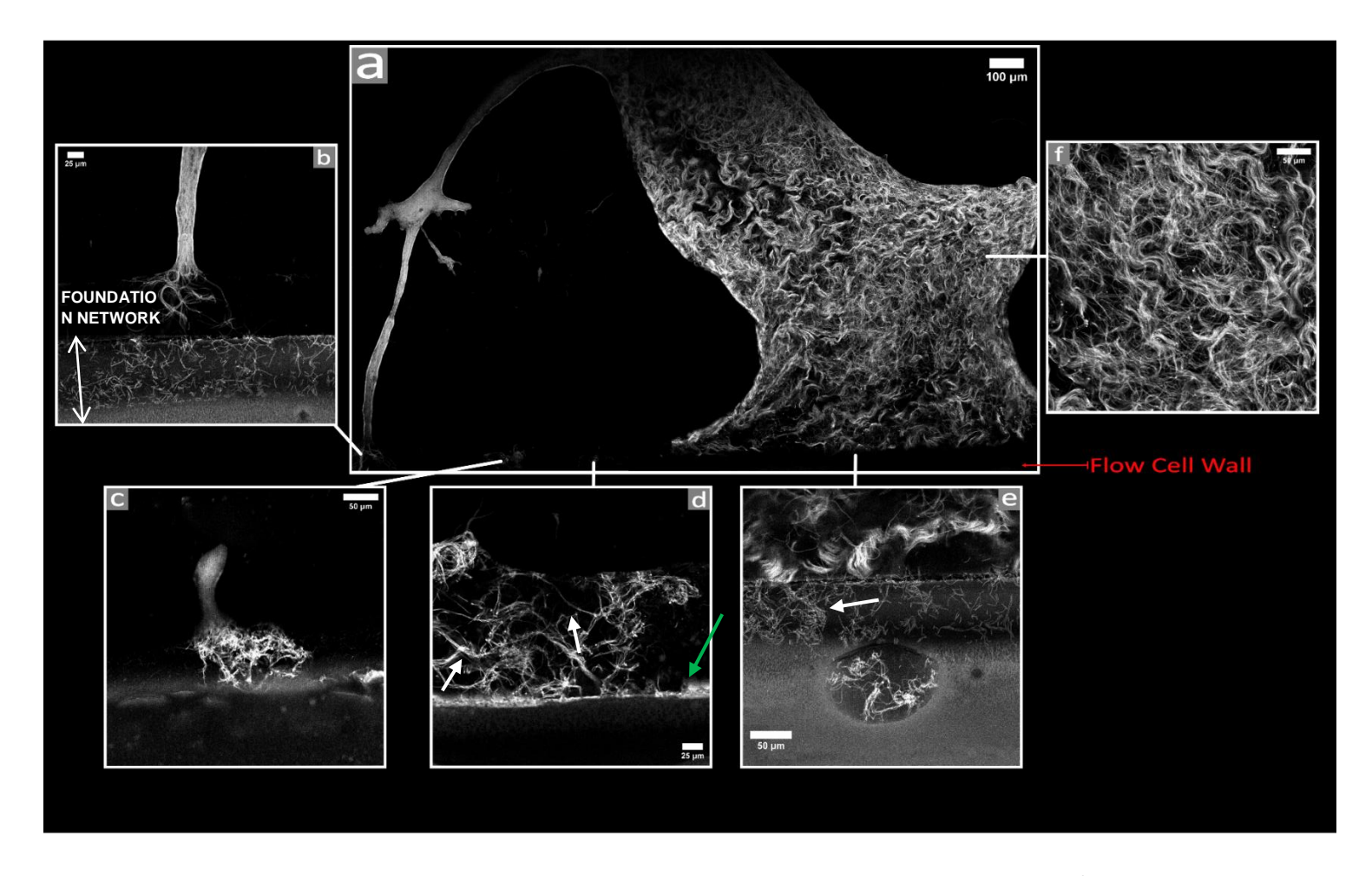


Figure 3.13. Fluorescent images of a *gfp*-expressing *B. subtilis* biofilm grown under a fluid flow, attached to the wall of the flow cell. a) Entire image of the whole biofilm. b) Elongated part of the main biofilm reaching towards the foundation network. c) A smaller biofilm with a main body and foundation network. d) ECM conditioning layer (green arrow) and emerging ropes and cell chains (white arrows) part of the foundation network. e) Image of the foundation network (arrow) right below the main biofilm body. f) Biofilm main body, made of Van Gogh bundles, ropes and spores. The flow cell biofilm was grown under a continuous flow of LB media at room temperature, for 48 hours. Entire flow cell was imaged using Leica SP5 (40x magnification).

### 3.4.2. Effect of 75 µg/mL GBLE on Flow Cell Biofilms

A concentration of 75  $\mu$ g/mL of GBLE was added to the inlet media of the flow system, to investigate any potential inhibitory effect of GBLE on flow biofilm. After allowing the system to run for 48 hours, fluorescent images of the biofilm developed within the flow cell were acquired using a CLSM (Fig. 3.14).

The addition of GBLE to the flow system resulted in a loss of organised Van Gogh bundle biofilm structure (Fig. 3.14a and b). While the flow cell biofilm described previously shows many Van Gogh bundles organised into wave- or cloud-like conformations with groups of filaments running parallel to each other. This does not occur with the addition of GBLE, where the Van Gogh bundles appear to have a less organized, more random pattern. The biofilm grown under 75  $\mu$ g/mL of GBLE shows reduced density as the biofilm structure appears more fragile. Within the biofilm, elongated structures appear (Fig. 3.14a and b, arrows). Because they are fluorescent, they are likely made of extracellular matrix (ECM) proteins and extracellular DNA (eDNA), similarly to the round ECM structures seen in the static biofilm grown under 100  $\mu$ g/mL GBLE (Chapter 2, Fig. 2.24b). These structures are also present at the edge of the biofilm (Fig. 3.14c), and light transmission microscopy reveals a few Van Gogh bundles wrapped around them (Fig. 3.14d, arrow).

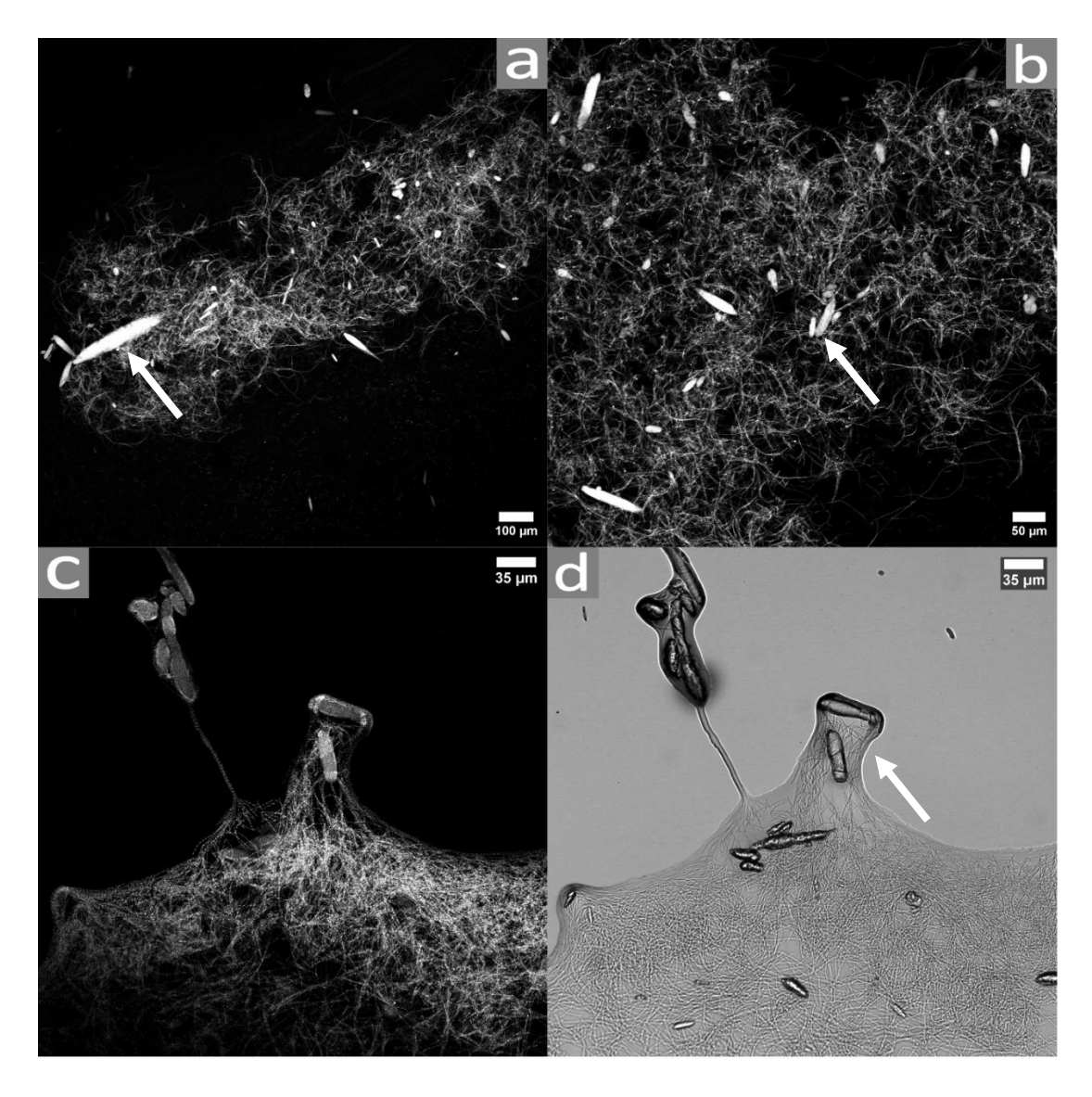


Figure 3.14. Fluorescent images of a *gfp*-expressing *B. subtilis* biofilm grown under a fluid flow, supplemented with 75  $\mu$ g/mL GBLE. Images a and b show the bulk biofilm structure, presenting disorganised and short Van Gogh bundles as well as elongated ECM structures (arrows). Images c (fluorescent microscopy) and d (light transmission microscopy) show the same biofilm area, with Van Gogh bundles and ECM structures (d, arrow). The flow cell biofilm was grown under a continuous flow of LB media, supplemented with 75  $\mu$ g/mL at room temperature, for 48 hours. Entire flow cell was imaged using Leica SP5 (40x magnification).

Furthermore, a change in intracellular fluorescence can be seen in response to GBLE. This also occurred in static biofilms exposed to GBLE (See Chapter 2, Fig. 2.27d). While the flow cell biofilm developed without GBLE shows a mixture of bacterial cells with and without changes in fluorescence, *B. subtilis* cells seem to show DNA condensation in majority of cells when GBLE is present. The fluorescence signal is so concentrated that the bacterial cells appear coccoid rather than rod-shaped (Fig. 3.15, arrow), likely due to DNA condensation at the cell centre and the CLSM detecting only the fluorescently labelled regions. However, the *B. subtilis* cells are most likely still maintaining their native rod shape.

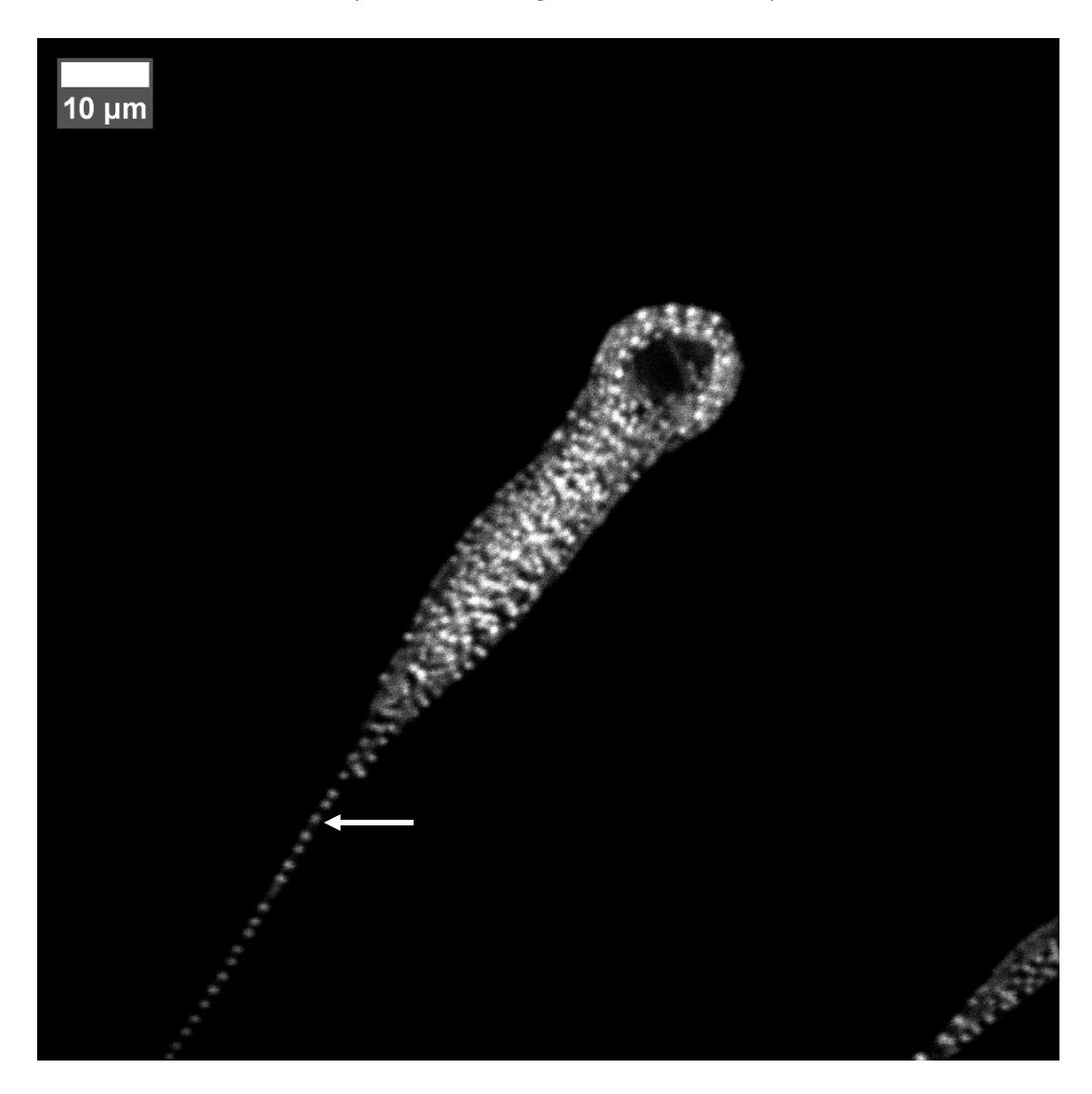


Figure 3.15. "The spoon". Fluorescent image of structure seen within the *B. subtilis* biofilm grown under a continuous fluid flow of LB media supplemented with 75 μg/mL GBLE. The image shows *B. subtilis* Van Gogh bundles made of cells that appear spherical (arrow), due to the condensation of DNA in the nucleoid upon addition of GBLE. The image was acquired using Leica SP5 (40x magnification).

### 3.4.3. Effect of 400 µg/mL GBLE on Flow Cell Biofilms

To investigate the antibiofilm activity of GBLE on flow cell biofilms, a B. subtilis biofilm was developed under continuous flow and supplemented with 400  $\mu$ g/mL GBLE suspension. This concentration was chosen as it was found to have antibiofilm activity on B. subtilis static biofilms in the previous study. After a period of 48 hours, the biofilm developed within the flow cell with 400  $\mu$ g/mL was imaged using CLSM (Fig. 3.16).

Unlike the previously described biofilms, there seems to be a complete loss of Van Gogh bundle formation under flow supplemented with 400  $\mu$ g/mL GBLE. While it is still possible to see Van Gogh bundles with 75  $\mu$ g/mL GBLE (Fig. 3.14a), when the concentration of GBLE increases to 400  $\mu$ g/mL, Van Gogh bundles cannot be seen at a broader scale (Fig. 3.16a). At higher magnification it is evident the biofilm is composed of short chains of cells which are intertwined with each other in a disorganised manner (Fig. 3.16c-e). These chains are far shorter than the Van Gogh bundles. The addition of 400  $\mu$ g/mL GBLE also seemed to reduce biofilm cohesion, compared to the biofilm grown without GBLE. This is seen in Fig. 16b, where many gaps can be seen within the biofilm.

Consistently to previously described flow biofilms, bacterial cells show DNA condensation (Fig. 3.16d, arrow), although this phenomenon is not as frequent as seen in the biofilm supplemented with 75  $\mu$ g/mL GBLE.

Overall, GBLE at higher concentrations seemed to interfere with biofilm development at a higher degree. The biofilm grown under 400  $\mu$ g/mL GBLE completely lacks the formation of long Van Gogh bundles, seen at 75  $\mu$ g/mL GBLE and without GBLE. The biofilm without GBLE exhibits a dense, highly organized structure composed of tightly packed single-cell filaments forming characteristic Van Gogh bundles, displaying spatial cohesion and rope-like structures. In contrast, the biofilm treated with 400  $\mu$ g/mL GBLE appears markedly disrupted, with a substantial reduction in Van Gogh bundle formation and spatial organization. Cells are dispersed and largely unaligned, lacking the cohesive bundling seen in the control.

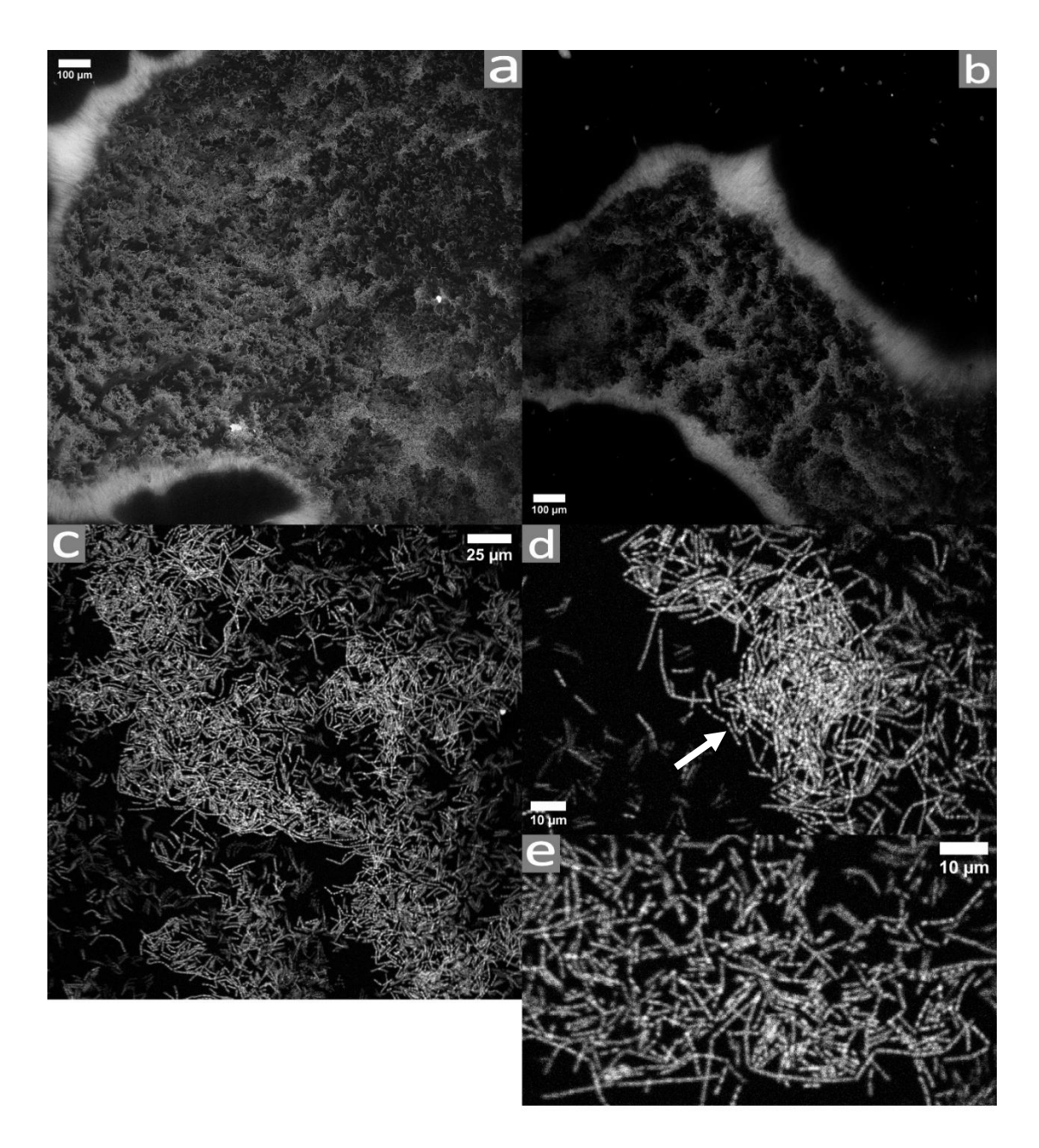


Figure 3.16. Fluorescent images of a *gfp*-expressing *B. subtilis* biofilm grown under a fluid flow, supplemented with 400  $\mu$ g/mL GBLE. Images a and b show the bulk biofilm structure, lacking Van Gogh bundles and with no apparent organisation. c) d) e) Images of higher magnification show short disorganised cell chains and changes in intracellular fluorescence, as cells shift from a rod to shorter and more round shape (d, arrow). The flow cell biofilm was grown under a continuous flow of LB media, supplemented with 400  $\mu$ g/mL at room temperature, for 48 hours. Entire flow cell was imaged using Leica SP5 (40x magnification.

### 3.5. Discussion

Bacteria and microorganisms are extremely resilient entities and in order to withstand and proliferate under challenging conditions, they adopt a biofilm form (Costerton et al., 1995) (Flemming et al., 2016). Biofilms develop in any kind of environments, and this shapes the morphology of the biofilm (Flemming and Wingender, 2010). Remarkably, bacteria are able to sense the changes in the environment, modulate gene expression and grow in a robust biofilm structure (Stoodley et al., 2002) (O'Toole et al., 2000).

# 3.5.1. Fluid Flow Forces Promote the Formation of Spore Aggregates and Rope-Like Structures

Biofilms grown under a continuous fluid flow presented significant changes in morphology compared to static biofilms. In the previous chapter, B. subtilis JWV042 static biofilms were grown and then imaged using CLSM. B. subtilis static biofilms showed standard biofilm structure, with rod-shaped cells encased in ECM, with no apparent Van Gogh bundle structures. These only appeared in static biofilms once GBLE was supplemented to the growing media. As seen in Fig. 3.3, in this study, flow cell biofilms seem to have a cloud-like appearance. Attached internally to the flow cell, the biofilm appears to be made of multiple Van Gogh bundles aligned with each other. Van Gogh bundles are more visible at the edge of the cloud biofilm, along with fluorescent small dots. Although tightly aligned Van Gogh bundles have been described in the context of colony agar biofilm expansion (van Gestel et al., 2015), they have not been described in biofilms grown under flow. Van Gogh bundles in the flow cell form clusters of aligned cells which can form wave like patterns or intertwine with each other. (Fig. 3.3 and 3.4). Currently, there are no studies investigating the morphological appearance of B. subtilis biofilms under a fluid flow. A majority of the studies around biofilms developing under a fluid flow utilise microfluidic devices and Pseudomonas spp. (Rusconi and Stocker, 2015) (Recupido et al., 2020). While this approach is able to investigate the formation of streamers and the impact of the parameters concerning the microfluidic channels on streamers characteristics, the overall morphology of the biofilm is neglected, because the microfluidic channels are too narrow to allow the free development of the bulk biofilm. Although understanding streamer development within a flow environment is important, there is a lack of information regarding how other bacteria form streamers and generally, how microorganisms shape their biofilm architecture in response to flow. In this study, B. subtilis biofilm morphology within a flow environment was unveiled. Under a fluid flow, bacteria are subjected to a number of different mechanical stresses, mainly shear stress (Stoodley et al., 2002) (Persat et al., 2015). Bacteria are able to adapt to shear stress by changing their metabolic response. Evidently, this is seen in this study as same species biofilms differ morphologically based on the environmental conditions. When grown under shear stress, bacteria were found to increase synthesis of ECM compounds (Rupp et al., 2005). In a research study conducted by Rodesney et al. (2017), Pseudomonas aeruginosa was seen to increase cyclic-di-GMP levels when subject to shear forces. Cyclic-di-GMP is a compound secreted intracellularly which triggers the shift from a planktonic to biofilm lifestyle and its increased synthesis by P. aeruginosa under flow indicates that the bacteria prefer the biofilm lifestyle under flow in order to withstand shear stress. The ability of microorganisms to sense and adapt to the environment is referred to as quorum sensing and when this occurs in response to mechanical forces, it is termed mechanosensing (Rutherford and Bassler, 2012) (Tsagkari et al., 2022). Mechanosensing in a flow environment leads to the formation of a stronger biofilm with increased surface attachment and overall biomass (Yan et al., 2017) (Tsagkari et al., 2022). While this present study lacks any measurements regarding biofilm strength, it is possible to assume that *B. subtilis* biofilms change their entire morphology to overcome the shear stress induced by flow. It is likely that mechanosensing in B. subtilis is inducing changes from the overall biofilm morphology down to the cellular level.

Fluid flow shaped not only the overall biofilm architecture, but also induced the formation of secondary structures, such as bacterial ropes and aggregates (Fig. 3.5, 3.8 and 3.9).

Fluorescence microscopy revealed aggregates composed of GFP-expressing *B. subtilis* cells (Fig. 3.5), indicating the presence of DNA-rich subpopulations. Given their size and morphology, these fluorescent objects are likely spores. Sporulation, typically triggered by harsh conditions, produces resilient structures that withstand stressors such as desiccation, temperature, and pH extremes (Errington, 2003) (Saggese et al., 2022). Spores contribute to biofilm persistence and are commonly detected in contaminated water and food environments (Driks, 2002) (Setlow, 2014). In this study, fluid flow alone appeared to induce sporulation and spore aggregation, suggesting that mechanical forces may act as a sufficient trigger. This is the first report of *B. subtilis* spore formation and aggregation in response to flow. Spores were frequently observed adhering to Van Gogh bundles (Fig. 3.5b), potentially driven by physical forces that promote contact and adhesion (Persat et al., 2015).

Additionally, flow-induced stress may modify spore surface properties, enhancing their stickiness (Driks, 2002) (Setlow, 2014). While spore resistance is well-studied, spore adhesion and aggregation under mechanical stress remain poorly understood, highlighting a key gap in knowledge of how *B. subtilis* adapts to dynamic flow conditions through differentiation and biofilm restructuring.

Multicellular lifestyle in bacteria is characterised by intercellular cooperation, where different subpopulations secrete molecules that are shared with non-producing cells. The development of a multicellular lifestyle is modulated by quorum sensing, which is a mechanism of cell-to-cell communication used to share information regarding the surrounding environment and modulate gene expression appropriately (Rutherford and Bassler, 2012). Ultimately, gene expression is what drives cellular differentiation and division of labour (Vlamakis et al., 2013). Subpopulations can clearly be seen under flow, as spore aggregates (Fig. 3.5), Van Gogh bundles and ropes (Fig. 3.8 and 3.9) are both present.

Remarkably, B. subtilis not only formed Van Gogh bundles, or cell chains, under flow, but also induced the development of Van Gogh ropes (Fig. 3.8and 3.9). Van Gogh ropes are composed of multiple B. subtilis cell chains aligned parallel to each other and twisted into a rope-like structure. The formation of Van Gogh bundles under flow may provide a survival advantage by allowing cells to remain attached to surfaces and resist being washed away, as bundling together increases collective stability against shear forces (Vlamakis et al., 2013) (Yan et al., 2017). Furthermore, adopting a rope structure likely enhances their mechanical strength because twisting bundles into a rope distributes the tensile strain more evenly across the individual cell chains, preventing breakage of single strands under stress (Goriely and Neukirch, 2006). This increase in tensile strength would confer an advantage by enabling the biofilm structures to better withstand the physical forces of the flowing environment, thus maintaining biofilm integrity and ensuring that bacteria remain anchored and protected despite the constant shear stress imposed by fluid flow (Flemming and Wingender, 2010) (Persat et al., 2015). In addition to the mechanical action of the flow, Van Gogh ropes might also be forming due to increased ECM production, which further enhances cohesion among the bundled cell chains.

Twist angle measurements of Van Gogh ropes further support the idea that these structures are mechanically adapted to flow conditions. Quantification of twist angles revealed that the ropes are not randomly bundled but instead exhibit consistent helical organization, with

moderate twist angles ranging from approximately 21° to 27° across several ropes (Fig. 3.11). This organized twisting may enhance the structural integrity of the rope by providing torsional resistance and distributing mechanical stress more uniformly along the rope (Goriely and Neukirch, 2006). Similar to the role of twist in engineered ropes or helical fibres, a controlled twist angle may prevent local deformation or buckling of individual chains, and increase resistance to tensile and shear forces within the flow environment (Goriely and Neukirch, 2006). The presence of a defined twist also suggests that rope formation is not merely a passive result of cell alignment but may involve active structural regulation, possibly mediated by extracellular matrix components or surface adhesion dynamics (Branda et al., 2005) (Beauregard et al., 2013). Notably, twist angle heterogeneity observed across different ropes may reflect varying local flow conditions or developmental stages of rope maturation, with tighter twists potentially correlating with regions of higher shear (Persat et al., 2015) (Stoodley et al., 1999). These findings suggest that rope formation could serve as a functional morphological adaptation, contributing to the mechanical robustness and long-range cohesion of the biofilm under unidirectional flow.

The formation of Van Gogh ropes in B. subtilis biofilms under unidirectional flow bears a striking resemblance to the mechanical behaviour observed in engineered twisted fibre systems such as polypropylene baling twine and plant fibre yarn composites. Kostić (2013) demonstrated that the tensile strength of baling twine increases with twist angle up to an optimal point, after which further twisting leads to a decline in strength due to fibre misalignment and internal stress accumulation. Similarly, Shah et al. (2013) modelled the tensile behaviour of plant fibre yarns and found that twisting enhances yarn cohesion and tensile load distribution, but excessive twist introduces oblique fibre orientation that reduces the ability to bear axial loads effectively. These principles directly parallel the behaviour of Van Gogh ropes, where moderate twist angles (21°-27°) likely represent a mechanically favourable range that maximizes cohesion among cell chains without compromising alignment with the direction of flow. In the microbial context, this may enhance the mechanical resilience of the ropes under shear stress, ensuring that individual filaments do not unravel or detach from the surface. Furthermore, the observed twist angle variation across ropes may reflect an adaptive response, similar to how engineered materials balance twist to achieve optimal tensile performance. Taken together, these studies suggest that B. subtilis may employ rope formation as a biological strategy to optimize mechanical integrity in dynamic environments, akin to design principles used in synthetic fibre systems.

In the context of *B. subtilis* biofilms, many cell types have been described, including motile single cells, referred to as explorers and sessile cell chains, also named settlers (Qin, Angelini and Chai, 2022). Although the literature reports that in biofilms, settlers have been found less abundant compared to the explorers, this study shows that the biofilm adhered to the flow cell is entirely made of Van Gogh bundles (Fig. 3.4), spore aggregates (Fig. 3.5) and Van Gogh ropes (Fig. 3.8 and 3.9). *B. subtilis* planktonic cells can be found in mutually exclusive cell states, which are dependent on various environmental factors. In planktonic cultures, long cell chains have been detected in the exponential phase, while single or pairs have been seen more abundantly in the stationary phase (Kearns and Losick, 2005). In colony agar biofilms, *B. subtilis* differentiates into genetically identical subpopulations to adapt challenges in the environment, as seen in Chapter 2, in response to GBLE. These subpopulations include matrix-producers, which are able to produce ECM components and are seen in cell chains. Matrix-producers are assisted by surfactin-producers in biofilm expansion, indicating the ability of the bacterium to further differentiate in multiple coexisting cell types (van Gestel et al., 2015) (Branda et al., 2005).

Fluid flow drastically changes biofilm morphology, clearly indicating that B. subtilis differentiates into subpopulations to adapt to shear stress. Because cell chains have been referred to as matrix producers, it is possible that, in order to withstand flow, matrix producers, along with surfactin producers, form the key components of the biofilm (van Gestel et al., 2015). These two subpopulations are known to form Van Gogh bundles (van Gestel et al., 2015), and since Van Gogh ropes are composed of multiple cell chains aligned and twisted together, it is likely that ropes are formed predominantly by matrix- and surfactin-producing cells. Biofilm formation begins when bacterial cells secrete ECM composed primarily of exopolysaccharides, proteins, and extracellular DNA (Flemming and Wingender, 2010). Upon ECM production, B. subtilis cells elongate, stick to each other, and align to form Van Gogh bundles. Under flow, these bundles appear to twist and adhere together into rope-like structures. This morphological adaptation confers clear advantages: for example in climbing plants, rope structures distribute mechanical strain more evenly across their bundled strands, enhancing tensile strength (Goriely and Neukirch, 2006). Such increased tensile strength prevents breakage of individual chains, allowing the biofilm to resist deformation and detachment under flow (Persat et al., 2015). While rope formation may partially arise as a by-product of ECM and surfactin production, this structure ultimately benefits the biofilm by enhancing adhesion to surfaces, resisting shear forces, and

maintaining community stability in dynamic fluid environments (Branda et al., 2005) (Vlamakis et al., 2013).

A biofilm under flow will not only be subjected to the forces exerted by flow, but will also be modulated by the mechanical selection of more adhesive bacterial cell types (Martínez-García et al., 2018). Therefore, the morphology of flow biofilms seen in this study, characterised by multiple Van Gogh bundles aligned and intertwined with each other, will also be due to the selection process caused by the flow. It is likely that Van Gogh bundles represent the most adhesive cell type in B. subtilis flow biofilms, due to being made of matrixand surfactin-producers (van Gestel et al., 2015). This high adhesive capacity likely refers both to cell-cell adhesion and adhesion to surfaces. Matrix producers secrete exopolysaccharides and proteins that facilitate cells sticking together, promoting robust cellcell cohesion within the bundles (Branda et al., 2005) (López et al., 2009). At the same time, surfactin producers modulate surface tension and promote initial surface attachment and spreading, which, alongside matrix components, enhances the ability of these cell chains to anchor firmly to surfaces (Kearns and Losick, 2003) (Arjes et al., 2020). Together, we suggest that these properties enable Van Gogh bundles to maintain structural integrity within the biofilm while also ensuring strong attachment to the substratum under fluid flow. Both forms of adhesion are crucial for effective biofilm formation, providing stability and resistance against shear stress in flowing environments (Flemming and Wingender, 2010) (Persat et al., 2015).

B. subtilis naturally adopts multicellular lifestyles, with cell—cell adhesion providing resistance to environmental challenges (Vlamakis et al., 2013). In this experiment, fluid flow induced multicellularity in B. subtilis JWV042, prompting cells to differentiate into specialised subtypes and cooperate to withstand shear forces efficiently. However, multicellularity in undomesticated microorganisms remains underexplored, as most studies use domesticated lab strains under optimal conditions (McLoon et al., 2011). These strains, having lost the ability to form structured biofilms, do not accurately represent wild-type behaviour (McLoon et al., 2011). This is the first study that used B. subtilis JWV042, a NCIB 3610 derivative that retains wild-type biofilm formation and motility, to better simulate natural biofilm development under flow.

### 3.5.1.1. Biofilm Attachment under Fluid Flow Forces

Investigating biofilm formation under flow is essential to understand the underpinning mechanisms and come up with effective biofilm control strategies. Biofilms under flow are morphologically different compared to other types of biofilms and depending on the environmental stress, bacteria and other microorganisms will adopt multicellular lifestyles to be able to proliferate (Vlamakis et al., 2013) (Tsagkari et al., 2022). Biofilms are often found in fluid flow systems, such as water distribution networks (Wingender and Flemming, 2011), wastewater treatment plants (Flemming et al., 2016), medical devices like catheters and stents (Donlan, 2001), industrial cooling systems (Di Pippo et al., 2018), and gas and oil pipelines (Dobretsov et al., 2009). While investigating *B. subtilis* JWV042 biofilm development under continuous fluid flow within a plastic flow cell, a biofilm attached to both sides of the flow cell was seen (Fig. 3.13). This biofilm seems to have a main body and an foundation network, Fig. 3.13f and 3.13d respectively. High magnification images of the foundation network of the flow cell biofilm were taken (Fig. 3.13b, c, d and e). This network appears to serve as foundation for the main biofilm body. It is likely that this attachment layer of the flow biofilm is the first step of biofilm formation in flow cell biofilms.

The stages of biofilm development within a fluid flow have not been investigated thoroughly; this is the first study describing an attachment layer in a *B. subtilis* flow cell biofilm. Fig. 3.13d shows fluorescent matter attached to the flow cell wall (green arrow), as it is likely to be extracellular matrix (ECM). It has been established that in order for the biofilm to survive in a flow system, ECM production is increased, as the matrix enhances structural stability and resistance to shear forces (Stoodley et al., 1999) (Shaw et al., 2004) (Klapper et al., 2002). For example, studies have shown that *B. subtilis* and *P. aeruginosa* biofilms upregulate matrix production under fluid shear to strengthen biofilm integrity and prevent detachment (Petrova and Sauer, 2012) (Yan et al., 2017). It is likely that at the first stages of wall colonisation under flow, *B. subtilis* JWV042 cells adhere to the flow cell wall and ramp up ECM synthesis. While some bacterial cells establish attachment and differentiate into matrixand surfactin-producers, more cells and nutrients will come in contact with the flow cell wall due to mass transport, aiding biofilm growth and development.

In the context of biofilm formation, the literature broadly describes the presence of a conditioning layer, which precedes bacterial adhesion to a surface, composed of organic and inorganic molecules and compounds as well as cellular components (Bhagwat et al., 2021)

(Garrett, Bhakoo and Zhang, 2008). The conditioning layer occurs due to the gravitational and/or fluid flow mechanical forces, as any particles, nutrients and cells present in the moving fluid deposit onto the walls surrounding the fluid (Garrett, Bhakoo and Zhang, 2008). This layer changes the properties of the substratum, including surface tensions, charge, ion composition and also surface potential (Garrett, Bhakoo and Zhang, 2008). These changes facilitate bacterial adhesion and proliferation (Bhagwat et al., 2021). Flow cell biofilms will likely also have a conditioning layer, however, there are no studies investigating this phenomenon. In this present study, in Fig. 3.13d, the layer of ECM seen is likely the conditioning layer of the *B. subtilis* JWV042 flow biofilm.

Protruding from the flow biofilm conditioning layer, Van Gogh bundles and ropes can be seen (Fig. 3.13d and 3.13e, white arrows). These bundles and ropes however do not seem to be part of the biofilm's main body, seen in Fig. 3.13f. This network of ropes and bundles seem to function as a foundation for the attachment of the main part of the biofilm to the ECM conditioning layer. This is clearly seen in Fig. 3.13c, where the biofilm foundation made of Van Gogh bundles and ropes are vertically attached to the flow cell wall and a small main body biofilm is elongating.

The presence of this foundation network could be driven by the flow dynamics within the flow cell. Near the surface, within the diffusion boundary layer where flow velocity is minimal, bacterial cells can initially attach and begin producing ECM, establishing the less dense foundation (Stoodley et al., 2002) (Klapper et al., 2002). As the biofilm grows outward into regions of faster flow, nutrient and oxygen availability increase due to mass transport, promoting higher cell density and ECM production, leading to the formation of a denser main biofilm body (Stewart, 2003) (Purevdorj et al., 2002). While this filamentous foundation network provides structural support, it may also represent a potential weakness. Because it is less dense and forms the primary attachment point to the surface, mechanical forces from the flow could shear off the entire biofilm if detachment occurs at this layer. In such an event, the dense main body could detach as a single unit, or fragments may remain attached depending on the extent of ECM cohesion (Stoodley et al., 2002). However, the Van Gogh bundles and ropes within the foundation likely enhance tensile strength and attachment stability by distributing shear forces, thus reducing the risk of detachment under flow. In addition, flow forces by the flow cell wall are near to zero, due to the boundary layer effect, minimising hydrodynamic forces on the foundation layer.

The stages of biofilm development within fluid flow conditions have not been thoroughly investigated; most studies focus primarily on overall morphology and architecture, such as streamer formation, biovolume changes, or shear response, leaving the early developmental stages under flow largely underexplored (Stoodley et al., 1999) (Thomen et al., 2017) (Pearce et al., 2019). This study is the first to describe an attachment layer composed of ECM and Van Gogh bundles in *B. subtilis* flow cell biofilms, highlighting the need for further research into the mechanical properties and failure points of biofilm foundation layers under shear stress.

The five step biofilm development model currently used to understand biofilm formation was established in 2002, based on in vitro experiments using *P. aeruginosa* (Stoodley et al., 1999). This model identifies five steps in biofilm formation: reversible attachment, irreversible attachment, maturation (I), maturation (II) and dispersion. Although this model is relevant for studying biofilms in laboratory settings in static cultures, it presents several limitations, as it does not reflect the complexity of biofilm formation in real-world environments (Sauer et al., 2022), and this highlights the need for an updated and tailored biofilm development model. In the five-step biofilm development model, initial attachment is characterised by planktonic cells which adhere to a surface due to a number of forces, which may include Van Der Waals, electrostatic, hydrophobic and adhesive proteins (Thomen et al., 2017) (Sharma et al., 2023). These same forces are also likely to play a role in bacterial attachment under hydrodynamic forces. As the fluid nears the wall, there is a diffusion boundary layer where flow is very slow, causing things to deposit without being washed off. Reversible attachment is usually followed by irreversible attachment. This step is characterised by ECM synthesis, and it has been established that ECM production is not only necessary for biofilm formation, but it also increased under environmental stresses (Yan et al., 2017) (Teschler et al., 2015). Fluorescent images from this present study reveal a thin layer of ECM, containing eDNA, adhered to the flow cell wall, indicating that irreversible attachment also occurs in flow cell biofilms. The third step of the latter is the first maturation stage, during which bacterial clusters are formed (Sauer et al., 2022). In this present study, instead of clusters, B. subtilis cells arrange themselves into Van Gogh bundles, which adopt a vertical orientation. Verticalization in the context of biofilm development under flow has been described by Pearce et al. (2019), who, using a mathematical model, established that bacterial cells at the upstream end of the biofilm are oriented vertically due to the drag and shear torques. In this current study, verticalization seems to occur at the foundation network of the biofilm and instead of involving single cells, it involves entire Van Gogh bundles and ropes (Fig. 3.12d). Once the foundation network is established, the biofilm develops into the main body, adopting wave-like appearance and differentiating into spores and other unknown subpopulations. Therefore, it may be reasonable to add another step, which will be termed 'extension', during which the foundation network extends into the main body and bacterial cells further differentiate.

It is well recognised that different flow forces produce distinct biofilm morphologies. For example, Recupido et al. (2020) observed that *P. fluorescens* under low shear formed isolated clusters with minimal ECM production. Similarly, in this study, less biomass was observed in the biofilm foundation layer where flow forces are negligible near the wall. Thomen et al. (2017) showed that *E. coli* adopts a "stress-escaping" strategy by first attaching and proliferating in flow-protected wall regions before expanding into areas exposed to higher shear. This suggests that *B. subtilis* may also initially settle on the flow cell wall to form a foundation network before differentiating into the dense main biofilm body (Fig. 3.13e). Paula et al. (2020) further support this concept, showing through mathematical modelling that biofilm clusters on surfaces merge to form larger structures.

According to the five steps biofilm development model, the final stage of biofilm formation is dispersion, a phenomenon in which bacterial cells detach and go on to establish more biofilms elsewhere (Sauer et al., 2022). Dispersion also occurs under flow and it is highly influenced by hydrodynamic forces, as bacterial cells' displacement is facilitated by the movement of flow. This is likely to occur in B. subtilis JWV042 flow biofilms, so that bacterial cells can attach and grow in other parts of the flow cell in the form of biofilms. However, fluorescent images obtained from this study indicate that, due to the forces exerted by the fluid flow, established B. subtilis biofilms can bend in their entirety and reach for downstream surfaces (Fig. 3.13a and 3.13b). In Fig. 3.13a, the biofilm main body stretches and bends all the way down towards the foundation network. Clusters of Van Gogh bundles can be seen branching down in Fig. 3.13b. The fact that a mature biofilm can, due to the forces of flow, bend and attach to new surfaces reshapes the general thinking when it comes to biofilm development, especially regarding the five-step biofilm development model. A biofilm establishing colonisation in this manner has not been documented before. Biofilms have been previously described as colloidal hydrogels, as ECM behaves like a crosslinked polymer and the bacterial cells like colloids (Ido et al., 2020). It is important to highlight that these features have been attributed to agar and pellicle biofilms, and not immersed biofilm structures. In agar and pellicle biofilms, bound water and water channels confer viscoelasticity to the biofilm (Ido et al., 2020), and in *B. subtilis*, the amyloid fibre TasA play a key role in the biofilm's hydrogel behaviour (Huang et al., 2019). In this study, the *B. subtilis* biofilm bending towards the surface upstream, in Fig. 3.13a, is likely behaving in this manner due to the viscous and elastic nature of biofilms.

Biofilms present mechanical heterogeneity, with the biofilm base being more stiff than upper regions, due to the biofilm's morphological and structural heterogeneity (Peterson et al., 2015). This is likely the reason why the biofilm in Fig. 3.13a is deforming the way it is, with the base attached to the substratum and the upper biofilm layer behaving like a viscoelastic fluid under fluid flow.

The findings of this study highlight the complexity of biofilms and their development, specifically, how the current understanding of biofilm development is simplistic and incomplete, as it does not take into account the heterogeneity of biofilm formation, which can be significant even within single species biofilms.

### 3.5.2. Effect of *Gingko biloba* Leaf Extract on Flow Cell Biofilms

In this study, in addition to investigating the effects of a fluid flow on *B. subtilis* biofilm morphology, the antibiofilm effect of GBLE was investigated in the context of flow biofilms. Because it is a leaf extract, GBLE could potentially represent a sustainable alternative for standard biofilm control strategies in pumped flow systems. So far, GBLE antibiofilm activity has been investigated using agar and static biofilms, and previous studies have highlighted the extract's ability to inhibit *S. aureus*, MRSA and enteropathogenic *E. coli* biofilms (Lee et al., 2014) (Wang et al., 2021). The findings from the previous chapter also indicate that GBLE has inhibitory effects on static *B. subtilis* biofilms. In order to investigate GBLE antibiofilm activity in a flow system, *gfp*-expressing *B. subtilis* biofilms were grown in flow cells under continuous flow and the inlet medium was supplemented with different concentrations of GBLE.

In both flow cell biofilms supplemented with GBLE, a general loss in wave- and cloud-like biofilm structures was seen, compared to the flow cell biofilm without GBLE (Fig. 3.3 and 3.4 and Fig 3.16 and 3.14). Additionally, both biofilms grown under GBLE showed overall reduced biomass. Interestingly, there seems to be a gradual loss of biofilm structure and biomass, as

this is more apparent in the biofilm supplemented with 400  $\mu$ g/mL, indicating a concentration-dependent response.

Findings from the previous chapter investigating the effect of different GBLE concentrations on *B. subtilis* planktonic growth showed that the extract delayed the exponential phase in bacterial growth curve experiments. If bacterial cells within a fluid flow behave in the same manner as they do in a planktonic culture, then it is likely that the exponential growth phase for *B. subtilis* cells in the fluid flow is being delayed due to GBLE. Coupled with fluid flow forces, which might also have a delaying effect on exponential growth phase by washing out quorum sensing molecules (Thomen et al., 2017), the addition to GBLE will inevitably delay flow cell biofilm development and result in a decrease in biofilm biomass.

If the antibiofilm effect of GBLE was only due to a delay in exponential growth phase, then the fluorescent images acquired would show a flow cell biofilm structurally similar to the biofilm without any GBLE, but smaller in size, as longer times would be required for growth. However, Fig. 3.11 and 3.13 also show the loss in organised Van Gogh bundles and ropes arrangement within the biofilms. In the flow cell supplemented with 75 µg/mL, B. subtilis bacterial cells seem to still attempt to form Van Gogh bundles (Fig. 3.11). However, Van Gogh bundles appear more fragmented, creating shorter filaments, and less cohesive compared to the flow cell biofilm in Fig. 3.3-3.4. Van Gogh bundles also present no organised structure or alignment, as they look randomly intertwined with each other. Additionally, as seen in Fig. 3.12, bacterial cells present a drastic change in intracellular fluorescence, to the point that they almost look spherical. DNA condensation was also seen in the previous chapter in B. subtilis static biofilms, upon addition of GBLE. As described in the previous chapter, nucleoid condensation in bacteria is a well-known structural response to stress, mediated by NAPs, topoisomerase activity, or direct interactions with small molecules, including plant phenolics (Ohniwa et al., 2006) (de Vries, 2010) (Hołówka and Zakrzewska-Czerwińska, 2020) (Luu et al., 2022) (Khameneh et al., 2019). Given that Ginkgo biloba contains diverse phenolic compounds, it is plausible that GBLE influences intracellular structures by inducing such condensation.

The cells making these Van Gogh bundles look completely different from the cells in the Van Gogh bundles and ropes making the flow cell biofilm without GBLE, indicating that either, the required *B. subtilis* subpopulation for adequate Van Gogh development is not differentiating or upon differentiation, their adequate role cannot be performed due to the presence of

GBLE. Therefore, it is possible that GBLE is influencing *B. subtilis* subpopulation, either before or after differentiation. Van Gogh bundles formation relies on matrix- and surfactin-producers (van Gestel et al., 2015), and therefore, the gradual loss of organised bundles and ropes with increasing concentration of GBLE indicates that the extract is hindering either the development of these *B. subtilis* subpopulations or their organised assembly, possibly by inhibiting ECM synthesis, as mentioned by previous studies. Lee et al. (2014) indicated that *Ginkgolic acid* C15:1 inhibited curli formation in enterohaemorrhagic *E. coli*. Curli fibres are a type of amyloids produced by *E. coli*, which play a key role in adhesion and biofilm formation (Barnhart and Chapman, 2006). Furthermore, findings from another study, carried out by Wang et al. (2021), showed that *Gingko biloba* exocarp extracts downregulated ECM and virulence genes of *S. aureus*/MRSA.

The key role of ECM in biofilm development has been widely recognised, and in biofilms under fluid flow, ECM confers mechanical stability and protection from environmental stresses (Flemming and Wingender, 2010) (Yan et al., 2017). Therefore, inhibition of ECM component will lead to the development of a fragile biofilm, even more so under flow forces. These findings may highlight the potential of GBLE for biofilm control and inhibition in pumped flow systems.

In addition to morphological changes and reduced biomass, GBLE-treated flow cell biofilms exhibited elongated fluorescent structures, hypothesized to be ECM aggregates. This interpretation is supported by the use of *gfp*-tagged histone proteins, which label *B. subtilis* DNA and potentially extracellular DNA (eDNA) within the ECM. These structures were more abundant at 75 µg/mL GBLE and sparse at 400 µg/mL. Similar ECM aggregates were observed in static biofilms exposed to 100 µg/mL GBLE, though those appeared circular in shape, suggesting that flow may influence aggregate elongation. GBLE is known to alter ECM production and composition, potentially affecting post-synthetic interactions among ECM components (Secchi et al., 2022). Additionally, EPS components may interact with GBLE, either structurally or through sequestration, as some extracellular polymeric substances are known to bind antimicrobial compounds and contribute to biofilm resistance (Singh et al., 2021). Such ECM aggregates have not been described before. The fact that ECM components undergo aggregation means that they cannot perform their functions within the biofilm, further indicating that GBLE has antibiofilm activity on flow cell biofilms.

Due to the fact that current biofilm control strategies involve the use of harsh chemicals, which are then disposed of in the sewage systems and have detrimental effects on biodiversity and ecosystems (Pascual, Llorca and Canut, 2007), sustainable and eco-friendly biofilm control alternatives are needed. These findings further strengthen the potential antibiofilm application of GBLE, which may represent a safe, plant-based and eco-friendly alternative to current biofilm control agents.

### 3.6. Conclusion

This study demonstrates that continuous fluid flow induces profound morphological adaptations in *B. subtilis* biofilms, including the formation of specialised structural features such as Van Gogh bundles, ropes, and spore aggregates. The identification of an attachment foundation layer composed of ECM and bundles expands the understanding of biofilm developmental stages under flow, revealing limitations in the traditional five-step biofilm formation model. These findings fill critical gaps in current knowledge by showing that mechanical forces alone can trigger sporulation and multicellular differentiation as adaptive survival strategies. Furthermore, the concentration-dependent inhibitory effects of GBLE on flow biofilms underscore its potential as an eco-friendly alternative to harsh chemical disinfectants. Future research should investigate the mechanical properties of biofilm foundation layers, the role of ECM-eDNA interactions under flow, and the efficacy of GBLE against multispecies biofilms in real-world flow systems. Overall, this chapter highlights the importance of studying biofilm development under dynamic environmental conditions to inform effective and sustainable biofilm management strategies in industrial settings.

### 3.7. References

Arjes, H.A., Vo, L., Dunn, C.M., Willis, L., DeRosa, C.A., Fraser, C.L. and Simmons, L.A. (2020) Biosurfactant surfactin has unique cellular effects in *Bacillus subtilis*. *Current Biology*. Vol. 30(22), pp. 4733–4741.e6.

Arnaouteli, S., Bamford, N.C., Stanley-Wall, N.R. and Kovács, Á.T. (2021) Extracellular DNA in *Bacillus subtilis* biofilms. *Microbial Biotechnology*. Vol. 14(5), pp. 1534–1544.

Barnhart, M.M. and Chapman, M.R. (2006) Curli biogenesis and function. *Annual Review of Microbiology*. Vol. 60, pp. 131–147.

Bhagwat, G., O'Connor, W., Grainge, I. and Palanisami, T. (2021) Understanding the fundamental basis for biofilm formation on plastic surfaces: role of conditioning films. *Frontiers in Microbiology*. Vol. 12, p. 687118.

Beauregard, P.B., Chai, Y., Vlamakis, H., Losick, R. and Kolter, R. (2013) Bacillus subtilis biofilm induction by plant polysaccharides. *Proceedings of the National Academy of Sciences of the United States of America*. Vol. 110, No. 17, pp. E1621–E1630.

Beech, I.B. and Sunner, J. (2004) Biocorrosion: towards understanding interactions between biofilms and metals. *Current Opinion in Biotechnology*, 15(3), pp. 181–186.

Branda, S.S., González-Pastor, J.E., Ben-Yehuda, S., Losick, R. and Kolter, R. (2005) Fruiting body formation by *Bacillus subtilis*. *Proceedings of the National Academy of Sciences of the United States of America*. Vol. 98, No. 20, pp. 11621–11626.

Bridier, A., Briandet, R., Thomas, V. and Dubois-Brissonnet, F. (2011) Resistance of bacterial biofilms to disinfectants: a review. *Biofouling*. Vol. 27(9), pp. 1017–1032.

Bridier, A., Leroy, C., Dubois-Brissonnet, F., Bénézech, T. and Briandet, R. (2015) Biofilm-associated persistence of food-borne pathogens. *Food Microbiology*. Vol. 45, pp. 167–178.

Borges, A., Abreu, A.C., Dias, C., Saavedra, M.J., Borges, F. and Simões, M. (2016) New perspectives on the use of phytochemicals as an emergent strategy to control bacterial infections including biofilms. *Molecules*. Vol. 21, No. 7, 877.

Bos, R., van der Mei, H.C. and Busscher, H.J. (1999) Physico-chemistry of initial microbial adhesive interactions – its mechanisms and methods for study. *FEMS Microbiology Reviews*. Vol. 23, No. 2, pp. 179–230.

Carpentier, B. and Cerf, O. (2011) Review - Persistence of *Listeria monocytogenes* in food industry equipment and premises. *International Journal of Food Microbiology*. Vol. 145(1), pp. 1–8.

Corcoran, M., Morris, D., De Lappe, N., O'Connor, J., Lalor, P., Dockery, P. and Cormican, M. (2014) Commonly used disinfectants fail to eradicate Salmonella enterica biofilms from food contact surface materials. *Applied and Environmental Microbiology*, 80(4), pp. 1507–1514.

Costerton, J.W., Lewandowski, Z., Caldwell, D.E., Korber, D.R. and Lappin-Scott, H.M. (1995) Microbial biofilms. *Annual Review of Microbiology*. Vol. 49, pp. 711–745.

Coughlan, L.M., Cotter, P.D., Hill, C. and Alvarez-Ordóñez, A. (2016) New weapons to fight old enemies: novel strategies for the (bio)control of bacterial biofilms in the food industry. *Frontiers in Microbiology*, 7, 1641.

de Vries, R. (2010) DNA condensation in bacteria: Interplay between macromolecular crowding and nucleoid proteins. *Biochimie*. Vol. 92(12), pp. 1715–1721.

Di Pippo, F., Di Gregorio, L., Congestri, R., and Tandoi, V. (2018) Biofilm growth and control in cooling water industrial systems. *FEMS Microbiology Ecology*. Vol. 94(5), fiy044.

Dobretsov, S., Dahms, H.U. and Qian, P.Y. (2006) Inhibition of biofouling by marine microorganisms and their metabolites. *Biofouling*. Vol. 22(1–2), pp. 43–54.

Donlan, R.M. (2001) Biofilm formation: a clinically relevant microbiological process. *Clinical Infectious Diseases*. Vol. 33(8), pp. 1387–1392.

Donlan, R.M. (2002) Biofilms: microbial life on surfaces. *Emerging Infectious Diseases*. Vol. 8(9), pp. 881–890.

Dragoš, A., Kiesewalter, H., Martin, M., Hsu, C.Y., Hartmann, R., Wechsler, T., Eriksen, C., Brix, S., Drescher, K., Stanley-Wall, N., Kümmerli, R. and Kovács, Á.T. (2018) Division of labor during biofilm matrix production. *Current Biology*. Vol. 28, No. 12, pp. 1903–1913.e5.

Driks, A. (2002) Maximum shields: the assembly and function of the bacterial spore coat. *Trends in Microbiology*. Vol. 10, No. 6, pp. 251–254.

Errington, J. (2003) Regulation of endospore formation in *Bacillus subtilis*. *Nature Reviews Microbiology*. Vol. 1, No. 2, pp. 117–126.

Flemming, H.-C. and Wingender, J. (2010) The biofilm matrix. *Nature Reviews Microbiology*. Vol. 8, pp. 623–633.

Flemming, H.-C., Wingender, J., Szewzyk, U., Steinberg, P., Rice, S.A. and Kjelleberg, S. (2016) Biofilms: an emergent form of bacterial life. *Nature Reviews Microbiology*. Vol. 14(9), pp. 563–575.

Fu, Y., Ji, J., Wang, J., Guo, H., Zhao, T. and Jiang, Y. (2021) Effects of sodium hypochlorite and quaternary ammonium compounds on mature Listeria monocytogenes biofilms in the food industry. *Food Control*, 120, 107522.

Garrett, T.R., Bhakoo, M. and Zhang, Z. (2008) Bacterial adhesion and biofilms on surfaces. *Progress in Natural Science*. Vol. 18(9), pp. 1049–1056.

Goriely, A. and Neukirch, S. (2006) Mechanics of climbing and attachment in twining plants. *Physical Review Letters*. Vol. 97, No. 18, 184302.

Hall-Stoodley, L., Costerton, J.W. and Stoodley, P. (2004) Bacterial biofilms: from the natural environment to infectious diseases. *Nature Reviews Microbiology*. Vol. 2(2), pp. 95–108.

Hołówka, J. and Zakrzewska-Czerwińska, J. (2020) Nucleoid-associated proteins: The small organizers that help to cope with stress. *Frontiers in Microbiology*. Vol. 11, p. 590.

Huang, J., Liu, S., Zhang, C., Wang, X., Pu, J., Ba, F., Xue, S., Ye, H., Zhao, T., Li, K., Wang, Y., Zhang, J., Wang, L. and Zhong, C. (2019) Programmable and printable *Bacillus subtilis* biofilms as engineered living materials. *Nature Chemical Biology*. Vol. 15(1), pp. 34–41.

Ido, N. (2020) Whole biofilm of *Bacillus subtilis* analyzed as a colloidal hydrogel: cells are colloids; ECM is a cross-linked network. *Soft Matter*. Vol. 16(23), pp. 5452–5461.

Jahid, I.K. and Ha, S.D. (2012) A review of microbial biofilms of produce: future challenge to food safety. *Food Science and Biotechnology*. Vol. 21, No. 2, pp.299–316.

Karanth, S., Feng, S., Patra, D. and Pradhan, A.K. (2023) Linking microbial contamination to food spoilage and food waste: The role of smart packaging, spoilage risk assessments, and date labeling. *Frontiers in Microbiology*. Vol. 14, Article 1198124.

Kearns, D.B. and Losick, R. (2003) Swarming motility in undomesticated *Bacillus subtilis*. *Molecular Microbiology*. Vol. 49(3), pp. 581–590.

Kearns, D.B. and Losick, R. (2005) Cell population heterogeneity during growth of *Bacillus subtilis*. *Genes & Development*. Vol. 19(24), pp. 3083–3094.

Khameneh, B., Iranshahy, M., Soheili, V. and Bazzaz, B.S.F. (2019) Review on plant antimicrobials: a mechanistic viewpoint. *Antimicrobial Resistance & Infection Control*. Vol. 8, p. 118.

Khan, M.A.A., Hussain, M. and Djavanroodi, F. (2021) Microbiologically influenced corrosion in oil and gas industries: A review. *International Journal of Corrosion and Scale Inhibition*, 10(1), pp. 80–106.

Kim, K., Drescher, K., Pak, O.S., Bassler, B.L. and Stone, H.A. (2014) Filaments in curved streamlines: rapid formation of *Staphylococcus aureus* biofilm streamers. *New Journal of Physics*. Vol. 16, No. 6, Article 065024.

Kip, N. and van Veen, J.A. (2015) The dual role of microbes in corrosion. *ISME Journal*. Vol. 9, pp. 542–551.

Klapper, I., Rupp, C.J., Cargo, R., Purvedorj, B. and Stoodley, P. (2002) Viscoelastic fluid description of bacterial biofilms. *Biotechnology and Bioengineering*. Vol. 80(3), pp. 289–296.

Kostić, S., Kocović, V., Petrović Savić, S., Miljanić, D., Miljojković, J., Djordjević, M. and Vukelić, D. (2024) The Influence of Friction and Twisting Angle on the Tensile Strength of Polypropylene Baling Twine. *Applied Sciences*. Vol. 14(7), p. 3046.

Kurz, S., Rösner, V., Weber, S., Klee, S., Faber, F., Nau, R., Brakhage, A.A. and Kniemeyer, O. (2022) Flow dynamics shape biofilm formation and nutrient distribution in *Pseudomonas aeruginosa* colonies. *NPJ Biofilms and Microbiomes*. Vol. 8, Article 59.

Latorre, A.A., Van Kessel, J.A.S., Karns, J.S., Zurakowski, M.J., Pradhan, A.K., Boor, K.J., Adolph, E., Sukhnanand, S. and Schukken, Y.H. (2010) Biofilm in milking equipment on a dairy farm as a potential source of bulk tank milk contamination with *Listeria monocytogenes*. *Journal of Dairy Science*. Vol. 93(6), pp. 2792–2802.

Lee, J.-H., Kim, Y.-G., Ryu, S.-Y., Cho, M. H. and Lee, J.-G. (2014) Ginkgolic acids and *Ginkgo biloba* extract inhibit *Escherichia coli* O157:H7 and *Staphylococcus aureus* biofilm formation. *International Journal of Food Microbiology*. Vol. 174, pp. 47–55.

Little, B.J., Lee, J.S. and Ray, R.I. (2008) The influence of marine biofilms on corrosion: a concise review. *Electrochimica Acta*. Vol. 54(1), pp. 2–7.

Liu, G., Bakker, G.L., Li, X., Kapteijn, F. and van Loosdrecht, M.C.M. (2016) Biofilm growth and clogging in a flow channel reactor. *Biotechnology and Bioengineering*. Vol. 113(12), pp. 2746–2754.

López, D., Vlamakis, H. and Kolter, R. (2009) Generation of multiple cell types in *Bacillus subtilis*. *FEMS Microbiology Reviews*. Vol. 33, No. 1, pp. 152–163.

Luu, C.K., Li, Z., Ye, X. and Hayes, C.S. (2022) Post-translational modifications of HBsu regulate DNA compaction, sporulation, and stress survival in *Bacillus subtilis*. *mBio*. Vol. 13(5), e02136–22.

Marchand, S., De Block, J., De Jonghe, V., Coorevits, A., Heyndrickx, M. and Herman, L. (2012) Biofilm formation in milk production and processing environments; influence on milk quality and safety. *Comprehensive Reviews in Food Science and Food Safety*. Vol. 11, No. 2, pp.133–147.

Martínez-García, E., Nikel, P.I., Chavarría, M. and de Lorenzo, V. (2014) The metabolic cost of flagellar motion in *Pseudomonas putida KT2440*. *Environmental Microbiology*. Vol. 16(1), pp. 163–176.

Martínez-García, R., Nadell, C.D., Hartmann, R., Drescher, K. and Bonachela, J.A. (2018) Cell adhesion and fluid flow jointly initiate genotype spatial distribution in biofilms. *PLoS Computational Biology*. Vol. 14, No. 4, e1006094.

McLoon, A.L., Guttenplan, S.B., Kearns, D.B., Kolter, R. and Losick, R. (2011) Tracing the domestication of a biofilm-forming bacterium. *Journal of Bacteriology*. Vol. 193(8), pp. 2027–2034.

NACE International (2013) *International Measures of Prevention, Application, and Economics of Corrosion Technologies (IMPACT)*. Available at: https://impact.nace.org/economic-impact.aspx

O'Toole, G., Kaplan, H.B. and Kolter, R. (2000) Biofilm formation as microbial development. *Annual Review of Microbiology*. Vol. 54, pp. 49–79.

Ohniwa, R.L., Morikawa, K. and Kim, J. (2006) Structural basis of nucleoid condensation in bacteria. *Trends in Microbiology*. Vol. 14(4), pp. 194–198.

Pascual, A., Llorca, I. and Canut, A. (2007) 'Use of ozone in food industries for reducing the environmental impact of cleaning and disinfection activities', *Trends in Food Science & Technology*, 18(S1), pp. S29–S35.

Paula, A.J., Hwang, G. and Koo, H. (2020) Dynamics of bacterial population growth in biofilms resemble spatial and structural aspects of urbanization. *Nature Communications*. Vol.11(1354).

Pearce, P., Song, B., Skinner, D., Li, H., O'Donnell, S., Murrell-Lagnado, R. and Rybenkov, V.V. (2019) Flow-induced biofilm formation in microfluidic devices. *Lab on a Chip*. Vol. 19, No. 6, pp. 1080–1091.

Persat, A., Nadell, C.D., Kim, M.K., Ingremeau, F., Siryaporn, A., Drescher, K., Wingreen, N.S., Bassler, B.L., Gitai, Z. and Stone, H.A. (2015) The mechanical world of bacteria. *Cell*. Vol. 161, No. 5, pp. 988–997.

Peterson, B.W., He, Y., Ren, Y., Zerdoum, A., Libera, M.R., Sharma, P.K., van Winkelhoff, A.J., Neut, D., Stoodley, P., van der Mei, H.C. and Busscher, H.J. (2015) Viscoelasticity of biofilms and their recalcitrance to mechanical and chemical challenges. *FEMS Microbiology Reviews*. Vol. 39(2), pp. 234–245.

Petrova, O.E. and Sauer, K. (2012) Sticky situations: key components that control bacterial surface attachment. *Journal of Bacteriology*. Vol. 194(10), pp. 2413–2425.

Purevdorj, B., Costerton, J.W. and Stoodley, P. (2002) Influence of hydrodynamics and cell signaling on the structure and behavior of *Pseudomonas aeruginosa* biofilms. *Applied and Environmental Microbiology*. Vol. 68(9), pp. 4457–4464.

Qin, Y., Angelini, L.L. and Chai, Y. (2022) Bacillus subtilis cell differentiation, biofilm formation and environmental prevalence. *Microorganisms*. Vol. 10, No. 6, p. 1108.

Recupido, F., Di Lauro, A., Olivieri, F., Diana, D., Guarino, A., Winter, R., Töpfer, N., Cermola, F., Fusco, S., Velotta, R., D'Ursi, A.M. and Duilio, A. (2020) Biofilm formation under laminar flow: microfluidic device for real-time monitoring of bacterial adhesion and biofilm development. *Scientific Reports*. Vol. 10, Article 18660.

Rodesney, C.A., Roman, B., Dhamani, N., Cooley, B.J., Katira, P., Touhami, A. and Gordon, V.D. (2017) Mechanosensing of shear by *Pseudomonas aeruginosa* leads to increased levels of the cyclic-di-GMP signal initiating biofilm development. *Proceedings of the National Academy of Sciences of the United States of America (PNAS)*. Vol. 114, No. 23, pp. 5906–5911.

Rupp, C.J., Fux, C.A. and Stoodley, P. (2005) Viscoelasticity of *Staphylococcus epidermidis* biofilms in response to fluid shear allows resistance to detachment and facilitates rolling migration. *Applied and Environmental Microbiology*. Vol. 71, No. 4, pp. 2175–2178.

Rusconi, R. and Stocker, R. (2015) Microbes in flow. *Current Opinion in Microbiology*. Vol. 25, pp. 1–8.

Rutherford, S.T. and Bassler, B.L. (2012) Bacterial quorum sensing: Its role in virulence and possibilities for its control. *Cold Spring Harbor Perspectives in Medicine*. Vol. 2, No. 11, a012427.

Saggese, A., Paone, N., Ricci, S., Di Luccia, B., Rigano, M.M. and Ricca, E. (2022) Non-essential role of YtvA in the onset of sporulation in *Bacillus subtilis*. *Microbial Cell*. Vol. 9, No. 5, pp. 98–110.

Sauer, K., Camper, A.K., Ehrlich, G.D., Costerton, J.W. and Davies, D.G. (2022) Expanding the biofilm concept: new insights into the life cycle of microbial communities. *Genes & Development*. Vol. 36(22), pp. 1699–1714.

Secchi, E., Savorana, G., Vitale, A., Eberl, L., Stocker, R. and Rusconi, R. (2022) The structural role of bacterial eDNA in the formation of biofilm streamers. *Proceedings of the National Academy of Sciences of the United States of America*. Vol. 119(12), Article e2113723119.

Setlow, P. (2014) Germination of spores of *Bacillus subtilis*: what we know and do not know. *Journal of Bacteriology*. Vol. 196, No. 7, pp. 1297–1305.

Shah, D.U., Schubel, P.J. and Clifford, M.J. (2013) Modelling the effect of yarn twist on the tensile strength of unidirectional plant fibre yarn composites. *Journal of Composite Materials*. Vol.47(4), pp. 425–436.

Sharma, S., Mohler, J., Mahajan, S.D., Schwartz, S.A., Bruggemann, L. and Aalinkeel, R. (2023) Microbial biofilm: a review on formation, infection, antibiotic resistance, control measures, and innovative treatment. *Microorganisms*. Vol. 11(6), p. 1614.

Shaw, T., Winston, M., Rupp, C.J., Klapper, I. and Stoodley, P. (2004) Commonality of elastic relaxation times in biofilms. *Physical Review Letters*. Vol. 93(9), p. 098102.

Simões, M., Simões, L.C. and Vieira, M.J. (2010) A review of current and emergent biofilm control strategies. *LWT – Food Science and Technology*. Vol. 43(4), pp. 573–583.

Singh, B.N., Singh, B.R., Singh, R.L., Prakash, D., Dhakarey, R., Upadhyay, G. and Singh, H.B. (2017) Oxidative stress and antibacterial activity of aqueous extract of *Moringa oleifera* leaves – an in vitro study. *Food and Chemical Toxicology*. Vol. 61, pp. 231–240.

Singh, S., Datta, S., Narayanan, K.B. and Rajnish, K.N. (2021) Bacterial exo-polysaccharides in biofilms: role in antimicrobial resistance and treatments. *Journal of Genetic Engineering and Biotechnology*. Vol. 19(1), p. 140.

Springer (2024) Microbiologically influenced corrosion of metals: annual global economic impact between US \$300 and 500 billion. npj Materials Degradation / Corrosion Reviews. Available at: https://link.springer.com/article/10.1007/s40735-024-00820-w

Stewart, P.S. (2003) Diffusion in biofilms. *Journal of Bacteriology*. Vol. 185(5), pp. 1485–1491.

Stoodley, P., Lewandowski, Z., Boyle, J.D. and Lappin-Scott, H.M. (1999) Structural deformation of bacterial biofilms caused by short-term fluctuations in fluid shear: an in situ investigation of biofilm rheology. *Biotechnology and Bioengineering*. Vol. 65, No. 1, pp. 83–92.

Stoodley, P., Sauer, K., Davies, D.G. and Costerton, J.W. (2002) Biofilms as complex differentiated communities. *Annual Review of Microbiology*. Vol. 56, pp. 187–209.

Teschler, J.K., Zamorano-Sánchez, D., Utada, A.S., Warner, C.J.A., Wong, G.C.L., Linington, R.G. and Yildiz, F.H. (2015) Living in the matrix: assembly and control of Vibrio cholerae biofilms. *Nature Reviews Microbiology*. Vol. 13(5), pp. 255–268.

Thomen, P., Robert, J., Monmeyran, A., Bitbol, A.-F., Douarche, C. and Henry, N. (2017) Bacterial biofilm under flow: first a physical struggle to stay, then a matter of breathing. *PLoS ONE*. Vol. 12(4), e0175197.

Tsagkari, E., Schlegel, S., Vassilakos, G., Stocker, R. and Rusconi, R. (2022) Mechanosensing in bacteria. *Proceedings of the National Academy of Sciences of the United States of America*. Vol. 119, No. 44, e2206888119.

UK Health Security Agency (2024) *Investigation into an outbreak of Shiga toxin—producing Escherichia coli (STEC) O145 in Great Britain, May to June 2024*. UKHSA. Available at: https://www.gov.uk/government/publications/shiga-toxin-producing-e-coli-outbreak-o145-may-to-june-2024

United Nations Environment Programme (2021) *Food Waste Index Report 2021*. Nairobi: UNEP. Available at: <a href="https://www.unep.org/resources/report/unep-food-waste-index-report-2021">https://www.unep.org/resources/report/unep-food-waste-index-report-2021</a>

van Gestel, J., Vlamakis, H. and Kolter, R. (2015) Division of labor in biofilms: the ecology of cell differentiation. *Microbiology Spectrum*. Vol. 3, No. 2, MB-0002-2014.

Vlamakis, H., Aguilar, C., Losick, R. and Kolter, R. (2013) Control of cell fate by the formation of an architecturally complex bacterial community. *Genes & Development*. Vol. 27, No. 14, pp. 1617–1624.

Wang, C., Wei, P. W., Song, C. R., Wang, X., Zhu, G. F., Yang, Y. X., Xu, G. B., Hu, Z. Q., Tang, L., Liu, H. M. and Wang, B. (2021) *Ginkgo biloba* exocarp extracts inhibit *Staphylococcus aureus* and methicillin-resistant *Staphylococcus aureus* biofilms by altering related gene expression. *Journal of Ethnopharmacology*. Vol. 269, p. 115602.

Wingender, J. and Flemming, H.C. (2011) Biofilms in drinking water and their role as reservoir for pathogens. *International Journal of Hygiene and Environmental Health*. Vol. 214(6), pp. 417–423.

World Health Organization (2023) *Estimates of the global burden of foodborne diseases*. [Online]. Available from WHO.

Yan, J., Sharo, A.G., Stone, H.A., Wingreen, N.S. and Bassler, B.L. (2017) Vibrio cholerae biofilm growth program and architecture revealed by single-cell live imaging. *Proceedings of the National Academy of Sciences of the United States of America*. Vol. 113, No. 36, pp. E5337–E5343.

Zhang, J., Dong, F., Liu, S., Zhang, D. and Wang, X. (2022) Biofilm streamer growth dynamics in various microfluidic channels. *Canadian Journal of Microbiology*. Vol. 68, No. 5, pp. 367–375.

# 4. Structural Adaptation of *Bacillus subtilis* Biofilms to Bidirectional Flow and the Disruptive Effect of *Ginkgo biloba* Leaf Extract

# 4.1. Abstract

Bacillus subtilis is a model organism for studying biofilm development and structural adaptation in response to environmental stimuli. This chapter investigates the effects of bidirectional fluid flow on submerged *B. subtilis* biofilms, with a particular focus on the emergence of complex morphological features such as Van Gogh bundles and previously undescribed folds. Using confocal laser scanning microscopy and quantitative image analysis, biofilms grown under bidirectional flow exhibited significantly greater biomass, porosity, and structural heterogeneity compared to those under unidirectional flow, described in the previous chapter. The formation of folds, elongated, raised structures with tapered ends and underlying channels, was exclusive to bidirectional flow and likely serves as an adaptation to fluctuating hydrodynamic stress, facilitating nutrient transport, mechanical stability, and spatial differentiation. Furthermore, treatment with *Ginkgo biloba* leaf extract (GBLE) significantly disrupted biofilm architecture, reducing biomass and structural integrity under bidirectional flow regimes. These findings highlight the remarkable plasticity of *B. subtilis* biofilms and underscore the potential of GBLE as a plant-derived antibiofilm agent suitable for dynamic environments.

## 4.2. Introduction

Biofilm development is a multi-step process governed by the interplay between environmental stimuli and genetic expression (Flemming et al., 2016). In bacterial biofilms, while extracellular polymeric substance (EPS) synthesis is genetically regulated, cells also begin to differentiate and specialise in different roles within the biofilm community (Vlamakis et al., 2013). Bacterial differentiation leads to the development of subpopulations: cells that are genetically identical but display distinct phenotypic characteristics. This process, referred to as bacterial bet-hedging or phenotypic heterogeneity, enhances survival and persistence in variable and dynamic environments by diversifying functional traits within the population (Veening, Smits and Kuipers, 2008) (Ackermann, 2015).

Bacillus subtilis (B. subtilis) biofilms are a well-studied model of phenotypic heterogeneity, with cells differentiating into distinct subpopulations that cooperate to build structurally

complex communities (Vlamakis et al., 2013) (Veening, Smits and Kuipers, 2008). Found in soil and the plant microbiome, B. subtilis forms colony biofilms composed of at least five cell types: matrix- and surfactin-producers, motile cells, protease-producers, and endospores; each contributing to biofilm stability and function (López et al., 2009). All these cooperate to establish strong microbial communities attached to surfaces, displaying structural complexity and 3D aerial projections. Surface features such as wrinkles are linked to mechanical stress and colony expansion under spatial constraints (Trejo et al., 2013). Expansion has also been associated with specialised filamentous cell chains called Van Gogh bundles, observed at the colony edge and formed through the coordinated activity of matrix- and surfactin-producing cells (van Gestel, Vlamakis and Kolter, 2015). Surfactin reduces surface tension, enabling sliding motility, while extracellular matrix (ECM) production stabilises the aligned cell chains. These types of cells have only been described in colony agar biofilms and have been associated with colony expansion. The previous research chapters (2 and 3) show the presence of Van Gogh bundles in response to Ginkgo biloba leaf extract (GBLE) as well fluid flow forces. Interestingly, GBLE promoted Van Gogh bundles in B. subtilis colony-agar biofilms and static biofilms. Van Gogh bundles were also seen in response to a continuous fluid flow, as they appeared to be the key structural component of flow cell biofilms. However, the understanding of how these differentiated cell types, or phenotypic heterogeneity, behave in other environments, such as submerged systems exposed to fluid flow, remains limited. Hence chapter 2 explored biofilm response under submerged unidirectional flow. Given that biofilms in real-world settings, such as pipelines, medical devices, and natural aquatic systems (Donlan, 2002), are constantly exposed to flow, it is essential to investigate how B. subtilis biofilms respond to these forces. As a genetically tractable and relevant model organism, B. subtilis offers a valuable system for exploring the spatial organisation, structural adaptation, and phenotypic adaptation of biofilms in response to hydrodynamic stress (Branda et al., 2001). While chapter 3 explored B. subtilis biofilm development under unidirectional flow, this chapter explores this under bidirectional flow. This is needed as bidirectional flow will create unique and alternating forces on the biofilm compared to unidirectional flow. This study aims to address this gap by characterising the architecture and cellular organisation of B. subtilis biofilms under bidirectional flow, thereby providing new insight into how bacterial communities may develop, survive, and function in complex, fluctuating environments.

Biofilm development is also a product of quorum sensing (QS). QS describes systems through which bacteria communicate at a cellular level and adapt to the surrounding environment (Miller and Bassler, 2001). Because of their ability to adapt to different environments, through processes such as bet-hedging and quorum sensing (QS), understanding bacterial biofilms is essential to overcome the challenges posed by biofilm growth. Biofilms grow anywhere, from teeth and gastrointestinal tracts to industrial pipelines (Costerton et al., 1999), and can become problematic in many sectors. For example, up to 80% of human infections have been attributed to biofilms by the US National Institute of Health (Khatoon et al., 2018). Biofilms are also widely associated with indwelling medical devices and lead to chronic infections, which are difficult to treat due to the resistance of biofilms to antibiotics (Mishra, Aggarwal and Khan, 2024). Biofilms are also relevant for the built environment. Legionella control is essential for water systems and cooling towers within buildings. This bacterium forms biofilms in water pipeline networks and water aerosols contaminated with Legionella can be inhaled by humans, causing pneumonia and influenza-like illnesses (Cámara et al., 2022). Additionally, biofilms are a challenge in the food and drink processing industry. Bacterial contamination of food products is often solely due to biofilms and lead to foodborne diseases, causing human morbidity and mortality. Listeria monocytogenes is often the causative pathogen of Listeriosis and 142 cases of foodborne Listeriosis were recorded in the United Kingdom in 2019, which lead to 23 deaths. Food contamination is also a great economic burden due to costs associated with product recall, transport and discarding. Despite disinfection efforts, biofilm growth still poses a challenge (Bridier et al., 2011) and therefore, innovative, sustainable and efficient antibiofilm solutions are needed in all sectors. Biofilms are the main cause of biofouling, bioclogging and microbial-induced corrosion (MIC). For example, biofouling of shipment vessels not only leads to increased maintenance costs, but also increased CO<sub>2</sub> emissions, due to a higher frictional resistance of the vessel. MIC also occurs within pipeline networks, including water systems as well as oil and gas flow pipelines. Microbial contamination of drinking water systems occurs primarily due to biofilm growth on the pipe walls, which are often resistant to disinfectants, leading to water contamination (Trusz et al., 2024). In addition, the extensive use of disinfectant to neutralise biofilms in drinking water systems can negatively impact the quality of drinking water and the disinfectants byproducts can have adverse effects on the ecosystem and biodiversity (Chen et al., 2020). Microorganisms can also form biofilms within petroleum pipelines, resulting in corrosion and pipeline damage and structural failure (Lenhart et al., 2014). Despite biofilms' relevance in water and energy flow systems, studies addressing biofilm growth in flow systems are quite limited. The vast majority these studies involve the use of microfluidic chambers or mathematical models and only a number of bacterial species have been investigated. Previous works investigating biofilm formation under a fluid flow utilise the common biofilm forming strains, such as Pseudomonas aeruginosa (P. aeruginosa), Pseudomonas fluorescens (P. fluorescens), Escherichia coli (E. coli) and Vibrio Cholera (V. cholera) (Recupido et al., 2020) (Martínez-García et al., 2018) (Lee, Secchi and Kang, 2023). Generally, these studies have addressed streamer formation, which can be described as filamentous structures made of bacterial cells and ECM, and were found to form between corners of microfluidic chambers (Recupido et al., 2020). In microfluidic devices, the use of very narrow pipes creates highly controlled less turbulent/more lamina flow structures, which lack the complexity of wider pipes. Despite the valuable insights provided by microfluidic studies, characteristics like the overall biofilm bulk structure, phenotypic heterogeneity and biofilm development within larger pipe structures is neglected. For example, streamers appear to be specific to microfluidic devices, while data presented in the previous chapter of this work highlight the development of macroscopic structures which resemble twisted ropes in response to a continuous flow during B. subtilis biofilm formation. This highlights the need of studies investigating macroscopic biofilm development under a fluid flow, using real life scenarios which reflect environments commonly used in industrial settings.

Hydrodynamic forces influence bacterial adhesion and detachment, QS systems, ECM production and overall biofilm characteristics. Biofilms not only respond to the mere introduction of a fluid flow, but are also susceptible to different flow regimes, such as changing velocities (Recupido et al., 2020). In most studied flow parameters are flow velocity and shear stress. A number of studies have investigated biofilm development at high/low velocity, highlighting significant morphological changes depending on the velocity. Multispecies biofilms grown under high flow velocity were thin but more dense compared to porous and less dense biofilms developed under low flow velocity (Khu, Changchun and Wang, 2023). In multispecies biofilms, velocity also affects microbial diversity of a biofilm, with more diverse bacterial communities under higher flow velocity (Douterelo et al., 2019). Another study carried out by Wang et al. (2014) identified optimal biofilm growth under intermediate velocity conditions and the same biofilms presented different ECM composition depending on the flow velocity. Shear stress, on the other hand, is thought to govern spatial

distribution of the biofilm. Shear forces are heterogeneous throughout the biofilm surface, further promoting morphological heterogeneity seen in biofilms (Romeu et al., 2024). Shear forces modulate bacterial transport and biofilm detachment (Kurz et al., 2022), as well as microbial diversity of multispecies biofilms (Tsagkari et al., 2022).

While it is important to investigate parameters like shear forces and flow velocity, there is a need to address other parameters, such as flow direction. The impact of changes in fluid flow direction on biofilm development and morphology has not yet been thoroughly investigated. In real-world applications, many fluid systems experience changes in flow direction, including pumped pipeline networks with alternating pumping cycles (Zhang et al., 2016), wastewater treatment plants employing oscillatory aeration and flow reversal for sludge management (Gao et al., 2011), membrane bioreactors using backwashing to mitigate fouling (Wu et al., 2017), and food processing CIP (clean-in-place) systems where reversing flow enhances cleaning efficiency (Bremer et al., 2006).

Unlike changes in velocity, which alter the magnitude of shear stress applied to biofilms, changing flow direction imposes oscillatory or reversing shear forces, which may disrupt bacterial adhesion, reorient cells, or influence the spatial distribution of EPS within the biofilm matrix (Stoodley et al., 1999) (Rusconi and Stocker, 2015). This mechanical perturbation is hypothesised to affect biofilm strength and cohesion differently compared to unidirectional flow (Jia et al., 2017). For instance, Jia et al. (2017) found that oscillatory flow regimes reduced *P. aeruginosa* biofilm thickness and density compared to steady flow, likely due to repeated detachment forces disrupting biofilm consolidation. Li et al. (2016) similarly showed that oscillatory shear reduced biofilm biomass in microchannels by preventing the maturation of microcolonies.

However, very few studies have investigated true bidirectional flow, where the direction of bulk fluid flow is periodically reversed rather than oscillated around a mean. A study by Hodges et al. (2004) demonstrated that bidirectional flow altered streamer formation dynamics of mixed bacterial species in porous media, resulting in different clogging patterns compared to unidirectional flow. Similarly, Wu et al. (2017) found that bidirectional backwashing in membrane bioreactors effectively removed EPS layers and reduced biofilm formation. These findings suggest that bidirectional flow can mechanically destabilise biofilms or prevent their structured development, although the underlying mechanisms remain unclear. Therefore, understanding how flow direction affects biofilm formation and

morphology is critical, as it could inform the development of novel biofilm control strategies that exploit directional changes to weaken biofilms or prevent their establishment altogether. For example, alternating flow direction could be integrated with antimicrobial dosing to enhance removal efficiency while reducing chemical usage.

This study builds upon previous work by exploring how B. subtilis biofilms develop under bidirectional flow, a dynamic condition rarely addressed in the literature but highly relevant to real-world applications. By combining confocal laser scanning microscopy (CLSM) with detailed image analysis, this research aims to shed light on the bulk 3D architecture and internal heterogeneity of biofilms exposed to alternating shear forces. Unlike microfluidic models, the flow cell system allows for the formation of mature, macroscale biofilms (Tolker-Nielsen and Sternberg, 2011), while preserving spatial structure, making it possible to observe features such as folds, channels, and Van Gogh bundles in situ. In addition to characterising the mechanical adaptation of biofilms to flow reversal, this study also investigates the antibiofilm potential of GBLE under bidirectional flow. While Chapter 3 demonstrated that GBLE weakens B. subtilis biofilms under unidirectional flow, this chapter evaluates its efficacy in a more mechanically complex setting. Given its reported antimicrobial properties and natural origin (Lee et al., 2014) (Wang et al., 2021), GBLE might represents a sustainable alternative to harsh chemical biocides, particularly in industrial or medical systems where flow regimes fluctuate. This work contributes novel insights into both the physical structuring and chemical susceptibility of biofilms in dynamically changing environments.

# 4.3. Material and Methods

#### 4.3.1. Bacterial Strain and Culture Conditions

*Gfp*-expressing *Bacillus subtilis* (JWV042 strain, Hbs-GFP endogenous localization, cat amyE::Phbs-hbs-gfp, cat marker) colonies on agar were obtained from Strathclyde Institute of Pharmacy and Biomedical Sciences (SIPBS). A flask containing 150 mL of Luria-Bertani (LB) broth (Sigma-Aldrich) was inoculated with a colony from the plate and incubated overnight at  $37^{\circ}$ C. The culture was supplemented with 5 µg/mL chloramphenicol to ensure selection of *gfp* mutants. Glycerol stocks were made from the culture and stored at -80°C. The stocks were then used for the rest of this study.

Gingko biloba leaf extract (GBLE) powder was obtained from Wuhan ReCedar Biotechnology Co., Ltd (Wuhan, China). The extract was resuspended in RNAse-free water to make working solutions and 400  $\mu$ g/mL were added to the culture media for the experiments assessing GBLE's activity in bidirectional flow.

Prior each experiment, *B. subtilis* JWV042 was cultured in LB broth overnight at  $37^{\circ}$ C in a shaking incubator at 150 rpm. The OD<sub>600</sub> of the inoculum was measured prior inoculation in each experiment and was adjusted to 0.3. All experiments were carried out in triplicates on separate occasions, using freshly prepared cultures each time to ensure biological replication, unless stated otherwise. All bacterial cultures and flow cell biofilms were grown using LB media, supplemented with 5  $\mu$ g/mL. All materials and reagent were sterile at the time of use and sample preparations was carried out in biological safety cabinets.

## 4.3.2. Bidirectional Fluid Flow System Design

In order to study biofilm development under a bidirectional fluid flow, a flow system which allowed for the development and direct microscopical imaging of bacterial biofilm was developed (Fig. 4.1).

Inlet media for the flow system was prepared in a 4L polycarbonate bottle (IBI Scientific) and autoclaved to achieve sterility. Subsequently, the inlet media was supplemented with 0 and 400 µg/mL GBLE suspension. From the inlet media bottle, silicone tubing was connected to a sterile plastic drip chamber, to avoid inlet media contamination from the inoculum, and then it was placed through a pump channel. Non autoclavable silicone tubing was sterilised through a series of washes. The tubing was first soaked overnight in 1%(w/v) Virkon solution and dried. Then, sodium hypochlorite was injected into the tubing using a sterile syringe, and this was followed by isopropyl alcohol (70%) wash. To achieve a continuous fluid flow, a peristaltic pump was used (VWR, PP4000 Series), at a set flow rate of 40 mL/h. Going through the peristaltic pump, the tubing was then attached to a plastic T junction, which allowed for the creation of two streams of fluid going into a convertible flow cell (IBI CFCAS0003; for a flow cell schematic, refer to Chapter 3, Fig. 3.2). The flow cell is where the biofilm developed. Using plastic tubing clamps, it was possible to control the direction of the fluid flow. By closing clamp 7 and 10 (Fig. 4.1) for 24 hours, the direction of the flow from the right to the left was maintained. After 24 hours, clamps 7 and 10 were opened and clamps 8 and 9 were closed, thereby allowing the media to flow from left to right for another 24 hours. The switch in direction was done once. Because of the presence of glass coverslips on the top and bottom of the cell, it was possible to image the biofilm using confocal fluorescent microscopy. From the flow cell, waste was collected in 4L polycarbonate bottles (IBI Scientific).

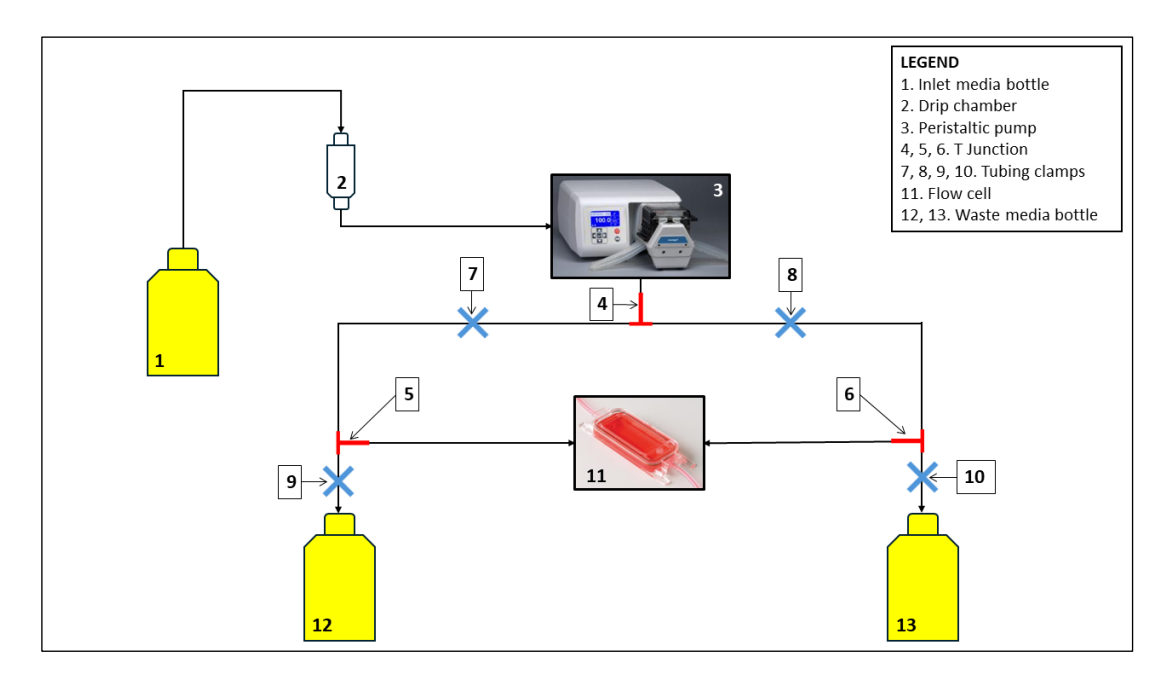


Figure 4.1. Schematic of the bidirectional fluid flow set up used to grow biofilms under a fluid flow.

In order to adjust the flow rate, the flow system was run for a period of time of 1 hour and the outlet media was collected in a beaker. RPM value was then adjusted to a flow rate of 40 mL/h. After pausing the flow, inoculation of the system was achieved via injecting 150  $\mu$ L of overnight *gfp*-expressing *B. subtilis* JWV042 liquid culture (OD<sub>600</sub> = 0.3). Following inoculation, the flow was restarted 1 hour post inoculation. The system was run for a total of 48 hours.

After the 48 hours, the flow was stopped and the tubing was clamped at either side of the flow cell, in proximity to the chamber. The tubing was cut at either side of the flow chamber using a sterile scalpel (Brand). In order to image the biofilm adhered to the internal surface of the flow cell, the media inside was aspirated using a sterile plastic syringe.

Biofilm imaging was performed using a Leica TCS SP5 confocal laser scanning microscope (Leica Microsystems, Germany) equipped with a motorised stage. For whole-chamber biofilm imaging in the flow-cell, a 4x/0.10 numerical aperture (N. A.) HI PLAN PH 0 air objective ( $\approx 40\times$  overall optical magnification through the eyepieces) was used to capture the overall biofilm structure across the chamber. The *gfp*-expressing *B. subtilis* JWV042 strain was excited using an argon laser at 488 nm, and emission was collected between 500–550 nm.

For finer structural details, the zoom function within the Leica LAS AF software was applied while maintaining the 4 x objective. Laser power and detector gain were kept constant across all samples to allow comparative quantification. All image acquisition was carried out at room temperature using Leica LAS AF software.

In order to minimise disruption to the morphology of the biofilm, the whole flow cell was placed under the objective lens.

# 4.3.3. Image Analysis

All confocal laser scanning microscopy (CLSM) images were analysed using ImageJ (Fiji). Biofilm biomass distribution along the Z-axis was assessed by measuring the biofilm area per slice from Z-stacks. A custom macro was developed to automate this process. The macro applied a custom intensity threshold to each slice, converted the thresholded image to a binary mask, and used the "Analyze Particles" function to calculate the area of thresholded biofilm in each slice. This process was repeated across all Z-slices. Mean gray value was quantified by applying the same custom threshold to each slice and measuring the mean gray value of the selected region to reflect biofilm density and fluorescence intensity. Porosity was calculated from thresholded binary masks as the ratio of biofilm area to total image area, expressed as a percentage. Fold height was measured using resliced Z-projections of stacks containing folds. For each fold, five equidistant height measurements were taken using the line tool and recorded in microns. Fold width was measured in XY projections using the line tool at five equidistant points along each fold. The relationship between fold height and width was then analysed in R. Channel width underneath folds was also measured using the line tool, taking five equidistant measurements per channel across the fold base. To assess the relationship between fold height and channel width, Pearson correlation was performed in R. Biofilm thickness was calculated using the formula: Thickness = Number of slices × Zstep size (µm). Z-step values were defined during image acquisition and maintained consistent across samples. All measurements were conducted on at least three biological replicates, and where applicable, results were summarised using mean ± standard deviation.

#### 4.4. Results

## 4.4.1. Effect of Unidirectional and Bidirectional Fluid Flow on Biofilms

Fluorescent images of biofilms grown under a bi-directional flow show significant changes in overall biofilm morphology compared to static biofilms and biofilms subjected to a

unidirectional continuous flow. Fig. 4.2 presents three fluorescent images depicting *gfp*-expressing *B. subtilis* JWV042 biofilms grown under varying flow conditions (without GBLE addition); a static biofilm (Fig. 4.2a), a biofilm grown under a unidirectional continuous fluid flow (4.2b) and an image of a biofilm grown under a bidirectional fluid flow (4.2c). Image 2a was obtained from the study described in Chapter 2, while details about image 4.2b can be found in Chapter 3. Generally, with the addition of a fluid flow, the biofilm morphology shifts from a standard biofilm architecture to numerous long Van Gogh bundle filaments. This can be clearly seen in Fig. 4.2. Interestingly, when the flow direction is changed, the biofilm appears more intricated, with more curves and bends, compared to when the flow is kept unidirectional. While the biofilm seen under unidirectional continuous flow shows less dense Van Gogh bundles (Fig. 4.2b), a degree of complexity is added to the biofilm when bidirectionality is introduced (Fig. 4.2c), as the Van Gogh bundles appear tightly packed and more interwoven. In addition, single Van Gogh filaments can clearly be seen in Fig. 4.2b, forming hair-like strings. These cannot be seen anymore under bidirectional flow, as Van Gogh bundles appear adhered to each other, forming thicker strands.

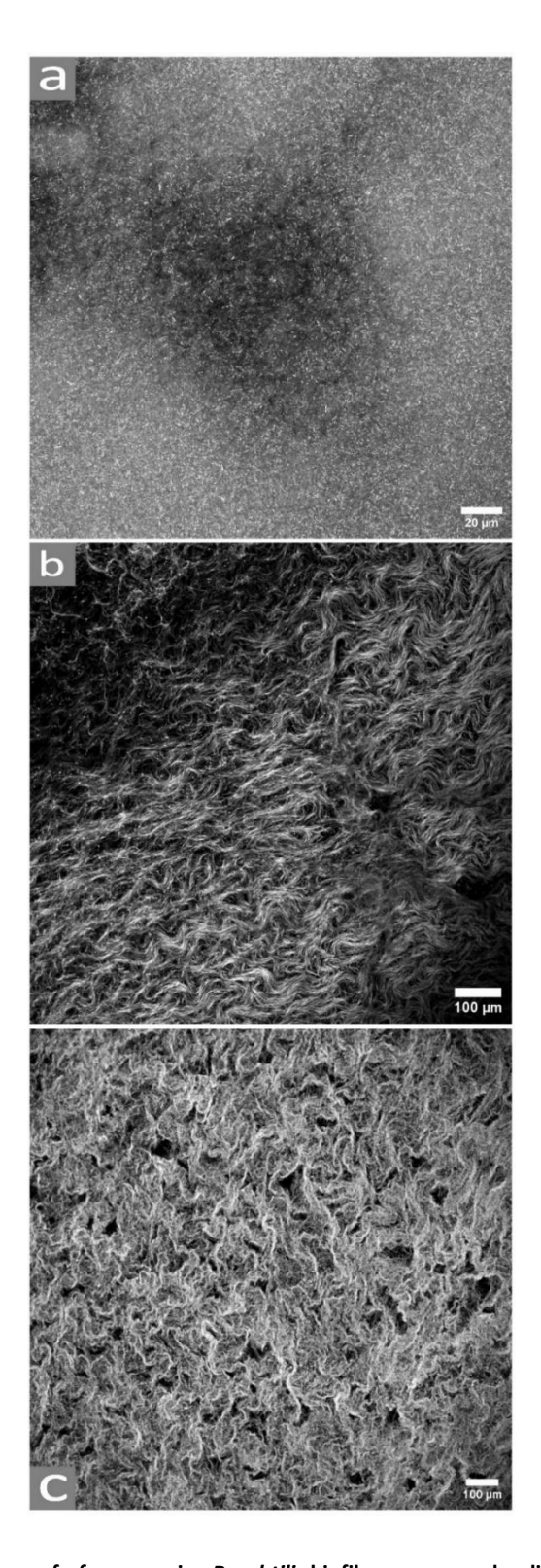


Figure 4.2. Fluorescent images of *gfp*-expressing *B. subtilis* biofilms grown under different flow condition. a) A *gfp*-expressing *B. subtilis* biofilms grown in absence of a fluid flow (Biofilms were grown for 48 hours, incubated at 37° in LB medium. Images acquired using SP5 Leica, 63X magnification). b) A *gfp*-expressing *B. subtilis* biofilm grown under a continuous fluid flow, showing multiple Van Gogh bundles aligned (biofilm was grown within flow cells in LB media, at room temperature, for 48 hours. Entire flow cells were imaged using Leica SP5, 40x magnification). c) A *gfp*-expressing *B. subtilis* biofilm grown under a bidirectional continuous fluid flow, showing an intricate pattern made of Van Gogh bundles.

Fig. 4.3 shows the mean gray value of biofilms grown under bidirectional and unidirectional flow conditions. Mean gray value (reported in arbitrary units, a.u.) represents the pixel intensity measured from the images and is directly proportional to biofilm density, with higher gray values indicating greater biomass accumulation. Biofilms grown under bidirectional flow exhibited a significantly higher mean gray value (~145 a.u.) compared to those grown under unidirectional flow (~100 a.u.), indicating the bidirectional flow biofilms were more dense.

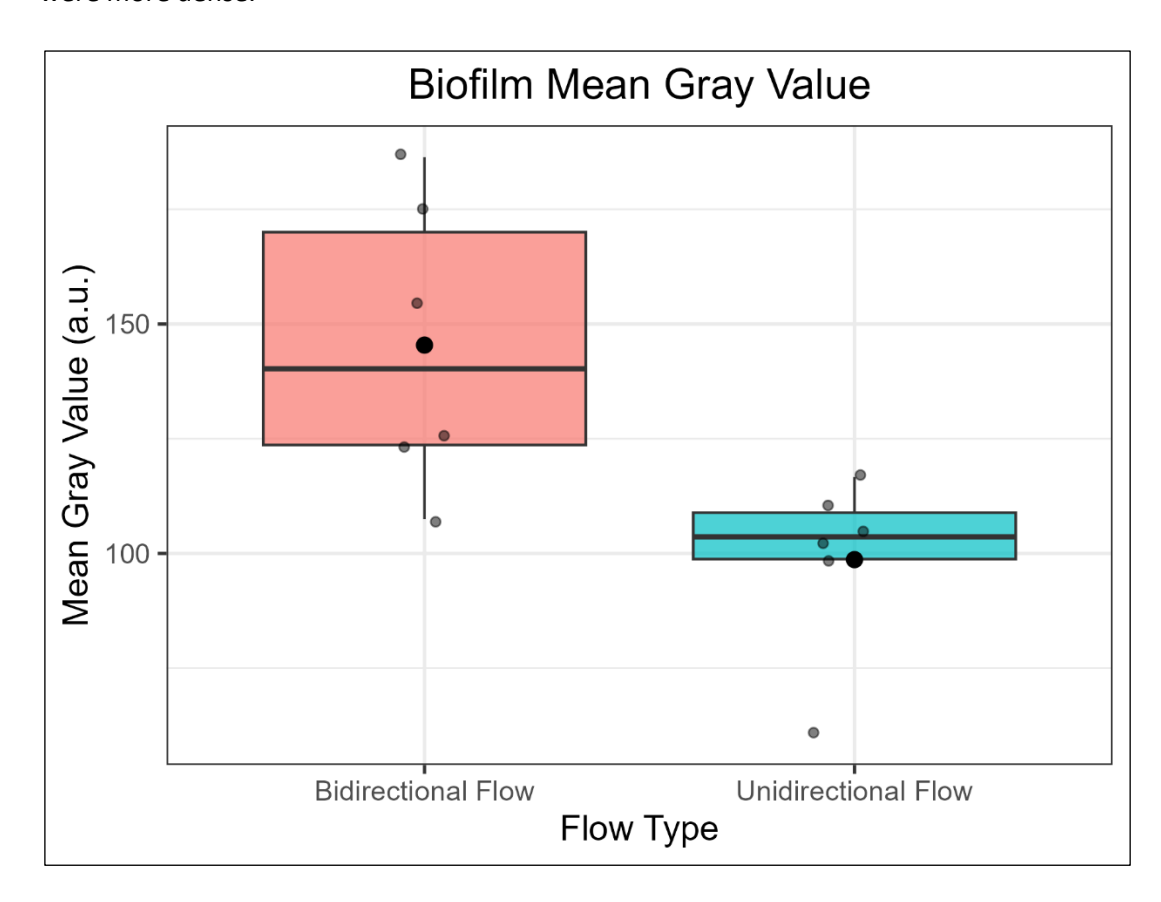


Figure 4.3. Boxplots represent the distribution of mean gray values (a.u.), which are directly proportional to biofilm density and biomass based on fluorescence intensity. Biofilms formed under bidirectional flow exhibited significantly higher mean gray values compared to those grown under unidirectional flow, indicating enhanced biofilm accumulation and structural complexity in response to changing flow direction.

Fig. 4.4 shows the porosity of biofilms grown under bidirectional and unidirectional flow conditions. Porosity is expressed as a percentage and reflects the proportion of void space within the biofilm structure. Biofilms grown under bidirectional flow exhibited significantly higher porosity values (~85%) compared to those grown under unidirectional flow (~40%).

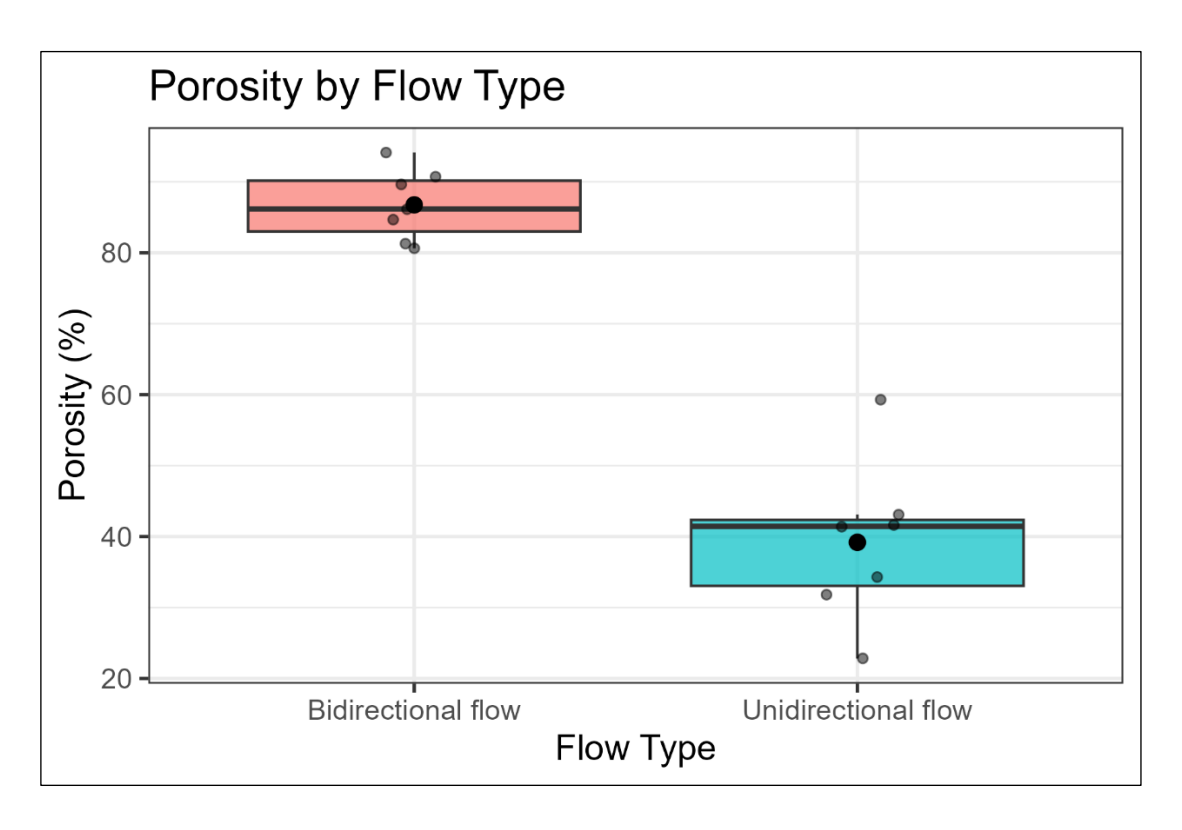


Figure 4.4. Porosity of biofilms grown under bidirectional and unidirectional flow conditions. Porosity (%) represents the proportion of void space within the biofilm structure. Boxes show the interquartile range with median values, and individual data points are plotted. Biofilms under bidirectional flow exhibited significantly higher porosity compared to unidirectional flow, indicating more open and porous biofilm architecture under bidirectional conditions.

## 4.4.2. Biofilm Architecture under Bidirectional Conditions

In order to further understand the architecture of *B. subtilis* biofilms under a bidirectional fluid flow, more fluorescent images were acquired at different scales (Fig. 4.5). As mentioned above, all biofilms exhibited structured surface strands, which are likely formed by parallel Van Gogh bundles adhered to each other. Van Gogh bundles were discovered by van Gestel, Vlamakis and Kolter (2015), and are defined as chains of *B. subtilis* cells. One Van Gogh bundle is one chain of cells. Under bidirectional flow, strands of Van Gogh bundles seem to follow a repetitive pattern around each other and seemingly empty areas, creating an undulated pattern. The wave-like structures appear of different width and fluorescent signal, with thicker strands showing more intense fluorescence, which will be referred to as Van Gogh strands (Fig. 4.5e, blue arrow). Fig. 4.5b shows another interesting feature seen uniquely in this type of *B. subtilis* biofilm: the folds (Fig 4.5b, red arrow). These structures, which are discussed further below, appear as a thicker layer of biofilm and have never been seen before. The biofilms also shows relatively deep gaps in between the thick Van Gogh strands, which appear to be completely empty (Fig. 4.5d, green arrow).

At higher magnification, images reveal a complex and organized network of bacterial cells. In Fig. 4.5d (yellow arrow), small fluorescent dots are notable. These structures have also been seen within biofilms grown under unidirectional continuous flow. Because green fluorescent protein (GFP) is bound to histone proteins in the genetically modified *B. subtilis* used for this study, the round fluorescent dots are either DNA condensed in the middle of the rod-shaped cells or *B. subtilis* endospores. The complex network of Van Gogh bundles becomes even more apparent in Fig. 4.5e (white square), where it is possible to see the thick strands (clusters of Van Gogh bundles) and singular Van Gogh bundles intertwining.

Overall, the change in fluid flow direction adds elements of complexity to the bacterial biofilm. While the biofilm under unidirectional flow was made of long singular Van Gogh bundles aligned adjacent to each other as well as rope-like structures, the biofilms in this present study show a complex and denser network structure, with thick strands made of Van Gogh bundles, as well as singular Van Gogh bundles adopting a net-like morphology in less dense areas of the biofilm.

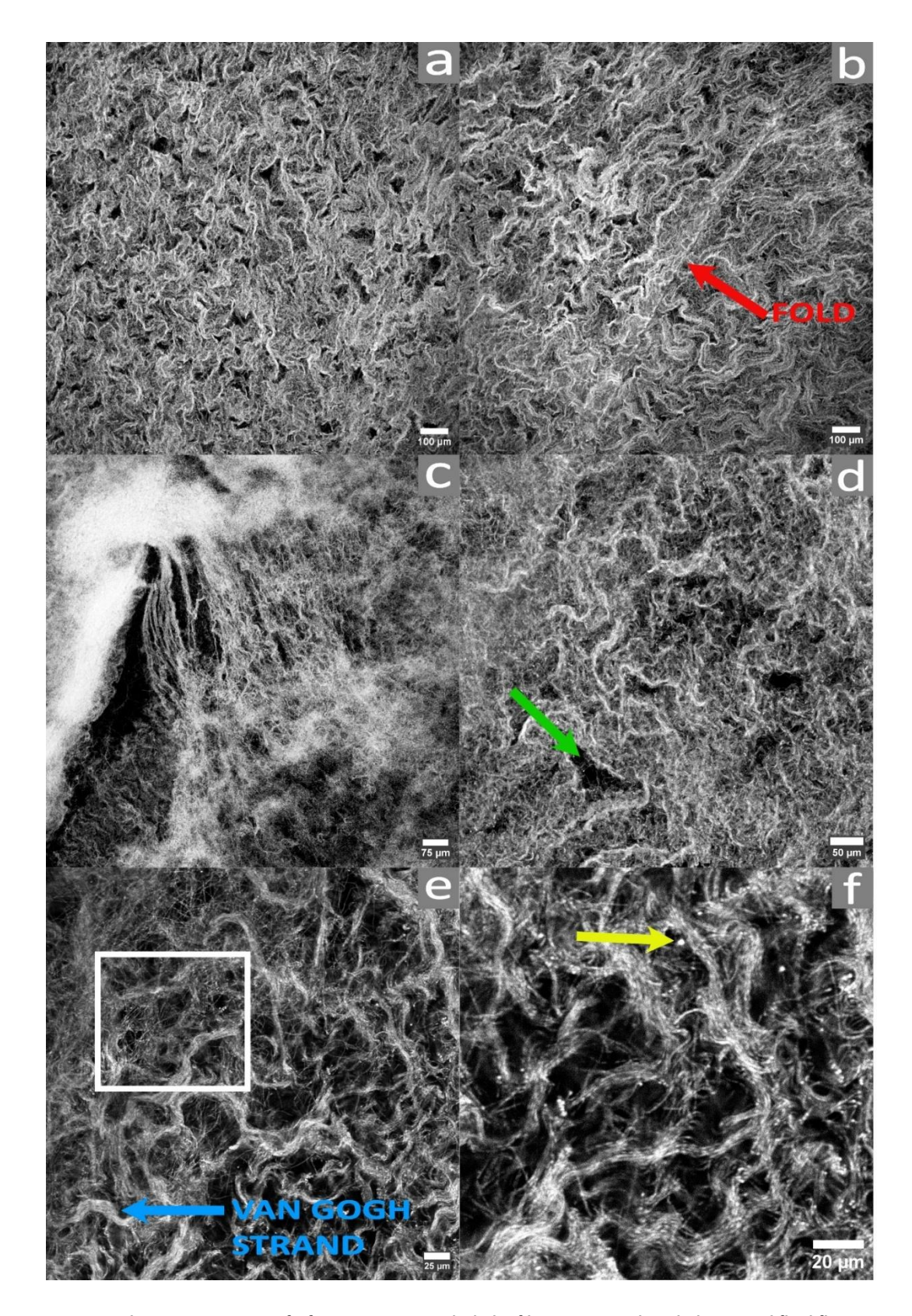


Figure 4.5. Fluorescent images of *gfp*-expressing *B. subtilis* biofilms grown under a bidirectional fluid flow. (a)–(f) Representative images show the structured surface topology characterised by parallel ridges and channels formed by Van Gogh bundles. (b) Fold-like structure unique to bidirectional flow biofilms (red arrow). (c) Aligned Van Gogh strands reaching towards a denser biofilm region. (d) Deep gaps between thick Van Gogh strands, with small branches protruding into the gaps (green arrow). (e) Thick Van Gogh strands

(blue arrow) and single Van Gogh bundle filaments intertwining (white square) (f). (f) Close-up of the intertwined Van Gogh bundle filaments and visible small fluorescent dots (yellow arrow), possibly representing condensed DNA or endospores (Entire flow cells were imaged using Leica SP5, 40x magnification).

# 4.4.3. Bidirectional Flow Induced the Formation of Folds

The most striking feature seen in flow cell biofilms grown under bidirectional flow is the presence of unique structures, seen in Fig. 4.6 and Fig. 4.7, which appear like long and acuminate (pointy) raised sections of the biofilm. These peculiar structures have not been reported before in any previous biofilm study and appear to be folds in the biofilm. Fig. 4.6 shows four images of the same biofilm region. This image was acquired as a Z stack, in order to thoroughly investigate the biofilm folds. Fig. 4.6a shows the overall region of the biofilm harbouring the fold structures (white arrows). The general biofilm morphology shows multiple filamentous strands of various width, made of Van Gogh bundles, creating the undulated patterns. Fig. 4.6b, 4.6c and 4.6d show the top, middle and bottom regions of the biofilm in Fig. 4.6a. In Fig. 4.6b, it is possible to clearly see fold 1.

Fig. 4.6c shows the same biofilm area at a depth between the top and bottom of the biofilm. Further evidence that these are folds is shown in Fig. 4.6d, which is a deeper slice within the biofilm. Linear gaps in the biofilm can be seen where the base of the fold is, which are the basal openings of the folds.

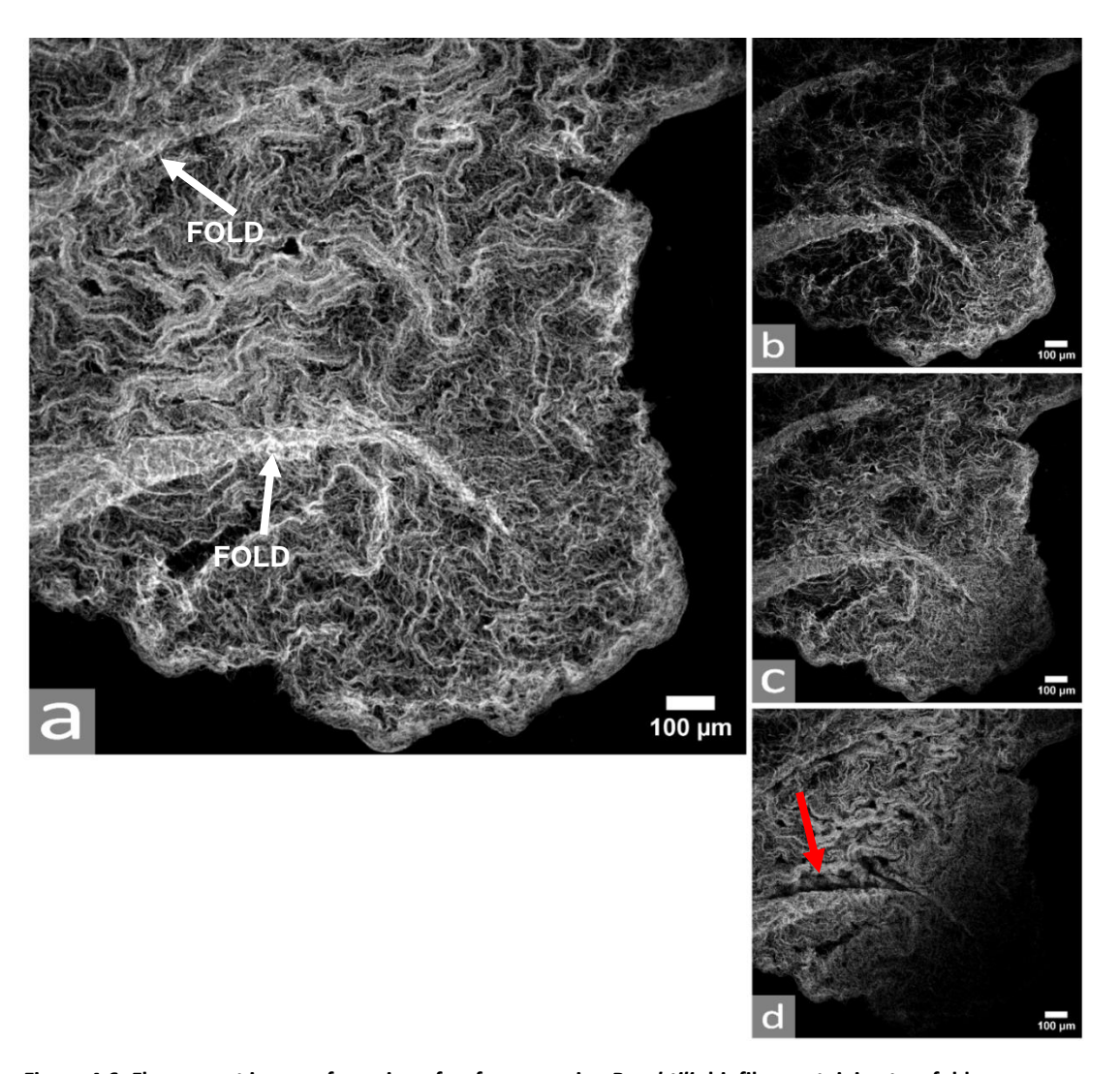


Figure 4.6. Fluorescent image of a region of a gfp-expressing *B. subtilis* biofilm containing two folds, developed under a bidirectional fluid flow, presented at different depths. a) Fluorescent image of the biofilm, showing two folds (white arrows), with fold 1 appearing bigger in size compared to fold 2. b) Top view of the highest point of the biofilm, highlighting the folds, as they appear raised compared to the rest of the biofilm. c) Midsection of the biofilm, showing multiple Van Gogh strands branching from the folds as well as the gap underlying fold 1. d) Bottom view of the biofilm, showing thick Van Gogh strands and the gaps underneath fold 1 (red arrow). (Biofilms were grown within flow cells in LB media, at room temperature, for 48 hours. Entire flow cells were imaged using Leica SP5, 40x magnification).

The fold-like structures were seen not only at the edge, but also in inner regions of the biofilm (Fig. 4.7). The overall architecture of the biofilm is similar to the ones described above, with multiple strands made of Van Gogh bundles, which adopt the complex groovy morphology. The folds in Fig. 4.7a appear wider and longer compared to the folds in Fig. 6a. and also show increased fluorescence, indicating increased density. Like in Fig. 4.6, Fig. 4.7 also presents fluorescent images of the folds at different depths, Fig. 4.7b, 4.7c and 4.7d show the top, middle and bottom of the folds, respectively. These folds are morphologically exactly the same as the ones in Fig. 4.6, as they show an overall elevated architecture compared to the

rest of the biofilm, and this can be clearly seen in Fig. 4.7b. The folds again create channels or gaps at their base created between the two fold limbs (Fig. 4.7b and 4.c).

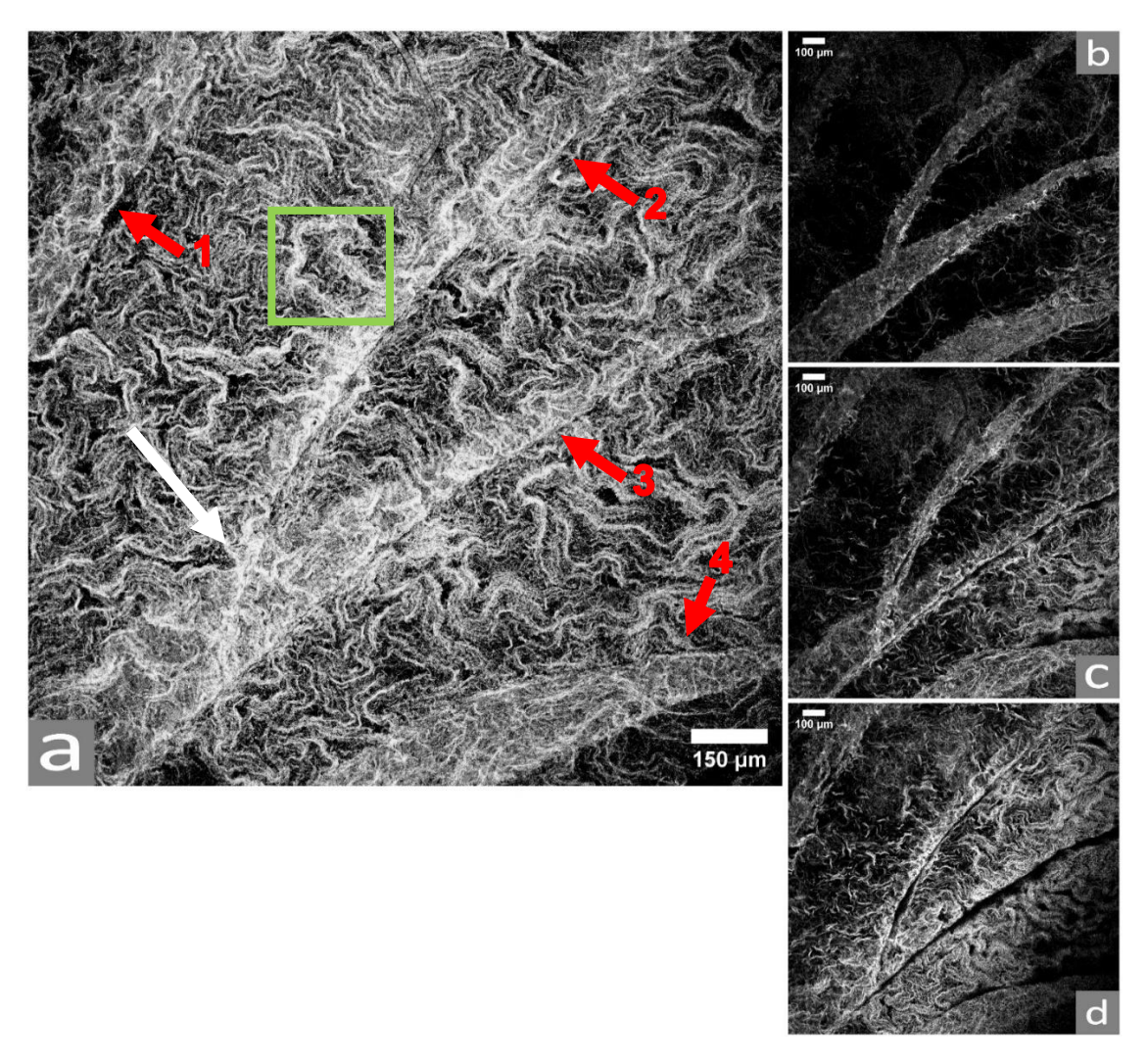


Figure 4.7. Fluorescent image of a region of a *gfp*-expressing *B. subtilis* biofilm containing four folds, developed under a bidirectional fluid flow, presented at different depths. a) Fluorescent image of the biofilm, showing four folds (red arrows), with fold 2 and 3 overlapping (white arrow) and a loop of Van Gogh strands emerging from fold 2 (green square). b) Top view of the highest point of the biofilm, highlighting the folds, as they appear raised compared to the rest of the biofilm. c) Midsection of the biofilm, showing multiple Van Gogh strands branching from the folds as well as the gap beginning to form under fold 2 and 3. b) Bottom view of the biofilm, showing thick Van Gogh strands and the gaps underneath the folds. (Biofilms were grown within flow cells in LB media, at room temperature, for 48 hours. Entire flow cells were imaged using Leica SP5, 40x magnification).

To quantitatively assess the morphology of folds observed in *B. subtilis* biofilms under bidirectional flow, fold height and width were measured and analysed across multiple samples (Fig. 4.8). Fig. 4.8a shows the distribution of fold heights, revealing a notable variation between individual folds, with median heights ranging from approximately 90  $\mu$ m to over 130  $\mu$ m, highlighting the structural heterogeneity of the biofilm folds. Fig. 4.8b presents fold width profiles measured at five positions spaced at equal percentage intervals

along the top of each fold, starting from the wider end. Since fold lengths vary, these positions represent proportional distances (e.g., 0%, 25%, 50%, 75%, and 100% of fold length), allowing for consistent comparison across folds of different sizes. The folds are not symmetrical; instead, they exhibit a tapered structure, with one edge consistently narrower and forming a point, while the opposite edge broadens out. Notably, some folds showed a more uniform width along their length. Fig. 8c presents the relationship (r = 0.387, p = 0.0216) between overall fold width and fold height. A weak, but statistically significant, correlation was observed. Collectively, these findings demonstrate that fold morphology is highly variable but follows a consistent structural trend. The Fold ID used in the analysis corresponds to the Fig. number and the specific fold number (e.g., Fold 6.1 refers to fold 1 in image 4.6).

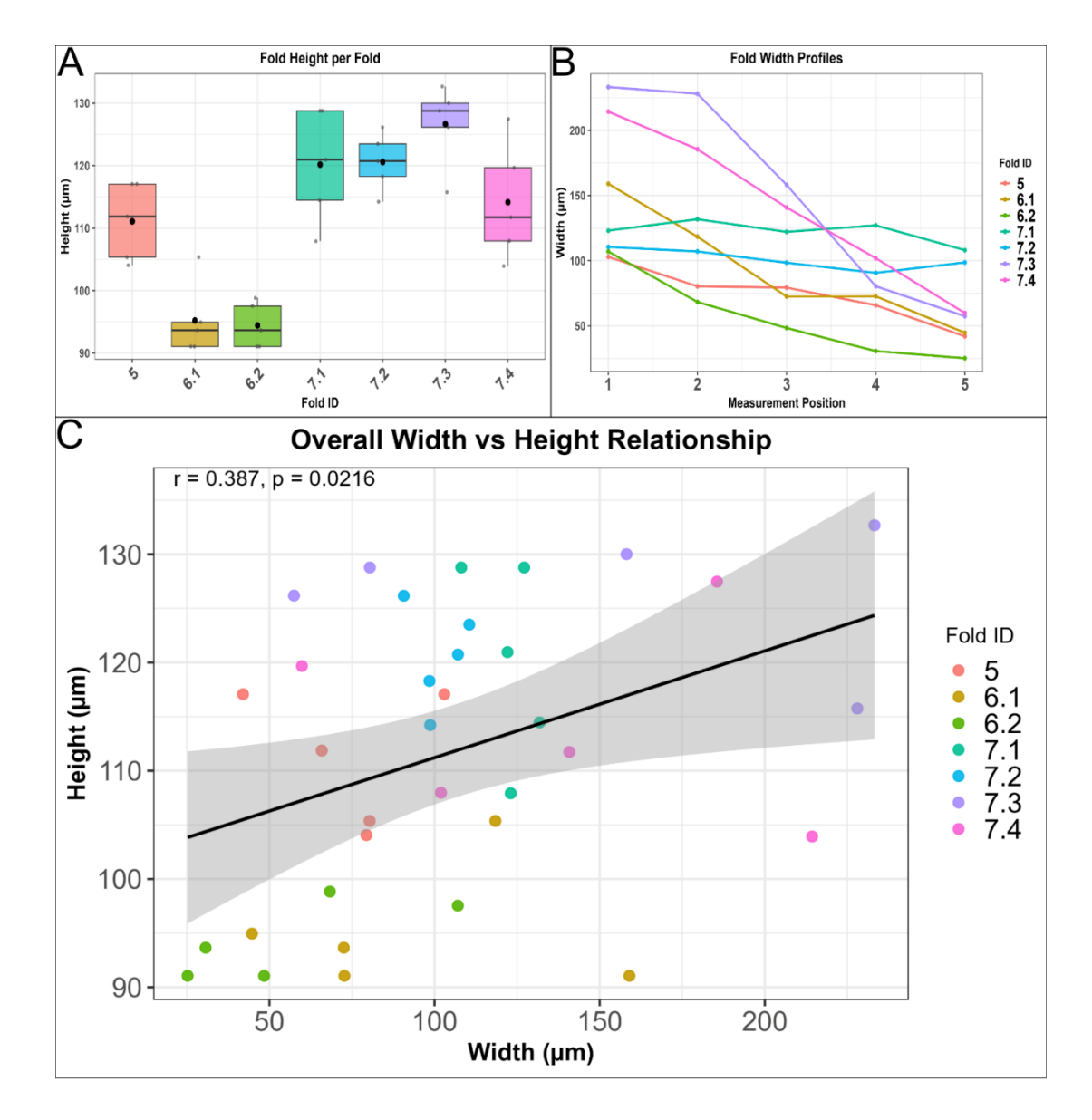


Figure 4.8. (A) Boxplot showing the measured heights of different biofilm folds. Each box represents the interquartile range (IQR), with the horizontal line indicating the median height. The vertical whiskers extend to the minimum and maximum values within  $1.5 \times IQR$ , while grey points show individual measurements. Black dots represent the mean height per fold. Height varies between folds, with some reaching over 130  $\mu$ m. (B) Fold width profiles measured at five equidistant points across each fold. The plots show that most folds taper toward the edges, with central regions generally wider. (C) Scatter plot showing the relationship between overall fold width and fold height, grouped by fold ID. A positive correlation is observed, suggesting that wider folds tend to be taller. The black line represents the linear regression fit, with the shaded area indicating the 95% confidence interval. The Fold ID number is representative of the figure number and fold number.

To further investigate the spatial organisation of folds, the width of the channels located directly beneath each fold was quantified (Fig. 4.9). Fig. 4.9a presents the distribution of channel widths across folds, with each boxplot showing the minimum (red), mean (blue), and maximum (green) channel width values per fold. Most channels had a mean width between  $30-60~\mu m$ , although certain folds, such as Fold 7.4 and Fold 5, showed wider channels. Notably, red markers indicate folds with minimum channel widths below  $20~\mu m$ , suggesting

some channels may be highly constricted. Spatial analysis of the width profiles revealed that the narrowing of the channels occurred predominantly toward the tapered end of the fold. Fig. 4.9b shows the fold height-to-channel width ratio for each fold. While some folds (e. g. Fold 5) exhibited high ratios, indicating tall folds with narrow channels, most folds maintained a ratio between 2 and 4. Fig. 4.9c displays the correlation between fold height and channel width. No significant correlation was observed (Pearson r = 0.066, p = 0.684), indicating that the height of a fold does not reliably predict the width of the underlying channel.

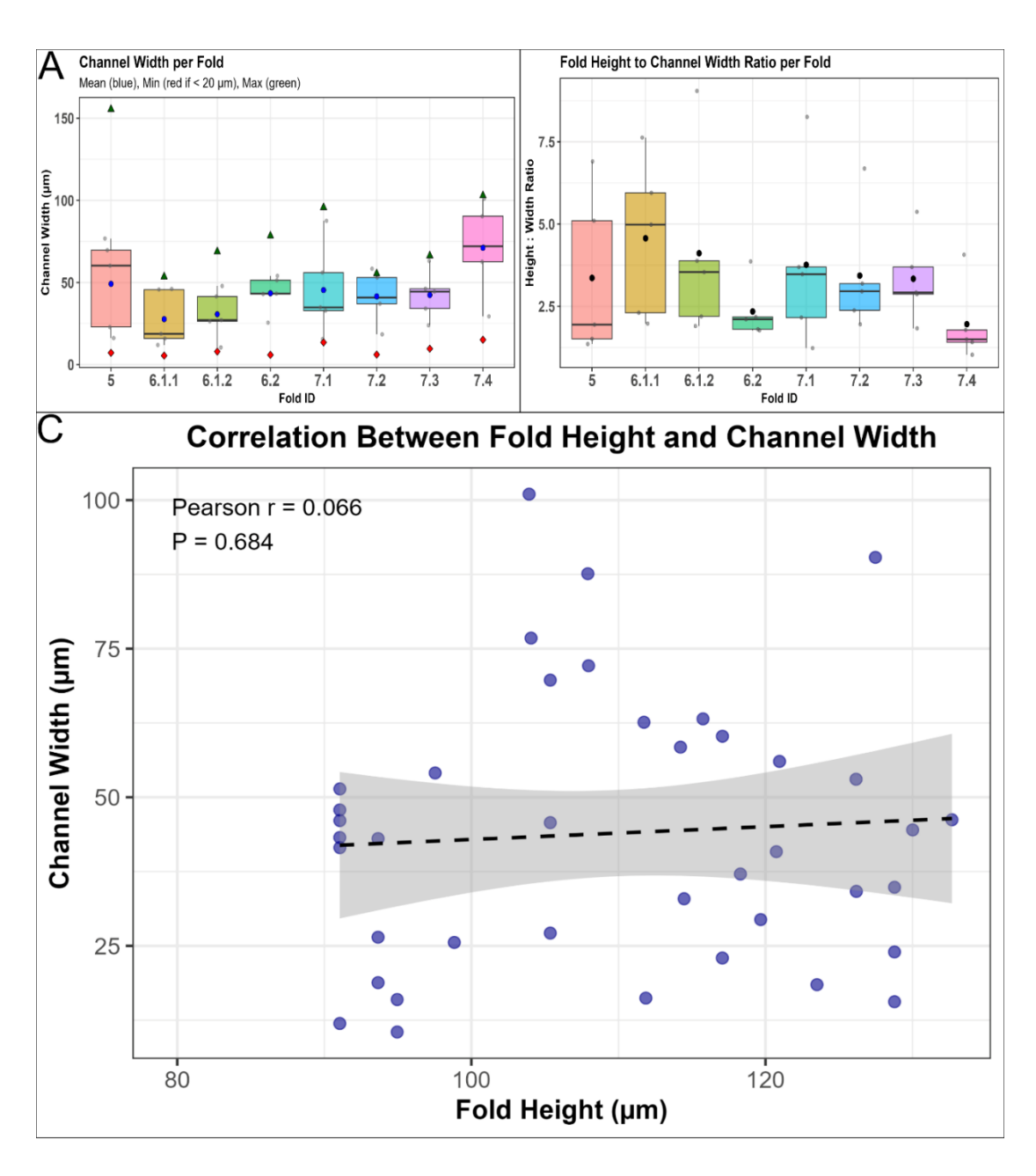


Figure 4.9. (A) Boxplots showing minimum (red), mean (blue), and maximum (green) channel widths beneath individual folds. Each box represents the interquartile range (IQR), with the horizontal line indicating the median width. The vertical whiskers extend to the minimum and maximum values within  $1.5 \times IQR$ , while grey points show individual measurements. Fold IDs correspond to fold number and figure panel from previous analyses. (B) Fold height-to-channel width ratio per fold, indicating structural variation across folds, with some folds (e.g., Fold 5) displaying high ratios suggestive of narrow channels beneath tall folds. (C) Scatter plot showing the relationship between fold height and channel width. A weak, non-significant correlation was found (Pearson r = 0.066, p = 0.684), indicating that fold height does not predict underlying channel width.

To determine whether the presence of folds influences the overall biofilm thickness, measurements were taken from regions of bidirectional flow biofilms with and without folds (Fig. 4.10). The data show that biofilm sections containing folds were significantly thicker

than regions without folds, with a median thickness of approximately 78  $\mu$ m, compared to ~55  $\mu$ m in regions without folds.

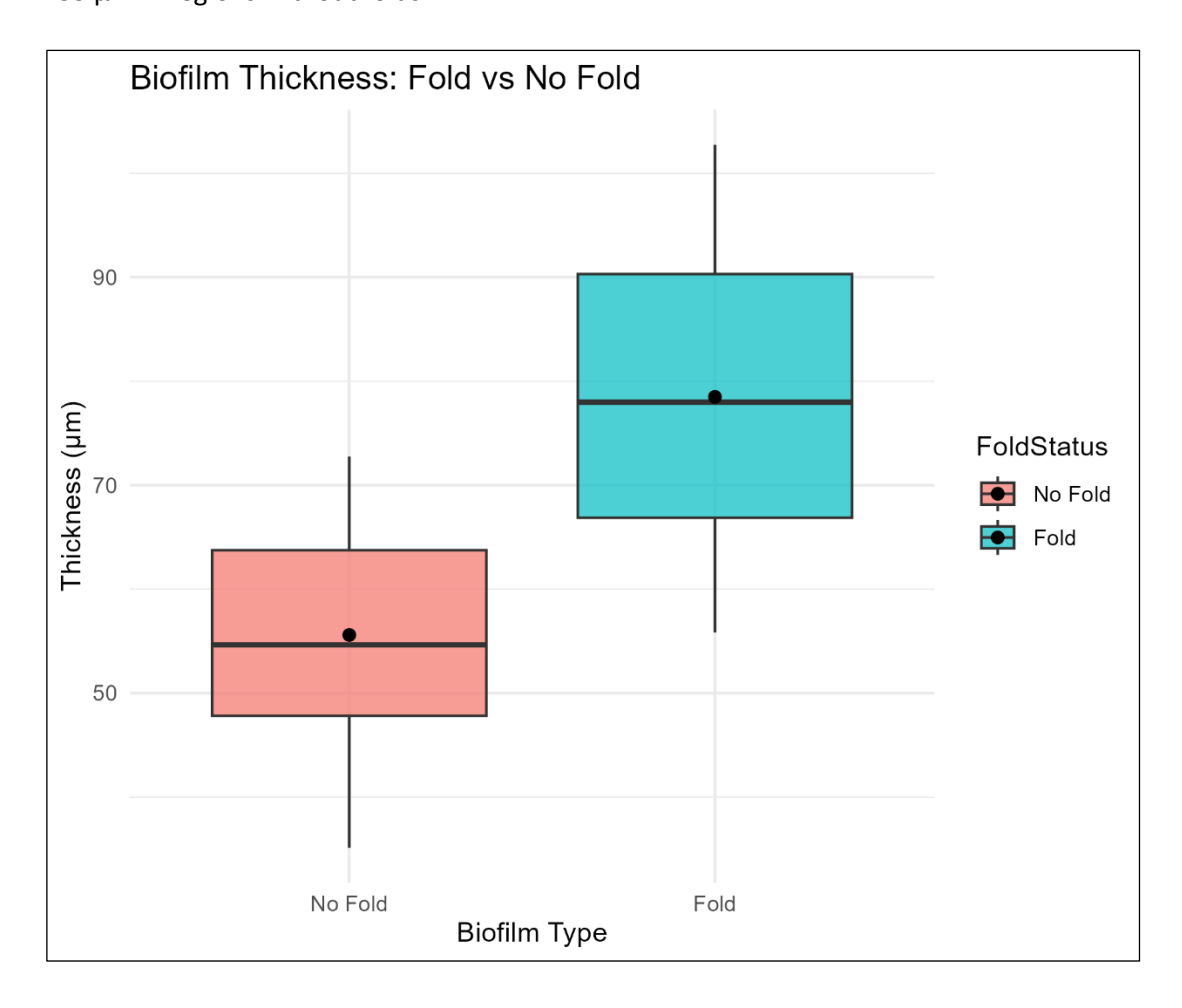


Figure 4.10. Boxplots represent the distribution of thickness measurements (µm) for each group. Biofilm regions containing folds exhibited significantly greater thickness compared to regions without folds. Median and mean values are shown by horizontal lines and black dots, respectively.

## 4.4.4. GBLE Disrupts Biofilm Architecture under Bidirectional Flow

Confocal laser scanning microscopy (CLSM) was used to analyse the structural organisation of B. subtilis biofilms grown under bidirectional flow with 400 µg/mL GBLE (Fig. 4.11). In contrast to biofilms without GBLE (Fig. 4.5), GBLE-treated biofilms (Fig. 4.11) showed a dramatic reduction in structural integrity. The typical Van Gogh strand architecture was largely absent, replaced by thinner, more dispersed Van Gogh bundles with a patchy distribution of fluorescence. The biofilm appears flattened, with reduced vertical complexity and disrupted cohesion. Some sparse Van Gogh ropes remain visible, particularly in Fig. 4.11a and 4.11b (white arrows), but they are less connected and lack the dense bundling observed in the untreated condition. Overall, GBLE interferes with biofilm formation under

bidirectional flow, leading to reduced biomass, altered architecture, and inhibition structural features (folds). These findings are consistent with observations from unidirectional flow biofilms treated with GBLE (Chapter 3), which also exhibited a drastic reduction in biofilm biomass and a near-complete loss of structural integrity.

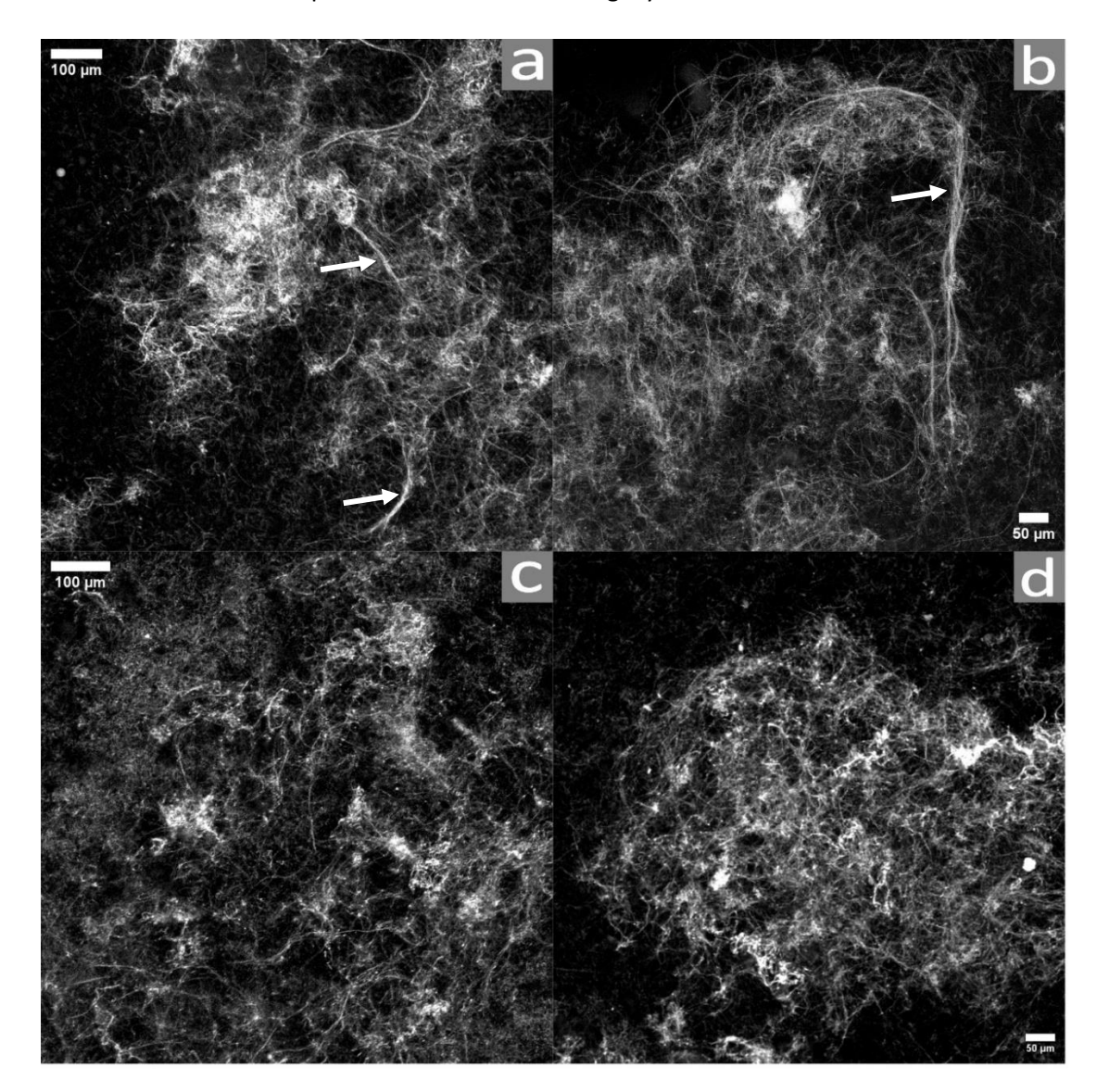


Figure 4.11. Images (a–d) show representative fields of view at various magnifications. The biofilm structure appears disrupted, with reduced biomass, fragmented filamentous structures, and loss of organised Van Gogh strand architecture. Van Gogh ropes still appear in image a and b (white arrows). The biofilm is less cohesive and displays decreased surface complexity compared to untreated biofilms.

To quantitatively assess the effect of GBLE on overall biofilm biomass, the total biofilm volume was measured in 3D CLSM image stacks for both untreated and treated samples under bidirectional flow (Fig. 4.12). The untreated group exhibited significantly higher total biofilm volume, while biofilms treated with 400  $\mu$ g/mL GBLE displayed a substantial reduction in total volume, with most samples falling below 1 × 10<sup>7</sup>  $\mu$ m<sup>3</sup>. The data show a clear and

consistent decline in biomass following treatment, supporting previous qualitative observations from CLSM images.

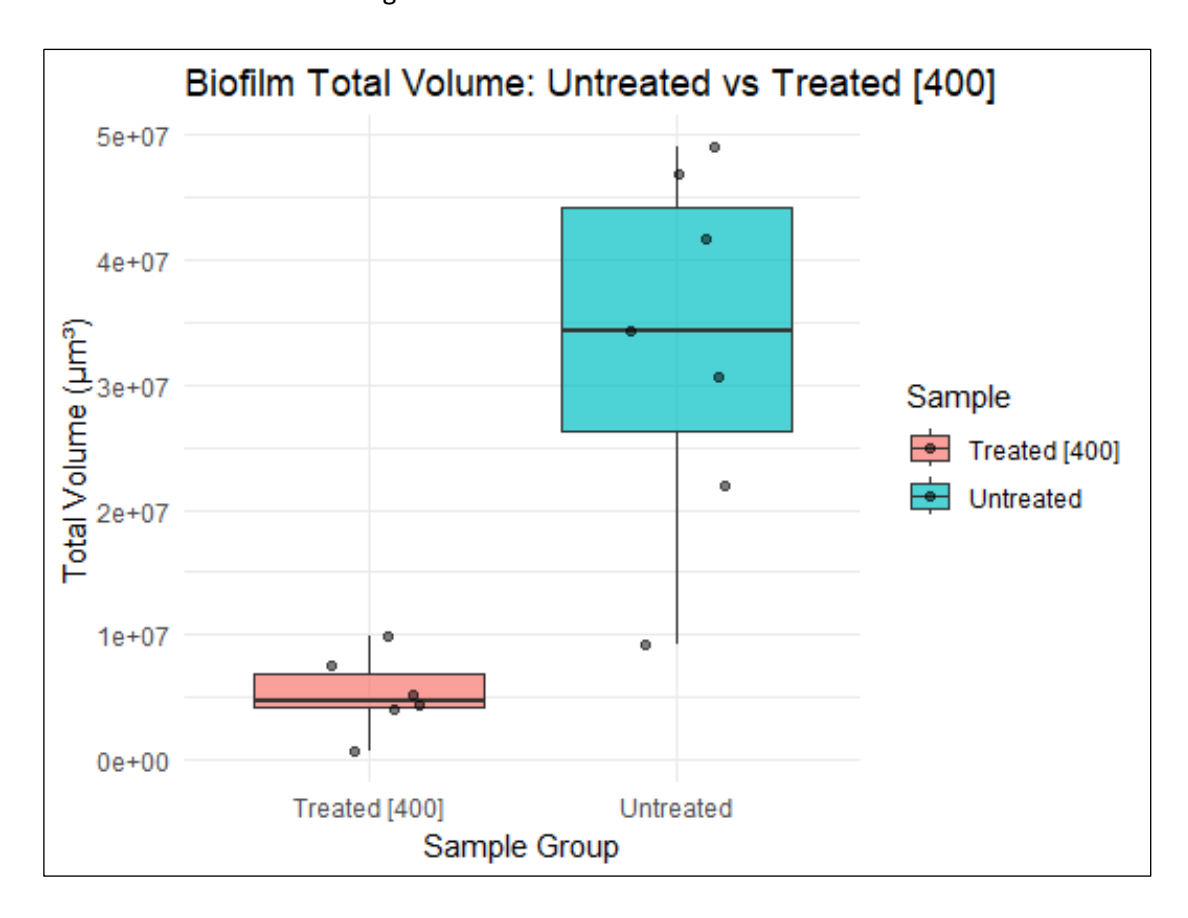


Figure 4.12. Boxplots represent total biofilm volume (μm³) from biofilms grown under bi-directional flow, grown either with GBLE (treated) or without GBLE (untreated). Data measured from 3D CLSM image stacks. Untreated biofilms displayed significantly greater total biomass compared to treated samples.

To further assess the impact of GBLE on biofilm development, the mean gray value of CLSM images was compared between untreated and treated *B. subtilis* biofilms under bidirectional flow (Fig. 4.13). The mean gray value, which represents overall image fluorescence, is directly proportional to biofilm density and biomass. Untreated biofilms exhibited significantly higher mean gray values, with a median value above 140 a.u., reflecting dense biofilm structures. In contrast, treated biofilms displayed markedly lower fluorescence intensity, with mean gray values consistently below 50 a.u. This substantial reduction in gray value corresponds to a sharp decline in biofilm density and matrix content, supporting both the visual observations from microscopy and the measured drop in total biofilm volume.

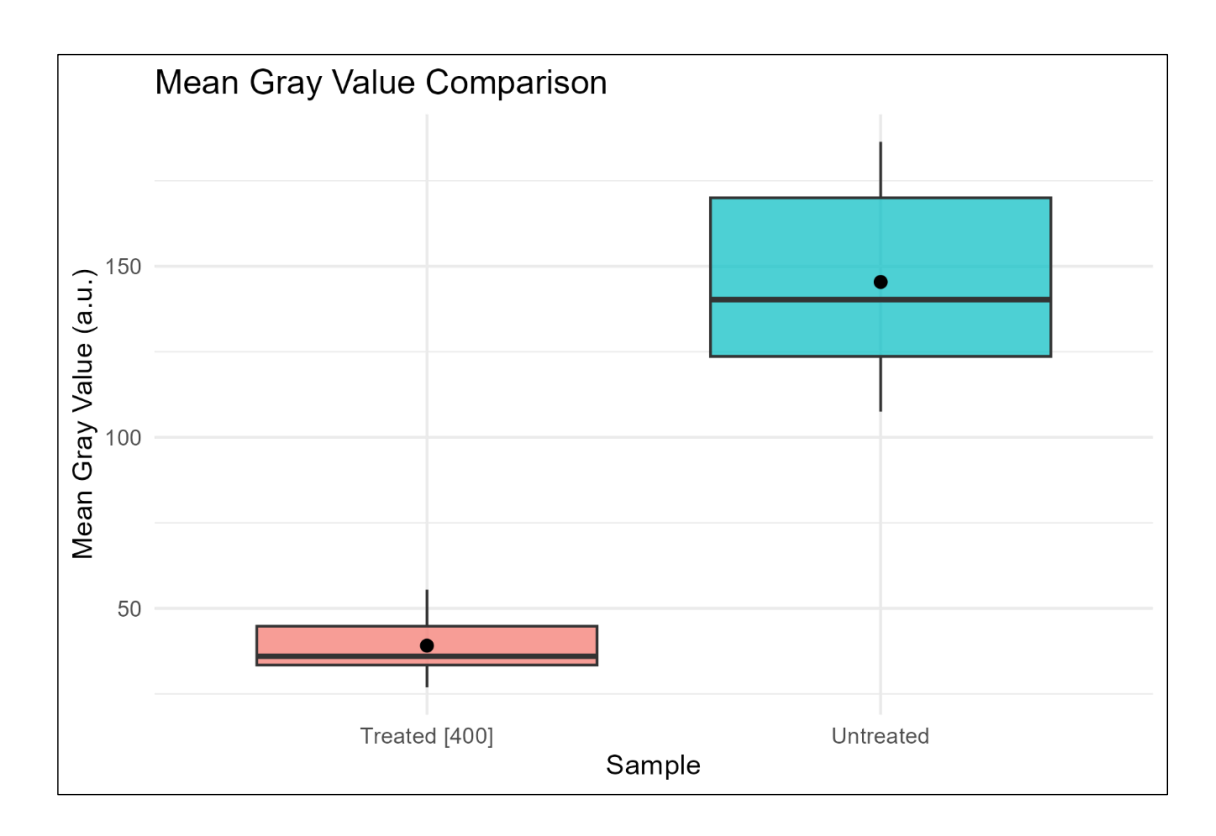


Figure 4.13. Boxplots represent mean gray value (a.u.), which is directly proportional to biofilm density and biomass. Biofilms treated with 400 μg/mL exhibited significantly lower fluorescence compared to untreated controls, indicating a strong reduction in overall biofilm accumulation following treatment.

## 4.5. Discussion

## 4.5.1. Effect of Unidirectional and Bidirectional Fluid Flow on Biofilms

This study highlights the striking structural complexity of biofilms developed under a bidirectional fluid flow. The biofilm's morphology change dramatically once a bidirectional flow is introduced, exhibiting additional architectural complexity, as seen in Fig. 4.2. Once either continuous unidirectional (chapter 3) or bidirectional flow (this chapter) is added, the bacterial cells arrange themselves in filamentous structures, also known as Van Gogh bundles. Van Gogh bundles have been described in the context of *B. subtilis* agar biofilms and have been seen at the edge of colony agar biofilms (van Gestel, Vlamakis and Kolter, 2015). Their function has been associated to colony expansion through sliding motility and have not been described in any other biofilm form.

A number of structural features have been observed here in biofilms grown under bidirectional flow. These are summarised in the table below.

**Table 4.1.** Characteristic architectural features of *Bacillus subtilis* biofilms developed under bidirectional flow, as visualised by confocal laser scanning microscopy (CLSM).

Biofilm Feature	Image
Net-like structure: composed individual, intertwined Van Gogh bundles that occupy and bridge the interstitial spaces between Van Gogh strands.	20 μm
Van Gogh strands: many Van Gogh bundles arranged in close parallel alignment.	20 рг
<b>Folds</b> : elevated three-dimensional structures containing underlying channel-like voids.	100 µm

In this study, Van Gogh bundles appear to be the main constituent of the flow cell biofilm, similar to the flow cell biofilms described in the previous chapter under unidirectional flow. However, the biofilms developed under bidirectional flow exhibit the development of thick strands made of several Van Gogh bundles that have arranged themselves in an intertwined manner (referred to as Van Gogh strands, see Table 4.1) (Fig. 4.2c), an effect that is not seen in biofilms grown under unidirectional flow (Fig. 4.2b). Under continuous bidirectional flow,

biofilms developed a distinct net-like architecture, with filamentous meshwork stretching between the strands (see Table 4.1) (Fig. 4.5a–b, d). This interconnected network becomes especially evident in Fig. 4.5e–f, highlighting the scaffold-like nature of the biofilm under bidirectional flow. The ability of single Van Gogh bundles to arrange in an organized manner has been observed in the previous chapter, as Van Gogh bundles formed rope-like structures under a continuous fluid flow.

Compared to unidirectional flow, biofilms grown under bidirectional flow exhibited a general increase in biofilm mean gray value. The observed increase in mean gray value under bidirectional flow (Fig. 4.3) suggests that these biofilms accumulate more biomass or exhibit greater cell density compared to those under unidirectional flow. This may be attributed to the enhanced mass transport and nutrient mixing provided by bidirectional flow patterns, which can disrupt stagnant zones and improve nutrient penetration into the biofilm matrix (Stoodley et al., 1999) (Stewart, 2003). In contrast, unidirectional flow may lead to nutrient gradients and localized depletion zones, limiting biomass accumulation over time.

Bidirectional flow may also induce cyclical shear forces that contribute to biofilm structural reinforcement rather than detachment. Moderate or fluctuating shear has been shown to promote stronger, denser biofilm architectures by stimulating extracellular polymeric substance (EPS) production and cell adhesion in *P. aeruginosa* (Purevdorj et al., 2002) (Liu and Tay, 2002). The net-like scaffold observed in the CLSM images (Fig. 4.5) under bidirectional flow is, possibly, a result of the bi-directional shear. Furthermore, a change in flow direction has been reported to prevent the establishment of channelized flow paths that typically emerge in unidirectional systems, which can limit biofilm expansion by directing nutrients away from certain regions (Wilking et al., 2013). By redistributing fluid forces and promoting more homogeneous nutrient exposure, bidirectional flow may promote biomass build-up throughout the structure rather than restricting growth to shear-protected niches. These findings align with previous studies that observed increased biofilm thickness and density under oscillatory or reversing flow regimes compared to steady flows in *S. aureus* and *S. epidermidis* (Melo and Bott, 1997) (Rupp et al., 2005).

The significantly higher porosity observed in biofilms developed under bidirectional flow (Fig. 4.4) indicates a more open and heterogeneous architecture compared to the biofilms formed under unidirectional flow. Porosity is a critical parameter that influences nutrient transport, waste removal, and microbial activity within biofilms (Xavier et al., 2005). The increased

porosity under bidirectional flow likely results from the cyclical shear stresses imposed by flow reversal, which can disrupt uniform layering and instead promote a scaffold-like architecture with interconnected voids (Stoodley et al., 1999) (Wilking et al., 2013). Previous studies have shown that fluctuating or oscillatory shear conditions enhance biofilm heterogeneity and internal channel formation in mixed-species biofilms (Stoodley et al., 1999). Bidirectional flow may intermittently displace weaker regions of the biofilm, facilitating the formation of voids and pores without causing complete detachment, thus enhancing structural complexity.

Additionally, an increased porosity under bidirectional flow may result from the formation and arrangement of filamentous Van Gogh bundles as seen in CLSM images, which appear to create a net-like matrix (see Fig. 4.5). These structures likely leave interstitial spaces between bundles, increasing overall porosity. In contrast, unidirectional flow tends to promote laminar growth along the direction of flow, often resulting in denser, layered biofilms with reduced void space (Stoodley et al., 2002) (Horn and Morgenroth, 2006). Greater porosity in biofilms under bidirectional flow may enhance diffusion of oxygen and nutrients into deeper layers, contributing to the higher biomass accumulation.

The combination of increased porosity and biomass under bidirectional flow likely provides a functional advantage for biofilm survival and persistence in dynamic environments. Higher porosity enhances mass transfer, allowing for more efficient diffusion of nutrients and oxygen throughout the biofilm matrix, which supports metabolic activity even in deeper layers (Stewart, 2003) (Horn and Morgenroth, 2006). Simultaneously, the increased biomass suggests robust structural development, which may improve resistance to shear stress and environmental fluctuations (Stoodley et al., 2002). Together, these features may enable the biofilm to better withstand the mechanical perturbations associated with the change in flow direction, while maintaining physiological activity and structural integrity.

The structural complexity of *B. subtilis* biofilms arises from cellular differentiation into specialised subpopulations, enabling a division of labour that conserves energy and promotes cooperative function. Five major cell types have been identified, including motile cells, matrix-producers, and surfactin-producers. Matrix-producers secrete EPS and TasA, while surfactin-producers synthesise surfactin, which lowers surface tension and acts as a signalling molecule (van Gestel, Vlamakis and Kolter, 2015). These two subpopulations coordinate to form Van Gogh bundles, which are multicellular chains that facilitate colony expansion (van

Gestel, Vlamakis and Kolter, 2015). Though previously observed at the edges of agar colony biofilms, this study demonstrates that Van Gogh bundles also emerge under submerged, bidirectional flow, forming three-dimensional strand-like structures. Their formation is likely driven by matrix- and surfactin-producing cells responding to fluid dynamics. While subpopulation behaviour in submerged *B. subtilis* biofilms remains understudied, the striking morphological differences observed between static, unidirectional, and bidirectional flow conditions (Fig. 4.2a–c) highlight the species' remarkable phenotypic plasticity in adapting biofilm architecture to environmental stress, ultimately enhancing survival and persistence.

## 4.5.2. Biofilm Architecture under Bidirectional Conditions

The change in direction of the flow triggers further complexity within the biofilm, as the Van Gogh bundle filaments adopt different conformation to create the observed net-like structure. The netlike structure is made of a framework of thick Van Gogh strands made of multiple Van Gogh bundles, with low density areas in between, which are either empty or filled with a low density matrix of individual Van Gogh bundles. In this study, it is likely that adopting the mesh structure is advantageous to the bacteria to withstand hydrodynamic forces.

*B. subtilis* biofilms behave as colloidal hydrogels, with cells as colloids and ECM mimicking cross-linked polymers (Ido et al., 2020). While there are limited studies on submerged biofilm mechanics, their high water content and viscoelasticity likely allows them to absorb mechanical stress. The porous, mesh-like structure observed here, reinforced by ECM-rich Van Gogh strands, likely dissipates hydrostatic pressure. As in inorganic hydrogels, a stable backbone prevents structural collapse (Foudazi et al., 2023), suggesting these strands might provide mechanical integrity under flow. The Van Gogh strands seen in this thesis are unique to bidirectional flow cell biofilms.

Bacterial adaptation is a result of quorum sensing (QS), where microorganisms synthesise a range of signalling molecules which allows bacteria to coordinate biochemical processes and downstream gene expression (Kalamara et al., 2018) in response to the environment. QS systems are essential for survival and modulate cooperative behaviours, allowing the development of phenotypic heterogeneity. This is apparent in biofilms, where cells simultaneously exhibit different biological states (Bareia, Pollak and Eldar, 2017). The *B. subtilis* biofilm developed under bidirectional flow seen in this study is a prime example of phenotypic heterogeneity. Presenting a degree of genetic and phenotypic diversity is

advantageous especially in environments that are constantly changing, such as in nature (Gasperotti et al., 2020) (Morawska, Hernandez-Valdes and Kuipers, 2021). Phenotypic heterogeneity is associated with bet-hedging, a risk-spreading strategy which entails the bacterial differentiation into offspring with different properties to maximise the probability of survival (Gasperotti et al., 2020). In addition, phenotypic heterogeneity enables division of labour, which is often seen in B. subtilis biofilms. Division of labour is also evident in this study, where B. subtilis cells form a mesh-like, porous biofilm to withstand the mechanical stress of bidirectional flow. This structural adaptation likely arises through the coordinated activity of distinct cell types, primarily matrix-producers and surfactin-producers, which differentiate in response to QS-regulated signalling (Kalamara et al., 2018) (van Gestel, Vlamakis and Kolter, 2015). Matrix-producers secrete EPS and amyloid fibres (TasA), providing the scaffold and cohesion required for biofilm integrity, while surfactin-producers reduce surface tension at the cell-liquid interface and facilitate the alignment and flexibility of cell chains that form Van Gogh bundles. These cell types operate synergistically, with QS enabling communication and spatial organisation within the biofilm, ensuring the emergence of a structurally stable architecture capable of resisting hydrostatic pressure under dynamic flow conditions.

#### 4.5.3. Bidirectional Flow Induces the Formation of Folds

Unique to *B. subtilis* biofilms grown under a bidirectional flow are the folds, elongated structures that appear raised compared to the rest of the biofilm and stretch through parts of the biofilm, displaying gradually decreasing width, culminating in an acuminate end (Fig. 4.6 and 4.7). The folds have been seen only in response to a bidirectional flow, not in a unidirectional flow. These structures present openings at the bottom, similar to a channel (Fig. 4.6d and 4.7d), with varying widths. Similar structures have not been seen before in bacterial biofilms.

Quantitative analysis of fold morphology (Fig. 4.8A–C) showed substantial variability in fold height between individual folds, with some reaching up to 130  $\mu$ m (Fig. 4.8A), and a general trend of decreasing width toward the fold tip (Fig. 4.8B). The observed tapering of folds, with a gradual decrease in width toward the tip, likely confers mechanical advantages under bidirectional flow. Tapered geometries are known to reduce mechanical stress by streamlining fluid flow, lowering pressure differentials across the structure (Kedebe and Winger, 2021) (Sung, Chong and Chung, 2023). In biofilms, this shape may help minimise

shear stress at the fold tip, decreasing the risk of detachment. The broader base provides structural anchorage, while the narrowing tip likely facilitates stress dissipation along the fold's axis, distributing mechanical load more evenly. This configuration may represent an adaptive response to fluctuating hydrodynamic forces, allowing the biofilm to maintain stability without compromising structural complexity.

These folds also accommodate or facilitate the formation of channels, which are known to play essential roles in nutrient delivery, waste removal, and fluid exchange within mature biofilms (Wilking et al., 2013) (Zhang et al., 2011). Previous studies have shown that in *B. subtilis* and *P. aeruginosa* biofilms form channels as part of a self-organised network to optimise mass transport and enable metabolic cooperation across the biofilm (Wilking et al., 2013) (Yan et al., 2016). In this context, the correlation between fold size and width could reflect a structural adaptation that allows the biofilm to maintain internal fluid flow through lateral channel-like openings observed at the base of the folds (Fig. 4.6d-7d), thereby sustaining growth in regions that would otherwise become nutrient-depleted.

Width measurements (Fig. 4.9A) of channels seen underneath the folds revealed significant heterogeneity among the channels, ranging from 10.5 μm to 101.002 μm, with, no significant correlation between fold height and channel width (Pearson r = 0.066, p = 0.684; Fig. 4.9C). Interestingly, one fold in particular (fold 6.1) contained two separate channels beneath it, a rare occurrence in this dataset. The presence of multiple channels beneath a single structural fold may serve to enhance fluid flow, nutrient distribution, or waste removal in regions experiencing higher metabolic activity or mechanical stress. Although the presence of multiple channels within a single biofilm wrinkle or fold has not been widely documented in *B. subtilis*, similar multi-channel architectures have been described in mature *P. aeruginosa* biofilms, where radial and branching channel networks facilitate internal convection and nutrient delivery (Wilking et al., 2013) (Drescher et al., 2013). In engineered or evolved biofilms, such as those subjected to flow or selective pressure, channel multiplicity may also represent spatial self-organisation for improving mass transport efficiency (Zhang et al., 2011).

The presence of internal channels integrated within folds can create preferential flow pathways that allow fresh nutrients and oxygen to penetrate deep into the biofilm matrix, bypassing the diffusional limitations typically associated with dense biofilms (Stoodley et al., 1999) (Stewart, 2003). Simultaneously, these channels enable the removal of metabolic byproducts and toxic compounds, maintaining a more stable internal microenvironment

conducive to sustained microbial activity (Stewart, 2003). From a mechanical perspective, such channels may act as pressure-relief zones, absorbing and redistributing fluid shear stress, particularly in systems like bidirectional flow where the direction of force changes. This flow-through architecture has been proposed as an evolved strategy in mature biofilms to balance structural stability with efficient exchange (Wilking et al., 2013) (Drescher et al., 2013).

B. subtilis is known to form wrinkles on the top surface of its biofilms. Wrinkles have been described thoroughly in colony agar biofilms as well as pellicle biofilms and occur when a mechanical stress is applied to the biofilm (Wilking et al., 2013). Wrinkles are a result of biofilm buckling, which involves surface detachment, creating empty channels underneath the wrinkle. These channels are thought to have a role in nutrient transport, driving nutrients from the edges of the biofilm towards the centre (Galdino, Benevides and Tenorio, 2020). While both folds and wrinkles are elevated structural features within B. subtilis biofilms, they differ in their context, formation, and mechanical origin. Wrinkles are seen in colony agar and pellicle biofilms, arise from buckling of the biofilm surface due to compressive stress, often caused by constrained growth or surface adhesion (Galdino, Benevides and Tenorio, 2020). These wrinkles involve surface detachment, creating empty subsurface channels that facilitate nutrient transport from the periphery to the biofilm centre. In contrast, the folds described in this chapter are exclusive to submerged biofilms exposed to bidirectional flow. Rather than forming through buckling, these folds appear as elongated, raised structures with acuminate ends, often containing lateral channel-like openings. Their formation is likely driven by dynamic hydrodynamic forces, rather than surface compression typical of colony biofilms. In submerged environments with alternating flow directions, biofilms are continuously exposed to cyclical mechanical loading, which may induce localized deformation and alignment of cells and extracellular matrix (ECM) over time (Stoodley et al., 2002) (Wilking et al., 2013).

Previous studies have demonstrated that pressure within channels of colony agar biofilms can be substantially lower than atmospheric pressure, generating internal pressure gradients that influence fluid transport and structural organisation (Wilking et al., 2012) (Seminara et al., 2012). Building on this, the present study suggests that *B. subtilis* biofilms exposed to a change in flow direction and hydrostatic pressure from the overlying fluid may similarly develop internal pressure differentials shaped by the geometry of folds and channels. These

gradients are likely to facilitate directional transport of nutrients and metabolites (Wilking et al., 2013), while also reducing localised mechanical stress (Stoodley et al., 2002). Furthermore, the presence of reduced pressure within channels may act as a stabilising factor by preventing collapse and maintaining the openness of internal voids, which are critical for efficient mass transfer and for preserving biofilm structure under dynamic flow conditions (Trejo et al., 2013).

Interestingly, regions of the biofilm containing folds were significantly thicker than regions without folds (Fig. 4.10), suggesting that fold formation is closely associated with localised biomass accumulation and enhanced matrix production. This increase in thickness may result from mechanical and physiological adaptations to the fluctuating forces present under bidirectional flow. Cyclical shear stresses are known to stimulate EPS production, which reinforces structural cohesion and allows the biofilm to resist deformation and detachment (Stoodley et al., 2002) (Wilking et al., 2013). A change in flow direction may lead to differential shear gradients across the biofilm surface, encouraging cell migration, alignment, and localised growth in specific regions. Matrix- and surfactin-producing subpopulations may respond to these gradients by depositing more biomass and matrix at mechanically favourable sites, reinforcing the structure (van Gestel, Vlamakis and Kolter, 2015).

From a functional standpoint, thicker folded regions may serve as load-bearing elements that help dissipate mechanical stress and anchor the biofilm against shear. Additionally, greater thickness can provide protective advantages, such as buffering embedded cells from hydrodynamic fluctuations, antibiotics, or nutrient limitation, and acting as diffusion barriers that preserve internal microenvironments (Stewart, 2003) (Flemming et al., 2016).

#### 4.5.4. GBLE Disrupts Biofilm Architecture under Bidirectional Flow

Treatment with 400  $\mu$ g/mL GBLE led to a marked reduction in *B. subtilis* biofilm biomass and structural complexity under bidirectional flow, as demonstrated by both confocal microscopy and quantitative analyses. Compared to the untreated condition, which exhibited dense networks of Van Gogh bundles, folds, and cohesive filamentous structures, GBLE-treated biofilms appeared flattened, patchy, and significantly disrupted (Fig. 4.11a–d). Quantitatively, this was reflected in a drastic decrease in total biofilm volume (Fig. 4.12) and mean gray value (Fig. 4.13), indicating a substantial loss in biomass and EPS density. The disintegration of organised Van Gogh strands and the loss of folds suggest that GBLE interferes with key processes involved in biofilm maturation and structural reinforcement.

These findings are consistent with those reported for unidirectional flow biofilms exposed to GBLE, as described in Chapter 2, where biofilms similarly exhibited major reductions in biomass, complexity, and cohesive architecture. While previous studies have shown that components of GBLE, notably flavonoids and terpene lactones, can disrupt quorum sensing, EPS production, and membrane integrity in various bacterial species, including Escherichia coli O157:H7, Staphylococcus aureus, and Staphylococcus haemolyticus (Kim et al., 2016) (Wang et al., 2021), the present work is the first to examine these effects on B. subtilis biofilms grown under bidirectional flow conditions. This flow regime introduces mechanical stresses absent in static systems, making the observed biofilm architectural changes and susceptibility to GBLE unique to this environmental context. Under flow conditions, such disruption is likely to interfere with processes such as the alignment and chaining of matrixproducing cells, which are thought to be critical for the development of large-scale biofilm structures. Although these specific processes were not directly measured in the present study, this interpretation is supported by prior observations that B. subtilis biofilm architecture relies on coordinated chaining and alignment of matrix-producing cells (Vlamakis et al., 2008) (Beauregard et al., 2013). The observed reduction in biofilm biomass and bundle-like architecture under GBLE treatment suggests a disturbance of these cellular behaviours during biofilm maturation. These findings further support GBLE's potential as a plant-based antibiofilm agent, particularly in industrial environments where mechanical forces typically promote robust biofilm development.

#### 4.6. Conclusion

This study demonstrates that *Bacillus subtilis* exhibits remarkable structural plasticity when exposed to bidirectional fluid flow, forming architecturally complex, highly porous, and mechanically adaptive biofilms. Unique features such as Van Gogh strands, net-like scaffolds, and previously undescribed folds with lateral channels were exclusive to bidirectional conditions and likely represent evolved responses to dynamic hydrodynamic stress. These adaptations promote biomass accumulation, structural stability, and metabolic resilience, underlining the capacity of bacterial populations to reorganise in response to environmental forces. The identification of folds as active, possible load-bearing and pressure regulating elements that facilitate internal flow, may offers novel insight into the functional morphology of submerged biofilms. Additionally, the disruption of these structures by *Ginkgo biloba* leaf extract (GBLE) highlights the potential of this plant-based antibiofilm agent to impair biofilm

development, under bidirectional flow. Together, these findings expand our understanding of how environmental flow regimes shape biofilm architecture and open new avenues for targeting biofilms in dynamic settings such as medical, industrial, or environmental systems.

# 4.7. References

Ackermann, M. (2015) A functional perspective on phenotypic heterogeneity in microorganisms. *Nature Reviews Microbiology*. Vol. 13(8), pp. 497–508.

Bareia, T., Pollak, S. and Eldar, A. (2017) Self-organization of bacterial diversification under stress. *Nature Microbiology*. Vol. 2(8), pp. 162–168.

Branda, S.S., González-Pastor, J.E., Ben-Yehuda, S., Losick, R. and Kolter, R. (2001) Fruiting body formation by Bacillus subtilis. *Proceedings of the National Academy of Sciences*. Vol. 98(20), pp. 11621–11626.

Bremer, P.J., Fillery, S., McQuillan, A.J. and Palmer, J.S. (2006) Cleaning-in-place in processing plants: chemical and physical considerations. *Food Engineering Reviews*. Vol. 2(2), pp. 107–122.

Bridier, A., Briandet, R., Thomas, V. and Dubois-Brissonnet, F. (2011) Resistance of bacterial biofilms to disinfectants: a review. *Biofouling*. Vol. 27(9), pp. 1017–1032.

Cámara, M., Rinaudo, M., Gebara, C., Leite, D.S., Solvi, M., Chauveheid, E. and Douterelo, I. (2022) Legionella biofilms: implications for public health and water systems. *Water Research*. Vol. 207, p. 117816.

Chen, C., Wang, H., Wang, Y., Li, X. and Ma, J. (2020) Disinfection by-products and their effects on the environment and human health in drinking water: A review. *Science of The Total Environment*. Vol. 713, p. 136654.

Costerton, J.W., Stewart, P.S. and Greenberg, E.P. (1999) Bacterial biofilms: a common cause of persistent infections. *Science*. Vol. 284(5418), pp. 1318–1322.

Donlan, R.M. (2002) Biofilms: microbial life on surfaces. *Emerging Infectious Diseases*. Vol. 8(9), pp. 881–890.

Douterelo, I., Jackson, M., Solomon, C., Boxall, J. and Fish, K.E. (2019) High flow rates affect the microbial ecology of drinking water biofilms. *Water Research*. Vol. 166, p. 115058.

Drescher, K., Dunkel, J., Nadell, C.D., van Teeffelen, S., Grnja, I., Wingreen, N.S., Stone, H.A. and Bassler, B.L. (2013) Architectural transitions in Vibrio cholerae biofilms at single-cell resolution. *Proceedings of the National Academy of Sciences*. Vol. 110(27), pp. 10783–10788.

Flemming, H.-C., Wingender, J., Szewzyk, U., Steinberg, P., Rice, S.A. and Kjelleberg, S. (2016) Biofilms: an emergent form of bacterial life. *Nature Reviews Microbiology*. Vol. 14(9), pp. 563–575.

Foudazi, R., Salehi, A., Mongrain, R.D. and Yeganeh, H. (2023) Mechanical properties and applications of hydrogels in biomedicine: A review. *Advanced Materials Interfaces*. Vol. 10(2), p. 2201330.

Galdino, A.C.M.S., Benevides, R.G. and Tenorio, M.A.C. (2020) Mechanical stress induces wrinkling in Bacillus subtilis biofilms. *Scientific Reports*. Vol. 10(1), p. 16650.

Gao, D.W., Liu, L., Liang, H. and Wu, W. (2011) Performance of a pilot-scale membrane bioreactor system under intermittent aeration and backwashing operation. *Bioresource Technology*. Vol. 102(3), pp. 2393–2397.

Gasperotti, A., Mazzoleni, S., Baglioni, A. and Bruno, L. (2020) Phenotypic heterogeneity in bacterial populations: a role in biofilm formation? *Microorganisms*. Vol. 8(12), p. 1845.

Hodges, S.R., Picioreanu, C., van Loosdrecht, M.C.M. and Heijnen, J.J. (2004) Biofilm formation in porous media under bidirectional flow conditions. *Biotechnology and Bioengineering*. Vol. 87(4), pp. 443–450.

Horn, H. and Morgenroth, E. (2006) Transport of oxygen, sodium chloride, and sodium nitrate in biofilms. *Chemical Engineering Science*. Vol. 61(5), pp. 1347–1356.

Ido, Y., Nagai, H., Shimizu, K., Nakanishi, Y., Iwaki, T., Watanabe, Y., Fukuda, J. and Taya, M. (2020) Biofilms as colloidal hydrogels: understanding biofilm mechanics. *Biofilm*. Vol. 2, p. 100028.

Jia, Y., Sun, H., Xie, X., Liu, Q. and Zhang, C. (2017) Oscillatory flow suppresses Pseudomonas aeruginosa biofilm formation. *Biofouling*. Vol. 33(5), pp. 405–415.

Kalamara, M., Spacapan, M., Mandic-Mulec, I. and Stanley-Wall, N.R. (2018) Quorum sensing drives the evolution of cooperation in Bacillus subtilis. *eLife*. Vol. 7, p. e35404.

Kedebe, D. and Winger, M. (2021) The effect of netting porosity on drag forces in aquaculture systems: A CFD study. *Aquacultural Engineering*. Vol. 93, p. 102170.

Khatoon, Z., McTiernan, C.D., Suuronen, E.J., Mah, T.F. and Alarcon, E.I. (2018) Bacterial biofilm formation on implantable devices and approaches to its treatment and prevention. *Heliyon*. Vol. 4(12), p. e01067.

Khu, D.-H., Changchun, H. and Wang, X. (2023) Biofilm morphology under various flow velocities in drinking water systems. *Journal of Environmental Management*. Vol. 330, p. 117099.

Kim, S., Lee, D.W., Kang, D.H., Kim, J., Jeong, Y. and Choi, H.J. (2016) Ginkgo biloba leaf extract inhibits biofilm formation of Pseudomonas aeruginosa. *International Journal of Molecular Sciences*. Vol. 17(1), p. 38.

Kurz, M.H., Reischke, M., Agrawal, P., Weinrich, S., Morgenroth, E. and Derlon, N. (2022) Hydrodynamic modulation of biofilm structure and function: effects on microbial diversity and detachment. *Water Research*. Vol. 212, p. 118114.

Lee, J., Kim, Y.J., Shin, S.Y., Lee, W.K., Lee, M.H. and Park, J.H. (2013) Antibacterial and antibiofilm activities of Ginkgo biloba extract against oral pathogens. *Journal of Medicinal Plants Research*. Vol. 7(40), pp. 2965–2971.

Lee, S.H., Secchi, E. and Kang, P.K. (2023) Rapid formation of bioaggregates and morphology transition to biofilm streamers induced by pore-throat flows. *Proceedings of the National Academy of Sciences of the United States of America*. Vol. 120(14), e2204466120.

Lenhart, J.J., Mehta, A.P., Ray, R.I., Lee, J.S. and Little, B.J. (2014) Microbially influenced corrosion in petroleum pipelines. *Journal of Pipeline Systems Engineering and Practice*. Vol. 5(1), p. 04013011.

Li, B., Bishop, D., Shao, J., Wu, C. and Nguyen, C. (2016) Oscillatory shear stresses regulate biofilm growth and architecture. *Biotechnology and Bioengineering*. Vol. 113(6), pp. 1270–1279.

Limoli, D.H., Jones, C.J. and Wozniak, D.J. (2015) Bacterial extracellular polysaccharides in biofilm formation and function. *Microbiology Spectrum*. Vol. 3(3).

Liu, Y. and Tay, J.H. (2002) The essential role of hydrodynamic shear force in the formation of biofilm and granular sludge. *Water Research*. Vol. 36(7), pp. 1653–1665.

López, D., Vlamakis, H., Losick, R. and Kolter, R. (2009) Generation of multiple cell types in Bacillus subtilis. *FEMS Microbiology Reviews*. Vol. 33(1), pp. 152–163.

Martínez-García, E., Calles, B., Arévalo-Rodríguez, M., de Lorenzo, V. and Santero, E. (2018) A microfluidic platform for studying biofilm formation and dispersal in Pseudomonas putida. *Environmental Microbiology*. Vol. 20(11), pp. 4124–4135.

Melo, L.F. and Bott, T.R. (1997) Biofouling in water systems. *Experimental Thermal and Fluid Science*. Vol. 14(4), pp. 375–381.

Miller, M.B. and Bassler, B.L. (2001) Quorum sensing in bacteria. *Annual Review of Microbiology*. Vol. 55, pp. 165–199.

Mishra, M., Aggarwal, S. and Khan, M.S. (2024) Biofilm-related infections: an emerging challenge for clinical treatment. *Frontiers in Microbiology*. Vol. 15, p. 123456.

Morawska, J., Hernandez-Valdes, J.A. and Kuipers, O.P. (2021) Diversity of bet-hedging strategies in microbial communities. *FEMS Microbiology Reviews*. Vol. 45(3), p. 060.

Purevdorj, B., Costerton, J.W. and Stoodley, P. (2002) Influence of hydrodynamics and cell signaling on the structure and behavior of Pseudomonas aeruginosa biofilms. *Applied and Environmental Microbiology*. Vol. 68(9), pp. 4457–4464.

Recupido, F., Cannas, D., Farci, A., Modolo, R., Bandiera, P., Pintus, G., Boi, F., Orrù, G. and Re, F. (2020) Impact of flow dynamics on biofilm structure and resistance. *Journal of Applied Microbiology*. Vol. 129(6), pp. 1465–1476.

Romeu, L., Douterelo, I., Fish, K.E. and Boxall, J.B. (2024) Spatial heterogeneity of shear stress shapes biofilm architecture in drinking water systems. *Water Research*. Vol. 246, p. 120660.

Rupp, C.J., Fux, C.A. and Stoodley, P. (2005) Development and architecture of Pseudomonas aeruginosa biofilms under flow conditions. *Applied and Environmental Microbiology*. Vol. 71(5), pp. 3026–3031.

Rusconi, R. and Stocker, R. (2015) Microbes in flow. *Current Opinion in Microbiology*. Vol. 25, pp. 1–8.

Seminara, A., Angelini, T.E., Wilking, J.N., Vlamakis, H., Ebrahim, S., Kolter, R., Weitz, D.A. and Brenner, M.P. (2012) Osmotic spreading of Bacillus subtilis biofilms driven by an extracellular matrix. *Proceedings of the National Academy of Sciences*. Vol. 109(4), pp. 1116–1121.

Stewart, P.S. (2003) Diffusion in biofilms. *Journal of Bacteriology*. Vol. 185(5), pp. 1485–1491.

Stewart, P.S. and Franklin, M.J. (2008) Physiological heterogeneity in biofilms. *Nature Reviews Microbiology*. Vol. 6(3), pp. 199–210.

Stoodley, P., Boyle, J.D., Lappin-Scott, H.M. and Elliott, T.S.J. (1994) Biofilm detachment in turbulent flow. *Biotechnology and Bioengineering*. Vol. 43(5), pp. 622–631.

Stoodley, P., Lewandowski, Z., Boyle, J.D. and Lappin-Scott, H.M. (1999) Biofilm structure and flow dynamics in laminar and turbulent flow reactors. *Water Research*. Vol. 33(1), pp. 122–132.

Stoodley, P., Sauer, K., Davies, D.G. and Costerton, J.W. (2002) Biofilms as complex differentiated communities. *Annual Review of Microbiology*. Vol. 56, pp. 187–209.

Sung, K., Chong, S.H. and Chung, J. (2023) Aerodynamic performance of porous road signs in crosswinds. *Journal of Wind Engineering and Industrial Aerodynamics*. Vol. 236, p. 105325.

Tolker-Nielsen, T. and Sternberg, C. (2011) Growing and analyzing biofilms in flow cells. *Current Protocols in Microbiology*. Vol. 21(1), pp. 1B.2.1–1B.2.17.

Trejo, M., Douarche, C., Bailleux, V., Poulard, C., Mariot, S., Regeard, C. and Raspaud, E. (2013) Elasticity and wrinkled morphology of Bacillus subtilis pellicles. *Proceedings of the National Academy of Sciences*. Vol. 110(6), pp. 2011–2016.

Trusz, T., Hall, M.J., Burton, S.G. and Gouws, P.A. (2024) Disinfectant resistance in drinking water biofilms. *Environmental Science & Technology*. Vol. 58(4), pp. 2674–2683.

Tsagkari, E., Douterelo, I., Wang, H., Fisher, M., Vieira, J., Ye, X. and Boxall, J. (2022) Shear stress promotes multispecies biofilm formation and community diversity in drinking water systems. *npj Biofilms and Microbiomes*. Vol. 8(1), p. 28.

van Gestel, J., Vlamakis, H. and Kolter, R. (2015) From cell differentiation to cell collectives: Bacillus subtilis uses division of labor to migrate. *PLoS Biology*. Vol. 13(4), p. e1002141.

Veening, J.W., Smits, W.K. and Kuipers, O.P. (2008) Bistability, epigenetics and bet-hedging in bacteria. *Annual Review of Microbiology*. Vol. 62, pp. 193–210.

Vlamakis, H., Aguilar, C., Losick, R. and Kolter, R. (2013) Sticking together: building a biofilm the Bacillus subtilis way. *Nature Reviews Microbiology*. Vol. 11(3), pp. 157–168.

Wang, H., Liu, Y., Wang, J., Liu, S., Xu, H. and Chen, F. (2014) Effect of flow velocity on biofilm formation and microbial community structure in rotating annular reactors. *Science of the Total Environment*. Vols. 466–467, pp. 579–585.

Wang, Y., Wang, D., Zhang, L., Wang, Y., Wu, Z., Liu, C. and Han, X. (2021) Antibacterial and antibiofilm effects of Ginkgo biloba extract against Pseudomonas aeruginosa. *Frontiers in Microbiology*. Vol. 12, p. 676345.

Wang, Y., Liu, H., Huang, L., Li, Z., Zhang, Z. and Peng, H. (2022) Ginkgo biloba leaf extract inhibits bacterial quorum sensing and biofilm formation. *Journal of Applied Microbiology*. Vol. 133(2), pp. 916–928.

Wilking, J.N., Zaburdaev, V., De Volder, M., Losick, R., Brenner, M.P. and Weitz, D.A. (2012) Liquid transport facilitated by channels in Bacillus subtilis biofilms. *Proceedings of the National Academy of Sciences*. Vol. 109(36), pp. 14038–14043.

Wilking, J.N., Angelini, T.E., Seminara, A., Brenner, M.P. and Weitz, D.A. (2013) Biofilms as complex fluids. *MRS Bulletin*. Vol. 38(4), pp. 271–276.

Wu, X., Wang, H., Lu, Z., Zhang, J. and Chen, Y. (2017) Effect of bidirectional backwashing on membrane fouling mitigation and microbial community in a membrane bioreactor. *Bioresource Technology*. Vol. 229, pp. 165–172.

Xavier, J.B., Picioreanu, C., Rani, S.A., van Loosdrecht, M.C.M. and Stewart, P.S. (2005) A framework for multidimensional modeling of activity and structure of multispecies biofilms. *Environmental Microbiology*. Vol. 7(8), pp. 1085–1103.

Yan, J., Moreau, H.D., Khodaparast, S., Perazzo, A., Feng, J., Vallotton, P., Heydari, T., Yawata, Y., Hobley, L., Biais, N., Doyle, P.S. and Persat, A. (2016) Environmental conditions regulate the impact of mechanical forces on bacterial aggregation. *Nature Communications*. Vol. 7, p. 12955.

Zhang, Q., Lambert, G., Liao, D., Kim, H., Robin, K., Tung, C.K., Pourmand, N. and Austin, R.H. (2011) Channel formation in Pseudomonas aeruginosa biofilms is controlled by intercellular signaling and nutrient availability. *Proceedings of the National Academy of Sciences*. Vol. 108(17), pp. 7280–7285.

Zhang, R., Yang, H., Liu, Y., Zhang, Z. and Xu, W. (2016) Effect of flow direction change on biofilm development and detachment in an alternating pumping pipeline. *Water Research*. Vol. 88, pp. 119–127.

Zhang, Y., Wang, X., Wang, Y., Zhang, C. and Wang, D. (2018) Antimicrobial activity of Ginkgo biloba extract against multidrug-resistant Staphylococcus aureus. *Phytotherapy Research*. Vol. 32(4), pp. 698–704.

# 5. Gene Expression Rewiring and Biofilm Morphogenesis in *Bacillus subtilis* Exposed to *Ginkgo biloba* Leaf Extract and Fluid Flow

# 5.1. Abstract

Biofilm formation in *Bacillus subtilis* is a complex, multicellular process tightly regulated by gene expression networks controlling matrix production, motility, stress response, and developmental pathways. These regulatory systems allow bacterial populations to adapt to environmental cues and form structured, resilient communities. This study investigates the molecular response of *B. subtilis* to *Ginkgo biloba* leaf extract (GBLE) under static and unidirectional flow, as well as flow conditions alone.

Using RT-qPCR and RNA-Seq, this study shows that GBLE broadly represses genes involved in biofilm formation (*bslA*, *tasA*, *remB*, *slrR*), sporulation and competence (*spoOA*, *comK*), motility (*sigD*, *LytA*), and stress response (*sigM*, *dps*, *YerD*). Despite this, RNA-Seq revealed upregulation of oxidative stress (*hmoB*, *yhfE*), polyamine metabolism (*speD*), and ribosome-supporting genes (*rsuA*), suggesting selective activation of survival pathways. In flow-grown biofilms, GBLE treatment led to pronounced downregulation of RNA-processing genes (*rnpB*, *ssrA*), correlating with disrupted Van Gogh bundle formation and reduced biomass seen in microscopic analysis seen in previous chapters.

To investigate how fluid dynamics influence biofilm development, gene expression in static, unidirectional, and bidirectional flow-grown biofilms was compared using RNA-Seq. Flow conditions broadly enhanced transcriptional activity, with bidirectional flow showing the greatest upregulation of RNA processing, stress-related, and developmental genes, including *rnpB* and the *skf* operon. This corresponded with the emergence of complex architectures such as Van Gogh bundles, ropes, folds, and channels seen in previous chapters. In contrast, unidirectional flow induced less structural organisation and a narrower transcriptional response.

Together, these findings highlight the impact of phytochemical and mechanical cues on *B. subtilis* biofilm formation. Flow regime shapes transcriptional breadth and structural complexity, while GBLE independently suppresses core developmental pathways regardless of culture condition.

#### 5.2. Introduction

Bacillus subtilis (B. subtilis) is a well-studied model for bacterial multicellularity and biofilm formation and is widely used to investigate regulatory transitions between motile and sessile (matrix-producing) lifestyles (López et al., 2010) (Dergham et al., 2021). Biofilm development in B. subtilis is a tightly regulated process involving multiple layers of genetic control, tailored in response to environmental stimuli such as nutrient limitation, surface contact, and population density (Vlamakis et al., 2013). The process begins with the activation of the master regulator SpoOA, a transcription factor triggered by environmental signals which then modulates the expression of downstream genes associated with sporulation, matrix production, and biofilm initiation (Hamon and Lazazzera, 2001). When phosphorylated, SpoOA activates matrix gene expression indirectly by repressing abrB, a global transition state regulator that inhibits early stationary-phase genes (Strauch et al., 1990). The repression of abrB allows the expression of sinl, which antagonizes SinR, a master repressor of matrix genes (Vlamakis et al., 2013). Once SinR is inactivated, key structural genes such as epsA-O, which is responsible for exopolysaccharide production, and tapA-sipW-tasA, the operon encoding the amyloid fibres TasA essential for structural scaffolding, are expressed (Kearns et al., 2005) (Branda et al., 2001).

Subsequently, the gene bslA, encoding a hydrophobin-like protein, plays a crucial role in forming the hydrophobic coat that confers architectural integrity and water repellency to mature biofilms (Hobley et al., 2013). Transcriptional regulators such as SIrR and RemA/RemB further modulate biofilm development by regulating the expression of matrix genes and surface motility components in a mutually exclusive manner, facilitating the switch between biofilm formation and motility (Chai et al., 2008) (Winkelman et al., 2009). Other important regulators include alternative sigma factors like  $\sigma^AD$ ,  $\sigma^AM$ , and  $\sigma^AW$ , which govern responses to motility, cell envelope stress, and antimicrobial compounds, respectively (Helmann, 2002). In addition to matrix regulation, B. subtilis biofilm development is tightly connected to cellular differentiation pathways, such as sporulation and competence, which are

coordinated with environmental stress responses through regulatory quorum sensing (Lopez et al., 2009) (Vlamakis et al., 2013).

Although much of our understanding of B. subtilis biofilms has been derived from planktonic culture models and colony-agar biofilms, bacterial communities growing in natural and industrial environments are often subjected to dynamic fluid conditions such as hydrodynamic shear, fluctuating nutrient/oxygen delivery, and pressure (Stewart and Franklin, 2008). These physical forces can significantly influence biofilm architecture, gene expression, and resistance to antimicrobial agents (Pereira et al., 2002) (Islam et al., 2014). The development of transparent flow cells and micro-/millifluidic platforms, combined with transcriptomic or fluorescent reporter assays, has demonstrated that shear history can reprogramme bacterial adhesion, matrix production, metabolism, and gene expression. For example, Streptococcus gordonii (S. gordonii) oral biofilms subjected to rocker-induced shear showed substantial transcriptomic reprogramming (Nairn et al., 2024), Pseudomonas (P. aeruginosa) cells exposed to microfluidic shear exhibited altered aeruginosa transcriptional profiles and biofilm physiology (Sanfilippo et al., 2019), and Escherichia coli (E. coli) monolayers grown in microfluidic channels displayed increased phenotypic heterogeneity in cell division and attachment under variable shear conditions (Hubert et al., 2024). Time-varying or oscillatory shear frequently supports thicker or more structured communities than steady flow in P. aeruginosa and S. gordonii, implying active mechanosensing that cannot be explained by mass transfer alone (Tsagkari et al., 2022) (Nairn et al., 2024). Hydrodynamic regime has also been linked to large-scale morphological transitions (pillars, streamers) and to shifts in developmental and stress loci, including recent analyses of friction-driven streamer growth under controlled flow (Wittig et al., 2025) (Valiei et al., 2012). Despite these advances, molecular interrogation of flow-grown biofilms remains limited by inconsistent shear quantification, low RNA yield, scarce datasets that pair mechanics with omics, and the still emerging integration of single-cell or spatial transcriptomics into shear-defined systems (Thomen et al., 2017) (Valiei et al., 2018) (Tsagkari et al., 2022) (Nairn et al., 2024). The work presented here addresses several of these gaps by comparing static, unidirectional, and bidirectional flow regimes in B. subtilis and linking transcriptional programmes with emergent architectures.

Moreover, conventional chemical biocides used to control biofilms raise concerns regarding environmental impact and resistance development, prompting interest in natural, plant-

derived alternatives. *Ginkgo biloba* leaf extract (GBLE) has been reported to possess antimicrobial and antioxidant properties, but its effects on bacterial biofilm gene regulation, particularly under hydrodynamic conditions, remain poorly understood.

This study aims to investigate the impact of GBLE on *B. subtilis* biofilm formation and gene expression under both static and flow-based environments. While the previous chapters focused on the morphological characteristics of biofilms using imaging techniques, including confocal microscopy and quantitative structural analysis, this chapter shifts focus toward the underlying molecular mechanisms. Using a combination of RT-qPCR and RNA Sequencing, we assessed the expression of key genes involved in matrix production, stress response, sporulation, and transcriptional regulation in response to GBLE treatment. Additionally, the study aims to investigate how unidirectional and bidirectional flow alone influence gene expression and biofilm-associated phenotypes to better reflect the complexity of real-world environments such as industrial pipelines, medical devices, and natural habitats. This dual approach provides insight into how bacterial communities respond to mechanical stresses and into how plant-based antibiofilm agents interact with bacterial regulatory networks.

This integrative approach is the first to evaluate the transcriptional response of *B. subtilis* biofilms to a natural antibiofilm agent and dynamic flow conditions. It offers novel insights into how mechanical forces and phytochemical treatments intersect to shape biofilm behaviour. The findings from this chapter contribute to a deeper understanding of bacterial adaptation in complex environments and may inform the development of more effective, plant-based strategies for biofilm control in both clinical and industrial settings.

#### 5.3. Material and Methods

## 5.3.1. Growth conditions

#### 5.3.1.1. Planktonic Experiments

Experiments were carried out to investigate the effect of GBLE on *B. subtilis* cultures grown in planktonic conditions at a transcriptional level. The same growth conditions were applied as in Chapter 2. In summary, conical flasks containing 300 mL of Luria-Bertani (LB) broth supplemented with a range of GBLE concentrations (0, 50, 75, 100, 150, 175, 200, 300, 400, 500 and  $600 \,\mu\text{g/mL}$ ) were inoculated with *B. subtilis* JWV042 glycerol stock and incubated for 48 hours at 37°C in a shaking incubator. The cultures were supplemented with 5  $\,\mu\text{g/mL}$  chloramphenicol to ensure selection of gfp mutants. Planktonic growth was carried out in

quadruplicates, using freshly prepared cultures to ensure biological replication, unless stated otherwise.

#### 5.3.1.2. Biofilms under Fluid Flow

Further experiments were carried out to investigate biofilm growth under fluid flow at a transcriptional level. *B. subtilis* biofilms were grown under two types of fluid flow: unidirectional and bidirectional flow. In another set of experiments, the same unidirectional and bidirectional flow experiments were performed with the addition of a continuous supply of 400 µg/mL GBLE. All experiments were carried out in triplicates on separate occasions, using freshly prepared cultures to ensure biological replication, unless stated otherwise. RNA was extracted from the outflow of the flow systems. A detailed description of growth conditions and flow cell set-ups is described in chapter 3 (Fig. 3.1, for unidirectional flow) and chapter 4 (Fig. 4.1, for bidirectional flow).

Bacterial cells were then collected from the flow systems for RNA extraction.

#### 5.3.2. Total RNA Isolation

1 mL of the bacterial culture obtained from each experiment was centrifuged at maximum rpm for 15 minutes. After discarding the supernatant, the bacterial pellet was resuspended in 5 volumes of RNA/ater (RNA|ater™ Stabilization Solution – Invitrogen™) and incubated for 30 minutes at room temperature. The sample was centrifuged once again, supernatant was removed and the pellet was resuspended in TE buffer (50 mM Tris, 20 mM EDTA) supplemented with 10 mg/mL lysozyme (Thermo Scientific™) and incubated at 30°C for 30 minutes. 50 μL of 10% SDS (UltraPure™ SDS Solution, 10%, Invitrogen™) and 85 μL of 5M NaCl solution were added to the sample, followed by 1 mL of TriZol reagent. Prior to vortexing the sample for 15 seconds, 300 μL of chloroform were pipetted into the sample. Subsequently, the sample was centrifuged at maximum speed for 10 minutes. Total RNA purification was performed following manufacturer's kit instructions (TRIzol™ Plus RNA Purification Kit - Invitrogen™). RNA purity and quality was checked by assessing the 280/260 ratio detected using BioTek Gen5.

# 5.3.3. cDNA Synthesis and Reverse Transcription Quantitative Polymerase Chain Reaction (RT-qPCR)

RNA was converted into cDNA using High-Capacity RNA-to-cDNA™ Kit (Applied Biosystems™) following manufacturer's instructions. The cDNA product was diluted accordingly for a final concentration of 4 ng per reaction.

RT-qPCR was used to investigate the genetic expression of genes that govern motility, sporulation, competency, autolytic activity and ECM synthesis and transcription regulation in *B. subtilis* in presence of different concentration of GBLE. The primers used in this study were designed using Primer-BLAST (NCBI) and optimal primer concentrations were determined using the Primer Concentration Optimization Protocol by Sigma-Aldrich. Using cDNA as the template for the qPCR reaction, the latter was carried out using GoTaq® qPCR Kit (Promega). RT-qPCR was carried on RNA extracted from the planktonic cultures only.

Primer sequences can be found in the appendix (see Table S5.1).

Data analysis was carried out according to the  $\Delta\Delta$ Ct method. Ct values were obtained for each gene of interest, as well as for two reference genes, 16srRNA and AroE, which were selected based on their stable expression. For each sample, the  $\Delta$ Ct value was calculated by subtracting the average Ct of the reference genes from the Ct of the target gene. To determine treatment-induced changes in gene expression,  $\Delta\Delta$ Ct values were calculated by comparing the  $\Delta$ Ct of each treated sample to the mean  $\Delta$ Ct of the corresponding gene in the control group. Fold changes in expression were then derived using the 2^- $\Delta\Delta$ Ct method (Livak and Schmittgen, 2001). Group-wise comparisons between treated and control samples were conducted using unpaired t-tests, and results were visualized as boxplots and annotated significance thresholds (p < 0.05). All analyses and plots were performed in R.

# 5.3.4. RNA-Seq, Data Processing and Differential Expression Analysis

To complement the targeted analysis provided by RT-qPCR, which is limited to the specific genes selected for investigation, RNA Sequencing (RNA-Seq) was employed as a global transcriptomic approach. Unlike RT-qPCR, RNA-Seq allows for an unbiased, genome-wide assessment of gene expression, enabling the identification of both known and novel transcriptional changes in response to treatment and flow conditions. RNA-seq analysis was carried out to get a more broad understanding of the effects of GBLE as well as fluid flow forces on *B. subtilis* cultures. The RNA extracted from planktonic cultures with 0, 400 and

600 μg/mL and the RNA extracted from the flow system experiments was sent to MVLS Shared Research Facilities – University of Glasgow. RNA sequencing was performed using a ribosomal RNA depletion adapted to bacterial samples. Total RNA was first treated with Qiagen FastSelect –5S/16S/23S (bacteria) to deplete rRNA and enrich for mRNA. Library preparation was carried out using the Illumina TruSeq Stranded Total RNA Library Prep Kit. Paired-end sequencing (2×100 bp) was conducted on an Illumina platform, aiming to generate approximately 10 million reads per sample.

RNA-Seq data processing was carried out in part on Galaxy (https://usegalaxy.org/) and R.

After quality control (FastQC) and adapter trimming (Cutadapt), reads were aligned to the *B. subtilis* BS3610 reference genome using HISAT2, and gene-level counts were obtained using featureCounts. Due to the lack of available reference genome for *B. subtilis* JWV042, *B. subtilis* BS3610 reference genome was used.

The resulting count matrix was imported into R for downstream analysis. Differential gene expression was performed using the DESeq2 package (Love et al., 2014). DESeq2 normalises raw count data to account for differences in sequencing depth and RNA composition between samples by estimating *size factors* for each library. These size factors are calculated from the median ratio of observed counts for each gene relative to a pseudo-reference sample, ensuring that the majority of genes have similar expression distributions across conditions. This approach corrects for sample-specific biases so that observed differences in gene counts are more likely to reflect true biological variation rather than technical variability, thereby making the samples directly comparable for statistical analysis.

For visualisation and clustering, variance-stabilising transformation (VST) was applied to the normalised counts. VST reduces the dependence of the variance on the mean expression level, producing homoscedastic data that are more suitable for analysis and heatmap generation.

Genes with an adjusted p-value (padj) below 0.05 were considered differentially expressed (Benjamini and Hochberg, 1995). Heatmaps of these genes were generated to visualize expression patterns across conditions. Where possible, locus tags were mapped to gene names and annotated using BLAST-based transfer from the *B. subtilis* 3610 and 168 reference (Barbe et al., 2009) (Nicolas et al., 2012).

# 5.4. Results

# 5.4.1. RT-qPCR: planktonic cultures supplemented with GBLE

In order to understand the effect of GBLE on the gene expression of *B. subtilis* JWV042, RNA was extracted from a series of planktonic cultures supplemented with GBLE. The RNA was then converted into cDNA and the expression of genes involved in biofilm formation, stress response, motility and general transcription regulation was quantified using the  $\Delta\Delta$ Ct analysis method in R.

#### 5.4.1.1. Biofilm-Associated Genes

#### 5.4.1.1.1. Bs/A

The expression of number of genes that govern biofilm formation was quantified and box plots were generated to visualise the change of relative expression between samples.

The first gene investigated was bs/A, which encodes for a bacterial hydrophobin, essential for biofilm stability (Hobley et al., 2013). Analysis showed a significant reduction in bs/A expression in response to increasing concentrations of GBLE (Fig. 5.1). As seen in the control, bs/A expression levels were consistently high, with a median fold change of approximately 1.6. However, the addition of GBLE resulted to a concentration-dependent downregulation of bs/A expression. Even at 50 µg/mL GBLE, a significant decrease in expression was observed, which became progressively more pronounced at higher concentrations. Interestingly, the measurements obtained from the culture supplemented with 400 µg/mL GBLE reached statistical significance (p < 0.05, \*), while other mid-to-high concentrations showed weaker trends. These results suggest a biologically consistent downregulation but with limited statistical power at most concentrations, due to high biological variability or insufficient replicates in the control.

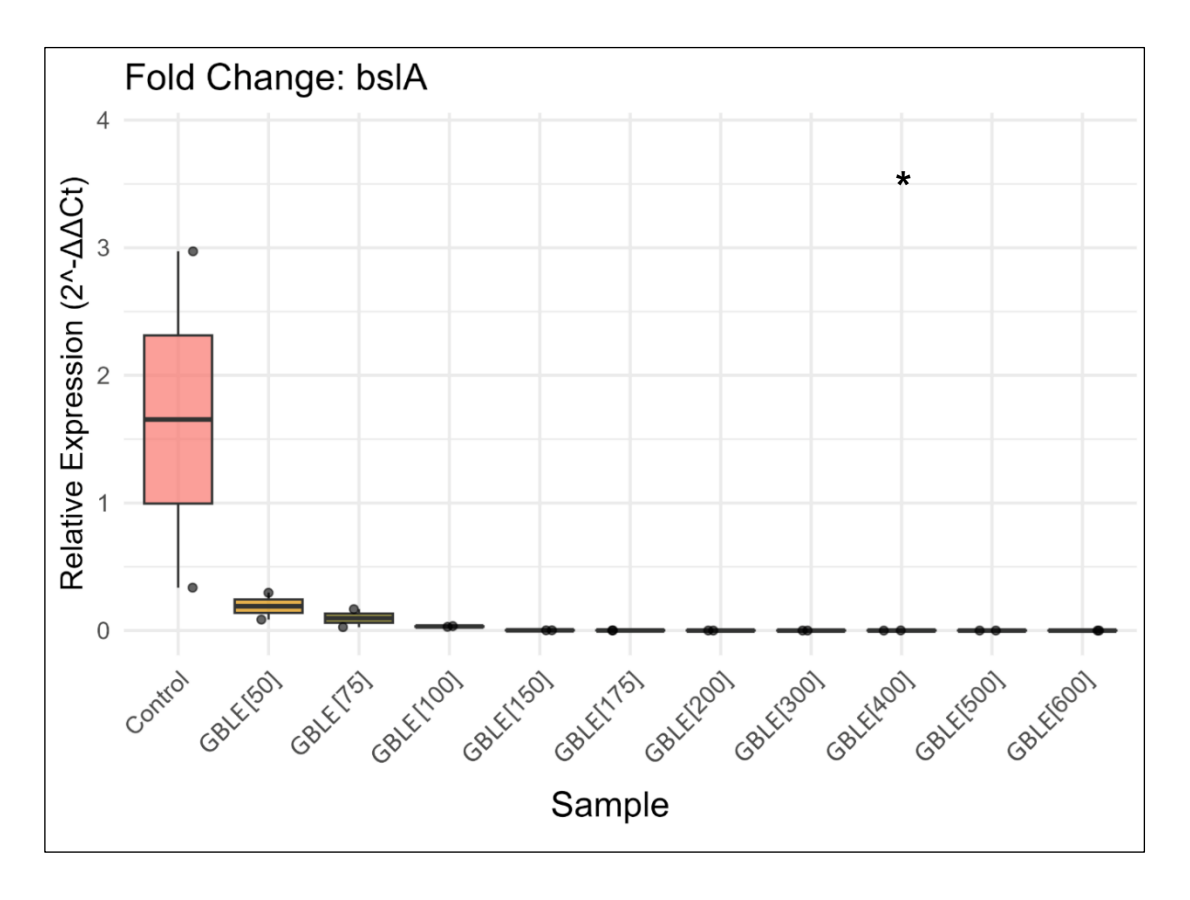


Figure 5.1. Relative expression of bslA in  $Bacillus\ subtilis$  planktonic cultures under increasing concentrations of GBLE, in  $\mu g/mL$ . RT-qPCR analysis shows fold change in bslA expression relative to the control condition. Boxes represent the interquartile range; horizontal lines indicate the median. P-value annotations are displayed above each group.

#### 5.4.1.1.2. TasA

The second biofilm-associated gene investigated was TasA. This gene encodes for a B. subtilis specific amyloid fibre, essential for biofilm stability and maturation (Romero et al., 2010). RT-qPCR analysis of TasA expression showed a noticeable reduction in expression in response to increasing concentrations of GBLE (Fig. 5.2). The control exhibited a median fold change of approximately 1.1. Mild repression was observed at lower doses (50–75  $\mu$ g/mL) with limited statistical support, while from 100  $\mu$ g/mL onwards, the reduction was marked and statistically significant. Cultures supplemented with concentrations 150, 175 and 200  $\mu$ g/mL yielded p-values < 0.01 (\*\*), while cultures grown with 100, 300, 500, and 600  $\mu$ g/mL maintained a p-value of < 0.05 (\*). This pattern reflects strong transcriptional silencing of TasA with high confidence across mid- to high-level treatments.

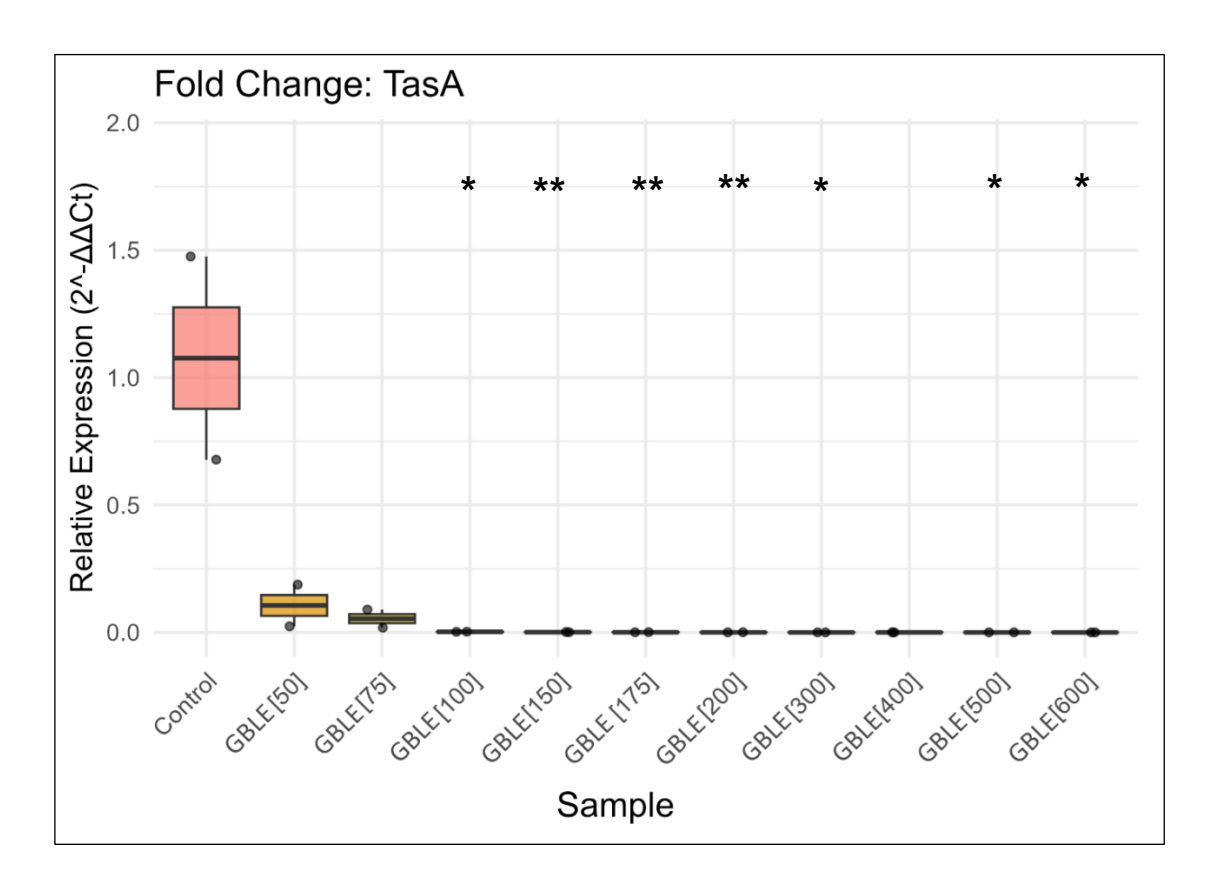


Figure 5.2. Relative expression of TasA in Bacillus subtilis planktonic cultures supplemented with increasing concentrations of GBLE, in  $\mu g/mL$ . RT-qPCR analysis shows fold change in TasA expression relative to the control condition. Boxes represent the interquartile range; medians are indicated by horizontal lines. P-value annotations are displayed above each group.

#### 5.4.1.1.3. SlrR

The third biofilm-associated gene targeted was sIrR, a key transcriptional regulator that works in coordination with SinR to control biofilm formation in B. subtilis, promoting matrix gene expression while repressing motility genes (Chai et al., 2010). Similarly to the genes described above, the expression of sIrR was strongly downregulated in response to increasing concentrations of GBLE (Fig. 5.3). The control group had a median fold of approximately 1.1, which sharply decreased at 50  $\mu$ g/mL GBLE and approached zero at higher concentration, highlight a concentration-dependent response. Early treatment points, 50 and 100  $\mu$ g/mL, showed no statistical significance, but from 150  $\mu$ g/mL onward, repression became statistically significant. Concentrations of 75, 150, 200, and 500  $\mu$ g/mL reached p-values less than 0.05 (\*), while 175, 300, and 600  $\mu$ g/mL resulted in p-values < 0.01 (\*\*).

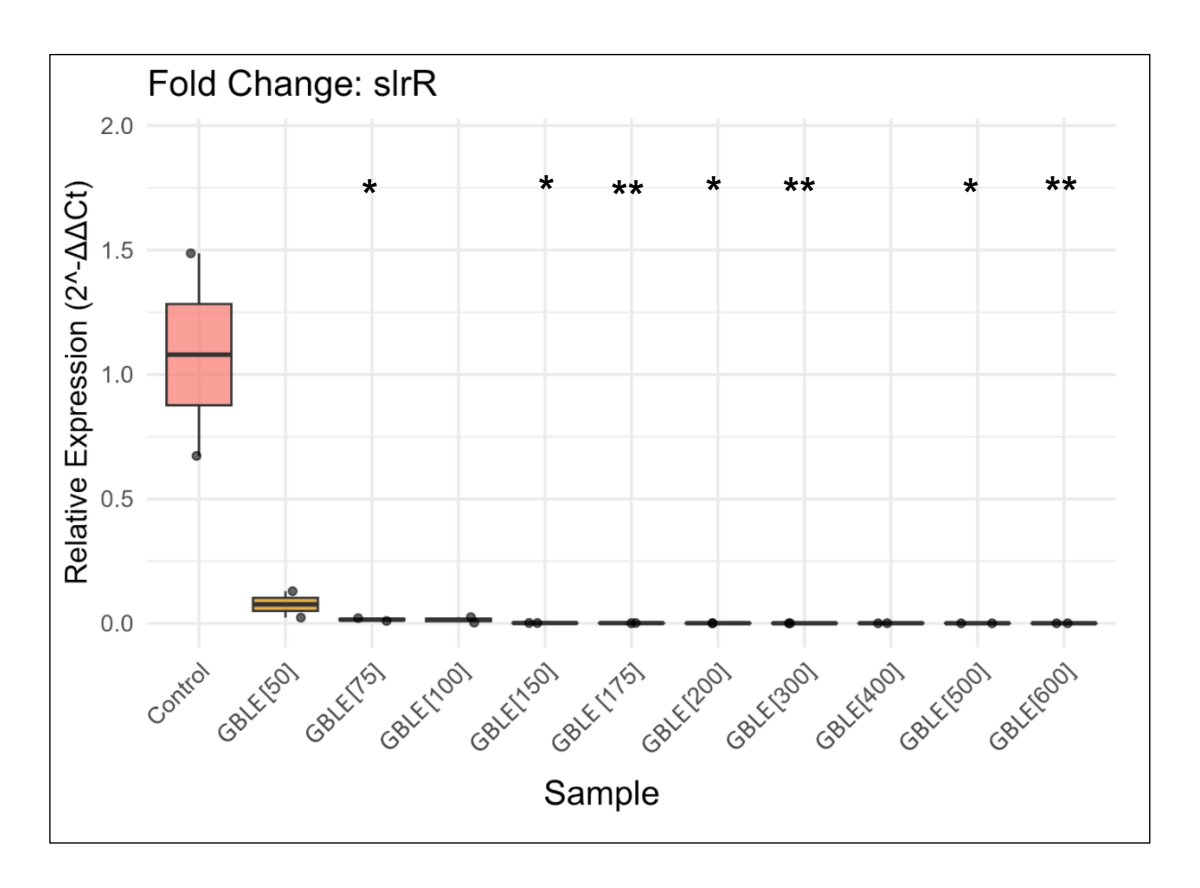


Figure 5.3. Relative expression of sIrR in Bacillus subtilis planktonic cultures under increasing concentrations of GBLE, in  $\mu g/mL$ . RT-qPCR analysis shows fold change in sIrR expression relative to the control condition. Boxes represent the interquartile range; medians are shown. P-value annotations are displayed above each group.

#### 5.4.1.1.4. RemB

remB is a regulatory gene involved in the development of biofilms in *B. subtilis*. It plays a role in supporting the production of matrix components and helps shape the overall structure of the biofilm (Kearns et al., 2005). In this study, expression of this gene was inhibited significantly with increasing GBLE concentrations, similarly to the previous biofilm-associated genes (Fig. 5.4). The addition of GBLE to the bacterial cultures rapidly led to a reduced expression of *remB*, reaching near-zero expression by 100 μg/mL GBLE. As previously seen, statistical significance was reached at concentrations of 100, 150, 175, and 300 μg/mL GBLE, which showed a p value of < 0.05 (\*). Higher concentrations of GBLE resulted in a stronger downregulating effect with p value < 0.01 (\*\*).

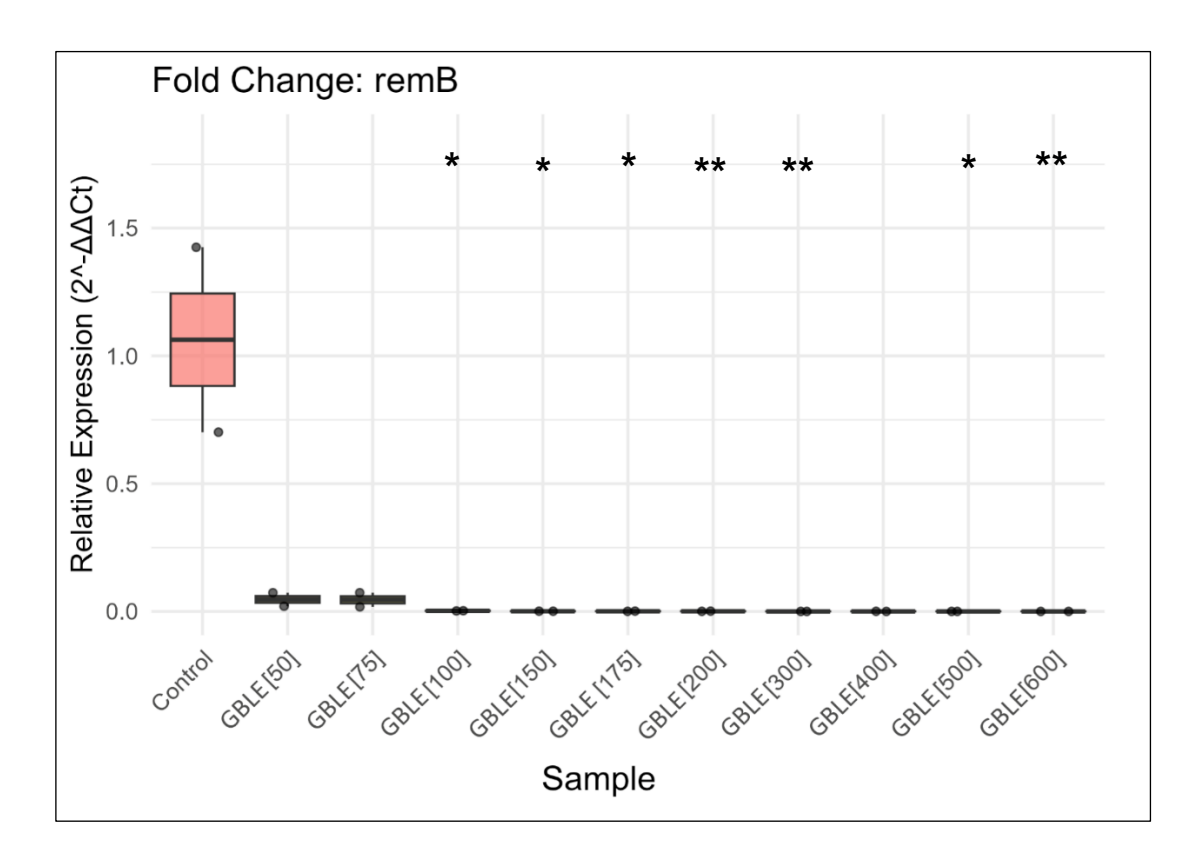


Figure 5.4. Fold change in *remB* expression in *Bacillus subtilis* planktonic cultures in response to increasing concentrations of GBLE, in  $\mu g/mL$ . RT-qPCR analysis shows fold change in *remB* expression relative to the control condition. Boxes reflect the interquartile range; medians are marked by horizontal lines. P-value annotations are displayed above each group.

#### 5.4.1.2. Sporulation and Competence

#### 5.4.1.2.1. SpoOA

*Spo0A* is the master regulator that initiates the sporulation process in *B. subtilis*. In addition to its role in sporulation, spo0A also plays a key role in biofilm development by activating genes involved in matrix production and repressing those associated with motility (Grossman, 1995) (Fujita et al., 2005). Upon addition of GBLE, spo0A showed significant transcriptional downregulation in response to increasing concentrations of GBLE (Fig. 5.5). Relative expression exhibited a consistent drop from a control median of approximately 1.1 to near zero levels at higher concentrations. Higher concentrations, 150 and 175 µg/mL achieved significance at p < 0.05 (\*), with concentrations of 200, 300 and 500 µg/mL yielding strong significance (p < 0.01 \*\*). Suppression persisted across higher concentrations, indicating robust downregulation of SpoOA upon addition of GBLE.

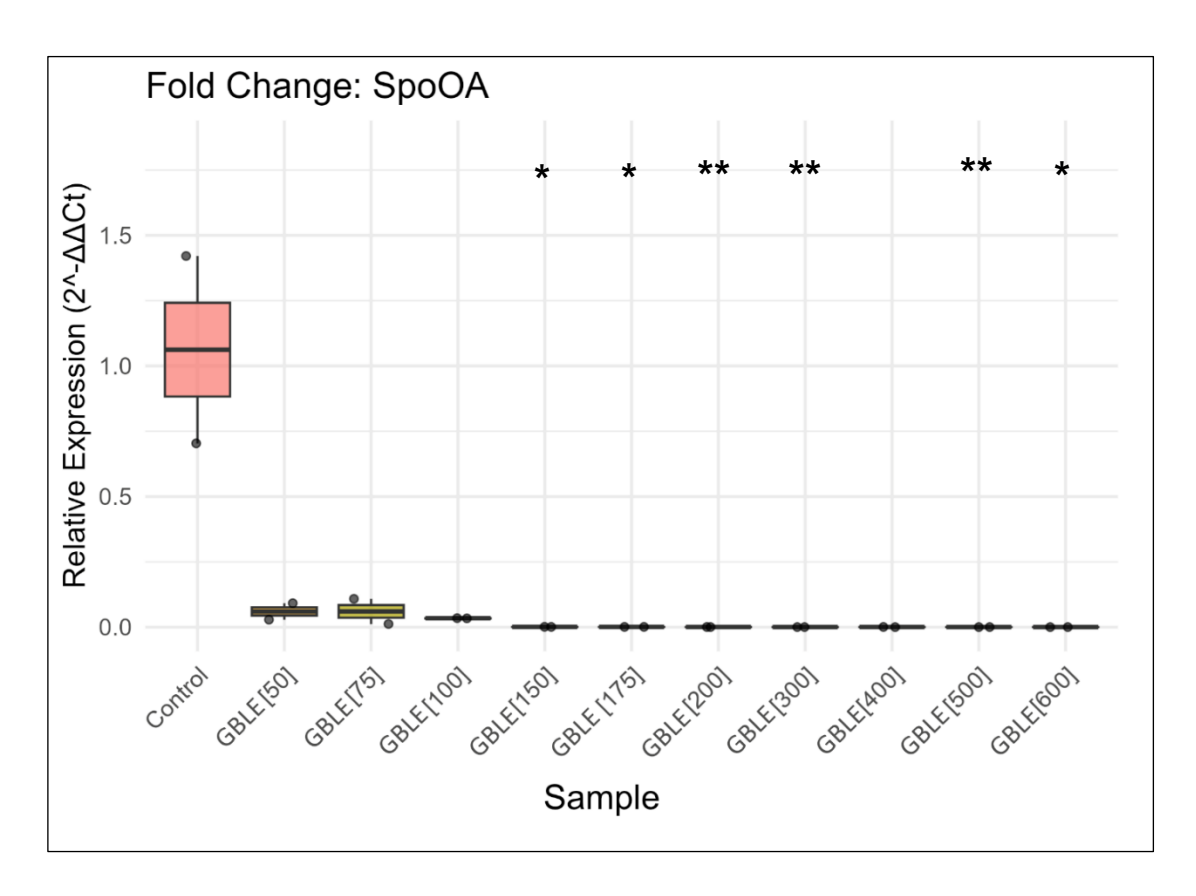


Figure 5.5. RT-qPCR analysis of *SpoOA* expression in *Bacillus subtilis* planktonic cultures following addition of increasing concentrations of GBLE, in  $\mu$ g/mL. RT-qPCR analysis shows fold change in *spoOA* expression relative to the control condition. Boxes show the interquartile range; medians are indicated. P-value annotations are displayed above each group.

# 5.4.1.2.2. ComK

Competency is the ability of bacteria to take up extracellular DNA and incorporate it into its genome. comK is competency transcription factor and plays a key role in entry into competency state (Hahn et al., 1995). RT-qPCR quantification of comK displayed a significant decrease in overall expression in response to increasing concentrations of GBLE (Fig. 5.6). Control samples showed a median fold change of approximately 1.3, while expression was rapidly downregulated below detectable levels at doses  $\geq$  100 µg/mL GBLE. Statistical significance was achieved between 175 and 300 µg/mL and at 600 µg/mL (p < 0.05; \*).

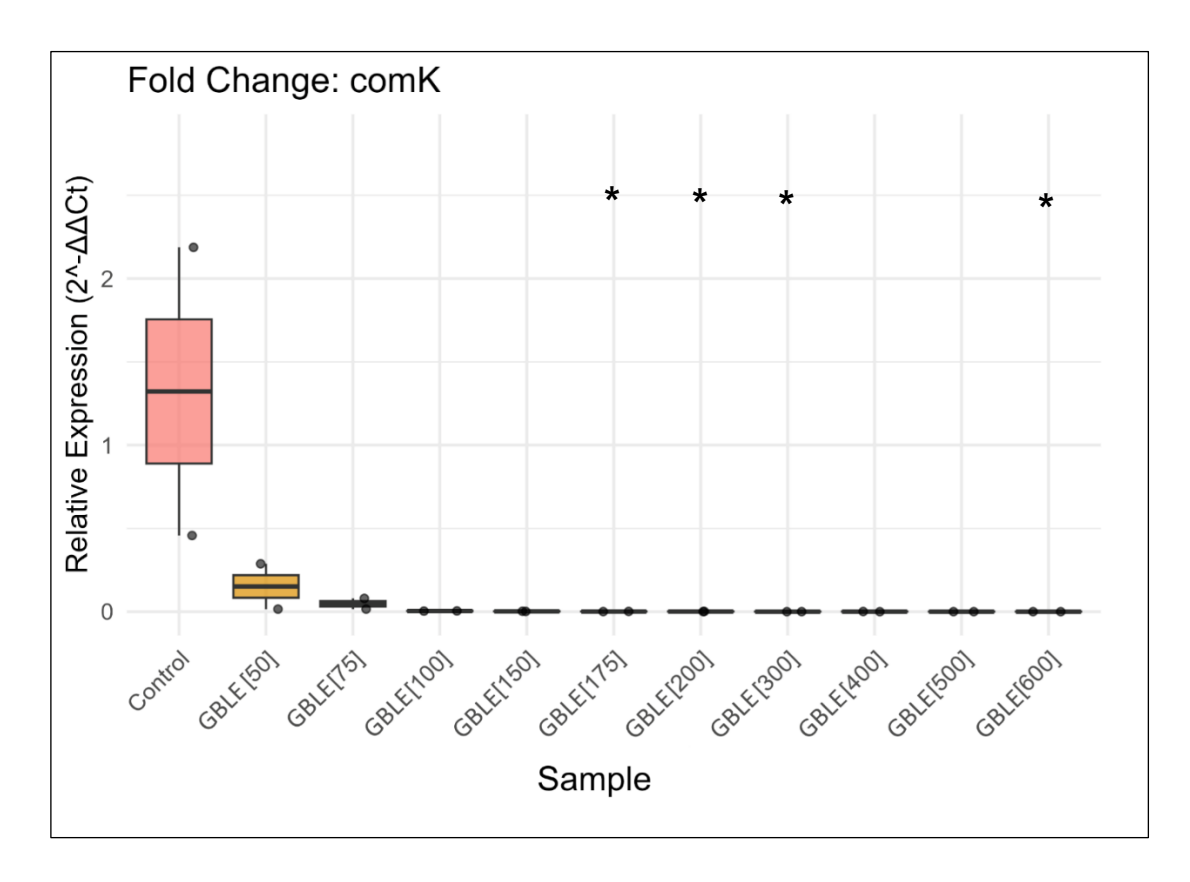


Figure 5.6. Fold change in comK expression in Bacillus subtilis planktonic cultures in response to increasing concentrations of GBLE in  $\mu g/mL$ . RT-qPCR analysis shows fold change in comK expression relative to the control condition. Boxes show interquartile range; medians are indicated by horizontal lines. P-value annotations are displayed above each group.

#### 5.4.1.3. Stress Regulation

Hypothesizing that GBLE was inducing a stress response in *B. subtilis* cultures, the expression of genes associated with stress response and adaptation was investigated using RT-qPCR.

#### 5.4.1.3.1. Dps

The *dps* gene is involved in oxidative stress protection in *B. subtilis*, where it encodes a DNA-binding protein that protects genomic DNA from damage by reactive oxygen species (Chen and Helmann, 1995). RT-qPCR analysis of *dps* showed consistent decrease in expression in response to increasing concentrations of GBLE (Fig. 5.7). Control samples exhibited a median expression of approximately 1.8, which was dramatically reduced even at 50  $\mu$ g/mL treatment. From 100  $\mu$ g/mL and up, *Dps* expression was nearly undetectable. However, only the culture treated with 400  $\mu$ g/mL GBLE yielding statistical significance (p < 0.05; \*).

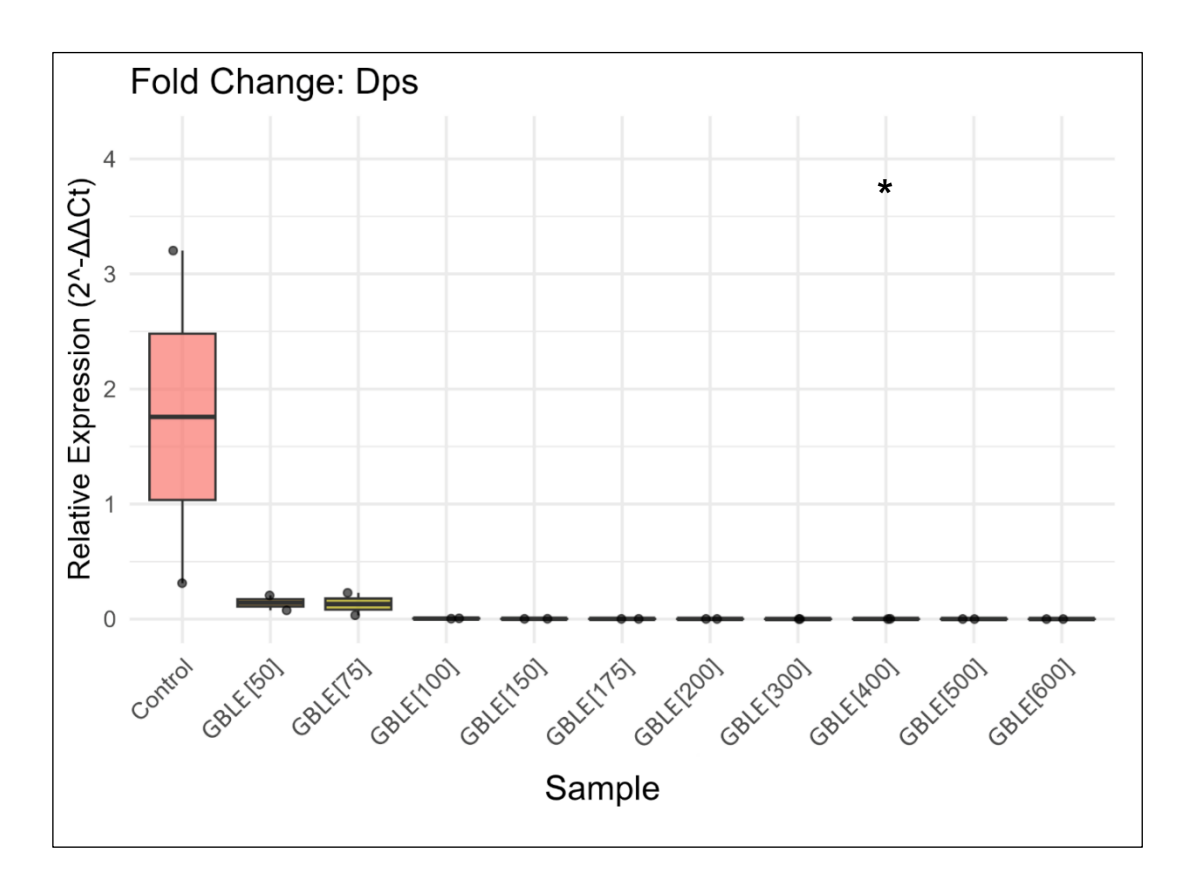


Figure 5.7. RT-qPCR analysis of Dps expression in Bacillus subtilis planktonic cultures under increasing concentrations of GBLE in  $\mu g/mL$ . RT-qPCR analysis shows fold change in dps expression relative to the control condition. Boxes show interquartile ranges, with horizontal bars indicating medians. P-value annotations are displayed above each group.

# 5.4.1.3.2. SigM

The sigM gene encodes an alternative sigma factor that plays a key role in the cell envelope stress response in B. subtilis, particularly in response to antibiotics and other agents that target the cell wall (Cao et al., 2002). RT-qPCR analysis revealed a strong genetic downregulation upon addition of GBLE (Fig. 5.8). The control group showed a median fold expression around 1.1, while expression dropped significantly from  $100 \, \mu g/mL$  GBLE and higher concentrations. Again, lower concentrations had weak to none statistical support, however significance became consistent from  $100 \, \mu g/mL$  GBLE upward (p < 0.05 \*, p < 0.01 \*\*).

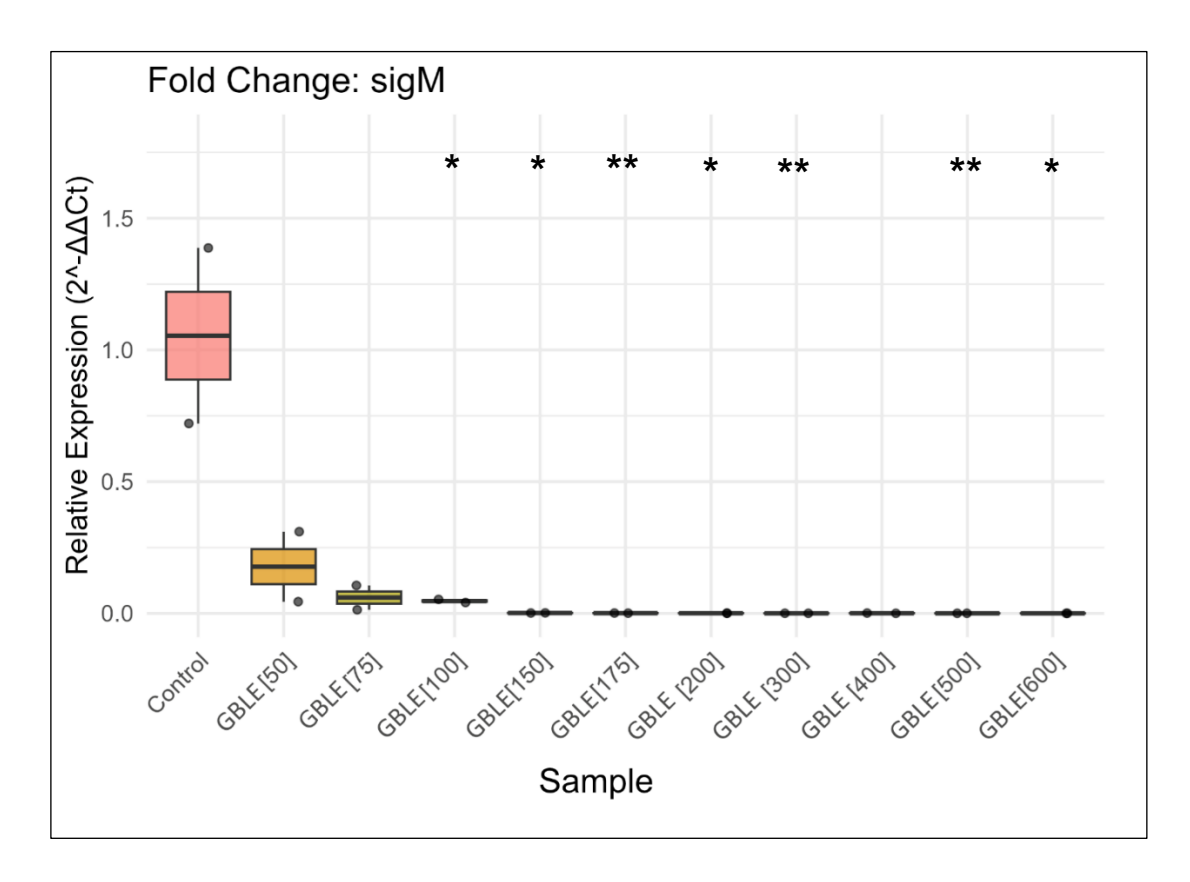


Figure 5.8. Expression of sigM in Bacillus subtilis planktonic cultures in response to increasing concentrations of GBLE, in µg/mL. RT-qPCR analysis shows fold change in sigM expression relative to the control condition. Boxplots represent interquartile ranges, with medians shown. P-value annotations are displayed above each group.

#### 5.4.1.3.3. YerD

yerD is a lesser characterized gene in *B. subtilis*, thought to be involved in adaptation to challenging environmental conditions, including stress and nutrient limitation (Nicolas et al., 2012). Similarly to previously analysed genes, yerD was substantially repressed across nearly all treatment cultures (Fig. 5.9). While the control group exhibited a median expression above 1.0, expression dropped sharply from 75 μg/mL GBLE onward. Statistical significance was achieved in most treated cultures with p values of < 0.05 (\*) and < 0.01 (\*\*). This suggests a strong and statistically supported downregulation of *YerD* with increasing concentrations of GBLE.

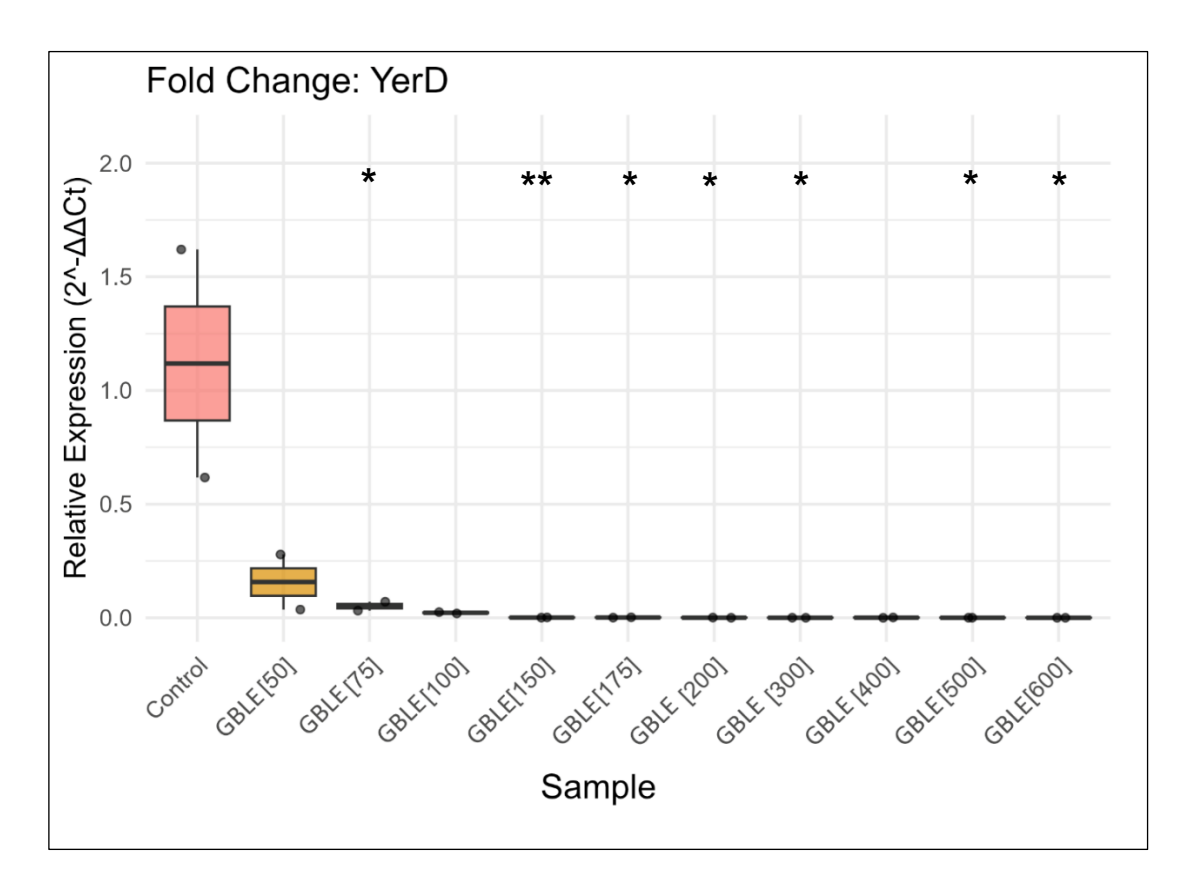


Figure 5.9. Expression of *YerD* in *Bacillus subtilis* planktonic cultures in response to increasing concentrations of GBLE in µg/mL. RT-qPCR analysis shows fold change in *yerD* expression relative to the control condition. Boxplots represent interquartile ranges, with medians shown. P-value annotations are displayed above each group.

#### 5.4.1.4. Transcription Regulation

In order to investigate the effect of GBLE on the expression of genes governing transcription regulation, key transcriptional regulators were quantified. While changes in the expression of these regulators can influence the expression of downstream genes, such effects are often context-dependent and may not lead to a uniform up- or downregulation of all genes (Fujita et al., 2005) (Britton et al., 2002) (Nicolas et al., 2012).

RT-qPCR analysis was performed to assess the expression of global transcriptional regulator *abrB* (Strauch et al., 1989), motility and flagella-related sigma factor regulator *SigD* (Helmann and Moran, 2002), and regulator of autolysin secretion *LytA* (Margot et al., 1999).

### 5.4.1.4.1. AbrB

Expression of global transcriptional regulator *abrB* decreased consistently with increasing GBLE concentrations (Fig. 5.10). While control samples had a median fold change of approximately 1.2, expression dropped sharply at 50 μg/mL and was nearly absent at 100

 $\mu$ g/mL and above. Importantly, several treatment groups demonstrated statistically significant differences: p < 0.05 (\*) for 150, 300, 500, and 600  $\mu$ g/mL; p < 0.01 (\*\*) for 175 and 200  $\mu$ g/mL. This pattern indicates a concentration-dependent transcriptional downregulation.

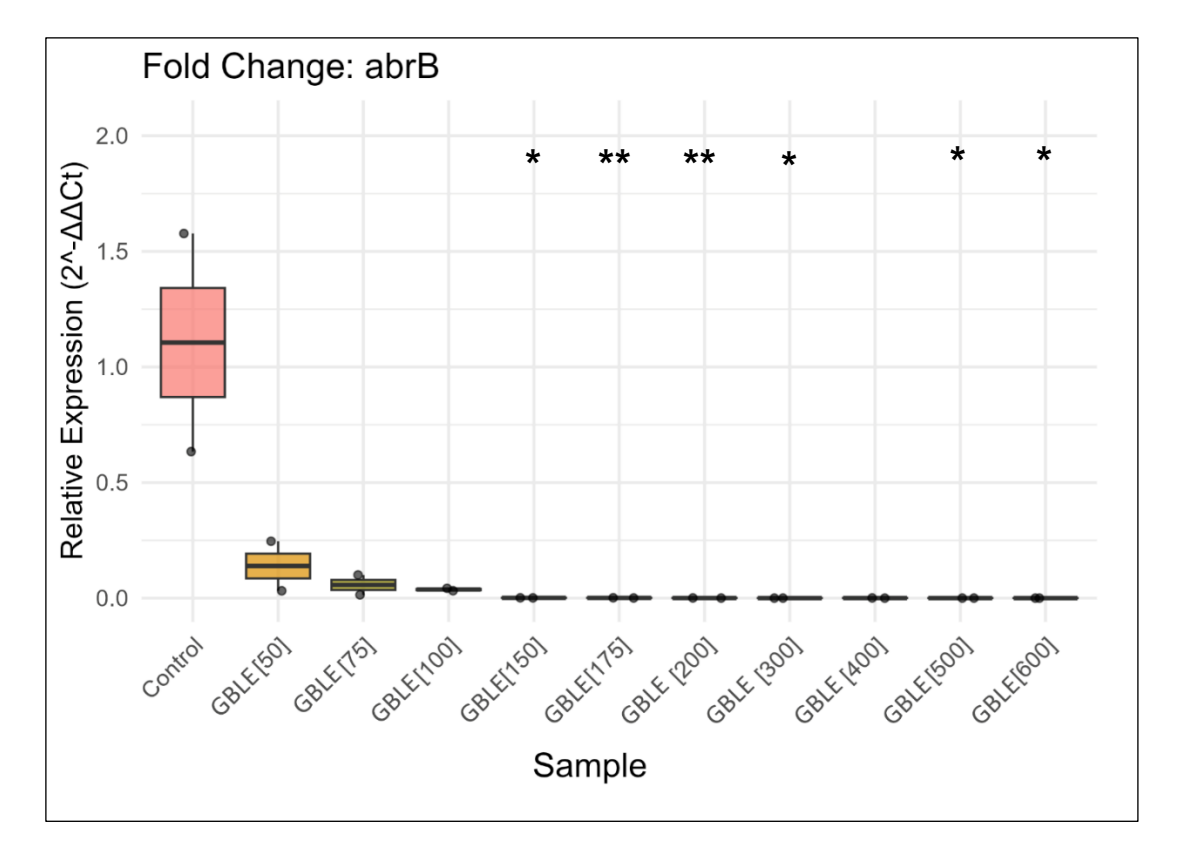


Figure 5.10. Fold change in *abrB* expression in *Bacillus subtilis* planktonic cultures treated with increasing concentrations of GBLE in µg/mL. RT-qPCR analysis shows fold change in *abrB* expression relative to the control condition. Boxplots represent interquartile ranges, with medians shown. P-value annotations are displayed above each group.

In order to investigate the effect of GBLE on the transcription regulation of motility, SigD gene expression was analysed in the RT-qPCR assay. Transcription of sigD showed a dramatic decrease in response to increasing concentrations of GBLE (Fig. 5.11). The control group showed consistent baseline expression of approximately 1.0, while all treated cultures displayed near-zero expression. Statistically significant downregulation was seen from  $100 \,\mu\text{g/mL}$  upward, with strong significance (p < 0.01, \*\*) at 100, 150, 300 and  $600 \,\mu\text{g/mL}$ , and moderate support (p < 0.05, \*) at 175 and  $200 \,\mu\text{g/mL}$ .

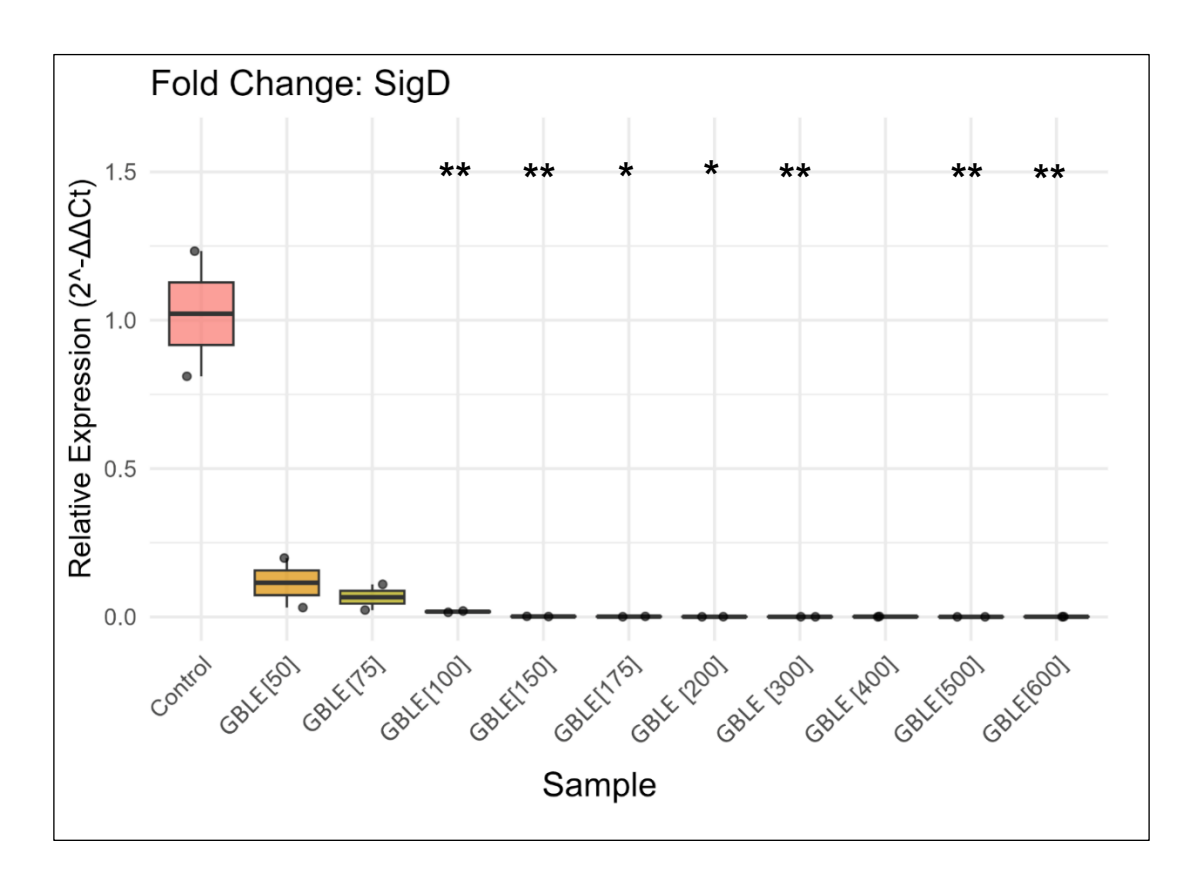


Figure 5.11. Expression profile of sigD in Bacillus subtilis planktonic cultures in response to increasing concentrations of GBLE in  $\mu g/mL$ . RT-qPCR analysis shows fold change in sigD expression relative to the control condition. Boxplots represent interquartile ranges, with medians shown. P-value annotations are displayed above each group.

#### 5.4.1.4.3. LytA

LytA is a gene often associated with cell wall turnover and autolysis as well as bacterial growth (Margot et al., 1999). RT-qPCR data indicated a significant decrease in expression with increasing GBLE concentration (Fig. 5.12). Statistically significant downregulation was seen from 100  $\mu$ g/mL onward, including strong significance at 175, 200 and 300  $\mu$ g/mL (p < 0.01, \*\*), and moderate significance at 100, 150, 500, and 600  $\mu$ g/mL (p < 0.05, \*).

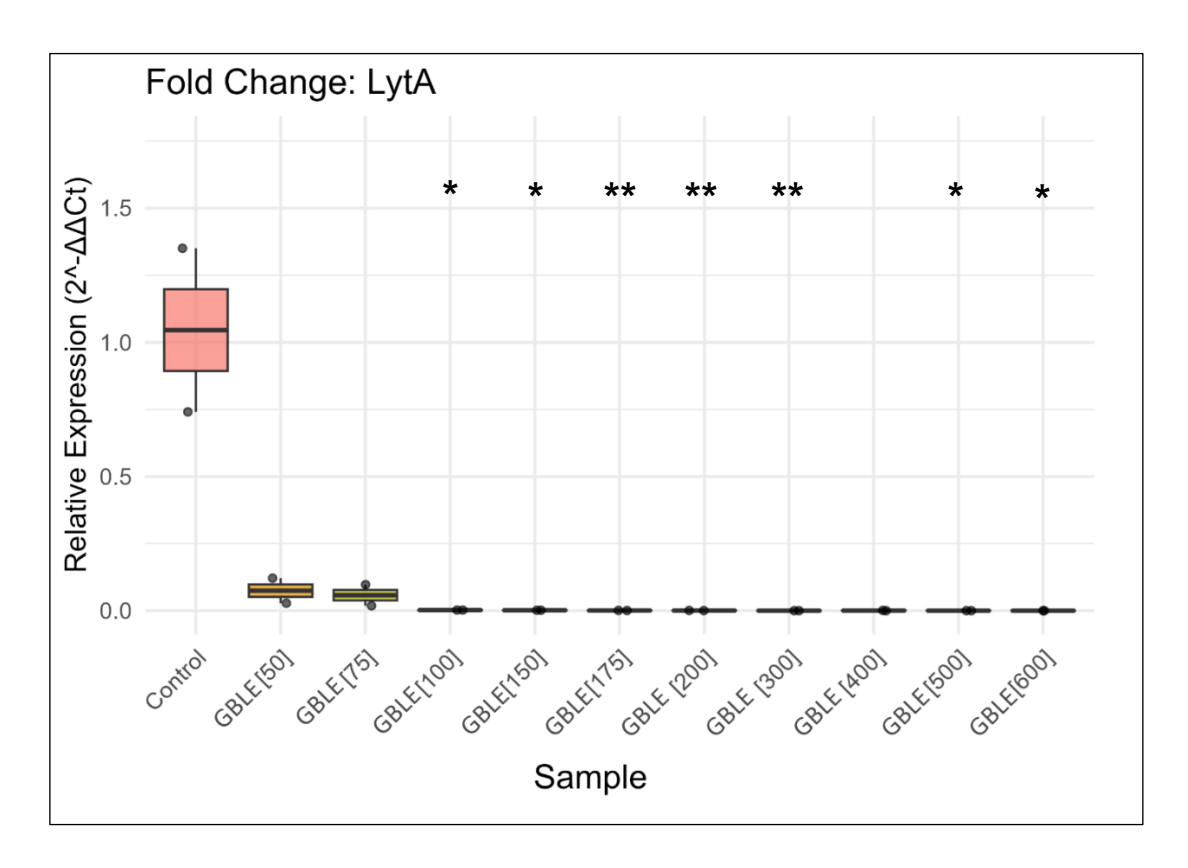


Figure 5.12. Expression levels of *LytA* in *Bacillus subtilis* planktonic cultures across increasing concentrations of GBLE, in µg/mL. RT-qPCR analysis shows fold change in *LytA* expression relative to the control condition. Boxplots represent interquartile ranges, with medians shown. P-value annotations are displayed above each group.

# 5.4.2. RNA-Sequencing Results

To investigate the global transcriptional response of *B. subtilis* JWV042 to GBLE, RNA-Seq was performed on planktonic cultures supplemented with 400  $\mu$ g/mL and 600  $\mu$ g/mL of GBLE, alongside untreated controls. Additionally, RNA-Seq was also performed on samples obtained from bacteria cultured under a unidirectional continuous fluid flow, a unidirectional continuous fluid flow with added 400  $\mu$ g/mL GBLE and a bidirectional fluid flow. Hierarchical clustering and heatmap visualization were used to highlight the most statistical significant genes across conditions.

Furthermore, RNA-Seq was carried out to validate the expression trends observed in the RT-qPCR analysis and to overcome its limitations by enabling the detection of transcriptional changes in genes not initially targeted in the RT-qPCR assays. This genome-wide approach provides a more comprehensive view of the bacterial response to GBLE treatment and flow regimes.

#### 5.4.2.1. Planktonic Cultures

To investigate the transcriptional response of planktonic *B. subtilis* cells to GBLE treatment, RNA-Seq analysis was performed comparing untreated controls to cells exposed to 400 and  $600 \,\mu\text{g/mL}$  GBLE. A heatmap of significantly differentially expressed genes (p < 0.05) is shown in Fig. 5.13, displaying hierarchical clustering of both genes and conditions. The colour scale represents relative expression levels, with red indicating high expression and blue indicating low expression.

The heatmap reveals clear expression changes in response to increasing GBLE concentration. The gene *yhfE*, which encodes a putative multidrug resistance transporter (Hu et al., 2005), showed a strong, concentration-dependent upregulation, indicating activation of stress-related efflux mechanisms. Two genes, *pucB* and *pucC*, both involved in purine catabolism, an essential pathway for nucleotide breakdown in *B. subtilis*, were clearly downregulated in the GBLE-treated samples compared to the control, suggesting that GBLE suppresses purine degradation. In *B. subtilis*, *pucB* and *pucC* are required for xanthine dehydrogenase activity, a key step in purine catabolism (Schultz, Nygaard and Saxild, 2001). This indicates that GBLE is suppressing purine degradation pathways. In *B. subtilis*, reduced purine catabolism could limit nitrogen and carbon recycling from nucleotides (Schultz, Nygaard and Saxild, 2001), potentially slowing growth or altering energy balance, which may contribute to the overall stress and biofilm-inhibitory effects observed under GBLE treatment. In contrast, *pucA*, another purine catabolism gene (Schultz, Nygaard and Saxild, 2001), showed mild upregulation under treatment.

yitJ, a gene potentially involved in sulphur-related metabolism (Lu et al., 2010), and *speD*, which helps produce molecules important for cell growth and stability (Sekowska et al., 1998), were also upregulated following GBLE treatment. Interestingly, *hmoB*, which is thought to help the cell manage iron and respond to oxidative stress (Gaballa and Helmann, 2002), also showed increased expression. Lastly, *rsuA*, a gene involved in the activity of the machinery used for protein production (ribosomes) (Douthwaite et al., 1995), was slightly upregulated, which could indicate increased protein synthesis activity.

These findings indicate that GBLE induces a complex transcriptional response in planktonic *B. subtilis* cells, downregulating specific metabolic pathways (e.g., purine catabolism via *pucB* and *pucC*), while upregulating genes related to stress adaptation, redox balance, and

biosynthetic processes. The concentration-dependent expression patterns suggest an escalating cellular response to the increasing intensity of GBLE exposure.

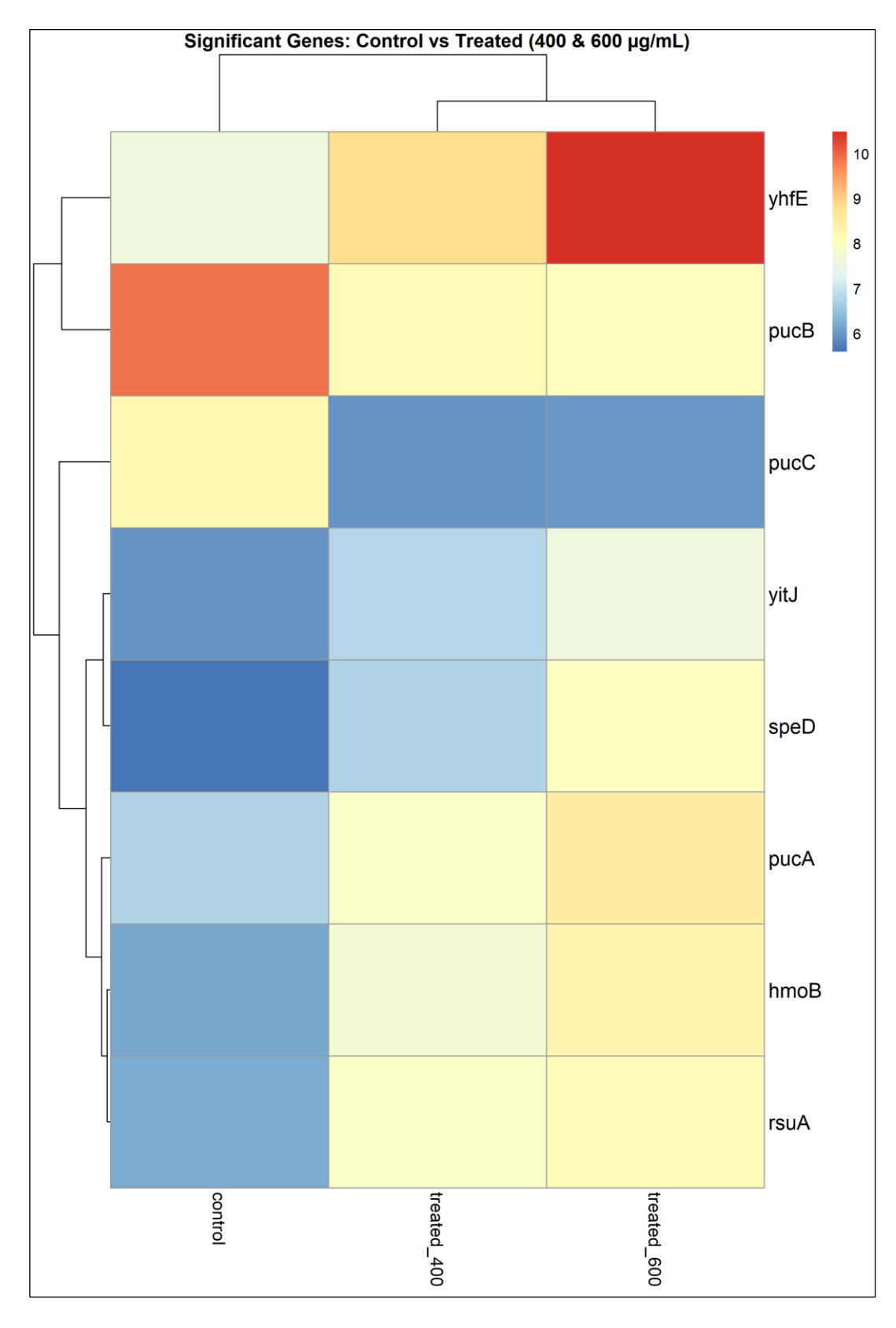


Figure 5.13. The heatmap displays hierarchical clustering of genes with significant differential expression (p < 0.05) across untreated control, 400  $\mu$ g/mL, and 600  $\mu$ g/mL GBLE-treated samples (labelled treated\_400 and treated\_600 respectively). Expression values were variance-stabilized and scaled; red indicates high expression, and blue indicates low expression.

These results partly support the RT-qPCR findings, which showed a general transcriptional repression. RNA-Seq data revealed a downregulation of purine metabolism, indicating a general metabolic suppression. In contrast, some stress- and survival-related genes such as *rsuA* and *hmoB* were upregulated, suggesting a selective activation of stress response elements. While RT-qPCR revealed repression of several global regulators (*sigM*, *spo0A*, *abrB*), this analysis was limited to a predefined set of genes. Therefore, the observed downregulation of these regulators does not necessarily reflect broader transcriptomic patterns, as revealed by the more comprehensive RNA-Seq approach.

# 5.4.2.2. Continuous Unidirectional Flow in Response to GBLE

To investigate the transcriptional response of *B. subtilis* under hydrodynamic stress, RNA sequencing was performed on cells grown in unidirectional continuous flow conditions with (uni\_treated) and without (uni\_untreated) 400 µg/mL GBLE.

RNA-Seq analysis revealed a few differentially expressed genes (Fig. 5.14). Notably, *rnpB*, which encodes the RNA component of RNase P involved in tRNA processing and essential for protein synthesis (Gunderson et al., 1987), was significantly more expressed in flow samples without GBLE. Similarly, *ssrA*, which plays a key role in restarting stalled protein production and maintaining its efficiency (Keiler et al., 1996), was upregulated in untreated flow samples, indicating a suppressive effect of GBLE on protein production.

In contrast, genes such as *fabHB*, involved in fatty acid biosynthesis (Schujman et al., 2001), and *yhfC*, a putative multidrug transporter potentially linked to stress resistance (Nicolas et al., 2012), were strongly repressed in response to GBLE treatment.

Also downregulated in response to GBLE is *ybdJ*, which encodes a predicted oxidoreductase that may contribute to redox balance or detoxification (Michna et al., 2016). Finally, *BS3610\_RS22550*, annotated as a hypothetical protein, also showed reduced expression in GBLE treated flow conditions. While its function remains unknown, consistent downregulation across multiple comparisons may indicate a role in flow-related adaptation or stress resilience.

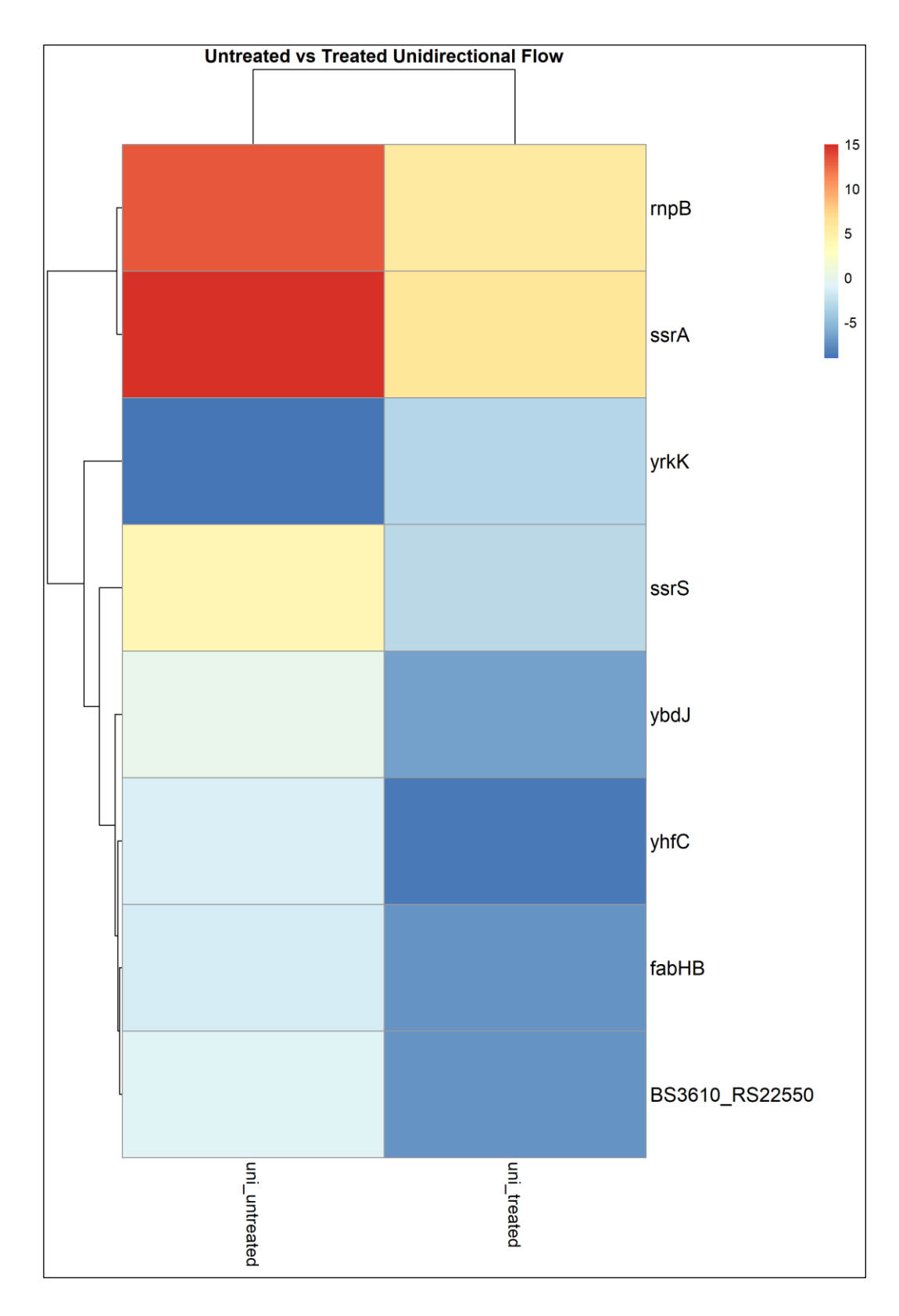


Figure 5.14. This heatmap shows differentially expressed genes between untreated and GBLE-treated (400  $\mu$ g/mL) *B. subtilis* cells grown under unidirectional flow. It displays genes with significant differential expression (p < 0.05), based on variance-stabilized RNA-Seq counts. Expression is colour-coded, with red representing higher and blue representing lower expression.

# 5.4.2.3. Planktonic Cultures and Continuous Unidirectional Flow (without GBLE)

To investigate the transcriptional response of *B. subtilis* to fluid shear stress, RNA sequencing was performed on bacterial cultures grown under standard planktonic conditions (control) and unidirectional flow (uni\_untreatead). Both conditions were run without the presence of GBLE. This comparison aimed to identify genes that are differentially expressed in response to the hydrodynamic environment, which simulates natural conditions such as those found in biofilm-forming or host-associated settings (Stoodley et al., 1999).

The analysis revealed distinct transcriptional signatures between the two growth conditions (Fig. 5.15), highlighting significant changes in RNA processing and genes linked to envelope biosynthesis.

The gene *rnpB*, encoding the RNA component of RNase P (involved in tRNA processing) (Guerrier-Takada et al., 1983), was strongly upregulated under unidirectional flow. Furthermore, *BS3610\_RS22555*, annotated as a hypothetical protein with no known function, showed relatively increased expression under unidirectional flow compared to static conditions. While its role is currently unclear, such hypothetical proteins are often candidates for uncharacterized stress response or metabolic functions (Galperin and Koonin, 2004). *pbpF*, encoding a penicillin-binding protein involved in peptidoglycan synthesis and cell wall remodelling (Popham and Young, 2003), was downregulated in unidirectional flow. In addition, *pucB*, associated with purine catabolism (Schultz, Nygaard and Saxild, 2001), also showed reduced expression in flow conditions, similar to the planktonic cultures in response to GBLE.

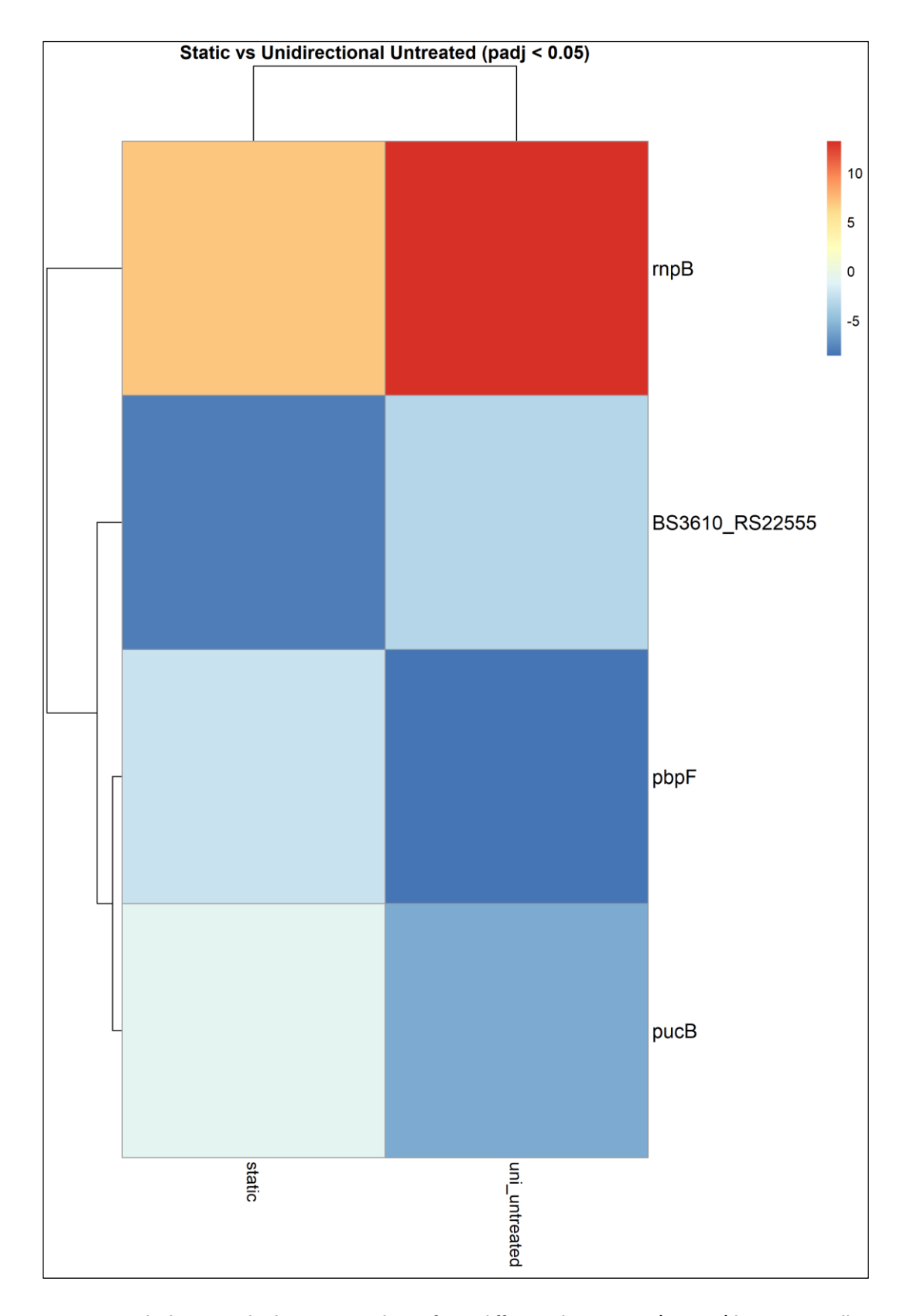


Figure 5.15. The heatmap displays genes with significant differential expression (p < 0.05) between *Bacillus subtilis* cells in static and unidirectional flow environments. Expression values were variance-stabilized and are shown using a colour scale, where red indicates high expression and blue indicates low expression.

#### 5.4.2.4. Planktonic cultures and Continuous Bidirectional Flow

To further assess the impact of fluid dynamics on *B. subtilis* gene regulation, RNA-Seq was performed to compare gene expression profiles between bacteria grown under static conditions and those exposed to bidirectional flow. The heatmap in Fig. 5.16 shows genes significantly differentially expressed (p < 0.05) between the two environments. Again, both conditions were run without the presence of GBLE.

Among the upregulated genes in bidirectional flow was *rnpB*, encoding the RNA component of RNase P, which plays a vital role in tRNA processing and protein synthesis (Guerrier-Takada et al., 1983). This finding is consistent with the previous unidirectional flow comparison (Fig. 5.16), where *rnpB* was also upregulated, suggesting that increased RNA processing activity is a shared adaptation to both flow environments. *BS3610\_RS01225* and *BS3610\_RS22545*, both annotated as hypothetical proteins, also showed increased expression. Interestingly, *BS3610\_RS22545* was upregulated under bidirectional flow, while *BS3610\_RS22555*, a nearby hypothetical gene, was slightly upregulated under unidirectional flow. Although their functions remain unknown, their similar response patterns and close genomic positions (*RS22545* and *RS22555*) suggest they may belong to the same transcriptional unit or participate in related flow-responsive pathways (Galperin and Koonin, 2004). Several *skf* operon genes (*skfC*, *skfF*, *skfG*) were also more highly expressed under bidirectional flow. These genes are associated with the sporulation killing factor system, involved in programmed cell death and cannibalism during early stationary phase (González-Pastor, Hobbs and Losick, 2003).

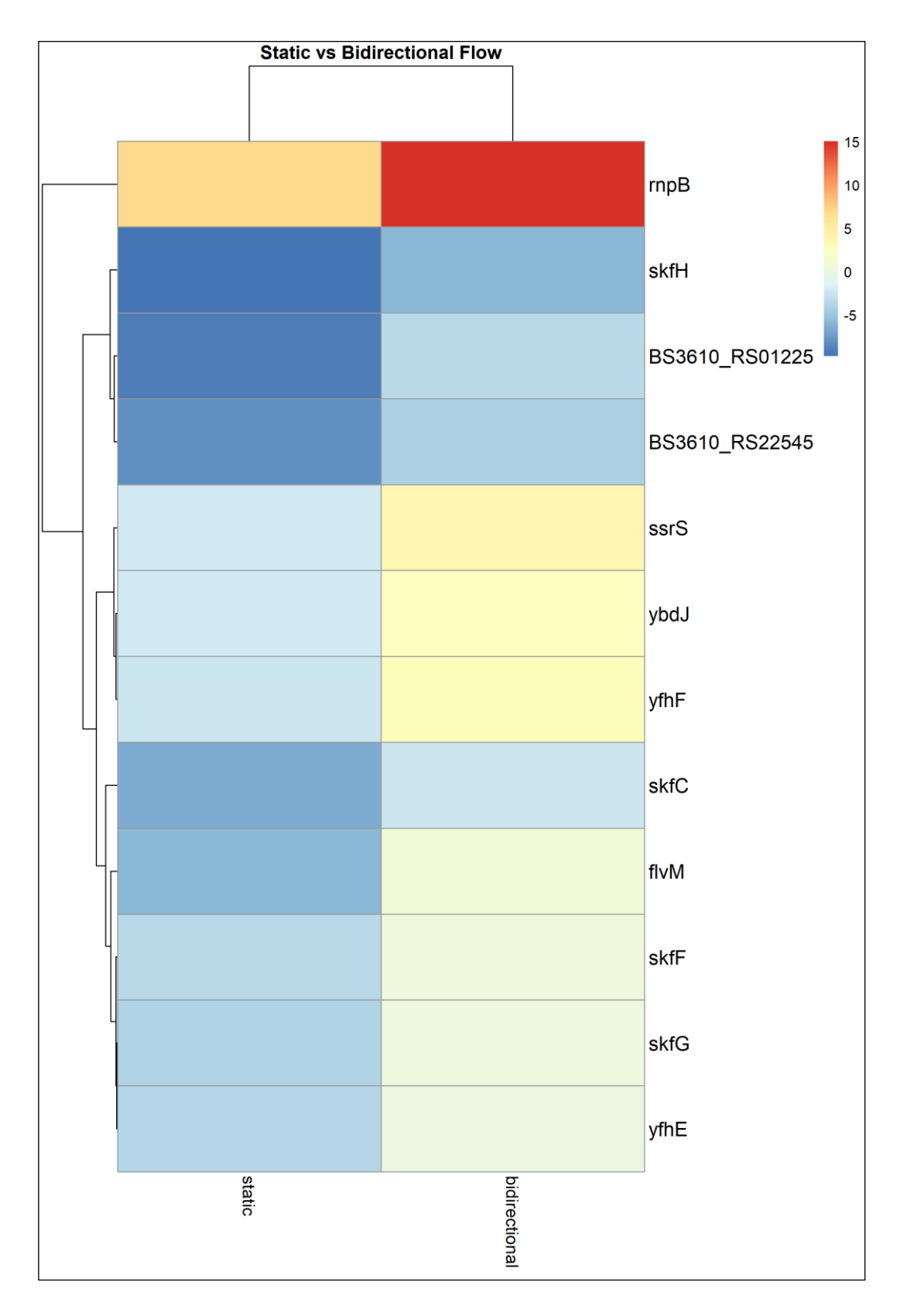


Figure 5.16. Heatmap showing differentially expressed genes (adjusted p < 0.05) in *Bacillus subtilis* cultures grown under static versus bidirectional flow conditions. Red indicates higher expression and blue indicates lower expression.

### 5.5. Discussion

### 5.5.1. Impact of GBLE on planktonic cultures

The molecular data presented in this chapter reveal a complex and multifaceted response of *Bacillus subtilis* to GBLE under planktonic conditions. RT-qPCR analysis consistently showed downregulation of key genes involved in biofilm formation (*bslA*, *tasA*, *slrR*, *remB*), biofilm formation and sporulation (*spo0A*), stress response (*dps*, *sigM*), motility (*sigD*), and transcriptional regulation (*abrB*, *comK*, *lytA*). This global gene repression suggests a strong transcriptional silencing effect exerted by GBLE, particularly at higher concentrations. This is consistent with Savoia (2012), who reported broad antimicrobial and antibiofilm activity of *Ginkgo biloba* extracts against diverse bacterial pathogens, although their study did not investigate *B. subtilis* or specific gene-level responses.

In order to study gene function in bacteria, mutants are often used. Mutants are organisms that have undergone a change in their DNA, which can alter how certain genes function. In bacteria, these changes can lead to visible differences in how the cells grow, move, or form structures like biofilms (Serrano et al., 2016). For example, the *B. subtilis* used in this study and previous chapters is a mutant, genetically modified to express gfp (green fluorescence protein). A number of studies have used *B. subtilis* mutants lacking the genes investigated in the RT-qPCR analysis of this present study; gene function and mutants' phenotype are summarised in Table 5.1.

Table 5.1. Functional roles and mutant phenotypes of key regulatory and structural genes involved in *Bacillus subtilis* biofilm development.

This table summarizes the known functions, associated mutant phenotypes, and relevant literature for genes central to *B. subtilis* multicellularity, matrix production, motility, stress response, and differentiation. References highlight studies that used targeted gene deletion or disruption to investigate biofilm physiology. These genes were explored by RT-qPCR analysis in this chapter.

Gene	Function	Mutant phenotype	Reference
bslA	Encodes a hydrophobin	Flat, wettable colonies	Hobley et al.,
	that coats and stabilizes	lacking aerial structures	2013; Arnaouteli
	the biofilm surface,	and wrinkles;	et al., 2016
	providing hydrophobicity	mechanically fragile	
	and structural integrity	biofilms	

TasA	Major amyloid protein forming the extracellular matrix; essential for biofilm scaffolding	Diffuse matrix, lack of amyloids leads to increased swarming; reduced matrix stability, non-structured pellicle formation	Romero et al., 2010
sIrR	Transcriptional regulator that represses motility and activates matrix genes	Unregulated motility, reduced matrix production, defects in biofilm structure	Chai et al., 2010
remB	Activator of extracellular polysaccharide (eps) and tapA-sipW-tasA operons; promotes matrix production	Smooth, unwrinkled colonies with defective pellicle and colony morphology; reduced ECM	Winkelman et al., 2009; Kearns et al., 2005
spoOA	Master regulator of sporulation; also initiates matrix genes and represses motility genes	Impaired sporulation; absence of wrinkles; structureless wide spread biofilm	Fujita et al., 2005; Grossman, 1995
dps	DNA-binding ferritin-like protein protecting against oxidative stress and starvation	Sensitive to oxidative damage; reduced survival in stationary phase	Chen and Helmann, 1995; Antelmann et al., 1997
sigM	Alternative sigma factor activating cell-envelope stress responses (especially under membrane-targeting stress)	Envelope defects, cell lysis, aberrant cell morphology	Cao et al., 2002
sigD	Controls motility (flagellar and autolysin genes) and cell separation	Motility-deficient, chain- forming cells; altered colony morphology	Kearns and Losick, 2003
abrB	Global regulator of transition-state genes; represses matrix and stress genes during exponential growth	Altered biofilm architecture; extensive motility	Strauch et al., 1990
сотК	Master regulator of competence; activates DNA-uptake and recombination machinery	Loss of competence; potential shifts in differentiation pathways	Berka et al., 2002
LytA	Autolysin involved in cell- wall hydrolysis, autolysis, and eDNA release	Tendency to form cell chains, decreased autolysis	Margot et al., 1999

Several features observed in the agar colony biofilms exposed to GBLE in Chapter 2 resemble phenotypes typically associated with specific *B. subtilis* mutants. For instance, changes in colony architecture and diffuse agar macrocolonies mirror the characteristics described in

 $\Delta bslA$ ,  $\Delta spoOA$ ,  $\Delta abrB$  and  $\Delta tasA$  mutants (Branda et al., 2006) (Kobayashi and Iwano, 2012). Interestingly, studies investigating the behaviour of  $\Delta tasA$  mutants noted an increase in swarming motility due to the lack of amyloid fibres, which interlock cells and limit motility (Romero et al., 2010). This was also described in  $\Delta abrB$  and  $\Delta spoOA$  mutants (Chai et al., 2008) (Kobayashi, 2007). Increased swarming motility was seen on the majority of the agar plates supplemented GBLE in Chapter 2. Overall, there are similarities between the phenotypes observed in this study resulting, in part, from downregulation of genes by GBLE, and the phenotypes where downregulation is driven by mutation. A few examples of *B. subtilis* agar biofilms grown in presence of GBLE can be found in Fig. 5.17.

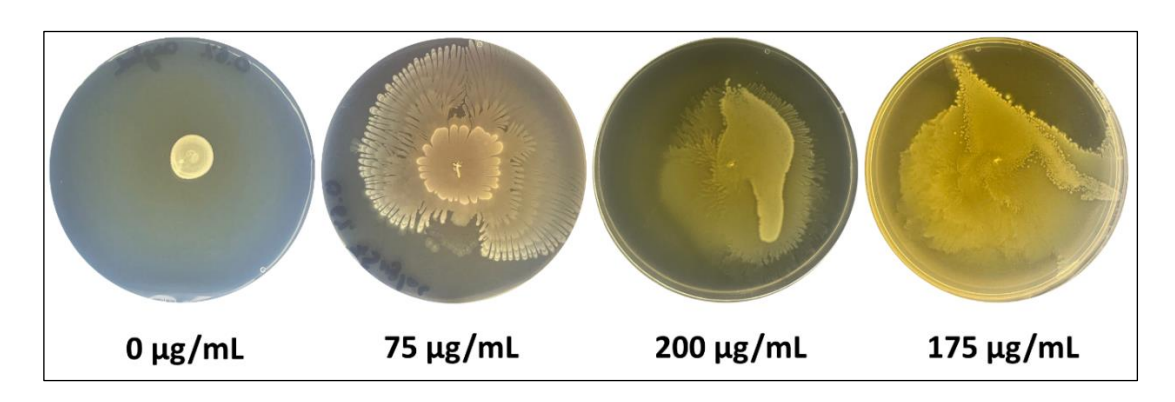


Figure 5.17. Representative macrocolonies of *B. subtilis* JWV042 grown on LB agar supplemented with increasing concentrations of *Ginkgo biloba* leaf extract (GBLE). At 0  $\mu$ g/mL (control), colonies appear compact and smooth. At 75  $\mu$ g/mL, colonies display expanded, dendritic morphology indicative of increased surface motility. At higher concentrations (175 and 200  $\mu$ g/mL), colonies show irregular, spreading morphologies with disrupted edges, suggesting GBLE-induced alterations in motility and cellular differentiation. Images illustrate dose-dependent morphological diversification in response to GBLE.

The increased swarming motility observed in GBLE-treated agar biofilms may represent an adaptive strategy by *B. subtilis* to escape localised stress. Swarming enables rapid surface colonisation and dispersal, allowing cells to relocate away from toxic microenvironments and seek more favourable niches (Kearns, 2010) (Guttenplan et al., 2013). Without the constraint of interlocking amyloid fibres, increased motility may serve as a survival mechanism in response to GBLE-induced membrane damage and transcriptional repression, supporting bacterial persistence under stress.

In Chapter 2, static biofilms showed extensive chaining (Fig. 5.18) and aberrant cell morphology (Fig. 5.18, arrow) in response to GBLE. This is consistent with findings investigating *B. subtilis* mutants lacking *sigM*, *sigD*, and *lytA*, which exhibit disrupted cell division, altered cell wall maintenance, and defective autolysin activity (Blackman et al., 1998) (Chen et al., 2009) (Yoshimura et al., 2004). These same genes were found to be

downregulated by GBLE in this chapter. Such morphological changes may offer a survival advantage by promoting stress-tolerant cell types, improving mechanical resilience, and limiting autolysis in a hostile environment (Branda et al., 2001) (López et al., 2009). Chaining may also support coordinated multicellularity and resistance to antimicrobial diffusion (Vlamakis et al., 2008) (Hall-Stoodley et al., 2004), helping cells persist under the membrane-disruptive and oxidative conditions induced by GBLE.

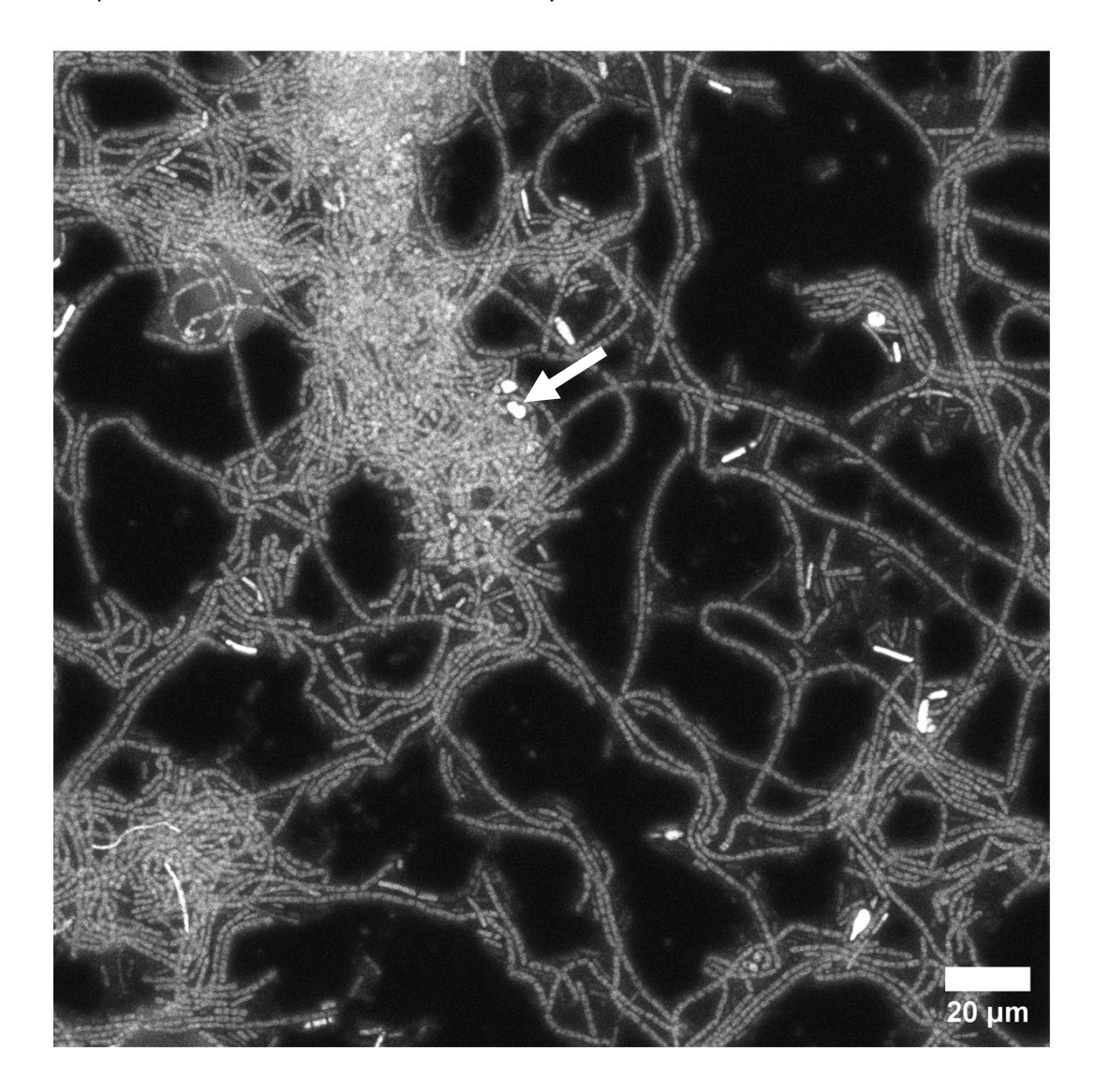


Figure 5.18. Confocal microscopy of *Bacillus subtilis* JWV042 pellicle biofilms treated with 100  $\mu$ g/mL GBLE. Biofilms were grown at the air–liquid interface and imaged using confocal laser scanning microscopy. The image reveals extensive chaining and highly organized filamentous structures. The white arrow highlights an example of aberrant cell morphology, with cells appearing rounded or irregularly shaped compared to the typical rod-shaped phenotype. This suggests that GBLE induces morphological alterations potentially linked to stress and cellular differentiation. Scale bar = 20  $\mu$ m.

GBLE contains a complex mixture of bioactive compounds, including flavonoids, ginkgolic acids, and terpene lactones, which are known to interfere with bacterial gene regulation in

E. coli and S. aureus. Several studies suggest GBLE can downregulate biofilm-associated genes by modulating gene expression networks. For instance, in E. coli O157:H7, ginkgolic acids and GBLE significantly reduced curli biosynthesis and fimbriae gene expression, thereby impairing biofilm formation (Lee et al., 2014). In S. aureus (including MRSA), Ginkgo biloba exocarp extract treatment led to downregulation of key biofilm regulatory genes such as icaA and sarA, and sigB at later time points (Wang et al., 2021). It is suggested here that, this may explain the observed downregulation of genes such as bsIA and tasA in B. subtilis, which encode surface-active and amyloid proteins critical for matrix formation. Bacteria use transcription factors (proteins that control when genes are active) and membrane-bound sensors (proteins that detect changes outside the cell) to decide when to produce biofilm proteins. GBLE could interfere with the tapA-sipW-tasA operon by interfering with the regulatory networks that control its expression. This operon is tightly regulated by transcription factors and membrane-bound sensor kinases that respond to environmental cues. GBLE is rich in bioactive compounds such as flavonoids and ginkgolic acids (Lee et al., 2014). For instance, the flavone luteolin, a structural analogue of some GBLE flavonoids, can inhibit histidine kinase activity by binding the HK853 sensor kinase in Thermotoga maritima (T. maritima), suggesting a plausible mechanism for perturbing bacterial two-component signalling systems (Zhou et al., 2019). This mode of action is supported by studies in E. coli and S. aureus, where Ginkgo extracts significantly downregulated biofilm-associated genes like csqA, csqB, icaA, and icaD, impairing matrix production and attachment (Lee et al., 2014) (Wang et al., 2021). Similar regulatory suppression could occur in B. subtilis, leading to reduced expression of the tapA-sipW-tasA operon and associated matrix genes, ultimately weakening the biofilm architecture.

Similarly, suppression of *sIrR*, *spo0A*, *abrB*, and *comK*, was also observed in this study. These genes are involved in biofilm commitment, sporulation, and competence, suggesting that GBLE might interfere with master regulators of cell fate. In a study investigating of the impact of flavonoids on *T. maritima*, the flavone luteolin was shown to inhibit histidine kinase activity (Zhou et al., 2019). Similarly, the flavonoids contained in GBLE may compromise cascade events essential for activating *Spo0A* and downstream genes in *B. subtilis*.

Interestingly, RNA-Seq analysis of the same condition revealed a broader picture, particularly at the global transcriptomic level. While purine catabolism genes (*pucB*, *pucC*) were indeed downregulated, supporting the metabolic suppression seen in the RT-qPCR, several genes

associated with stress adaptation (*hmoB*, *yhfE*), sulphur and polyamine metabolism (*yitJ*, *speD*), and translational machinery (*rsuA*) were upregulated.

In *B. subtilis, hmoB* helps the cell manage oxidative stress by regulating iron metabolism (Gaballa and Helmann, 2011), while *yhfE* is believed to encode a transporter involved in pumping out toxic compounds, contributing to multidrug resistance (Hu et al., 2005). The upregulation of these genes and the simultaneous downregulation of other stress-related genes (seen in the RT-qPCR) suggests that alternative stress-related mechanisms may be mobilized, perhaps to manage intracellular redox fluctuations or chemical stress induced by GBLE. The upregulation of *yhfE* aligns with reports that ginkgolic acid C15:1 can penetrate bacterial membranes and compromise their integrity. Hua *et al.* (2017) demonstrated this effect in *Bacillus amyloliquefaciens*, while Wen *et al.* (2022) observed iron-homeostasis disruption by ginkgolic acid C15:1 against *S. aureus* and *E. coli*. While direct evidence for efflux activation by ginkgolic acids is lacking, membrane and iron-stress perturbations caused by GBLE could trigger *B. subtilis* stress responses that include increased *yhfE* expression.

Similarly, *hmoB*, encoding a constitutively expressed haeme monooxygenase capable of degrading haeme and releasing iron (Gaballa and Helmann, 2011), was upregulated under GBLE treatment. This response may indicate GBLE-induced perturbations in haeme or iron homeostasis, which in *B. subtilis* can lead to altered expression of iron-responsive genes, rather than a direct oxidative stress-driven effect.

The upregulation of *speD* and *rsuA* observed here may reflect a metabolic shift toward biosynthesis and stress-tolerant growth. In *B. subtilis*, *speD* encodes S-adenosylmethionine decarboxylase in the spermidine biosynthetic pathway. Spermidines are polyamines that help stabilise DNA and membranes and support stress resilience (Sekowska et al., 2000) (Rhee, Lee and Park, 2007). Although *rsuA* is best characterised in *E. coli* as the 16S rRNA and it enhances survival under stress (Abedeera et al., 2023), *B. subtilis* encodes related rRNA pseudouridine synthase *rsuA* that modify rRNA and can influence ribosome function (Niu, Lane and Ofengand, 1999). Taken together, these changes may represent an adaptive response by a subpopulation of *B. subtilis* cells to counteract GBLE-induced stress. Phenotypically, treated biofilms displayed highly organised filamentous structures (See Chapter I), potentially linked to the upregulation of *speD* and *rsuA*, as increased polyamine synthesis and ribosomal activity would support the differentiation and persistence of stress-adapted cells. These adaptations may serve to maintain protein synthesis and cellular

homeostasis in a hostile environment, even as developmental and biofilm-specific genes are downregulated.

Overall, this suggests that not all cells are uniformly silenced by GBLE. Rather, a surviving subpopulation mounts a secondary, focused transcriptional response, indicative of phenotypic heterogeneity, a hallmark of *B. subtilis* biofilm adaptation (Ackermann, 2015).

The differences seen in RT-qPCR and RNA-Seq could be attributed to methodological and biological differences. RT-qPCR, being a targeted approach, focused on specific stress and biofilm-associated genes, many of which were transcriptional regulators. Their downregulation might reflect early silencing or post-transcriptional regulatory mechanisms not captured at the global level. In contrast, RNA-Seq provides a snapshot of overall transcriptional activity and may detect compensatory or alternative stress responses that are activated at later stages or through distinct regulatory pathways.

Taken together, these results indicate that GBLE imposes a substantial transcriptional burden on *B. subtilis*, leading to repression of coordinated biofilm development and cellular differentiation pathways. However, the organism attempts to compensate through the activation of select metabolic and protective responses. This dual strategy, suppression of complex community behaviours alongside activation of survival-linked stress and biosynthetic pathways, may explain the bacterial phenotypes observed in Chapter 2. The ability of *B. subtilis* to partially adapt, despite global repression of canonical biofilm genes, underscores its transcriptional plasticity and hints at the robustness of bacterial stress response networks even under phytochemical challenge.

#### 5.5.2. Impact of GBLE on Cultures under Unidirectional Fluid Flow

RNA-Seq analysis of bacterial cultures grown under continuous flow with and without GBLE revealed significant transcriptional changes.

Among the genes significantly downregulated in GBLE-treated unidirectional flow biofilms were *rnpB* and *ssrA*, which play crucial roles in RNA processing and translational quality control, respectively. *rnpB* encodes the RNA component of RNase P, an essential ribozyme involved in the maturation of the 5' ends of pre-tRNAs, a fundamental step in protein synthesis (Li and Altman, 2004). *ssrA*, also known as *tmRNA*, rescues stalled ribosomes through trans-translation and is essential for cellular survival under stress conditions, including nutrient limitation and antibiotic exposure (Keiler et al., 2000). Its deletion in *B*.

subtilis has been associated with impaired sporulation (Muto et al., 2000). The observed repression of *rnpB* and *ssrA* suggests that GBLE may interfere with core RNA metabolism, possibly mimicking nutrient deprivation or exerting direct inhibitory effects on RNA processing pathways. Notably, these transcriptomic changes align with the severe morphological disruption observed microscopically, where GBLE-treated biofilms displayed disorganised Van Gogh bundles and markedly reduced biomass (Fig. 5.19). Since Van Gogh bundles represent filamentous cellular arrangements critical for mechanical integrity and expansion under flow (van Gestel, Vlamakis and Kolter, 2015), their disorganisation may reflect a collapse in coordinated growth and multicellularity, likely driven by impaired protein synthesis and ribosomal function.

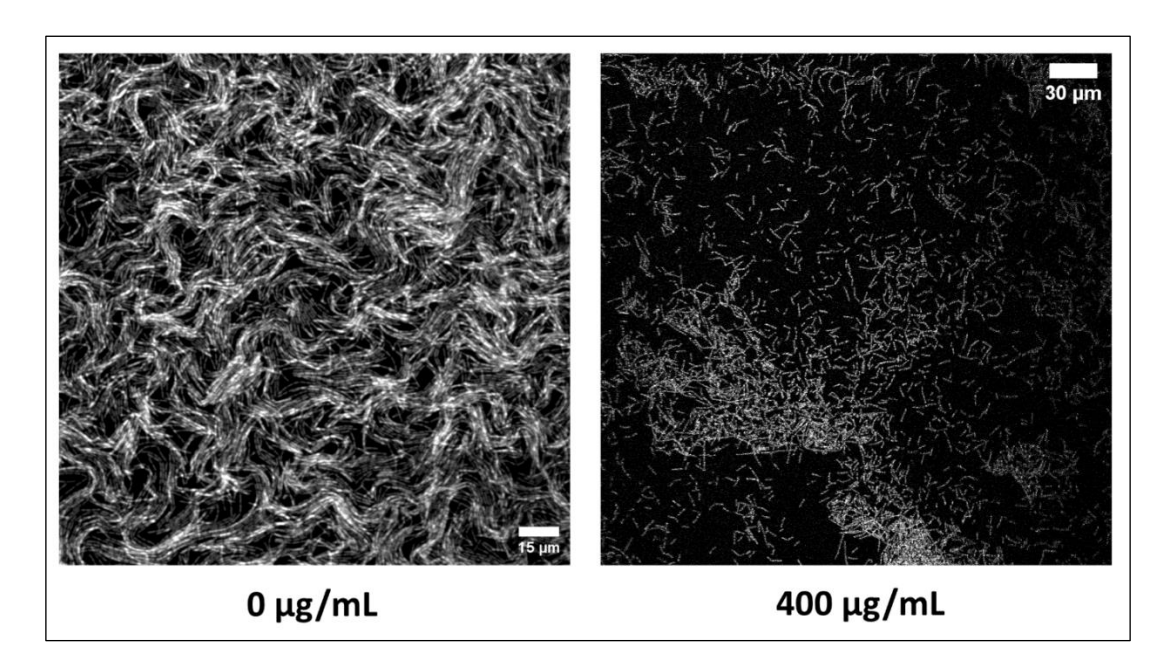


Figure 5.19. Confocal laser scanning microscopy of Bacillus subtilis JWV042 flow-cell biofilms with and without GBLE treatment. Left: Untreated control biofilms (0  $\mu$ g/mL) display dense, filamentous architecture and well-structured surface coverage. Right: Biofilms treated with 400  $\mu$ g/mL GBLE show disrupted morphology, reduced filamentation, and sparse surface colonisation, indicating a loss of structural integrity and biofilm cohesion. Scale bars = 100  $\mu$ m.

Notably, *fabHB*, encoding β-ketoacyl-ACP synthase involved in fatty acid biosynthesis, was downregulated in response to GBLE. Because fatty acids are essential components of the cell membrane and extracellular matrix precursors, the repression of *fabHB* suggests a reduction in lipid synthesis that could weaken membrane integrity and limit the production of matrix materials required for robust bundle and rope formation. (Dawan and Ahn, 2022). Other genes (*ssrS*, *ybdJ*, *yhfC*, *BS3610\_RS22550*) were similarly repressed, further indicating a dampening of growth-associated functions. In contrast, *yrkK* was upregulated, potentially as

part of a stress-response mechanism contributing to cell envelope stabilisation under flow conditions. Together, these transcriptional shifts align with the structural changes observed microscopically, suggesting that GBLE disrupts membrane and matrix production, thereby reducing biofilm biomass and preventing the development of Van Gogh bundles and ropelike architectures commonly seen in untreated flow-grown biofilms (Daglia, 2012).

Despite differing growth conditions, *B. subtilis* biofilms exposed to GBLE under both static and unidirectional flow conditions exhibited hallmark features of oxidative and membrane stress. In static cultures, GBLE triggered the upregulation of oxidative stress-related genes such as *hmoB* and *yhfE*. As *yhfE* has been reported to be involved in multidrug efflux (Hu et al., 2005), its upregulation here likely enhancing efflux to expel membrane-disruptive components like ginkgolic acids. Similarly, in flow conditions, the upregulation of membrane-associated genes (*fabHB*, *yrkK*) suggests that GBLE's membrane-targeting effects also prevail under shear stress, inducing cells to modify their lipid biosynthesis to restore membrane integrity.

Notably, while static cultures under GBLE responded with increased expression of *rsuA* and *speD*, genes which support ribosome function and DNA/membrane stabilization (Douthwaite et al., 1995) (Sekowska, Bertin and Danchin, 1998), flow cultures under GBLE showed strong downregulation of *rnpB* and *ssrA*, key components of RNA processing and translational quality control (Li and Altman, 2004) (Keiler, Waller and Sauer, 1996). This divergence may reflect the compounded stress of fluid shear and antimicrobial exposure in flow environments, which not only disturbs membrane structure but also impairs core metabolic processes such as tRNA maturation and ribosome rescue. Therefore, flow biofilms suffered greater biomass reduction and structural disorganisation, while static biofilms retained organised filamentous bundles. These findings align with prior observations that dynamic flow intensifies antimicrobial susceptibility by enhancing mass transfer and disrupting protective gradients (Shuppara et al., 2025). The transcriptional profiles suggest that static cultures may harbour a more resilient subpopulation capable of maintaining translational capacity and structural cohesion under GBLE-induced oxidative stress, whereas flow-grown cells undergo deeper metabolic suppression and structural collapse.

### 5.5.3. Impact of a Continuous Unidirectional Flow on *B. subtilis*

Transcriptomic comparison between static and unidirectional flow-grown *B. subtilis* biofilms (in the absence of GBLE) revealed distinct expression patterns associated with RNA processing, cell wall dynamics, and metabolic regulation.

The RNA-processing gene rnpB, was markedly upregulated under unidirectional flow. This gene encodes the catalytic RNA component of RNase P and is responsible for generating mature tRNAs (Li and Altman, 2004). Its upregulation here is thus consistent with an increased demand for tRNA maturation under stress conditions. In *B. subtilis*, mature tRNAs are essential for translating the structural, adhesive, and stress-response proteins required for biofilm matrix assembly, stable surface attachment, and adaptation to stress (Guerrier-Takada et al., 1983).

The RNA-processing gene *rnpB*, which encodes the catalytic RNA component of RNase P responsible for generating mature tRNAs (Li and Altman, 2004), was markedly upregulated under unidirectional flow, consistent with an increased demand for tRNA maturation under stress conditions. In *B. subtilis*, mature tRNAs are essential for translating the structural, adhesive, and stress-response proteins required for biofilm matrix assembly, stable surface attachment, and adaptation to stress (Guerrier-Takada et al., 1983). Increased *rnpB* expression may therefore reflect a transcriptional adjustment to ensure sufficient translational capacity to support these biofilm-related processes under flow conditions. This was seen in Chapter 2, where biofilms grown under continuous flow, mainly made of long Van Gogh bundles, showed increased architectural complexity compared to static biofilms (Fig. 5.20).

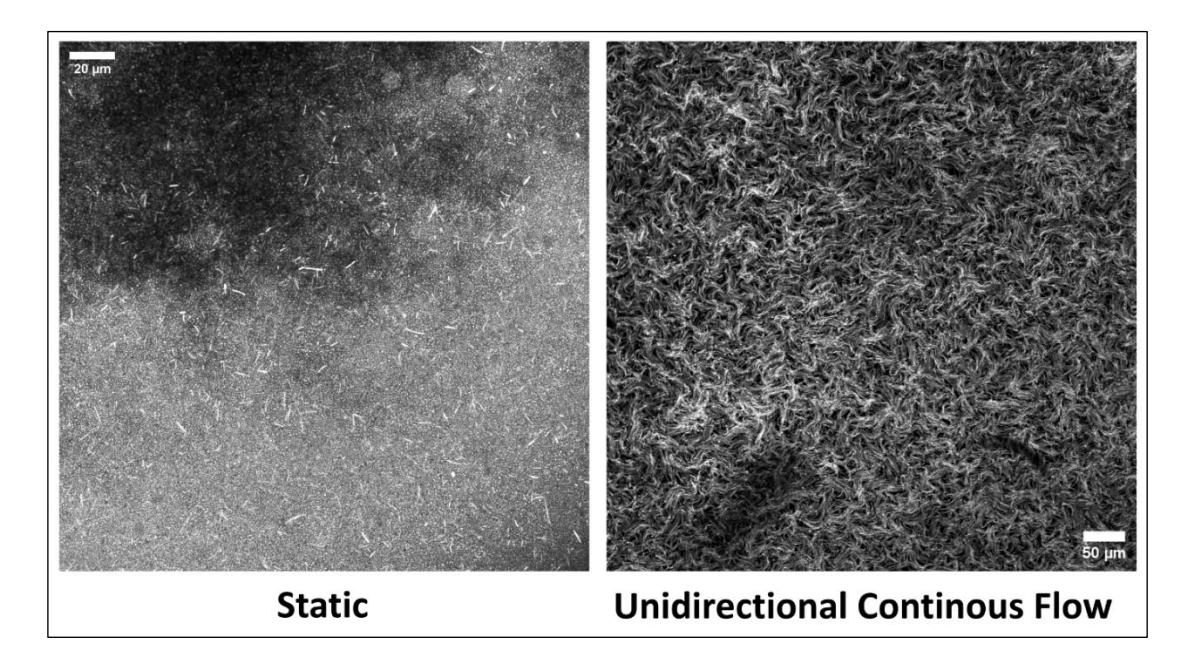


Figure 5.20. Confocal laser scanning microscopy comparison of *Bacillus subtilis* JWV042 biofilms formed under static versus unidirectional continuous flow conditions, both without GBLE. Left: Under static conditions, standard biofilm development is observed. Right: In contrast, continuous flow promotes dense, highly structured biofilm formation with tightly packed and aligned Van Gogh bundles. These findings highlight the role of hydrodynamic forces in promoting robust biofilm architecture. Scale bars =  $20 \mu m$  (static) and  $50 \mu m$  (flow).

In contrast, genes such as *pbpF*, *BS3610\_RS22555*, and *pucB* were all significantly downregulated in flow-grown biofilms. *pbpF*, encoding a penicillin-binding protein involved in peptidoglycan remodelling, has been implicated in maintaining cell shape (Popham and Setlow, 1996). In this present study, *pbpF* was downregulated under unidirectional flow, indicating a reduced transcriptional investment in peptidoglycan synthesis and modification. This change coincided with the formation of biofilms entirely made of Van Gogh bundles and Van Gogh ropes (aligned and twisted Van Gogh bundles, a unique architectural feature observed exclusively in *B. subtilis* flow biofilms, see Chapter 3). Van Gogh bundles are multicellular filaments made of directionally aligned chains of cells (van Gestel et al., 2015). Downregulation of cell wall remodelling genes such as *pbpF* may reflect altered cell wall dynamics during biofilm formation under flow, supporting the preservation of continuous connections between neighbouring cells and aiding their alignment in flowing environments.

Likewise, the downregulation of *pucB*, part of the purine degradation pathway, may indicate a metabolic shift away from nitrogen salvage under nutrient-replenished flow conditions, where purine recycling is less critical (Schultz, Nygaard and Saxild, 2001). The hypothetical gene *BS3610\_RS22555*, which currently has no assigned function, was uniquely downregulated under flow, indicating a transcriptional response specific to mechanical

stimulation; however, further function assignment studies are needed. These gene expression trends align with phenotypic differences between static and flow biofilms: while static biofilms often accumulate dense, vertically stratified communities with local nutrient limitation, flow biofilms exhibit more dynamic architectures adapted for surface adherence, resource acquisition, and mechanical resilience (Shuppara et al., 2025). The enhanced expression of *rnpB* may support rapid adaptation and growth under flow, while repression of cell wall and metabolic remodelling genes reflect a biofilm phenotype optimized for hydrodynamic environments.

### 5.5.4. Impact of a Continuous Bidirectional Flow on *B. subtilis*

Comparison of *B. subtilis* transcriptomes between static and continuous bidirectional flow conditions show a broad upregulation of genes associated with RNA processing, stress adaptation, and cell–cell interactions, supporting the observed development of architecturally complex biofilms.

Similarly to the unidirectional flow-grown cultures, the most strongly upregulated genes was *rnpB*, which encodes the RNA component of RNase P and is essential for tRNA maturation and active protein synthesis (Li and Altman, 2004). This increase suggests enhanced translational demand to support the growth and differentiation of cells within the mechanically dynamic and spatially organised biofilm structures characteristic of bidirectional flow. Microscopically, these biofilms exhibited a highly distinctive architecture composed of Van Gogh bundles and strands, raised folds with channels underneath (Fig. 5.21).

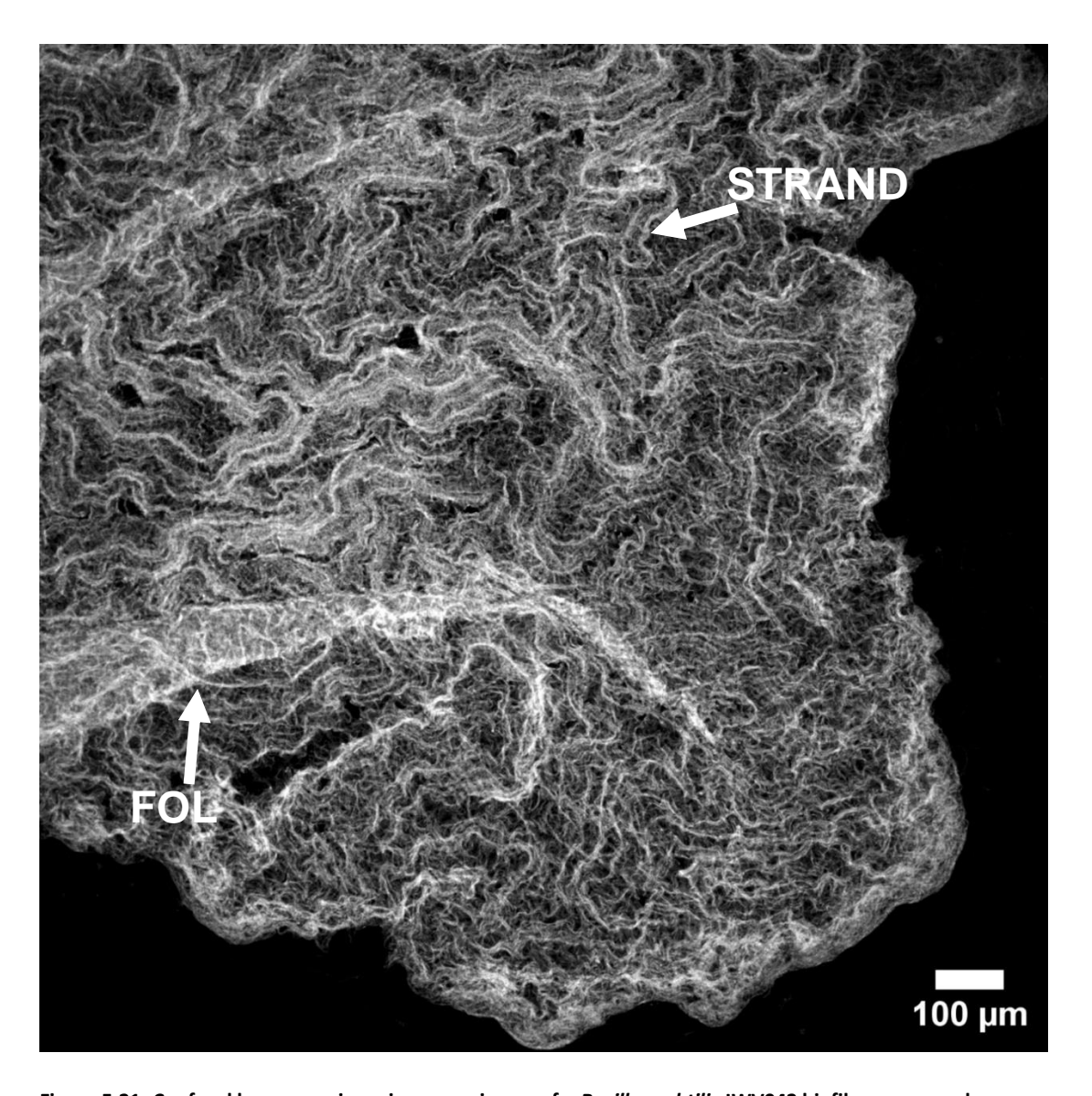


Figure 5.21. Confocal laser scanning microscopy image of a *Bacillus subtilis* JWV042 biofilm grown under bidirectional flow conditions. The biofilm exhibits pronounced architectural complexity, with visible folds and aligned strands forming a dense, interconnected matrix. These structural features suggest enhanced mechanical stability and spatial organisation, likely induced by the dynamic shear forces of alternating flow. Scale bar =  $100 \ \mu m$ .

The expression of multiple *skf* operon genes (*skfH*, *skfC*, *skfF*, *skfG*), which are part of the cannibalism toxin system (Gonzalez-Pastor et al., 2003), may reflect increased cell–cell competition, potentially triggered by mechanical cues or subpopulation differentiation within complex fluidic environments. Phenotypically, activation of the *skf* operon enables a subset of cells to produce toxins that lyse non-committed siblings, thereby releasing nutrients and reinforcing population-level fitness under resource-limited (Gonzalez-Pastor et al., 2003) (Ellermeier et al., 2006). In the context of bidirectional flow, the spatial and mechanical heterogeneity introduced by reversing fluid shear may amplify differentiation cues, causing segments of the biofilm to initiate programmed cell death or delayed

sporulation (López et al., 2009). This could explain the observed morphological complexity, such as the elevated folds, promoting spatial segregation of subpopulations, with toxin-producing cells forming structured scaffolds while lysed cells contribute to matrix enrichment or nutrient cycling. Such coordinated cannibalistic behaviour may support biofilm expansion, stress resilience, and internal channel formation by selectively pruning less-fit cells and allocating communal resources toward structurally and metabolically robust subpopulations.

Moderate upregulation of *ssrS*, *ybdJ*, *yfhF*, and *yfhE* may indicate a concurrent need to stabilise ribosome function and mitigate oxidative stress. In *B. subtilis*, *ssrS* encodes 6S RNA, a small regulatory RNA that binds RNA polymerase and modulates transcription during stationary phase and stress (Cavanagh et al., 2008); *ybdJ* encodes a predicted oxidoreductase that may participate in redox homeostasis (Michna et al., 2016); *yfhF* encodes a Fe–S cluster biogenesis protein, essential for protecting enzymes from oxidative damage (Ayala-Castro, Saini and Outten, 2008); and *yfhE* encodes a putative ferritin-like protein involved in iron storage and detoxification (Smith et al., 2010). These changes align with prior findings that spatially structured flow biofilms often experience oxygen gradients and metabolic heterogeneity (Stewart and Franklin, 2008).

When comparing unidirectional and bidirectional flow regimes against static cultures, both flow types upregulated *rnpB* and genes linked to ribosomal activity, indicating a shared push toward higher translational capacity and coordinated multicellularity. However, the broader and more coordinated transcriptional activation under bidirectional flow, including the *skf* operon and multiple stress-associated genes, may reflect the additional mechanical complexity and directional shifts imposed by bidirectional shear. Unlike the linear elongation of bundles seen in unidirectional flow, bidirectional flow promotes the emergence of more elaborate morphologies, such as folded architectures and channels, which likely require finely tuned spatial regulation and communication across the biofilm. Thus, while both flow conditions drive architectural sophistication, bidirectional flow appears to trigger a more diverse and possibly developmentally advanced transcriptional program, aligning with its enhanced morphological complexity.

#### 5.6. Conclusion

This chapter shows that *Bacillus subtilis* responds to GBLE with widespread repression of biofilm, sporulation, and stress-related genes under static conditions.

In summary, integrating RT-qPCR and RNA-Seq across static, unidirectional, and bidirectional flow shows that GBLE exerts a broad, condition-invariant repression of core developmental circuits in B. subtilis. In static systems, GBLE consistently downregulated biofilm matrix genes (bslA, tasA), sporulation and fate regulators (spoOA, abrB, comK), motility and stress regulators (siqD, siqM, dps), indicating suppression of biofilm commitment, motility and stress-responsive development. In parallel, we observed selective upregulation of survivalsupport pathways, including oxidative/iron-linked functions (hmoB, yhfE), polyamine metabolism (speD), and ribosome-supporting RNA modification (rsuA), consistent with a shift toward maintaining core cellular functions under phytochemical pressure. Under flow plus GBLE, findings showed a marked downregulation of RNA-processing/translation qualitycontrol genes (rnpB, ssrA), a signature consistent with constrained tRNA maturation and ribosome rescue; importantly, this molecular pattern coincided with disrupted Van Gogh bundle formation and reduced biomass documented in earlier chapters. By contrast, flow alone expanded transcriptional breadth and architectural complexity: bidirectional flow produced the strongest upregulation of RNA-processing, stress, and developmental modules (including rnpB and the skf operon) and aligned with the emergence of folds and channels, whereas unidirectional flow elicited a narrower transcriptional response, but showed architecturally complex structures such as Van Gogh ropes.

Together, these findings show that GBLE modulates multicellular development in *B. subtilis*, while mechanical conditions strongly shape the depth and nature of the transcriptional and phenotypic response. Static cultures show partial resilience to GBLE, unidirectional flow intensifies collapse in response to GBLE, and bidirectional flow enables complex, flow-adapted biofilm architecture.

### 5.7. References

Abedeera, S.M., Jayalath, K.S., Xie, J., Rauff, R.M., and Abeysirigunawardena, S.C. (2023) Pseudouridine synthase RsuA confers a survival advantage to bacteria under streptomycin stress. *Antibiotics*. Vol.12(9), 1447.

Ackermann, M. (2015) A functional perspective on phenotypic heterogeneity in microorganisms. *Nature Reviews Microbiology*. Vol.13(8), pp. 497–508.

Antelmann, H., Engelmann, S., Schmid, R., Sorokin, A., Lapidus, A. and Hecker, M. (1997) Expression of a stress- and starvation-induced dps/pexB-homologous gene is controlled by the alternative sigma factor σ^B in *Bacillus subtilis*. *Journal of Bacteriology*. Vol.179(23), pp. 7251–7256.

Arnaouteli, S., MacPhee, C.E. and Stanley-Wall, N.R. (2016) Just in case it rains: building a hydrophobic biofilm the *Bacillus subtilis* way. *Current Opinion in Microbiology*. Vol.34, 7–12.

Ayala-Castro, C., Saini, A. and Outten, F.W. (2008) Fe—S cluster assembly pathways in bacteria. *Microbiology and Molecular Biology Reviews*. Vol.72(1), pp. 110–125.

Barbe, V., Cruveiller, S., Kunst, F., Lenoble, P., Meurice, G., Sekowska, A., Vallenet, D., Wang, T., Moszer, I., Médigue, C., Danchin, A. and Glaser, P. (2009) From a consortium sequence to a unified sequence: the *Bacillus subtilis* 168 reference genome a decade later. *Microbiology*. Vol.155(6), pp. 1758–1775.

Benjamini, Y. and Hochberg, Y. (1995) Controlling the false discovery rate: a practical and powerful approach to multiple testing. *Journal of the Royal Statistical Society: Series B* (Methodological). Vol.57(1), pp. 289–300.

Berka, R.M., Hahn, J., Albano, M., Draskovic, I., Persuh, M., Cui, X. and Dubnau, D. (2002) Microarray analysis of the *Bacillus subtilis* K-state: genome-wide expression and competence regulator binding. *Molecular Microbiology*. Vol.43(5), pp. 1171–1185.

Blackman, S.A., Smith, T.J. and Foster, S.J. (1998) The role of autolysins during vegetative growth of *Bacillus subtilis* 168. *Microbiology*. Vol.144(Pt 1), pp. 73–82.

Branda, S.S., González-Pastor, J.E., Ben-Yehuda, S., Losick, R. and Kolter, R. (2001) Fruiting body formation by *Bacillus subtilis*. *Proceedings of the National Academy of Sciences USA*. Vol.98(20), pp. 11621–11626.

Branda, S.S., Chu, F., Kearns, D.B., Losick, R. and Kolter, R. (2006) A major protein component of the *Bacillus subtilis* biofilm matrix. *Molecular Microbiology*. Vol.59(4), pp. 1229–1238.

Britton, R.A., Eichenberger, P., Gonzalez-Pastor, J.E., Fawcett, P., Monson, R., Losick, R. and Grossman, A.D. (2002) Genome-wide analysis of the stationary-phase sigma factor (σH) regulon of *Bacillus subtilis*. *Journal of Bacteriology*. Vol.184(17), pp. 4881–4890.

Cao, M., Wang, T., Ye, R. and Helmann, J.D. (2002) Antibiotics that inhibit cell wall biosynthesis induce expression of the *Bacillus subtilis* σ<sup>N</sup>W and σ<sup>M</sup> regulons. *Molecular Microbiology*. Vol.45(5), pp. 1267–1276.

Cavanagh, A.T., Chandrangsu, P., Wassarman, K.M. and Winkler, W.C. (2008) 6S RNA regulation of transcription in Bacillus subtilis. *Journal of Bacteriology*. Vol.190(3), pp. 877–886.

Chai, Y., Chu, F., Kolter, R. and Losick, R. (2008) Bistability and biofilm formation in *Bacillus subtilis*. *Molecular Microbiology*. Vol.67(2), pp. 254–263.

Chai, Y., Kolter, R. and Losick, R. (2010) Reversal of an epigenetic switch governing cell chaining in *Bacillus subtilis* by protein instability. *Molecular Microbiology*. Vol.78(1), pp. 218–229.

Chen, L. and Helmann, J.D. (1995) Bacillus subtilis MrgA is a Dps (DNA-binding protein from starved cells) homologue: evidence for protective role in oxidative stress. *Journal of Bacteriology*. Vol.177(16), pp. 4614–4622.

Chen, R., Guttenplan, S.B., Blair, K.M. and Kearns, D.B. (2009) Role of *sigD*-dependent autolysins in *Bacillus subtilis* population heterogeneity. *Journal of Bacteriology*. Vol.191(18), pp. 5775–5784.

Cho, T.H.S., Pick, K. and Raivio, T.L. (2023) Bacterial envelope stress responses: Essential adaptors and attractive targets. *Biochimica et Biophysica Acta (BBA) - Molecular Cell Research*. Vol.1870(2), p. 119387.

Daglia, M. (2012) Polyphenols as antimicrobial agents. *Current Opinion in Biotechnology*. Vol.23(2), pp. 174–181.

Dawan, J. and Ahn, J. (2022) Bacterial stress responses as potential targets in overcoming antibiotic resistance. *Microorganisms*. Vol.10(7), p. 1385.

Dergham, Y., Sanchez-Vizuete, P., Le Coq, D., Deschamps, J., Bridier, A., Hamze, K. and Briandet, R. (2021) Comparison of the genetic features involved in *Bacillus subtilis* biofilm formation using multi-culturing approaches. *Microorganisms*. Vol.9(3), 633.

Douthwaite, S., Powers, T., Lee, J.Y. and Noller, H.F. (1995) Defining the structural requirements for a functional ribosomal RNA pseudouridine synthase. *EMBO Journal*. Vol.14(21), pp. 4718–4726.

Ellermeier, C.D., Hobbs, E.C., González-Pastor, J.E. and Losick, R. (2006) A three-protein signaling pathway governing immunity to a bacterial cannibalism toxin. *Cell*. Vol.124(3), pp. 549–559.

Fujita, M., González-Pastor, J.E. and Losick, R. (2005) High- and low-threshold genes in the SpoOA regulon of *Bacillus subtilis*. *Journal of Bacteriology*. Vol.187(4), pp. 1357–1368.

Gaballa, A. and Helmann, J.D. (2002) A peroxide-induced zinc uptake system plays an important role in protection against oxidative stress in *Bacillus subtilis*. *Molecular Microbiology*. Vol.45(4), pp. 997–1005.

Gaballa, A. and Helmann, J.D. (2011) Bacillus subtilis Fur represses one of two paralogous haem-degrading monooxygenases. *Microbiology*. Vol.157(11), pp. 3221–3231.

Galperin, M.Y. and Koonin, E.V. (2004) "Conserved hypothetical" proteins: prioritization of targets for experimental study. *Nucleic Acids Research*. Vol.32(18), pp. 5452–5463.

González-Pastor, J.E., Hobbs, E.C. and Losick, R. (2003) Cannibalism by sporulating bacteria. *Science*. Vol.301(5632), pp. 510–513.

Grossman, A.D. (1995) Genetic networks controlling the initiation of sporulation and the development of genetic competence in *Bacillus subtilis*. *Annual Review of Genetics*. Vol.29, pp. 477–508.

Guerrier-Takada, C., Gardiner, K., Marsh, T., Pace, N. and Altman, S. (1983) The RNA moiety of ribonuclease P is the catalytic subunit of the enzyme. *Cell*. Vol.35(3 Pt 2), pp. 849–857.

Gunderson, J.H., Sogin, M.L., Wollett, G., Hollingdale, M., de la Cruz, V.F., Waters, A.P. and McCutchan, T.F. (1987) Structural conservation among divergent RNase P RNA. *Proceedings of the National Academy of Sciences USA*. Vol.84(16), pp. 5823–5827.

Guttenplan, S.B., Blair, K.M. and Kearns, D.B. (2013) Regulation of flagellar motility during biofilm formation in *Bacillus subtilis*. *FEMS Microbiology Reviews*. Vol.37(6), pp. 849–871.

Hahn, J., Roggiani, M. and Dubnau, D. (1995) The major role of *comK* in competence development in *Bacillus subtilis* is to activate the transcription of *comK*-dependent late competence genes. *Journal of Bacteriology*. Vol.177(12), pp. 3601–3605.

Hamon, M.A. and Lazazzera, B.A. (2001) The sporulation transcription factor Spo0A is required for biofilm development in *Bacillus subtilis*. *Molecular Microbiology*. Vol.42(5), pp. 1199–1209.

Helmann, J.D. (2002) The extracytoplasmic function (ECF) σ factors. *Advances in Microbial Physiology*. Vol.46, pp. 47–110.

Helmann, J.D. and Moran, C.P. Jr. (2002) RNA polymerase and sigma factors, in Sonenshein, A.L., Hoch, J.A. and Losick, R. (eds.) *Bacillus subtilis and Its Closest Relatives: From Genes to Cells*. Washington, D.C.: ASM Press. pp. 289–312.

Hobley, L., Ostrowski, A., Rao, F.V., Bromley, K.M., Porter, M., Prescott, A.R., MacPhee, C.E., van Aalten, D.M.F. and Stanley-Wall, N.R. (2013) BslA is a self-assembling bacterial hydrophobin that coats the *Bacillus subtilis* biofilm. *Proceedings of the National Academy of Sciences USA*. Vol.110(33), pp. 13600–13605.

Hu, X., Van Alst, N.E., Hasona, A., Crowley, P.J., He, X., Lux, R., Anderson, M.H. and Bleiweis, A.S. (2005) Characterization of *yhfE* in *Bacillus subtilis*: a putative multidrug resistance transporter. *Journal of Bacteriology*. Vol.187(20), pp. 7045–7052.

Hua, Z., Wu, C., Fan, G., Tang, Z. and Cao, F. (2017) The antibacterial activity and mechanism of ginkgolic acid C15:1. *Microbiological Research*. Vol.205, pp. 45–53.

Hubert, A., Tabuteau, H., Farasin, J., Loncar, A., Dufresne, A., Méheust, Y. and Le Borgne, T. (2024) Fluid flow drives phenotypic heterogeneity in bacterial growth and adhesion on surfaces. *Nature Communications*. Vol.15, Article 6161.

Islam, N., Maslanka, M., Sova, M., Castiglia, C., Greco, F., Wyss, D., Eaton, P., Kallipolitis, B., Benton, O. and Sermet, I. (2014) Proteomic analysis of *Staphylococcus aureus* biofilm cells grown under fluid shear. *Proteome Science*. Vol.12, 21.

Kearns, D.B., Chu, F., Branda, S.S., Kolter, R. and Losick, R. (2005) A master regulator for biofilm formation by *Bacillus subtilis*. *Molecular Microbiology*. Vol.55(3), pp. 739–749.

Kearns, D.B. and Losick, R. (2003) Swarming motility in undomesticated *Bacillus subtilis*. *Molecular Microbiology*. Vol.49(3), pp. 581–590.

Kearns, D.B. (2010) A field guide to bacterial swarming motility. *Nature Reviews Microbiology*. Vol.8(9), pp. 634–644.

Keiler, K.C., Waller, P.R.H. and Sauer, R.T. (1996) Role of a peptide tagging system in degradation of proteins synthesized from damaged messenger RNA. *Science*. Vol.271(5251), pp. 990–993.

Kobayashi, K. and Iwano, M. (2012) BsIA (YuaB) forms a hydrophobic layer on the surface of *Bacillus subtilis* biofilms. *Molecular Microbiology*. Vol.85(1), pp. 51–66.

Lee, J.H., Kim, Y.G., Ryu, S.Y., Cho, M.H., Lee, J. (2014) Ginkgolic acids and *Ginkgo biloba* extract inhibit *Escherichia coli* O157:H7 and *Staphylococcus aureus* biofilm formation. *International Journal of Food Microbiology*. Vol.174, pp. 47–55.

Li, Y. and Altman, S. (2004) In search of RNase P RNA from microbial genomes. *RNA*. Vol.10(10), pp. 1533–1540.

Livak, K.J. and Schmittgen, T.D. (2001) Analysis of relative gene expression data using real-time quantitative PCR and the  $2^-\Delta \Delta Ct$  method. *Methods*. Vol.25(4), pp. 402–408.

López, D., Vlamakis, H. and Kolter, R. (2009) Generation of multiple cell types in *Bacillus subtilis*. *FEMS Microbiology Reviews*. Vol.33(1), pp. 152–163.

López, D., Vlamakis, H. and Kolter, R. (2010) Biofilms. *Cold Spring Harbor Perspectives in Biology*. Vol.2(7), a000398.

Love, M.I., Huber, W. and Anders, S. (2014) Moderated estimation of fold change and dispersion for RNA-seq data with DESeq2. *Genome Biology*. Vol.15(12), p. 550.

Lu, C., Ding, F., Chowdhury, A., Pradhan, V., Tomsic, J., Holmes, W.M., Henkin, T.M. and Ke, A. (2010) SAM recognition and conformational switching mechanism in the *Bacillus subtilis* yitJ S box/SAM-I riboswitch. *Journal of Molecular Biology*. Vol.404(5), pp. 803–818.

Margot, P., Mauël, C. and Karamata, D. (1999) The gene *lytE* of *Bacillus subtilis* 168 encodes a cell wall hydrolase. *FEMS Microbiology Letters*. Vol.170(2), pp. 147–155.

Michna, R.H., Zhu, B., Mäder, U. and Stülke, J. (2016) SubtiWiki 2.0—an integrated database for the model organism *Bacillus subtilis*. *Nucleic Acids Research*. Vol.44(D1), pp. D654—D662.

Muto, A., Fujihara, A., Ito, K., Matsuno, J., Ushida, C., Himeno, H. and Miyazaki, M. (2000) Requirement of transfer-messenger RNA for the growth of *Bacillus subtilis* under stresses. *Genes to Cells*. Vol.5(8), pp. 627–635.

Nairn, B.L., Mabbett, A.N., Riggio, M.P., Ramage, G., Nobbs, A.H. and Jenkinson, H.F. (2024) Shear stress modulates gene expression and phenotypic traits in *Streptococcus gordonii* oral biofilms. *Journal of Bacteriology*. Vol.206(5), pp. e00536-23.

Nicolas, P., Mäder, U., Dervyn, E., Rochat, T., Leduc, A., Pigeonneau, N., Bidnenko, E., Marchadier, E., Hoebeke, M., Aymerich, S., Becher, D., Bisicchia, P., Botella, E., Delumeau, O., Doherty, G., Denham, E.L., Fogg, M.J., Fromion, V., Goelzer, A., Hansen, A., Härtig, E., Harwood, C.R., Homuth, G., Jarmer, H., Jules, M., Klipp, E., Le Chat, L., Lecointe, F., Lewis, P., Liebermeister, W., March, A., Mars, R.A., Nannapaneni, P., Noone, D., Pohl, S., Rinn, B., Rügheimer, F., Sappa, P.K., Samson, F., Schaffer, M., Schwikowski, B., Steil, L., Stülke, J., Wiegert, T., Devine, K.M., Wilkinson, A.J., van Dijl, J.M., Hecker, M., Völker, U., Bessières, P. and Noirot, P. (2012) Condition-dependent transcriptome reveals high-level regulatory architecture in *Bacillus subtilis. Science*. Vol.335(6072), pp. 1103–1106.

Niu, L., Lane, B.G. and Ofengand, J. (1999) RsuA, the 16S rRNA pseudouridine synthase of *Escherichia coli*. *RNA*. Vol.5(3), pp. 327–336.

Pereira, M.O., Kuehn, M., Wuertz, S., Neu, T.R. and Melo, L.F. (2002) Effect of flow regime on the architecture of a *Pseudomonas fluorescens* biofilm. *Biotechnology and Bioengineering*. Vol.78(2), pp. 164–171.

Popham, D.L. and Young, K.D. (2003) Role of penicillin-binding proteins in bacterial cell morphogenesis. *Current Opinion in Microbiology*. Vol.6(6), pp. 594–599.

Rhee, H.J., Lee, E.J. and Park, C. (2007) Physiological polyamines: simple primordial stress molecules. *Journal of Cell and Molecular Medicine*. Vol.11(4), pp. 685–703.

Romero, D., Aguilar, C., Losick, R. and Kolter, R. (2010) Amyloid fibers provide structural integrity to *Bacillus subtilis* biofilms. *Proceedings of the National Academy of Sciences of the United States of America*. Vol.107(5), pp. 2230–2234.

Sanfilippo, J.E., Larkin, J.W., Wallace, E.W.J., Deighan, P., Taff, S.D., Whiteley, M. and O'Toole, G.A. (2019) Microfluidic-based transcriptomics reveals core and species-specific responses of *Pseudomonas aeruginosa* biofilms to shear stress. *mSystems*. Vol.4(4), pp. e00181-19.

Serrano, M., Zilhão, R., Ricca, E., Ozin, A.J., Moran, C.P. and Henriques, A.O. (2016) A Bacillus subtilis secreted protein with a role in endospore coat assembly and the modulation of spore properties. *Journal of Bacteriology*. Vol.198(9), pp. 1373–1388.

Schujman, G.E., Paoletti, L., Grossman, A.D. and de Mendoza, D. (2001) FapR, a bacterial transcription factor involved in global regulation of membrane lipid biosynthesis. *Developmental Cell*. Vol.1(6), pp. 783–792.

Schultz, A.C., Nygaard, P. and Saxild, H.H. (2001) Functional analysis of 14 genes that constitute the purine catabolic pathway in *Bacillus subtilis* and evidence for a novel regulon controlled by the PucR transcription activator. *Journal of Bacteriology*. Vol.183(11), pp. 3293–3302.

Sekowska, A., Bertin, P., Danchin, A. (1998) Characterization of polyamine synthesis pathway in *Bacillus subtilis* 168. *Microbiology*. Vol.144(4), pp. 971–982.

Sekowska, A., Coppée, J.Y., Le Caer, J.P., Martin-Verstraete, I. and Danchin, A. (2000) S-adenosylmethionine decarboxylase of *Bacillus subtilis* is closely related to archaebacterial counterparts. *Molecular Microbiology*. Vol.36(5), pp. 1135–1147.

Shuppara, A.M., Padron, G.C., Sharma, A., Modi, Z., et al. (2025) Shear flow patterns antimicrobial gradients across bacterial populations. *Science Advances*. Vol.11(11), eads5005.

Smith, J.L., Kopylov, M., Vyas, K., Cushing, S., Wawrzyn, G. and Holzenburg, A. (2010) Structural studies of ferritin-like proteins from bacteria. *Biochimica et Biophysica Acta (BBA) - General Subjects*. Vol.1800(8), pp. 745–753.

Stewart, P.S. and Franklin, M.J. (2008) Physiological heterogeneity in biofilms. *Nature Reviews Microbiology*. Vol.6(3), pp. 199–210.

Stoodley, P., Lewandowski, Z., Boyle, J.D. and Lappin-Scott, H.M. (1999) Structural deformation of bacterial biofilms caused by short-term fluctuations in fluid shear: an in situ investigation of biofilm rheology. *Applied and Environmental Microbiology*. Vol.65(4), pp. 1758–1765.

Strauch, M.A., Spiegelman, G.B., Perego, M., Johnson, W.C., Burbulys, D. and Hoch, J.A. (1989) The transition state transcription regulator *abrB* of *Bacillus subtilis* is a DNA binding protein. *EMBO Journal*. Vol.8(5), pp. 1615–1621.

Strauch, M., Webb, V., Spiegelman, G. and Hoch, J.A. (1992) The *Bacillus subtilis* transition state regulator *abrB* is a DNA binding protein. *EMBO Journal*. Vol.11(12), pp. 3977–3984.

Thomen, P., Robert, J., Monmeyran, A., Bitbol, A.F., Lacroix, F., Baudoin, M. and Létang, P. (2017) Bacterial biofilm under flow: First a physical fluctuation. *Scientific Reports*. Vol.7, 953.

Tsagkari, E., Connelly, S., Liu, Z., McBride, A. and Sloan, W.T. (2022) The role of shear dynamics in biofilm formation. *npj Biofilms and Microbiomes*. Vol.8, Article 33.

Valiei, A., Kumar, A., Mukherjee, P.P., Liu, Y. and Thundat, T. (2012) A web of streamers: biofilm formation in a porous microfluidic device. *Lab on a Chip*. Vol.12(24), pp. 5133–5137.

van Gestel, J., Vlamakis, H. and Kolter, R. (2015) From cell differentiation to cell collectives: *Bacillus subtilis* uses division of labor to migrate. *PLOS Biology*. Vol.13(4), e1002141.

Vlamakis, H., Aguilar, C., Losick, R. and Kolter, R. (2013) Control of cell fate by the formation of an architecturally complex bacterial community. *Genes & Development*. Vol.27(7), pp. 1393–1403.

Vlamakis, H., Chai, Y., Beauregard, P., Losick, R. and Kolter, R. (2013) Sticking together: building a biofilm the *Bacillus subtilis* way. *Nature Reviews Microbiology*. Vol.11(3), pp. 157–168.

Wang, B., Wei, P.W., Wan, S., Yao, Y., Song, C.R., Song, P.P., Xu, G.B., Hu, Z.Q., Zeng, Z., Wang, C., Liu, H.M. (2021) *Ginkgo biloba* exocarp extracts inhibit *S. aureus* and MRSA by disrupting biofilms and affecting gene expression. *Journal of Ethnopharmacology*. Vol.271, 113895.

Wen, Z., Zhao, Y., Gong, Z., Tang, Y., Xiong, Y., Chen, J., Chen, C., Zhang, Y., Liu, S., Zheng, J., Li, D., Deng, Q. and Yu, Z. (2022) The Mechanism of Action of *Ginkgolic Acid* (15:1) against Gram-Positive Bacteria Involves Cross Talk with Iron Homeostasis. *Microbiology Spectrum*. Vol.10(1), article e00991-21.

Winkelman, J.T., Blair, K.M. and Kearns, D.B. (2009) RemA (YIzA) and RemB (YaaB) regulate extracellular matrix operon expression and biofilm formation in *Bacillus subtilis*. *Journal of Bacteriology*. Vol.191(13), pp. 3981–3991.

Wittig, C., Wagner, M., Vallon, R., Crouzier, T., van der Wijngaart, W., Horn, H. and Bagheri, S. (2025) The role of fluid friction in streamer formation and biofilm growth. *npj Biofilms and Microbiomes*. Vol.11, Article 17.

Yoshimura, M., Asai, K., Sadaie, Y. and Yoshikawa, H. (2004) Interaction of *Bacillus subtilis* extracytoplasmic function sigma factors, SigM and SigW, with the anti-sigma factor YhdL. *Genes & Genetic Systems*. Vol.79(1), pp. 35–43.

Zhou, Y., Liu, X., Li, C., Liu, M., and Jiang, L. (2019) Structural basis for the inhibition of the autophosphorylation activity of HK853 by luteolin. *Molecules*. Vol.24(5), 933.

# 5.8. Appendix

**Table S5.1.** Primers used in the RT-qPCR investigation in this chapter.

Gene	Primer Sequence
blsA-F	ACA AAA CAC TTC CTG CCG CT
<i>blsA-</i> R	GTT GCA ACC GCA AGG CTG
TasA-F	CAA GCC GTT CCA CTG TGT AG
TasA-R	AAC CGC TCC TGA ATA TGA TGG
sIrR-F	AGC GGC GGT GAA GAA GAA T
<i>slrR-</i> R	GCT TGT ACG GCT TGC ACT AA
remB-F	AGA AAC ACA AGG TGG TGC CT
remB-R	ATA GAT TTG GGC GTG CCG TT
SpoOA-F	ATC TTC CTG CCC AAA GGC TG
SpoOA-R	GCA TCT AGA CGG ACT TGC GG
comK-F	TCG ACG ATA CGG AAG TGA CG
comK-R	ATC GGC AGC TCC ATC GTT TT
Dps-F	TCTGTCAAAGAAGCTGCTGG
<i>Dps</i> -R	CCGTTTTTCAGCTCTTCCGC
SigM-F	GCTCTCCATGACAAAAGACAAGC
SigM-R	ATGCCCGCATAAAGGTTTCC
YerD-F	GTCTGCCATGAGCTACGGTTC
<i>YerD-</i> R	CTTTTGAGAGCGCCGTAACA
abrB-F	TGC TCA GCG CCT TCT TTA CT
<i>abrB-</i> R	ACC TTA AAC TTG CAG GCG GT
SigD-F	AAG ATT GGC TGC CCA GAA CC
SigD-R	CGG GCG ATA CAT TCC GAA GA
lytA-F	GTC TGG CGA TAC ATC TTC ACCT
<i>lytA-</i> R	CGG GTT GCG GGG TTA ATA GT
16srRNA-F (Ref)	AAG TCG AGC GGA CAG ATG G
16srRNA-R (Ref)	CCA GTT TCC AAT GAC CCT CCC C
AroE-F (Ref)	GGG GAA GGC TTC GTG AAG TC
AroE-R (Ref)	CCC ACA GAC GTT GTA TGG ATG

# 6. Conclusion Chapter

### 6.1. Introduction

Biofilms represent one of the most resilient and adaptable modes of bacterial existence, capable of thriving in a vast range of environmental, clinical, and industrial contexts. This thesis set out to investigate how *Bacillus subtilis*, a well-established model for biofilm research, responds to two specific and ecologically relevant pressures: dynamic fluid flow and exposure to a natural extract, *Ginkgo biloba* leaf extract (GBLE). By integrating structural and molecular analyses across static, unidirectional, and bidirectional flow regimes, the work aimed to build a multi-scale understanding of how mechanical and phytochemical cues intersect to shape biofilm behaviour.

The decision to focus on *B. subtilis* JWV042, a wild-type derivative of NCIB3610 with constitutive GFP expression, provided both ecological relevance and experimental flexibility. This strain retains the full genetic repertoire required for robust, architecturally complex biofilm formation, while enabling high-resolution visualisation of structural features through confocal and fluorescence microscopy. Across four experimental chapters, the research progressed from investigating GBLE's effects on static biofilms, to exploring its impact on macroscale architectures formed under continuous flow, to examining structural adaptation to bidirectional flow, and finally to uncovering transcriptional responses underpinning these morphological outcomes.

This concluding chapter draws together the findings of these interconnected studies, evaluates their contribution to the field, and considers both the broader scientific implications and potential applications. It also outlines future research directions that could extend and translate these findings into practical biofilm management strategies

# 6.2. Integration of Structural Findings

Across the structural studies presented in this thesis, a consistent theme emerged: *B. subtilis* biofilms exhibit remarkable morphological plasticity when exposed to different hydrodynamic regimes. The progression from static to unidirectional and bidirectional flow systems revealed not only increasing architectural complexity but also the emergence of structural features previously undescribed in the literature, most notably Van Gogh ropes, strands and channel-harbouring raised folds.

Under static conditions, GBLE's effects were most readily observed at the level of colony and static morphology. In Chapter 2, static biofilms grown at the air—liquid interface showed a clear concentration-dependent reduction in biomass and alteration of structural organisation. Rather than exerting a bactericidal effect, GBLE influenced biofilm morphology, leading Van Gogh bundle formation and DNA condensation. Fluorescent amyloid staining revealed an increase in matrix-associated fibres under GBLE, suggesting a compensatory response aimed at reinforcing structural stability under chemical stress. Colony biofilms on agar displayed comparable concentration-dependent inhibition, with affected colonies exhibiting reduced wrinkling and surface relief, concentration-dependent cellular differentiation, with increased swimming motility.

The transition to continuous unidirectional flow in Chapter 3 revealed how mechanical forces fundamentally alter biofilm architecture. Even in the absence of GBLE, flow-grown biofilms formed distinctive Van Gogh bundles (long aligned chains of cells) and Van Gogh ropes (long and twisted chains of cells). Fluorescent microscopy enabled in situ visualisation of these bundles, along with the novel discovery of extracellular matrix (ECM)-rich attachment foundation layers that anchored the biofilm to the substratum. These features likely contribute to the enhanced mechanical stability observed under constant shear. GBLE supplementation in the flow system disrupted this organisation in a concentration-dependent manner, fragmenting Van Gogh bundles, reducing biomass accumulation, and altering surface coverage. Importantly, these structural changes were achieved without wholesale biofilm removal, indicating targeted interference with higher-order organisation rather than indiscriminate detachment.

In bidirectional flow systems (Chapter 4), biofilm architecture reached a new level of complexity. A change in flow direction introduced greater biofilm porosity, increased biomass, and the exclusive formation of raised folds with internal channels, structures that may enhance nutrient transport, promote spatial differentiation, and distribute mechanical stresses. This structural heterogeneity reflects a sophisticated adaptation to unpredictable hydrodynamic forces. GBLE treatment in this mechanically complex environment again reduced biomass and disrupted multicellular structures, including folds and Van Gogh bundles.

Taken together, these structural studies demonstrate that:

- Hydrodynamic conditions are primary drivers of biofilm morphology, with bidirectional flow promoting the highest degree of architectural complexity observed in this work.
- 2. GBLE consistently disrupts higher-order structural organisation across static and flow environments, acting through mechanisms distinct from simple growth inhibition.

By integrating static, unidirectional, and bidirectional systems, this work extends classical biofilm models, which largely focus on microcolony-scale development, into the macroscale, real-world contexts where mature biofilms persist. The identification of novel structures such as Van Gogh ropes and ECM foundation layers in flow, not only deepens our understanding of *B. subtilis* multicellularity but also introduces new morphological targets for antibiofilm strategies.

### 6.3. Integration of Molecular Findings

While the structural analyses revealed how *B. subtilis* biofilms physically adapt to different hydrodynamic regimes and to GBLE challenge, the molecular data provided a complementary view of the regulatory systems underpinning these adaptations. By combining RT-qPCR with RNA-Seq in static systems, and RNA-Seq in unidirectional, and bidirectional flow conditions, it was possible to identify transcriptional signatures that both explain observed morphological changes and reveal new layers of complexity in biofilm regulation.

One of the most consistent findings was GBLE's broad suppression of genes central to biofilm formation and developmental progression. Core matrix-associated genes, including *bslA* (encoding the hydrophobin-like surface layer protein) and *tasA* (encoding the primary amyloid fibre component), were significantly downregulated across all conditions. This transcriptional repression aligns with the reduced wrinkling and increased swimming in agar colony biofilms. The downregulation of *spo0A*, a master regulator of sporulation and biofilm development, suggests that GBLE impacts global decision-making pathways, potentially shifting the population away from differentiation into matrix-producing and spore-forming subpopulations.

Motility-associated (*sigD*) and stress-response genes (*sigM*, *dps*) were similarly repressed under GBLE treatment, indicating a broad attenuation of adaptive programmes that would normally enhance biofilm robustness. Interestingly, RNA-Seq data revealed selective activation of oxidative stress defence (*hmoB*, *yhfE*), polyamine metabolism (*speD*), and

ribosomal support (*rsuA*) genes in the presence of GBLE, suggesting that while global biofilm development is suppressed, cells may divert resources towards basal survival and protein synthesis maintenance.

Flow regimes induced distinct transcriptional responses in *B. subtilis* biofilms, closely matching the morphological differences observed microscopically.

In unidirectional flow, key changes included upregulation of *rnpB* (RNA component of RNase P, tRNA processing) and downregulation of *pbpF* (cell wall remodelling) and *pucB* (purine catabolism). These shifts suggest adaptations in RNA processing and envelope structure under constant shear, consistent with the presence of Van Gogh bundles but reduced higher-order cohesion.

In bidirectional flow, the response was broader, with *rnpB* again strongly upregulated alongside *skf* operon genes linked to programmed cell death and nutrient recycling. Two hypothetical proteins (*BS3610\_RS01225* and *BS3610\_RS22545*) were also induced, the latter showing a related expression pattern to *BS3610\_RS22555* in unidirectional flow, suggesting potential co-regulation. These changes align with the greater structural heterogeneity, folds, and channels observed under alternating shear forces.

Overall, unidirectional flow favoured targeted adjustments to cell envelope and RNA metabolism, whereas bidirectional flow triggered a more complex transcriptional programme, potentially underpinning the increased resilience and diversity of structures seen in these biofilms.

Together, these molecular insights reinforce three key points:

- GBLE acts primarily by disrupting the transcriptional programmes required for biofilm maturation, particularly those controlling matrix production, developmental transitions, and stress resilience.
- Flow directionality shapes gene expression profiles in ways that directly influence morphological outcomes, with bidirectional flow promoting both structural and transcriptional diversity.
- The interaction between mechanical and phytochemical stressors is non-linear, with bidirectional flow in particular fostering a partially resistant transcriptional state that may blunt the effects of GBLE on biofilm integrity.

By aligning gene expression patterns with observed morphologies, this thesis provides a systems-level view of *B. subtilis* biofilm adaptation. These findings extend current models of biofilm regulation by showing how environmental mechanics and chemical pressures converge at the transcriptional level to shape community structure and function.

### 6.4. Broader Scientific Implications

The findings of this thesis contribute to the growing recognition that biofilm development cannot be fully understood without considering the interplay between mechanical forces and chemical cues. While traditional biofilm models, such as the five-step attachment-maturation-dispersion framework, have been instrumental in describing fundamental processes, they often treat environmental pressures as static or singular influences. The present work demonstrates that hydrodynamic conditions and phytochemical stress from plant-derived compounds can exert simultaneous, intersecting effects on both biofilm architecture and its underlying regulatory networks.

One of the most significant contributions of this research is the extension of biofilm developmental theory into macroscale, flow-relevant environments. The identification of Van Gogh bundles as the main components of flow cell biofilms, Van Gogh ropes, channel-harbouring raised folds, and ECM foundation layers within *B. subtilis* biofilms grown in flow cells reveals levels of architectural organisation not accounted for in current conceptual models. These structures are not random artefacts but appear to be functional adaptations, conferring mechanical stability, enhancing nutrient transport, and creating spatial niches for differentiation. Their discovery underlines the need for biofilm models that incorporate hydrodynamic complexity and higher-order architecture, especially for industrial and environmental contexts where mature biofilms experience sustained or fluctuating flow.

From a regulatory perspective, the integration of molecular and structural data offers new insight into how biofilms reconfigure their transcriptional landscape in response to environmental challenges. The bidirectional flow findings, in particular, suggest that fluctuating mechanical stresses can stimulate broad transcriptional activation, fostering structural diversity and possibly enhancing resilience. This aligns with recent theoretical models proposing that biofilms behave as adaptive collectives, capable of reorganising both physically and genetically in response to multi-factorial stress. By showing that GBLE's impact

on gene expression is modulated by flow conditions, this work highlights the importance of context-dependent evaluation of antibiofilm strategies.

The phytochemical component of this research also has broader implications for the study of natural product-based antibiofilm agents. While much work on plant-derived antimicrobials focuses on their planktonic activity or bulk biomass reduction, the present findings emphasise the need to assess their influence on biofilm-specific structures and differentiation pathways. GBLE's suppression of key matrix and developmental genes, alongside targeted disruption of higher-order architecture, demonstrates that biofilm control can be achieved without complete eradication. This positions GBLE, and potentially other phytochemicals with similar modes of action, as promising candidates for sustainable biofilm management strategies in sectors where chemical toxicity and environmental persistence are concerns, although further research is needed.

Finally, the combined mechanical—chemical framework developed here has theoretical significance beyond *B. subtilis*. While the model organism's genetic tractability made it ideal for dissecting the relationship between structure, function and regulation, the principles uncovered, such as flow driven differentiation, context-modulated transcriptional responses, and phytochemical targeting of biofilm-specific pathways, are likely to apply to other environmental and industrially relevant bacteria. By integrating hydrodynamic and phytochemical perspectives, this work contributes to a more holistic understanding of biofilm ecology, bridging laboratory observations with the complex realities of natural and engineered systems.

## 6.5. Applied Relevance

The structural and molecular insights gained in this thesis have direct implications for the management of biofilms in industrial, medical, and environmental systems. Biofilm-related problems are costly and persistent, ranging from pipeline fouling and heat exchanger inefficiency to chronic infections and contamination of food-processing surfaces. By elucidating how *B. subtilis* adapts to mechanical and phytochemical pressures, this research provides a framework that can be adapted to other biofilm-forming species of industrial and clinical concern.

The discovery that flow regime strongly influences biofilm architecture and resilience is especially relevant for systems where hydrodynamics can be controlled or engineered. In

industrial water circuits, bioreactors, and filtration systems, adjusting flow direction periodically could be exploited as a mechanical control strategy, weakening structural features that confer stability, such as tightly aligned bundles or ECM-rich foundation layers. The bidirectional flow experiments in this thesis show a change in flow direction alters not only morphology but also gene expression profiles, suggesting that mechanical destabilisation could be timed to coincide with chemical treatments for synergistic effects.

The GBLE findings also have promising translational potential. As a plant-derived extract with demonstrated antibiofilm activity, GBLE offers an alternative to harsh synthetic biocides, aligning with the growing demand for sustainable, environmentally benign antimicrobials. While targeting biofilm-specific structures and regulatory pathways without causing broad bactericidal effects, GBLE may reduce the risk of resistance development and minimise collateral damage to beneficial microbial communities. This makes GBLE, or its active components, viable candidates for integration into biofilm prevention coatings, cleaning protocols, or dosing regimens in systems where chemical load and toxicity are major concerns.

In medical contexts, while *B. subtilis* is not a pathogen, the principles observed here, such as suppression of matrix genes, interference with higher-order architecture, and the modulation of stress responses, are relevant to biofilms formed by clinically important species. Devices such as catheters, stents, and wound dressings could benefit from surface treatments incorporating phytochemical agents with modes of action similar to GBLE, especially in combination with mechanical disruption methods like pulsed or oscillatory flow.

For environmental applications, the interplay between hydrodynamic forces and phytochemical exposure highlighted in this thesis can inform biofilm management in natural and engineered water systems. In irrigation networks, aquaculture facilities, or wastewater treatment plants, strategic use of flow variation combined with sustainable antibiofilm agents could help control unwanted biofilm accumulation while maintaining system performance and ecological balance.

Overall, the applied message of this work is clear: effective biofilm control strategies must account for the physical environment. By showing that hydrodynamic conditions can both strengthen and weaken biofilms, and that phytochemicals like GBLE can selectively target structural and regulatory elements, this research supports the development of integrated, multi-modal approaches to biofilm management that are both effective and sustainable.

### 6.6. Future Directions

The findings of this thesis open several avenues for further research, spanning fundamental questions in biofilm biology to applied strategies for sustainable control. Building on the structural and molecular framework developed here, future studies could refine our understanding of the interplay between hydrodynamic forces, phytochemical challenge, and biofilm adaptation.

From a fundamental science perspective, one priority is to dissect the mechanistic basis of the novel structures observed in this work, including Van Gogh ropes, ECM-rich foundation layers, and channel-harbouring folds. High-resolution time-lapse imaging and correlative microscopy could capture their formation dynamics, while targeted genetic knockouts could clarify the roles of specific matrix components and regulatory pathways in their development in flow environments. Similarly, detailed chemical characterisation of the extracellular matrix under different flow regimes and GBLE exposures could reveal how physical and chemical cues influence matrix composition and functionality.

On the molecular side, further RNA-Seq and proteomic studies could expand on the transcriptional patterns identified here. Time-course analyses would be particularly valuable, revealing how quickly biofilms adjust their gene expression after changes in flow regime or phytochemical exposure. Integrating these omics approaches with metabolomics could uncover metabolic adaptations that support survival under dual mechanical and chemical stress.

In terms of phytochemical research, the active constituents of GBLE responsible for its antibiofilm activity remain to be fully identified. Fractionation and bioassay-guided purification could isolate these compounds, enabling more targeted application and dosage optimisation. Structural analogues or synthetic derivatives could then be tested for enhanced potency or stability, broadening the potential use of GBLE-inspired treatments in industrial and medical contexts.

For applied biofilm control, the integration of hydrodynamic variation and phytochemical dosing offers a promising multi-modal approach. Future pilot-scale studies in relevant industrial or environmental systems, such as food processing lines, cooling towers, or aquaculture tanks, could assess how flow regimes impact biofilm accumulation and whether

combining these regimes with GBLE reduces biomass more effectively than either method alone.

Finally, there is scope to expand this research into mixed-species biofilms, which dominate real-world settings and often display enhanced resilience compared to monocultures. Understanding whether the structural and regulatory effects of GBLE and flow directionality observed in *B. subtilis* translate to multispecies communities will be critical for assessing the ecological validity of these strategies.

In summary, the next phase of work should aim to connect the mechanistic detail uncovered here with the operational realities of biofilm management. By continuing to integrate structural, molecular, and applied perspectives, future research can build on the foundations laid by this thesis to develop innovative, sustainable, and context-specific solutions for biofilm control.

### 6.7. Closing Remarks

This thesis has explored the structural and molecular adaptability of *B. subtilis* biofilms in response to two parameters: the forces of fluid flow and the phytochemical challenge of GBLE. By moving from static systems to unidirectional and bidirectional flow environments, and from whole-biofilm architecture to transcriptional regulation, the research has shown that biofilm behaviour is shaped by the combined and context-dependent effects of physical and chemical cues.

The work has contributed novel insights to biofilm science: the discovery of previously unreported structures such as Van Gogh ropes, strands, ECM-rich foundation layers, and channel-harbouring folds in flow cell biofilms; the demonstration that flow fundamentally alters both morphology and gene expression; and the identification of GBLE as a biofilm-specific disruptor. Together, these findings extend current models of biofilm development and highlight the importance of integrating environmental mechanics into studies of biofilm control.

Beyond its scientific contributions, this thesis points towards practical strategies for sustainable biofilm management, investigating hydrodynamic flow environments with plant-derived compounds to weaken biofilm defences without relying solely on harsh biocides. By bridging fundamental research and applied potential, the work underscores a central

message: effective biofilm control requires understanding the systems in which biofilms live, not just the organisms themselves.

In closing, the findings presented here deepen our understanding of bacterial multicellularity, reveal new targets for intervention, and offer a foundation for innovative, environmentally responsible approaches to managing biofilms in both industrial and medical contexts.